Dipl.-Ing. David Pfeifer, BSc.

Highly photostable red-emitting pH Indicators for Optical Sensors

Dissertation

Zur Erlangung des akademischen Grades
Doktor der technischen Wissenschaften

eingereicht an der

Technischen Universität Graz

Betreuer:
Assoc.Prof. kand. Sergey Borisov
Institut für Analytische Chemie und Lebensmittelchemie

Graz, Februar 2020

Worries are pointless. If there is a solution, there is no need to worry.
If no solution exists, there is no point to worry.

Buddha

Eidesstattliche Erklärung

Ich erkläre an Eides statt, dass ich die vorliegende Arbeit selbstständig verfasst, andere als die angegebenen Quellen/ Hilfsmittel nicht benutzt, und die den benutzten Quellen wörtlich und inhaltlich entnommenen Stellen als solche kenntlich gemacht habe. Das im TUGRAzonline hochgeladene Textdokument ist mit der vorliegenden Dissertation identisch.

Datum

Unterschrift

Statutory Declaration

I declare that I have authored this thesis independently, that I have not used other than the declared sources / resources, and that I have explicitly marked all material which has been quoted either literally or by content from the used sources.

Date

Signature

Danksagung

An dieser Stelle, ist es Zeit DANKE zu sagen, DANKE an alle die mich in der jüngeren Vergangenheit begleitet haben, aber auch an die, die mich durch ihre langjährige Unterstützung zu dem gemacht haben, was ich jetzt bin – stolzer Bruder; (teilweise) erwachsener Sohn; lustiger, ehrlicher, liebender Freund – und am Ende meiner Dissertation. Um auf niemanden zu vergessen, hab ich hier versucht Erlebnisse und Eindrücke festzuhalten, für die ich euch danken will und somit solltet ihr euch auch ohne Namen in der einen oder anderen Zeile wiederfinden, und mit einem Lächeln im Gesicht daran zurückdenken.

Mein Leben hätte doch deutlich weniger Farbe. Ohne euer Zutun wäre ich nicht über eine so lange Zeit im ständigen Gedanken an Sensoren, Farbstoffen aber auch immer wieder auf der Suche nach Lösungen und Erklärungen. Ohne die Unterstützungen am Weg zu fertigen Arbeiten, neuen Projekten oder zu erhaltenen Stipendien, wäre vieles anders gelaufen.

Wie viele Danksagungen hast du über die Jahre schon gelesen, in denen festgehalten wurde, welchen unfassbaren Mehrwert deine Anwesenheit, deine Unterstützung, deine Zeit zum Reden oder einfach deine Hilfe in schier unlösbaren Situationen, die du löst, einfach weil du es kannst. Ohne all das wäre ich jetzt nicht da, nicht an diesem Punkt. In der Hoffnung auf zukünftige, gemeinsame (Organisations)-Zeit.

Mentor der ersten Stunde. Freund und Helfer eines jungen Grazers, der die große Welt sehen will. Gegenseitige Motivation in unterschiedlichsten Lebenslagen, auch in harten 2:14:02 Stunden ist unser Schlüssel zum Erfolg und zu unserer Freundschaft. Unsere Ideen sind nicht enden wollend, vielleicht wollen wir uns doch noch um das ein oder andere gemeinsame Business kümmern und blaue Krähen fangen. Für mich ist eines glasklar, da gibt's in Zukunft noch so einiges zum Erleben.

Wie viele verrückte, genial, absurde, lustige, körperlich ertüchtigende Ideen wären mir ohne dein Zutun verwehrt geblieben, einher mit doch bemerkenswerten, zählbaren, teilweise unerwarteten Erfolgen seit Anbeginn meiner bunten Zeit und auch noch weit darüber hinaus.

Sturm auf Graz, Sturm auf Sport, Sturm auf geile Tage, Sturm auf ein Montagsseidel, Sturm im Herzen. Strohwitwerkollegen mit Bemutterungsinstinkten, Katzensitter mit gewissen Vorzügen, Macibuddies an wilden Tagen, aber warum schauts jetzt so?

Einmal LausbubInnen, immer LausbubInnen – so würde ich diverse Karpfenabflussverstopfungsaktionen, Laborputzwartungstage, sportliche Erfolgsabende, Seidelexpressfahrten, Chaoszurechtfindwochen, Frustbewältigungsgetränkenachmittage, Kletterabende, Lösungsorientierte Sprechstunden, Daydrinkings oder Kochorgien beschreiben. Ihr seid der Grund, warum ich es auch so lange auf der Uni wirklich gut ausgehalten habe.

Abseits der fachlichen Unterstützung und der gemeinsamen, lehrreichen Zeit in Graz, fernab der Unigebäude verbinden uns Lesezeiten im Liegestuhl, Riesenenten, harte, teils nervenraubende Kartenspiele, gemeinsam den ersten Schnee des Jahres in Polen bestaunen und den Augen nicht trauend den Heimweg antreten, weil ihr mir Spaß versprochen habt, gibt's Spaß auch weiterhin.

Emotionale Ernsthaftigkeiten, Büroweinaustrinkaktionen und Biertrinkerin werden, USA-Highlights, neue Frisuren ausprobieren – Vertrauen schenken, Mittags mal einen Abstecher ins Kaisers machen, die besten Verkostungen ergattern, Wein auf Bier, oder Bier auf Wein – mit euch kann alles sein.

Arbeiten machen sich nicht von alleine, gemeinsame Forschungsinteressen bringt Vorteile, zählbare Ergebnisse und neue Setups aber auch zahllose Säulen, Ansätze, Vergiftungen, Messungen. Ohne euch wäre viel nicht zustande gekommen, was den Grundstock dieser Arbeit ausmacht. Albert Einstein sagte sehr treffend – *Zwei Dinge sind zu unserer Arbeit nötig: Unermüdliche Ausdauer und die Bereitschaft, etwas, in das man viel Zeit und Arbeit gesteckt hat, wieder wegzuwerfen.*

Es war einmal vor den Sensoren, da hatte ich weniger Haare (im Gesicht!) und trank was gegoren. Mit von der Partie waren Kampfzwerge, erste Matrosen, Mordgelüste, Zuckernarren, Knieprobleme, Ohrwaschlkakteen und Kühlschrankverkäufer.

Nie mehr Schule, keine Schule mehr – war damals im Sommer 2008 unser Motto – wohin uns unsere Wege führen würden, war uns nicht klar – doch Freunde fürs Leben wollten wir bleiben – Worte, die halten, in der Vergangenheit, in der Gegenwart und in der Zukunft.

Ständiger Rückhalt, immerwährende Motivation und unbändiges Interesse an meinem Erfolg, ist nichts was leicht von der Hand geht, aber es zu spüren ist eines der schönsten Dinge im Leben und ohne das wäre ich auch jetzt nicht da. Ihr seid der Ursprung und die Zukunft, der Grund, warum Graz meine Heimat ist, ich mich aber eher als Oststeirer in Graz statt als Vollblutgrazer fühle, ihr macht mich stolz und überglücklich ein Teil von euch zu sein. Ihr habt mich unterstützt, als ich als 5-jähriger in die Schule wollte, der Schularzt mich als nicht bereit für die erste Klasse abgestempelt hat – 25 Jahre danach würde ich jetzt behaupten – er hatte keine Ahnung was in mir steckt, ihr schon. Was kann man sich mehr wünschen, als ein Teil von immer wachsenden, hervorragend funktionierenden Familien zu sein, wo man immer willkommen ist.

Laut Dudendefintion bist du für mich eine Frau, die besonders geschätzt oder geliebt wird – meine Herzdame. Aber das reicht für dich bei Weitem nicht aus. Du schaffst es bester Freund, Ideen- und Ratgeber, Reiseorganisator, Spontan-Planer, Katzenmama, Chefkoch und eben meine Freundin alles auf einmal zu sein. Du bist der Motor, der mich kreativ und spontan werden lässt, du bist der Ruhepol der mich zurück auf die Couch holt. Deine Wichtigkeit in meinem Leben, deine Unterstützung zur Verwirklichung unserer Ideen und du an meiner Seite, das gehört einfach so.

Diese Arbeit widme ich meiner Familie und meiner Freundin Chrissi.

Abstract

In this thesis, novel pH sensitive indicator dyes for optical pH and carbon dioxide sensors are presented. It is mainly focused on the synthesis and characterization of their photophysical properties and consequently the suitability for optical sensors. The results of the thesis are summarized in three main parts.

In the first part, new pH-sensitive perylene bisimide indicator dyes have been synthesized and used for fabrication of optical sensors. The highly photostable dyes show absorption/emission bands in the red/near-infrared (NIR) region of the electromagnetic spectrum, high molar absorption coefficients (up to 100 000 M^{-1} cm^{-1}) and fluorescence quantum yields close to unity. Physical entrapment of the indicators into polyurethane hydrogel enables pH determination in alkaline pH ranges. It is also shown that plastic carbon dioxide solid state sensors can be manufactured via immobilization of the pH indicator in a water-insoluble polymer, along with a quaternary ammonium base.

In the second part, a palette of several new BODIPY pH indicators bearing different receptors have been prepared and tested as transducers in polymer-based optical carbon dioxide sensors. Apart from classical BODIPY chromophores absorbing at around 505 nm, π-extended analogs showing absorption maxima at around 635 and 665 nm are prepared. All the dyes possess excellent brightness due to combination of high molar absorption coefficients and fluorescence quantum yields. Furthermore, the π-extended BODIPYs show unmatched photostability. Carbon dioxide sensors are manufactured via immobilization of the dyes into ethyl cellulose along with tetraoctylammonium hydrogencarbonate. The sensitivity of these sensors is mainly guided by the nature of the receptor and can be tuned over a very wide range covering all important applications. Materials for referenced sensing with phase fluorometry and ratiometric imaging with RGB cameras are also prepared.

In the last part, a multistep synthesis and characterization of core-extended terrylene diimide dyes is presented. The synthesis includes a cascade of Pd-catalyzed Suzuki couplings, bromination of the terrylene core, and further functionalization. Novel asymmetric core-enlarged dyes bearing phenyl-groups or 4-benzoyl-morpholino-groups in bay-position are prepared to increase solubility, enhance the hydrophilic character of the structure built up by naphthalene building blocks and subsequently prevent aggregation. The dyes exhibit high molar absorption coefficients, bright red to far-red fluorescence emission, and extraordinary high photostability. Furthermore, several unsuccessful synthetic attempts are carried out to introduce a pH-sensitive PET receptor by adapting previously applied procedures used for perylene and terrylene diimide dyes.

Kurzfassung

Im Rahmen dieser Arbeit wurden erfolgreich pH-sensitive Materialien verschiedener Farbstoffklassen hergestellt. Neben der Synthese dieser Materialien konnte auch die praktische Anwendung in optischen fluoreszenzbasierten Sensorsystemen gezeigt werden.

Im ersten Teil der Arbeit wurde eine Reihe ultraheller, rot emittierender, pH-sensitiver Perylen Bisimid Farbstoffe, mit lateraler Erweiterung des chromophoren π-Systems hergestellt. Diese können aufgrund ihrer hervorragenden Eigenschaften für die Messung alkalischer pH Werte und Kohlendioxid verwendet werden Des Weiteren weisen die synthetisierten Farbstoffe ausgesprochen gute photophysikalische Merkmale, wie außergewöhnlich hohe Photostabilität, Absorptions- und Emissionsbanden im roten bis nahinfraroten spektralen Bereich, hohe molare Absorptionskoeffizienten (bis 100 000 M^{-1} cm^{-1}) sowie Fluoreszenz Quantenausbeuten nahe 1 auf. Einerseits wurden die Farbstoffe für die Verwendung in optischen pH Sensoren auf physikalischem Weg in polyurethanbasierte Hydrogele immobilisiert, weiters konnte gezeigt werden, dass sie sich auch für die Herstellung von optische Kohlendioxidsensoren eignen.

Im zweiten Teilbereich dieser Doktorarbeit wurden BODIPY-basierte pH-sensitive Farbstoffe synthetisiert, die sich als exzellente fluoreszente Indikatoren für optische Kohlendioxidsensoren erwiesen. Die hergestellten BODIPYs weisen je nach Struktur des Farbstoffgrundgerüsts Absorptionsmaxima von 505 nm bis 665 nm auf und bestechen durch ihre überdurchschnittlich guten photophysikalischen Eigenschaften. Besonders hervorzuheben ist hier der Farbstoff, mit dem größten π-System, der eine bis dato unübertroffene Photostabiltät aufweist. Durch das Anbringen unterschiedlicher pH-sensitiver Rezeptoren können die sensorisch relevanten Eigenschaften der Farbstoffe variiert werden und in weiterer Folge die Sensitivitätsbereiche der hergestellten Kohlendioxidsensoren je nach Applikation eingestellt werden.

Der letzte Teil der Arbeit beschäftigte sich mit der anspruchsvollen und mit nicht trivialem, zeitlichem Aufwand verbundenen Synthese von Terrylen Diimid Farbstoffen, welche in ihrer Grundstruktur erst seit den späten 1990er Jahren synthetisch zugänglich sind. Diese Farbstoffe gehören, wie auch die oben schon erwähnten Perylen Bisimide zur Stoffklasse der Rylen Farbstoffe. Da Terrylene durch ihre Struktur zur Aggregation neigen und auch einen starken hydrophoben Charakter aufweisen, wurde versucht, durch Substitution am Core, die Löslichkeit in organischen Lösungsmittel zu erhöhen und die oben genannten Eigenschaften zu optimieren. Die hergestellten Farbstoffe zeigen hohe molare Absorptionskoeffizienten, helle Fluoreszenz im roten bis in den tief roten spektralen Bereich, sowie ausgezeichnete Photostabilität. Jedoch konnten diese Materialien nicht mit pH-sensitiven Rezeptoren versehen werden.

Content

Part I

Introduction

1 Scope and Outline of the Thesis

Numerous fields of science, technology and industry rely on the monitoring of pH and closely related analytes such as carbon dioxide. Not surprisingly development of new sensor materials for these parameters is of utmost importance. Optical luminescent sensors represent a promising alternative to commonly used analytical tools e.g. electrochemical sensors. Due to a number of practically attractive features provided by optical sensors such as variation of utilization formats, detection of numerous analytes and their non- or only minimal invasiveness, improvements are of high interest.

In the last decades many new indicators and sensors have been developed and some of them were also commercialized. However, most of the pH sensors are based on UV-Vis indicators and only a few rely on far-red and NIR ones. The aims of this thesis are synthesis and characterization of ultra-bright NIR pH-sensitive dyes, further preparation and characterization of new optical sensing materials on their basis and application of the new sensors in bioanalytics and other fields.

This thesis is written as cumulative work and manuscripts presented are already accepted, under revision or are prepared for submission in peer-reviewed journals. Additionally, given prefaces to the manuscripts should briefly address the connection to the thesis and refer to parts of the theoretical background. Future prospects and a outlook will provide ideas for future work on indicator dyes, their implementation in optical sensors and their applicability within this thesis.

The first part is dedicated to the theoretical background about luminescence, fluorescent dyes, optical sensors and indicators. It highlights the advantages of optical sensor technology but also its limitations. The second part presents the outcome of the realized projects.

Chapter 3 (p. 39) presents new ultra-bright red emitting perylene bisimide dyes used for sensing of pH and carbon dioxide. This chapter is mainly dedicated to synthesis and characterization of several new pH sensitive, easily accessible core-extended perylene bisimide dyes and materials for optical pH and carbon dioxide sensing prepared on the basis of these dyes. The indicators feature efficient absorption in the orange-red part of the spectrum, strong red/far-red fluorescence, and high photostability, molar absorption coefficients up to 100 000 M^{-1} cm^{-1} and fluorescence quantum yields close to unity.

Chapter 4 (p. 73) describes a palette of novel green to red emitting BODIPY pH-sensitive indicator dyes and their usage for fluorescent sensing and imaging of carbon dioxide. All the dyes possess excellent luminescence brightness and additionally the π-extended BODIPYs show unmatched photostability. Due to the modular synthesis concept, the sensitivity can be tuned over a wide range covering all relevant applications. We also designed sensing materials for ratiometric imaging with RGB cameras and referenced material for phase-fluorometric read-out.

Chapter 5 (p. 121) is dedicated to synthesis and characterization of core-extended terrylene bisimide dyes. Terrylene bisimide dyes are a relatively young class of dyes, with absorption and emission bands in the red/far red region of the spectrum, due to their structural properties they are usually hydrophobic and prone to aggregation. Novel asymmetric core-enlarged dyes have been synthesized bearing phenyl-groups or 4-benzoyl-morpholino-groups in bay-position to increase solubility in organic solvents and the hydrophilic character as well as to prevent from aggregation. Furthermore, several synthetic attempts were carried out to introduce a pH sensitive PET receptor by adapting applied procedures used for perylene bisimide indicators.

2 Theoretical Background

2.1 Luminescence – Basic Principles

A high quantity of optical sensors are based on luminescence. Luminescence in general is the process of light emission induced by relaxation of an excited electron back to its ground state. All occurring luminescence phenomena are visualized most commonly in the Jablonski diagram (Figure 2-1). Excitation of an electron by absorption of a photon from its ground state (S_0) to an energetically higher level (10^{-15} sec) – the excited singlet state (S_1) is the base for various de-excitation pathways which can occur.

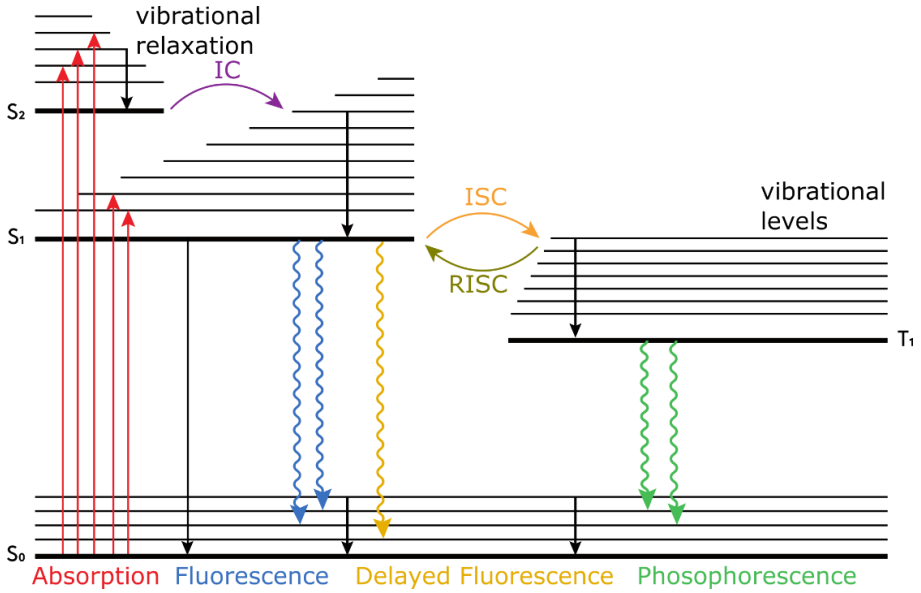

Figure 2-1 Jablonski diagram: visualization of the excitation process (absorption), radiative de-excitation processes (fluorescence, delayed fluorescence and phosphorescence) and non-radiative relaxation. S_0, S_1 and S_2 represent the singlet ground state and the energetically excited states, respectively. T_1 is the excited triplet state. Non radiative transition processes between levels of different energy are internal conversion (IC), intersystem crossing (ISC) and reverse intersystem crossing (RISC).

First, the direct relaxation from the excited singlet state back to the ground state takes place, usually in the nanosecond time-scale – the radiative de-excitation process is called *fluorescence*. However, also non-radiative de-excitation processes such as *vibrational relaxation* to the energetically lowest excited state or *internal conversion* may occur right before the emission of photons. *Internal conversion* is the transition from an energetically highest excited state (e.g. S_2) to the lowest one (e.g. S_1). *Internal Conversion* between the lowest excited level S_1 and the ground state S_0 might be possible, but due to the larger energy gap less efficient. Second, *phosphorescence* may occur if the excited electron undergoes a non-radiative *intersystem crossing*, i.e. changes its spin due to a spin-

orbit coupling and photons are emitted subsequently to the relaxation of an excited triplet state (T_1) back to the ground state (S_0). The *intersystem crossing* process is a slow process, thus phosphorescence lifetimes are in the microsecond to second time range. Finally, delayed fluorescence (strongly temperature dependent) is the emissive relaxation process from the excited singlet state S_1 back to the ground state S_0 after ISC to T_1 followed by a reversed ISC back to S_1 took place. Thereby the emission spectrum is like a normal fluorescence spectrum because of the S_1-S_0 relaxation but the lifetimes are much longer due to two occurring ISC processes.

For description of luminescence properties some terms are essential to know. First, the *molar absorption coefficient,* defined as absorption divided by the absorption pathlength and the amount concentration. Second, *quantum yield* which defines how efficient a molecule emits light upon excitation, which describes competing non-radiative de-excitation processes and light emitting de-excitation processes. To combine these two phenomena the term *luminescence brightness* is defined, as the mathematical product of *molar absorption coefficient* and *quantum yield*. *Luminescence lifetime*, is the average time, a molecule stays in its excited state before emitting a photon. *Stokes' shift*, describes the wavelength/energy difference between the maxima of the absorption and emission spectra due to the loss of energy required for non-radiative de-excitation processes. In general large *Stokes' shifts* are preferred because they allow excitation at the absorption maximum and collection of almost the whole luminescence. Certain interactions of an excited luminophore and a quencher molecule in the close environment such as electron transfer, proton transfer, energy transfer, complex formation or collisions with heavy atoms are also possible and can change any of the above mentioned properties, which is called *quenching*. If *quenching* processes are observed and correlated to specific species this can be used as analytical information in luminescent sensors. Apart from quenching there are other cases of non-radiative energy transfer processes such as Förster Resonance Energy Transfer (FRET) providing analytical information. Herein, energy can be transferred from an excited donor molecule to another acceptor molecule in its ground state under specific circumstances.[1–3]

2.1.1 Fluorescent Dyes

Going back in history, already our ancestors were fascinated of luminescence phenomena provided by nature such as glowing fireflies, northern lights and bioluminescent bacteria or algae. As mentioned above, light emission originates from competitive deactivation processes from the lowest excited state back to the ground state of a molecule, in terms of *fluorescence* – direct relaxation from the excited singlet state to the ground state. On the one hand, there are natural fluorophores and on the other hand so called fluorescent indicator dyes. The spectral properties of these dyes are sensitive to the presence of a certain substance.[2,4] Herein, a brief overview of commonly used fluorescent dyes, relevant for this thesis will be given in this section. Furthermore, detailed information about particular classes of dyes and specific indicators and their properties utilized for manufacturing of state-of-the-art pH as well as state-of-the-art carbon dioxide sensors will be provided in the next sections.

Xanthene dyes – especially in terms of pH sensitive indicator dyes, xanthene dyes are the most commonly used group in optical pH sensors, with representatives such as fluorescein derivatives, seminaphthofluoresceins (SNAFL) or seminaphtharhodafluors (SNARF). Fluoresceins possess efficient absorption at around 490 nm, whereas π-extended derivatives exhibit bathochromically shifted absorption and emission bands. Xanthene dyes have gained immense popularity in biological and medical research.[5,6]

Rhodamine dyes – in general, rhodamine fluorophores also belong to the large class of xanthene dyes. Due to high molar absorption coefficients, high fluorescence quantum yields and excellent photostability rhodamine dyes are widely used for laser dyes, fluorescence standards but they are also applied in optical sensor technologies or as molecular switches.[7,8]

HPTS and derivatives – displaying an important class of pH sensitive indicators utilized for fabrication of pH and carbon dioxide.[9,10] The most popular representative 8-Hydroxypyrene-1,3,6-trisulfonate is a triple charged indicator, which is highly soluble in water with a pK_a value in the physiological relevant range. It is commonly applied in commercially available pH sensors. HPTS is usually excitable in the blue region and exhibits fluorescence emission in the green part of the electromagnetic spectrum.[11]

Cyanine dyes – are a highly versatile class of fluorophores possessing efficient long-wavelength absorption and emission bands. Thus, they are interesting candidates for designing new pH sensitive dyes for ratiometric two-wavelength measurements and imaging techniques.[12] Moreover, the dye platform including cyanine, hemicyanine and squaraine feature extraordinary biocompatibility and low toxicity to living cells. On the other hand, cyanine dyes are also known for their poor photolability, limiting their use in optical sensors, especially for long-term applications.[13,14]

Rylene dyes – are a class of polycyclic aromatic molecules built up by naphthalene building blocks. The smallest representatives are naphthalene derivatives followed by perylenes, terrylene up to even higher homologues. Dyes of this group may show high molar absorption coefficients, quantum yields close to unity, high photostability and a high versatility to chemical modifications. Thus, this class of dyes has been applied in many fields of academic and industrial research.[15,16] Due to the relevance for this thesis rylene dyes will be discussed in more detail in the next sections.

Boron-dipyrromethene dyes (BODIPY) – this class of dyes gained spectacular popularity as useful fluorescent tools for various applications occasionally because of relatively high molar absorption coefficients (>50000 $M^{-1} \cdot cm^{-1}$), high fluorescence quantum yields and good photostability.[17,18] Especially for the use as indicator dye BODIPYs are advantageous because practically any chelator at almost any position of the BODIPY core can be attached to design modularly customized indicators with required spectroscopic and analyte binding properties. Again, boron-dipyrromethenes will be described in more detail in the next sections.

2.2 Rylene Dyes

Rylene dyes belonging to the class of polycyclic aromatic compounds built up by naphthalene blocks attached to each other in *peri*-position. The first perylene was published in the early 20th century.[19] Higher non-functionalized homologues – terrylene and quaterrylene – were developed in the 1950s by *Clar et al.*[20,21] Since the solubility in organic solvents, as well as the applicability of such non-functionalized molecules is limited, introduction of functional groups was the aim of further work. First quaterrylene- and terrylene bisimide dyes were published by the group of *Müllen* in the 1990s.[22,23] The structures of the homologues can be split up in *bay/core*-position, where the naphthalene building blocks are attached to each other in *peri*-position and *imide*-position (**Figure 2-2**). *Avlasevich et al.* summarized synthetic routes for an additional enlargement of the π-system of rylene core by Suzuki coupling and a cycloaddition of benzene, yielding in highly photostable, bright fluorescent dyes.[24,25]

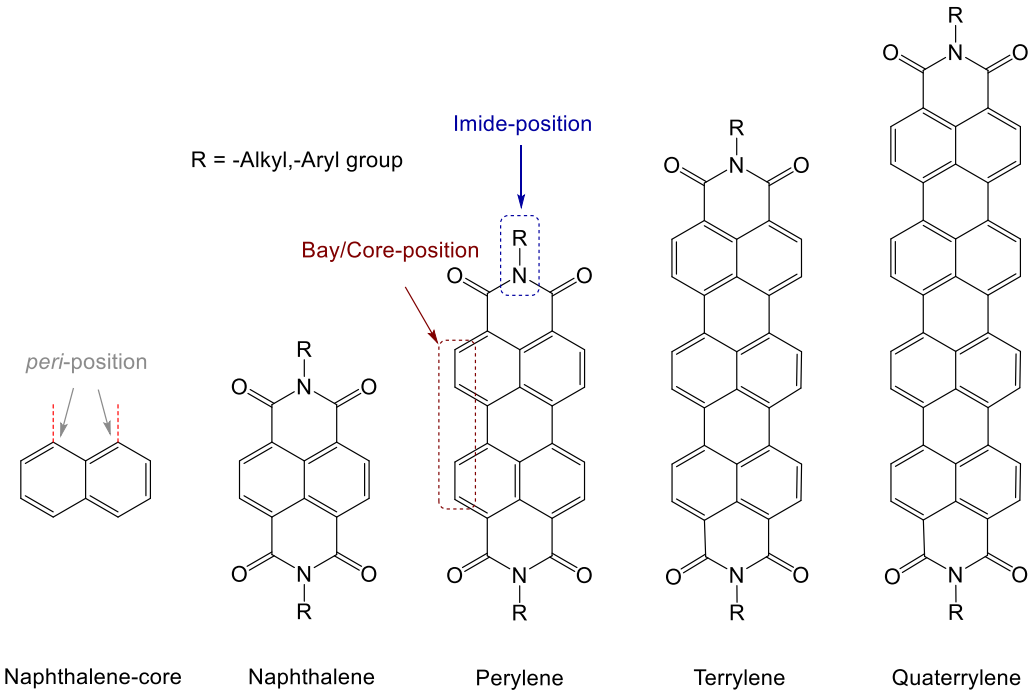

Figure 2-2 Chemical structures of naphthalene building block and rylene bisimide dyes.

Moreover, functionalized rylene derivatives have been successfully implemented in several challenging applications such as optoelectronics[26,27] and photovoltaic devices[28], light emitting diodes[29] and energy transfer cascades[30] to mention only a few. Furthermore, there have been recent scientific advances focusing on the design of new chromophores and their impact on optical properties, self-organization and molecular interactions well summarized in a review.[16]

2.2.1 Perylene Bisimide Dyes

Perylene tetracarboxylic acid bisimide or perylene diimide (PBI or PDI) dyes and pigments have received substantial attention in academic and industrial research over the last decades. PBI dyes are the smallest π-extended analogues of naphthalene bisimides. Indeed, core-unsubstituted perylenes absorb efficiently in the green to yellow part of the spectrum and emit green-yellowish light with high QYs close to unity. However, substitution with electron-donating groups in bay-position cause distinct bathochromic shift of the spectra. Generally, the dyes are known for their high molar absorption coefficients and quantum yields close to unity. Furthermore, excellent chemical as well as outstanding photochemical stability render them interesting for numerous fields of applications.[31]

Apart from high grade industrial applications as pigments since the 1950s, more recent applications of perylene bisimides have taken place in the development of electronic materials, functional supramolecular architectures[15], single molecule fluorescence techniques and fluorescent labelling.[25,32] They are used as high performance materials in n-type semiconductors due to the high electron affinity of rylene bisimide dyes.[15,33] Furthermore, PBIs have been commonly investigated for bulk-heterojunction organic solar cells based on non-fullerene acceptors due to high absorption ability, high electron mobility and photo- as well as temperature stability.[16,34,35]

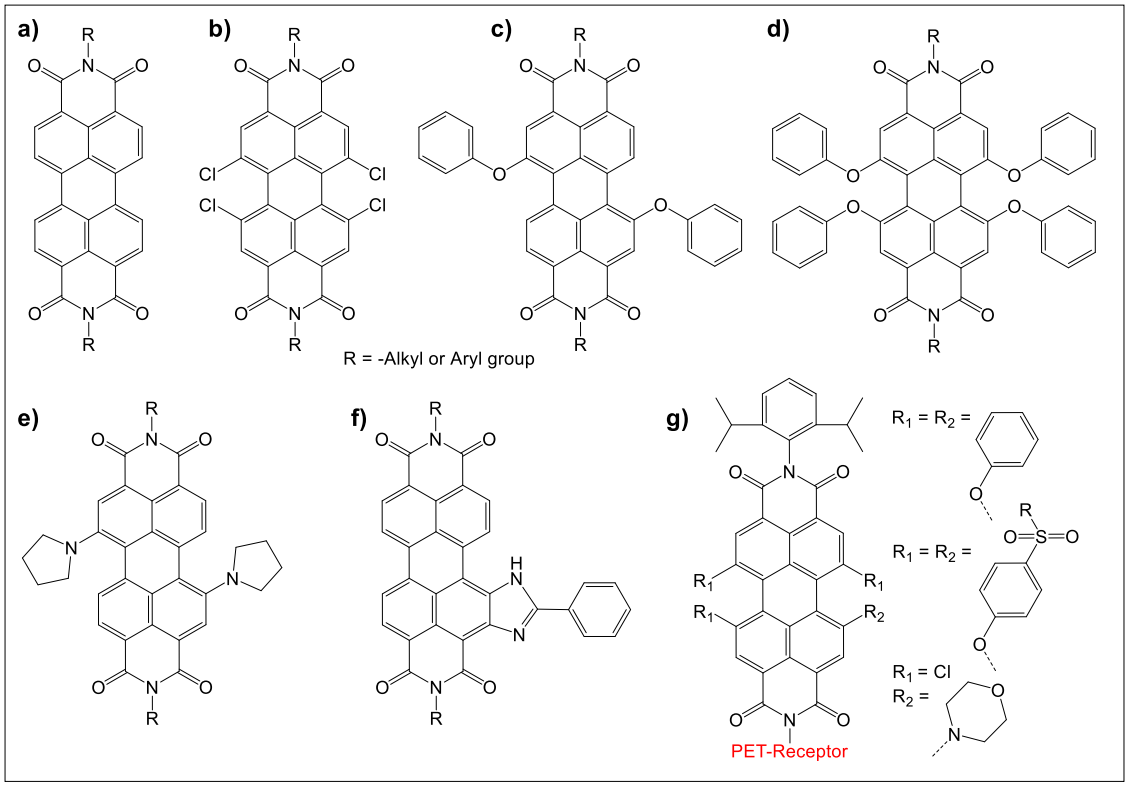

Figure 2-3 Chemical structures of perylene bisimide dyes. a) classical perylene bisimide; b-e) perylene bisimides with bay-substitution; f) perylene bisimide with 2-phenyl-imidazol substitution in bay-position; g) red and far red emitting, pH sensitive perylene bisimide dyes with bay-substitution, bearing a PET-receptor in imide-position.

However, the excellent photophysical properties and the versatility of chemical modifications make perylene bisimide dyes highly attractive as indicators for optical sensors and (bio)labels.[36–42] Unfortunately, perylene dyes which are strongly emissive in the red part of the spectrum are seldom. Particularly, introduction of phenoxy-substituents[43,44] or amino-groups[36,42,45] in bay-position shifts fluorescence emission to the red to far red-part of the electromagnetic spectrum. With attachment of two or four phenoxy groups (**Figure 2-3c, d**) in bay-region the absorption maxima are bathochromically shifted compared to the unsubstituted dye (**Figure 2-3a**) by ~20 nm and 50nm for the tetraphenoxy-substituted dye, respectively. These fluorophores feature high quantum yields, small solvent effects on the optical properties and high photostability. Moreover, introduction of amino-moieties such as two electron-donating pyrrolidino groups (**Figure 2-3e**) affect the spectral properties in a stronger way, absorption maxima are shifted 160 nm bathochromically to 686 nm and emission is transferred to the far red region. However, this shifts caused by a charge transfer are accompanied by strong decrease in fluorescence brightness.[23,24,42,45,46] On the other hand, introduction of electron-withdrawing substituents in bay-position such as chlorine (**Figure 2-3b**) or bromine only cause small spectral changes.[47,48] Since it is known that substitution in imide-position has a negligible influence on the absorption and emission properties, this position is well-suited for introducing pH sensitivity or functionalization to increase solubility and prevent aggregation.

A class of laterally extended 2-phenyl-imidazole-substituted perylenes reported by *Langhals et al.* represent a notable exception (**Figure 2-3f**).[49] Extension of the perylene core, causes a significant bathochromic shift into the deep red spectral region and the dyes exhibit high fluorescent brightness. The versatility of chemical modification and optical properties of this promising class of dyes represented an excellent platform for designing novel pH sensitive fluorescent probes for the work performed in context with ultra-bright red-emitting photostable perylene bisimide dyes described in **Chapter 3** (p.39).

Aigner et al. reported several red emitting PBI indicators with above mentioned substituents in bay-position (**Figure 2-3g**) to tune the spectral properties. The dyes have been rendered pH sensitive by introduction of photoinduced electron transfer (PET) receptors in imide-position.[36,41,50] Furthermore, effective tuning of the dynamic pH range can be achieved by selection of an appropriate PET group (halogenated phenoxide groups or amines). Tetraphenoxy based PBIs show emission in the red, feature high fluorescence brightness and excellent photostability. For further usage in optical pH sensors the dyes were embedded hydrogel matrices. However, aggregation of dyes was observed, that can be overcome with covalent coupling to the host polymer. It is also shown that several PBI probes were successfully applied for sensing intracellular pH by fluorescence lifetime imaging microscopy (FLIM).[50] More detailed description about optical pH sensors will be given in **Section 2.5.1** (p. 22).

Accessibility of larger bathochromic shifts to the NIR-region can be easier achieved by enlarging the π-system of the core with additional naphthalene building blocks to yield higher homologues such as terrylene diimide dyes, described in detail in the next section.

2.2.2 Terrylene Bisimide Dyes

Terrylene bisimide or terrylene diimide (TBI or TDI) dyes, are a relatively young member in the class of rylene dyes. The first red emitting TDI was synthesized by *Holtrup et al.* in 1997, driven by the motivation to close the gap between yellow emissive perylene bisimides and the NIR emitting quaterrylene bisimides.[23] As mention above, both terrylenes as well as perylenes are based on a conjugated framework of naphthalene units, summarized in the class of rylene dyes. In contrast to perylenes, terrylene dyes contain an additional naphthalene building block, without further substitution, these dyes are noticeable more hydrophobic and prone to aggregate. In general, this class of dyes feature high luminescence brightness, extraordinary good photostability, and bathochromically shifted absorption/emission bands (about 100 nm per additional naphthalene unit compared to classical perylene bisimide) in the far red to NIR region of the spectrum and additionally versatility in respect to chemical modification.[16,25,51] Nevertheless, due to difficult and time-consuming synthesis procedures TDIs have only be investigated for academic research but not gained industrial attention yet.[16,52–54] Advantages of long-wavelength fluorophores and their applicability in optical sensors will be given in **Section 2.5.1** (p.22).

Terrylene dyes are also commonly used as central building blocks of dendrimers as model compounds for biomolecules or as light-harvesting antenna complexes.[55] In such complexes short wavelength absorbing chromophores (e.g. perylenes) are located at the outside and the energy is transported to long-wavelength-absorbing acceptor chromophores such as terrylene bisimides located in the center. Hence, bichromophoric systems enable very efficiently energy transport over large distances in the scale of molecules.[56,57] To achieve such synthetic approaches, functionalization in bay-position, is of high importance.[58]

The synthetic pathways shown in **Figure 2-4** were investigated by the group of Müllen, to overcome drawbacks of synthetic methods published previously.[32,51,58] Synthesis of terrylene imides suffer from problems such as (i) use of toxic stannyl compounds; (ii) long reaction times; (iii) use of molten KOH for the final cyclodehydrogenation or (iv) unavailability of functional groups for further reactions.

The first synthetic route is a straightforward one-pot procedure which is reminiscent of direct coupling reactions of 1,8-naphthalendicarboximides affording the corresponding perylene bisimide dyes.[59] The obvious synthesis of symmetric and asymmetric terrylene bisimide 3 is a kind of base-promoted heterocoupling reaction of naphthalendicarboximid 2 and perylenedicarboximide 1 using 1,5-diazabicyclo[4.3.0]non-5-ene (DBN) and *t*-BuONa in diglyme. In principle, under this conditions three combinations – two homocouplings and one heterocoupling are competing, to force the formation of TDI 3 fourfold excess of 2 are required. This kind of reaction is also the simplest way for monofunctionalization of terrylene bisimides. The synthesis of monocarboxy-functionalized TDI 10 can be carried out under the same conditions only using functionalized naphthaldicarboximide 9 instead of 2. However, introduction of halogen-functionalized

naphthalcarboximide is not favorable with this method, due to very low yields, since the bromo substituted imide does not survive the strong basic conditions.

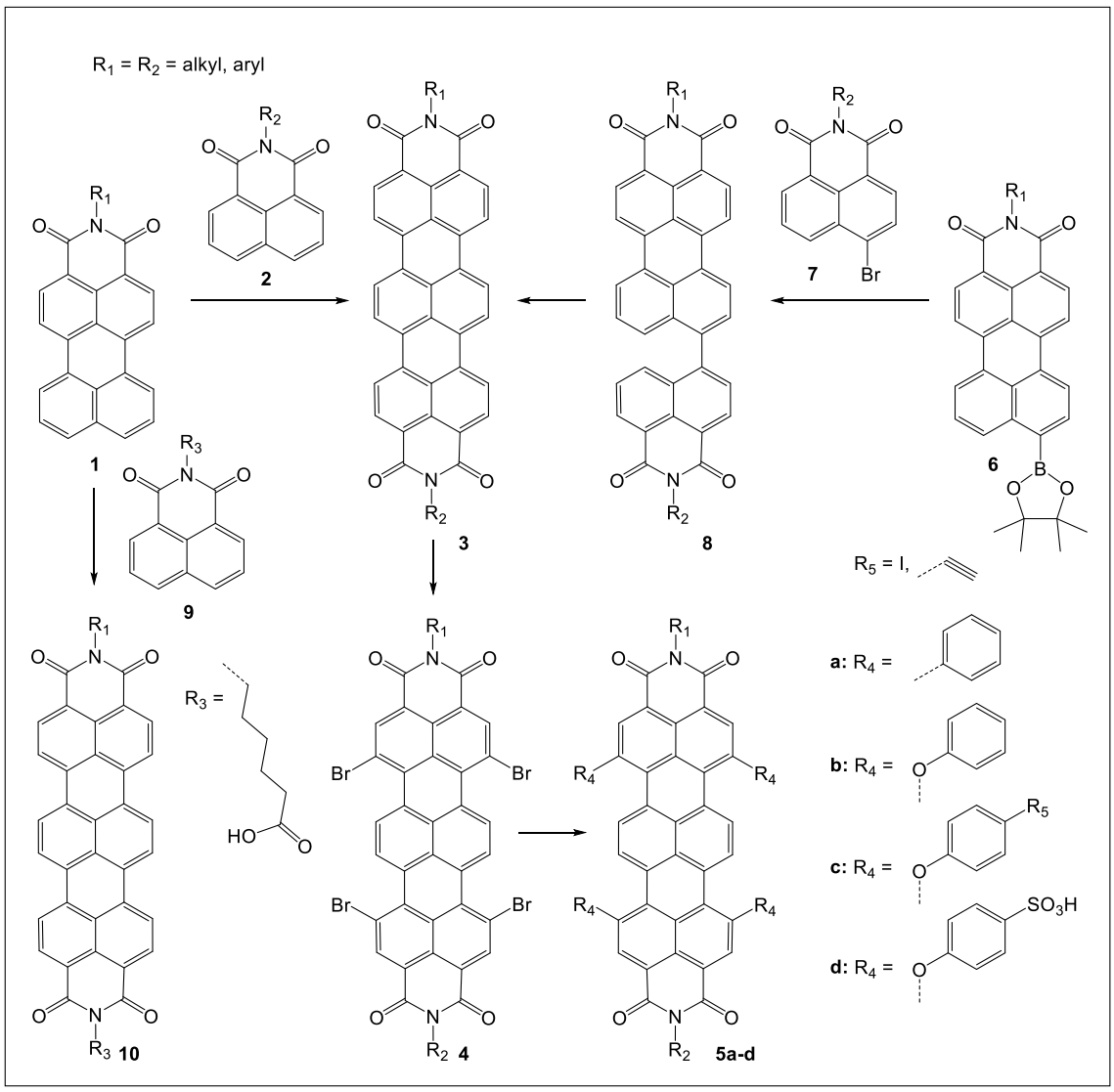

Figure 2-4 Commonly used strategies for synthesis of a symmetric or asymmetric terrylene bisimide **3**. Strategy for functionalization in imide-position starting from **1** and using an already functionalized naphthalimide **9**. Bromination in bay-position of **3** can be achieved in one step and is crucial for further functionalization to yield tetra-substituted terrylene bisimide dyes **5a-d**.

The second route includes a Pd-catalyzed Suzuki cross-coupling[60,61] of boronic ester 6 with 4-bromonaphthalendicarboximide 7 to give the not fully conjugated intermediate 8. This reaction is followed by a highly effective cyclization via cyclodehydrogenation using K_2CO_3 as base and ethanolamine under mild conditions to yield TDI 3.[51]

The next step, introduction of bromine in bay-region is of high importance for further functionalization of the core and was reported by *Weil et al.*[58] Bromination of TDI 3 is carried out in chloroform with elemental bromine under exclusion of light to give the tetrabrominated TDI 4. Due to bromination, absorption bands are more or less unaffected but the most intense emission

band is bathochromically shifted and solubility is significantly increased. Introduction of substituents in bay-region reduces planarity of the fluorophoric system and results in a significant increase of solubility in organic solvents. Furthermore, extension of the chromophoric core with aromatic substituents causes a noticeable bathochromic shift of absorption and emission bands. For such large conjugated systems like terrylenes increase of solubility is an important issue. Introduction of bulky 2,6-diisopropyl groups in imide-position is one option, on the other hand a commonly used strategy is displayed by substitution with phenoxy groups in bay-region. Examples of tetraphenoxy-TDIs are shown in **Figure 2-4** (5b-d). The simplest TDI bearing four phenoxy substituents 5b exhibit good solubility in commonly used organic solvents but is only slightly soluble in polar solvents and insoluble in water. For specific applications like biolabeling or fluorescence lifetime imaging (FLIM) techniques water solubility is required, which can be enabled by introduction of negatively charged sulfonyl groups like in 5d. That could be completely accomplished by treatment of the tetraphenoxy-TDI 5b with sulfuric acid to yield water soluble TDI 5d.[32,51] Furthermore, bay-substitution with functionalized phenols can serve a multifunctional core molecule applicable for formation of dendric multichromophores.[58] Concerning the spectral properties symmetric tetraphenyl-TDI 5a and tetraphenoxy-TDI 5b exhibit bathochromically shifted absorption maxima at 702 nm and 671 nm in chloroform, respectively compared to TDI 3 (λ_{Abs} 651 nm).[51,54]

Recently, Uersfeld et al. reported a simplified method to build up terrylene dyes from naphthalene and perylene units *via* efficient Suzuki/C-H-arylation coupling cascade. The presented synthetical development also allows purification by precipitation and crystallization and accessibility of terrylene monoimides, which may facilitate the synthesis of new dyes.[62]

Due to the limited number of organic compounds exhibiting intense fluorescence in the red to far red region of the electromagnetic spectrum and the pronounced good photophysical stability as well as investigation of challenging reported synthetic methods the class of terrylene represents an interesting platform for design of new dyes described in **Chapter 5** (p. 121).

2.3 BODIPY Dyes

The first set of 4,4-difluoro-4-bora-3a,4a-diaza-s-indacene fluorescent dyes (further on abbreviated BODIPY, difluoroboron dipyrromethene) was reported in 1968 by Treibs and Kreuzer[63] and turned out to be one of the most promising, furnished with highest potential and gained extraordinary popularity among the great number of fluorescent dyes.[17,64,65] The conventional BODIPY structure is shown in **Figure 2-5**. The number of research paper increased tremendously since the mid-1990s due to the recognition of broad applicability of this dye class in biological labeling, in electroluminescent devices or as fluorophores. BODIPY dyes provide many outstanding features which are responsible for their ever-growing success:

- Robustness against light and chemicals
- Relatively high absorption coefficients ε and fluorescence quantum yields Φ
- Negligible triplet-state formation
- Narrow emission bandwidths with high peak intensities
- Good solubility
- Resistance towards self-aggregation in solution
- Excitation/emission wavelength in the visible spectral region
- Fluorescence lifetimes τ in the nanosecond range

Furthermore, fine-tuning of their spectral and photophysical properties can be done by chemical modification at the appropriate positions of the BODIPY core. The versatility of synthetic pathways of BODIPYs enables a modular design of new dyes in respect to the desired structural, spectroscopic and photophysical characteristics. There are three widely used synthetic pathways for synthesis of BODIPY dyes.

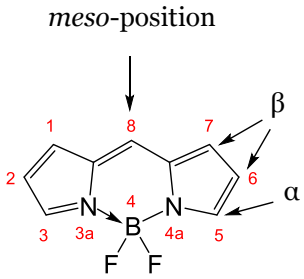

Figure 2-5 Chemical structure of 4,4-difluoro-4-bora-3a,4a-diaza-s-indacene (BODIPY).

The first route starts with an acid-catalyzed condensation of pyrrole 1 with aldehydes 2 to yield rather light- air- and acid-sensitive dipyrromethanes 3. Because of the instability of the compound an immediate oxidation with DDQ (2,3-dichloro-5,6-dicyano-*p*-benzoquinone) or *p*-chloranil (2,3,5,6-tetrachloro-*p*-benzoquinone) are recommended followed by basic complexation with boron trifluoride etherate to yield the boron difluoride complex 5 (**Figure 2-6**). Due to the

chemical robustness of the BODIPY core post-synthetic modifications on the *meso*-aryl substituent are possible, without remarkable decomposition of the dye.

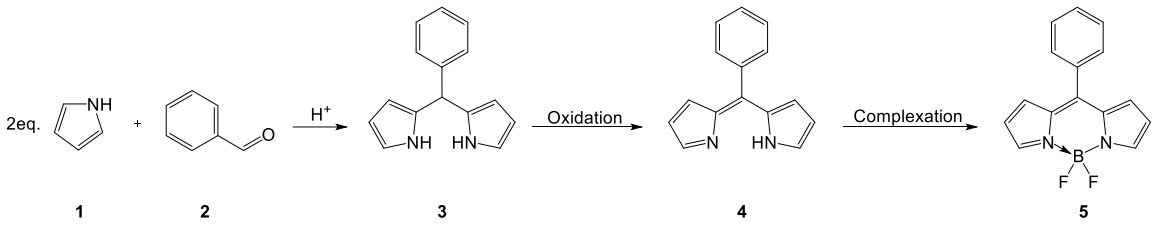

Figure 2-6 Synthesis route starting with condensation of a pyrrole with an aromatic aldehyde, subsequent oxidation and following complexation to BF_2-chelated dipyrromethenes (BODIPY) **5**.

In the second route to BODIPY condensation of a pyrrole 1 is used, this time with an acylium equivalent 6 (an acid chloride, an acid anhydride or an orthoester) to yield the acylpyrrole intermediate 7, which can react with an excess of pyrrole 8 to a dipyrrinium salt 9. Again, complexation with excess of a base and boron trifluoride etherate give the BODIPY product (**Figure 2-7**). An advantage of this method is the synthesis of asymmetric dyes because the isolated acylpyrrole 7 can be condensed with a second pyrrole moiety 8 to yield an asymmetric dipyrrinium salt 9.

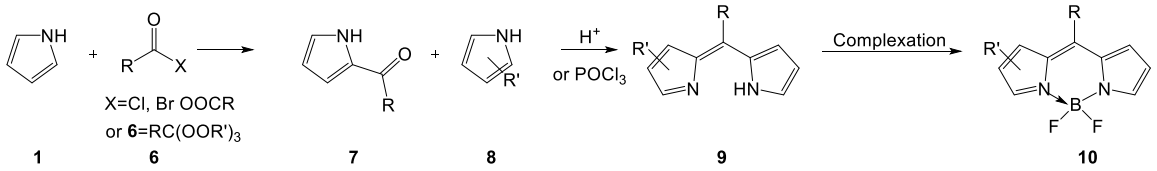

Figure 2-7 Synthesis of BODIPY through acylation of a pyrrole, condensation and final complexation with BF_3EtO_2.

The third route includes a one-pot condensation of 2 equivalents of pyrrole-2-carbaldehyde 11 using phosphorus oxychloride and further on complexation with BF_3EtO_2. For this procedure only little purification is required and the residual BODIPY dye is obtained in exceptionally high yields (**Figure 2-8**). Nevertheless, this route only yield in *meso*-unsubstituted BODIPY dyes.

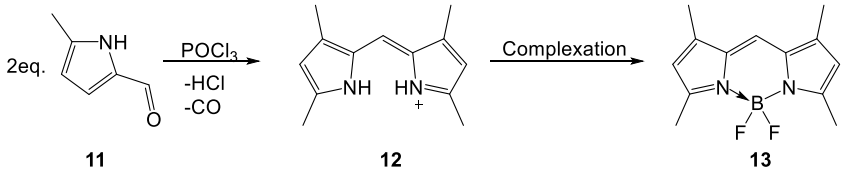

Figure 2-8 One-pot condensation-decarbonylation to yield dipyrrins, followed by complexation to BODIPY **13**.

Apart from the conventional BODIPY structure (**Figure 2-5**) numerous modifications at the BODIPY core have been reported, especially in order to shift both absorption and emission bands bathochromically into the red and far-red part of the electromagnetic spectrum.[66] Advantages of this bathochromic shift making the dyes even more attractive as fluorescent probes for sensing and (bio)imaging.[64,67–69] Summarizing, there are mainly two functionalization strategies how to accomplish the task of red shifting the spectral properties (i) extension of the conjugated system *via* substitution in α- or β-position of the core and (ii) synthesis of aza-BODIPY dyes (replacement of the *meso*-carbon by an aza-nitrogen atom). Examples for modifications are shown in **Figure 2-9**.

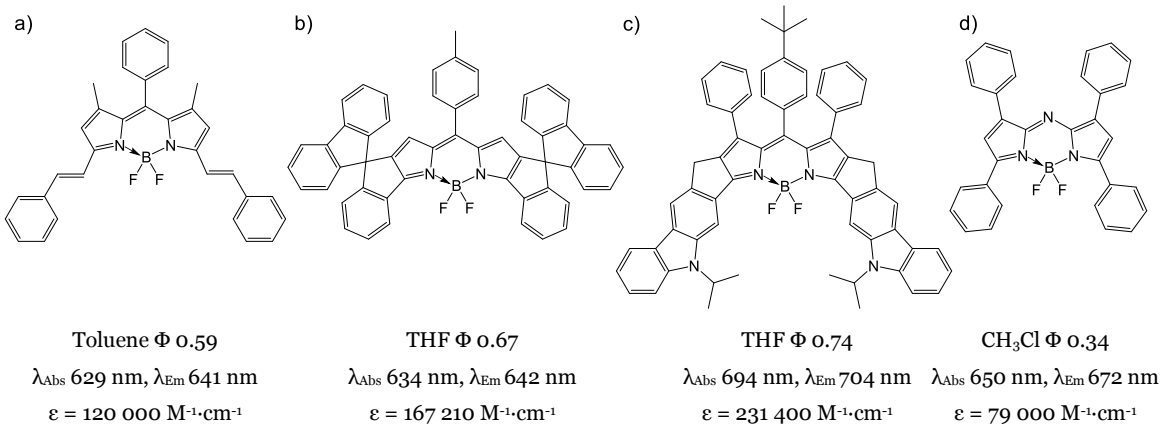

Figure 2-9 Chemical structures of modified BODIPY structures and photophysical properties. a-c) BODIPYs with extended conjugated system by substitution in α - or β -position; d) aza-BODIPY.

Introduction of two styryl substituents at the 3,5'-position of the BODIPY core (**Figure 2-9a**) results in a red shift of about 130 nm relatively to a conventional BODIPY structure as reported by *Rurack et al.*[70] Furthermore, substitution in *para*-position of the phenyl rings of the styryl substitution shifts the emission bands to the NIR region.[71] *Kowada et al.* presented a π-extended, rigid BODIPY (**Figure 2-9b**) structure containing spirofluorene moieties which also show a significant bathochromic shift of the absorption and emission spectra, with maintained high quantum yield.[72,73] In a more recent work *Rappitsch et al.* demonstrated a set of BODIPYs bearing π-extended pyrroles with a carbazol motif. The dyes possess bathochromically shifted sharp absorption and emission bands, high molar absorption coefficients and high quantum yields (**Figure 2-9c**).[74] A highly efficient strategy to shift the spectral bands to the red/NIR region is the synthesis of an aza-BODIPY, in such a structure the *meso*-carbon is substituted by an electronegative nitrogen atom. *Killoran et al.* reported a bathochromic shift of approximately 80 nm of the Tetra-aryl aza-BODIPY (**Figure 2-9d**) to the comparable tetra substituted BODIPY analogue.[75] Furthermore, the bathochromic shift can be enhanced by introduction of electron-donating groups such as -OMe and -NMe_2 in *para*-position of the phenyl substituents at the 3,5-positions of the core.[76]

Due to the increasing interest in BODIPY dyes a few other modification strategies of the core were investigated and they can also be explored for design of new fluorescence indicators. Introduction

of analyte sensitive groups (e.g. amino moieties for pH sensitivity or crown-ethers for cation sensitivity) is mainly based on two synthetic routes (**Figure 2-10**). On the one hand, direct condensation of a functionalized aromatic aldehyde with a pyrrole yield a BODIPY with phenyl substitution in *meso*-position of the core, acting as PET-functionality (Pathway 1).[77] On the other hand, taking advantage of the acidity of 3,5-methyl groups and enable the condensation of the fluorophore with a functionalized aromatic aldehyde in a Knoevenagel-reaction type to obtain a styryl-substituted BODIPY. This route yields an analyte sensitive BODIPY, acting as ICT probe (Pathway 2).[71] Commonly used examples for pH sensitive groups introduced to BODIPY chromophores are dimethylaniline substituents, applied for acidic pH ranges or phenol-groups for alkaline region (pH > 9), respectively.[71,77–79]

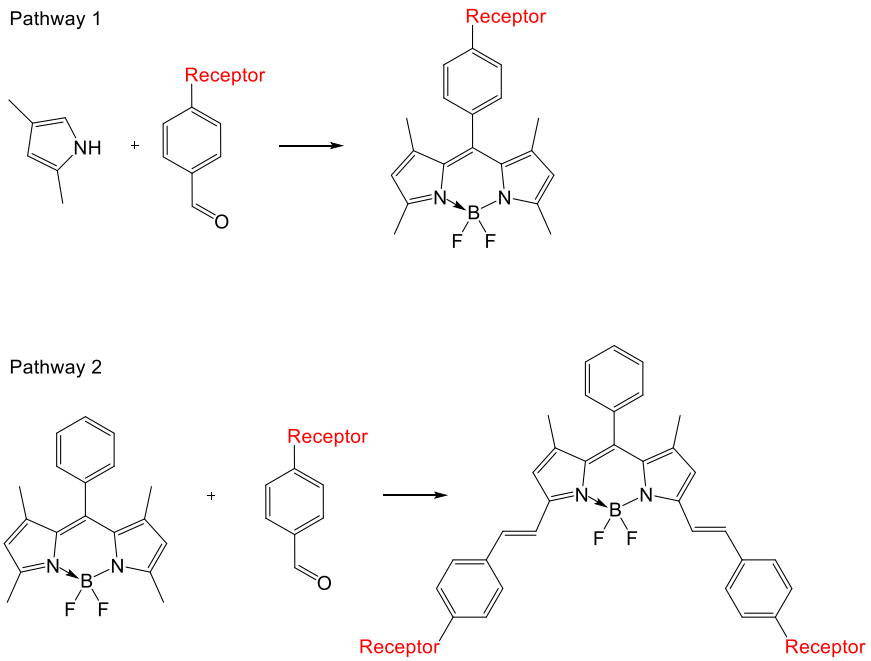

Figure 2-10 Routes for introduction of analyte sensitive groups (receptor units) at the BODIPY core.

BODIPYs and their beneficial properties are excellent fluorescent building blocks for design of novel indicators. Outstanding features concerning high chemical and photochemical stability, high brightness (high ε and Φ) paved the way to the popularity of BODIPYs. Moreover, practically any chelator at almost any position of the BODIPY core can be attached to design modularly customized indicators with required spectroscopic and analyte binding properties.

This immense versatility of modifications of BODIPY indicators and the concomitant tuning of their spectral properties were the driving forces for the work performed in context with green to red emitting BODIPY dyes described in **Chapter 4**(p. 73).

2.4 Chemical Sensors

Analyse of our environment in respect of presence of substances and their quantities is an essential part of everyday life. In the past, traditional analytical analysis has to be done in well-equipped laboratories performed by qualified personnel and included prior time intensive sample collection and preparation. However, for a long time there was a trend towards centralized high-tech analytical laboratories but decades ago the tendency changed – with invention of the personal computer. In recent years, the interest of automation in chemical analysis and continuous monitoring of various analytes in industrial processes, environmental monitoring as well as in academic research has been growing – the initial expansion in the use of chemical sensors rapidly developed.

A chemical sensor is an analytical device responding continuously and reversibly to the presence of a specific analyte, transducing the chemical information into a measureable electrical signal.

A widely used appropriate description is given by the Cambridge definition of a chemical sensor: "*Chemical sensors are miniaturized devices that can deliver real time and on-line information on the presence of specific compounds or ions in even complex samples.*"[80]

Generally, the composition of a sensor can be separated in 3 main parts: a receptor unit, a transducing platform and signal processing. The sensing starts with interaction of the receptor with a specific analyte; followed by transduction of the obtained chemical information into a measureable electrical or optical signal and the final step – processing of this signal. For an ideal sensor there are some required criteria which should be fulfilled:

- A fast responding, small and low-cost device which is easy to use
- Portable device enabling field measurements with little sample preparation
- Selectivity and sensitivity towards a specific analyte
- Transformation of chemical information into an electrical signal
- Long-term stability during measurement and storage

Recent developments in the field of sensors extended the range of measurement principles applied in sensor technology which are usually classified by the utilized transduction method. In this thesis, the focus will be on optical chemical sensors, wherein the transduction is most commonly based on absorbance, luminescence or refractive index.[81]

2.5 Optical Chemical Sensors

In optical sensors, similar to most chemical sensors, the analyte recognition is done by the receptor, whereas the generation of a measurable signal is part of the transducer. In an optical sensor the transduction is based on optical properties of the analyte itself or an analyte-sensitive material (e.g. indicator dye). This change of the optical properties can be based on reflectance, refractive index, light scattering, absorbance or luminescence, which is described in detail in several reviews.[5,12,82–84]

Optical sensors have to fulfill different requirements belonging to the field of use and the expected measurement conditions, but some fundamental parameters to characterize the performance of an optical sensor are:[81]

- *Selectivity:* A signal of the sensor should ideally only be generated in the presence of the analyte of interest and should not be interfered by other species with analyte similar properties. Generally, this is hardly dependent on the receptor.
- *Sensitivity,* meaning the increase of the signal with the concomitant increase of the analyte concentration. Furthermore, other essential parameters such as *dynamic range*, *detection limits* and *resolution* are effected by the sensitivity characteristics.
- *Response time* of a sensor is usually given by a value such as t_{90} or t_{95}, which describes the required time to achieve 90% or 95% of the signal change.
- *Stability* of the measured signal is of high importance for the sensor performance especially for long-term measurements. On the other hand, stability of the sensor should be given during long-term storage (long shelf life). An occurring signal change without change of the analyte concentration is called *drift* of a sensor.
- *Robustness:* Sensor materials are sometimes exposed to harsh conditions such as high light intensities, extreme temperatures, chemical or mechanical stress, and ideal sensor should withstand them.

In comparison to classical, well established, and for the most part advantageous routine techniques (e.g. electrochemical sensors) optical sensors exhibit some advantages considering the functionality without any need of a reference electrode. This make them easier to miniaturize and robust against electromagnetic influences. On the one hand, analyte-insensitive reference materials can be combined with the analyte-sensitive material e.g. in the same matrix or the same sensing layer. On the other hand, one can make use of self-referencing indicators, which are more robust due to the lower complexity of the sensor system. For this reasons, fabrication of optical chemical sensors in various formats spanning from nanoscale (e.g. nanoparticles) up to macroscale (e.g. planar sensor foils) is possible. Furthermore, the properties of light allow transmission of signal over long distances, which enables the local separation of sensing unit and read-out unit. Thus, read-out can be carried out contactless via optical windows, a beneficial way of sensing e.g. for sterile samples or food packaging applications.[82]

Generally, optical sensors can be divided in two categories, on the one hand direct sensors, which make use of intrinsic optical properties of an analyte itself, such as absorbance or luminescence. On the other hand there are so called reagent-mediated sensing systems, therefore optical properties of an analyte-sensitive indicator dye are utilized for monitoring of specific analyte concentration.

Herein, this thesis focuses on reagent-mediated sensors, particularly on absorption and fluorescence based pH-sensitive indicator dyes. Concerning absorption based sensors, changes in the absorption bands are observable. In the case of fluorescence indicator based sensors, presence of the analyte of interest (e.g. H^+) changes emission intensity, emission wavelength or lifetime of the indicator, which is used as source of analytical information. In general, fluorescent pH indicators offer higher sensitivity than absorption-based indicators.[4]

Due to occurring quenching processes via different indicator-analyte interactions one can distinguish between three most common groups of fluorescent pH indicators: (i) fluorophores undergoing photoinduced electron transfer (PET); (ii) those showing photoinduced proton transfer (PPT) and (iii) dyes exhibiting neither photoinduced electron transfer nor photoinduced proton transfer but significant changes of absorption and emission spectra upon deprotonation due to an intramolecular charge transfer process (ICT).[1]

Photoinduced Proton Transfer (PPT) – Fluorophores of this type show higher acidity (lower pK_a) in the excited state compared to the ground state. Therefore, the emitting form is the basic form because excitation of the acidic form is always followed by excited-state deprotonation. Hence, emission spectra are pH independent, in contrast to the excitation spectra, which make dyes of this group useful for ratiometric (two-wavelength) measurements. Commonly used dyes of this type are 8-h*ydroxypyrene-1,3,6-trisulfonat* (HPTS) and *7-hydroxycoumarins*.

Photoinduced Electron Transfer (PET) – The group with the greatest number of representatives is based on photoinduced electron transfer. In fact, this originates in the modular design, attaching a functional (PET) group such as phenols or amines to a pH insensitive dye. Such combination results in a redox process between PET group and excited fluorophore. For the more common reductive PET, the HOMO of the chromophore is located energetically lower than the HOMO of the deprotonated receptor, thus internal quenching by PET can occur upon excitation. Hitherto, the HOMO of the protonated receptor is located lower than the HOMO of the chromophore, no PET can be observed (**Figure 2-11**). Thus, increasing protonation yields higher fluorescence. Emission spectra show virtually an "on-off" character upon (de)protonation, whereas shapes of excitation and emission spectra are not strongly affected.

The quenching efficiency is affected by the combination of a strong electron-donating PET group and a strong electron-accepting chromophore, consequently not every chromophore can be quenched efficiently by every PET group.[36] Usually, the PET group and the chromophore are separated by a spacer resulting in the "turn-on/off" character, however partial conjugation of the PET group or electronic effects can yield a small spectral shift.

The high versatility of PET based indicator dyes make them interesting for pH sensors. The design of new indicators by combination of an intrinsically pH insensitive chromophores with apparently unlimited variety of PET-groups, enables on the one hand the adjustment of the spectral properties and on the other hand the tuning of the sensitivity independently. Commonly used representatives of this type are fluorescein, perylene and BODIPY dyes.

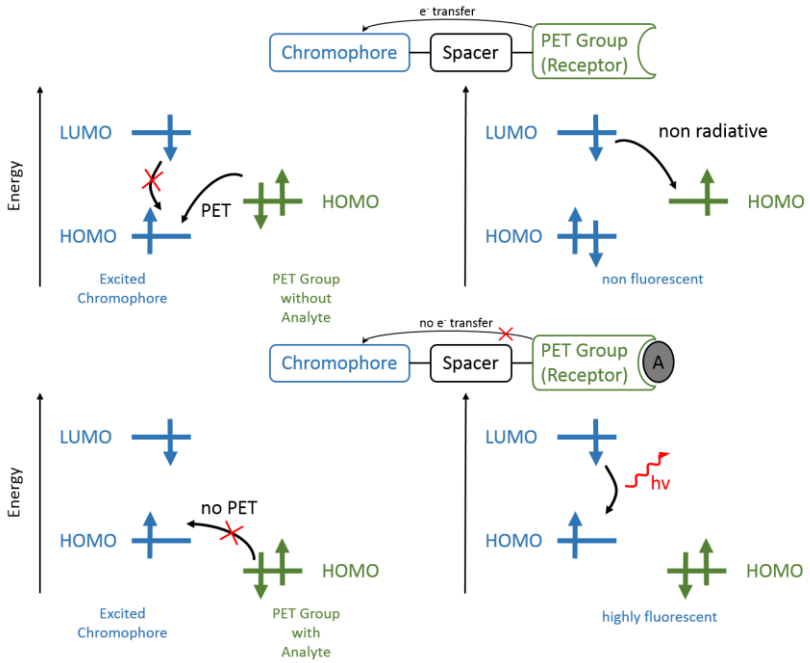

Figure 2-11 Schematic principle of the reductive photoinduced electron transfer and the inhibition of the effect due to a binding of an analyte (e.g. H^+) and a resulting change of the energy level of the molecule orbital of the PET group.

In this thesis the modular approach has been utilized: several pH sensitive chromophores were designed by varying their PET groups and the influence of the chromophore core itself was investigated. Furthermore the spectral properties of the indicators were adjusted to apply them in various referenced sensor materials (**Chapter 4**, p. 73).

Intramolecular Charge Transfer (ICT) – Fluorophores of this group show neither photoinduced proton transfer properties nor a "switch on-off" character such as PET dyes but significant changes of absorption and emission spectra upon deprotonation, caused by an intramolecular charge transfer. This effect originates from the direct attachment of the sensitive functional group at the conjugated system of the fluorophore and the resulting influence of the HOMO-LUMO levels of the latter. In such a case both emission and absorption spectra are affected in shape as spectral maxima. Increasing pH results in increase of signal intensity of absorption and emission bands of the acidic species by a concomitant decrease of signal intensity of the spectral bands of the basic form, which enables ratiometric dual wavelength measurements. Most important representatives are fluorescein and other xanthene dyes (e.g. SNAFL, SNARF), which are widely used for pH determination in physiological applications due to commercial availability.

In this thesis one chapter is dedicated to the design of pH sensitive dyes with functionalization directly at the conjugated system of the chromophore, which enables ratiometric sensing of pH (**Chapter 3**, p. 39).

2.5.1 State-of-the-Art Optical pH Sensors

Undoubtedly, pH determination is one of the most frequently performed analytical measurements in a multitude of sciences and industry, from biotechnology and medical diagnostic to environmental monitoring, to mention only a few. pH is determined to be a fundamental parameter in life. Therefore, precise, fast and robust measurement devices are requested, which are able to fulfill the distinct requirements of particular applications.

As a promising alternative to the most commonly used measurement devices such as (potentiometric) pH glass electrodes or ion-sensitive field effect transistors (ISFET) optical pH sensors (optodes) have been intensively investigated in the last four decades. Optical pH sensors are able to overcome various disadvantages of the above mentioned conventional methods such as challenging miniaturization, occurrence of electrical interferences or the limitation of single point measurements. Furthermore, optodes exhibit high sensitivity within their dynamic range, are suitable for continuous measurements and combined with optical fibers minimally invasive remote sensing can be provided. Optical sensors are also advantageous for other reasons such as their high mechanical flexibility, cost-effective production that in principle enables disposable character of the sensing materials, and the possibility of large-scale production. Besides this, there is a high potential for optical sensor applications in environmental, *in vivo* medical diagnostics and pharmaceutical fields. Particularly, planar optodes proved to be excellent tools for imaging of pH distribution combined with high resolution CCD cameras and nanoparticles are of high interest for extra- and intracellular imaging. However, optical pH sensors also have to overcome drawbacks, such as limited long-term stability due to photobleaching and leaching of the indicator dye or mentionable temperature dependency. Such limitations can be directly addressed through the suitable selection of indicator and matrix materials and adequate reference techniques.[5,6,85–87] Moreover, due to the pK_a value of the pH indicator the dynamic range of the sensor is limited to around $pK_a \pm 1.5$ pH units, thus mitigation of the limited dynamic range can be forced by fabrication of broad range sensors.[41,88,89]

In this section state-of-the-art sensor materials will be described. The main core of pH sensing materials is the pH sensitive dye, altering its optical properties due to changes of the surrounding pH, which is then used as source of analytical information.

As the indicator dye is the component ensuring pH response, the quantitatively main component is the matrix in which the dye is embedded. There are different ways of immobilization. On the one hand, physical entrapment is a relatively simple way. On the other hand, covalent coupling of the indicator to the matrix is the method of choice to prevent leaching of the dye. Though, this is usually a complex and time-consuming process and needs appropriate materials with functional groups for

binding. pH sensor matrices have to fulfill some requirements such as mechanical and chemical stability, they should feature an adequate water uptake and therefore should be proton permeable. Commonly used representatives are hydrophilic matrices such as polyurethane hydrogels or less hydrophilic ones like sol-gels. A disadvantage of optical pH sensors is their cross-sensitivity to ionic strength, for this reason the pH indicator should provide a low charge and should be embedded in an uncharged host matrix, to minimize this effect.[5]

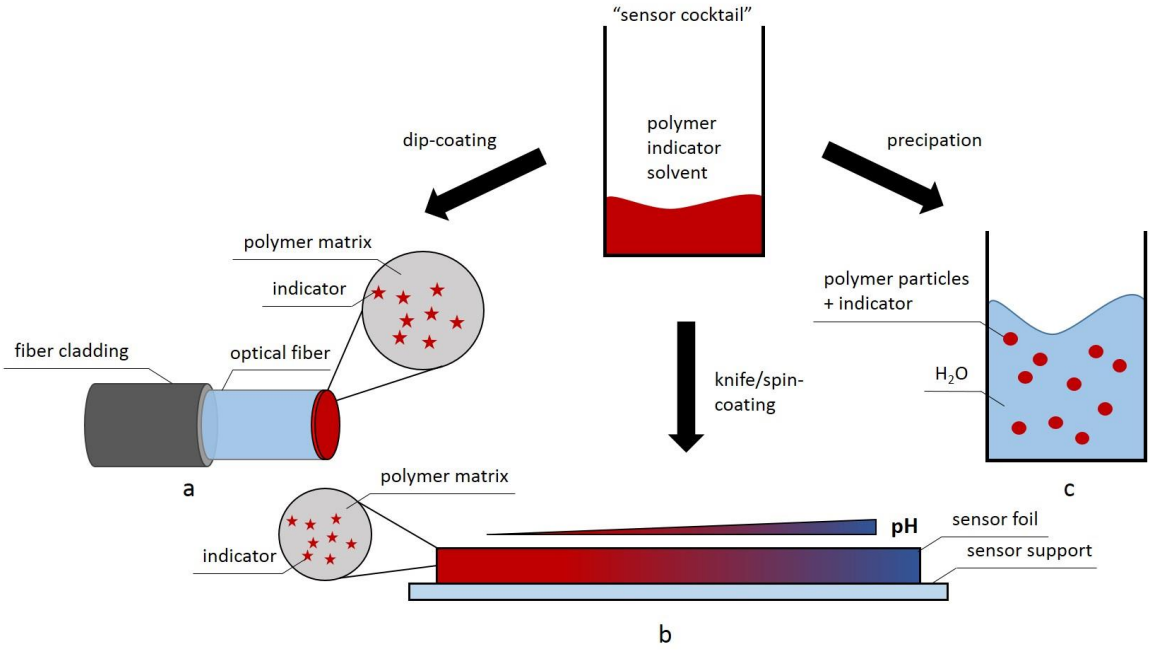

Figure 2-12 Scheme for the preparation of fluorescent pH sensing materials. a) dip-coated optical fiber; b) planar sensor foil; c) water dispersed nanoparticles with incorporated indicator.

A great number of colorimetric absorption based pH sensitive dyes has been reported in literature which is explained by the simplicity of the method and rather broad availability of colorimetric pH indicators.[90,91] However, these chemosensors can only be realized in a limited number of formats, and share the problem that the light from the light source is not only absorbed and reflected on the sensor surface but also on all other optical components (e.g. connections between filters and fibers) and this interferences are difficult to quantify. Measurements in scattering media, cells and tissues are virtually impossible. Therefore, fluorescent pH indicators received more attention in consideration of their higher sensitivity, compatibility with well-established referencing techniques such as dual lifetime referencing (DLR)[92] and the implementation in various formats. They can be utilized for manufacturing of a variety of sensor formats such as planar optodes, nanoparticle formulation, fiber-optic sensors or microsensors which enable high versatility of applications (**Figure 2-12**).[5,82,86]

All above mentioned parameters for an optical sensor (p. 19) can be extended by some crucial criteria for the design of fluorescence-based sensors ranging from pH sensitive dye properties itself

to the compatibility with optical components used for the sensing device. Generally, the list of parameters that need to be optimized collectively and simultaneously depends on the particular application:

- High brightness (defined as product of molar absorption coefficient and quantum yield) allowing utilization of lower dye concentrations in the sensor material
- High chemical and photochemical stability
- Easy accessibility to structural modification
- Tunable properties (spectral as well as sensing)
- Compatibility of the indicator with commercially available light sources
- Low cross-talk to ionic strength and temperature

Fluorescent pH indicators are of particular interest and the synthesis of new dyes is a fast growing field of research, therefore numerous such probes were reported in the literature during the last decades as mentioned before. They are mostly represented by xanthene dyes (e.g. fluorescein, SNAFL or SNARF)[11,93–99], naphthalimides[8,100–104], hydroxycoumarins[105,106] and derivatives of 8-hydroxypyrene-1,3,6-trisulfonic acid (HPTS)[9,11,99,107–109] (**Figure 2-13**). But many of them have severe limitations such as limited photostability and high tendency to self-quenching of xanthene dyes, low molar absorption coefficients of naphthalimides or high cross-sensitivity to ionic strength of triple negatively charged HPTS. Moreover, the above mentioned indicators provide absorption and emission profiles in the UV-Vis range (400-600 nm).

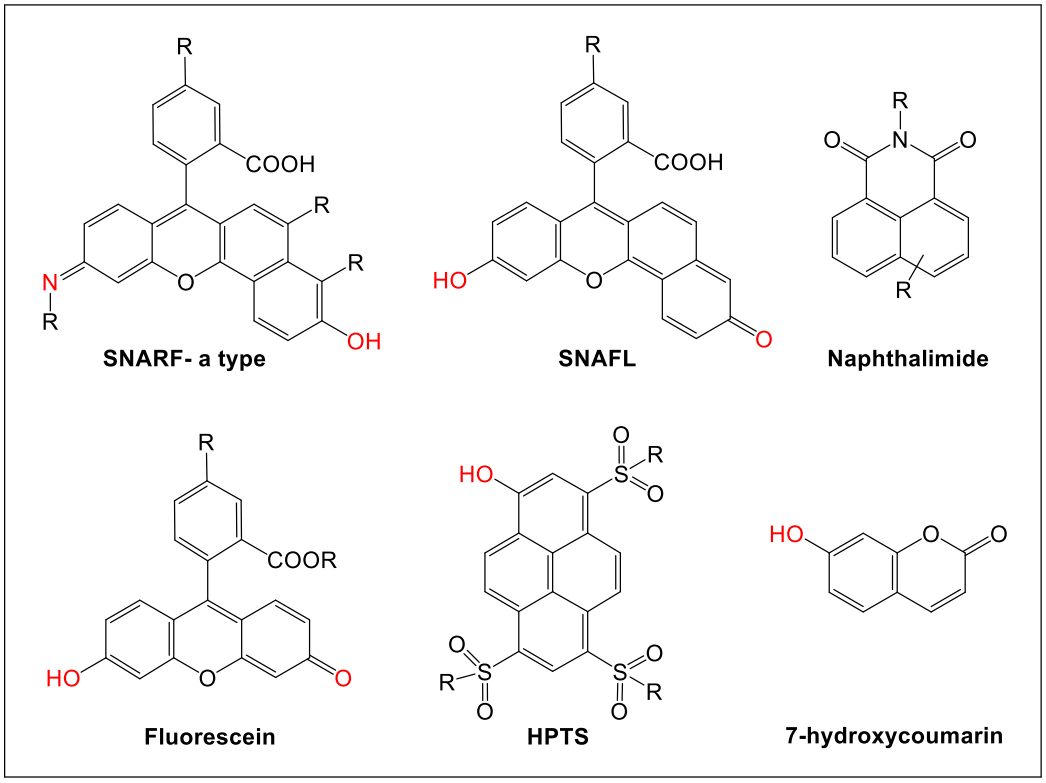

Figure 2-13 Chemical structures of popular pH indicators with absorption/emission profiles in the UV-Vis range.

The most commonly used group of pH indicators applied in optical sensors are *xanthene dyes* due to a wide commercial availability and the particular applicability for biological and medical sensing. Fluorescein is the most prominent representative of this group with efficient absorption around 490 nm and emission in the green part of the electromagnetic spectrum. Due to the existence of several protonation equilibria of fluorescein, the most important ones in aqueous media are the mono- and dianionic forms with deprotonated carboxylic and phenolic groups.[95] Regarding π-extended derivatives such as seminaphthofluoresceins (SNAFL)[94] or seminaphtharhodafluors (SNARF)[93] dyes the absorption and emission are bathochromically shifted. To increase the poor photostability of xanthene dyes introduction of electronegative halides in 2' and 7' positions are a preferable approach, but it´s directly connected to a concomitant decrease of the pK_a values.[96] Xanthene dyes can be physically incorporated in various matrices such as hydrogels,[96] sol-gels[110] or poly(styrene-block-vinylpyrrolidone) nanobeads.[11] Furthermore, also covalent immobilization of xanthene derivatives in several amino-modified materials have been reported in literature.[111,112]

Table 2-1 Overview of typical photophysical properties of fluorescent pH indicators used in optical sensors.

Dye class	Abs_{max} nm	$\varepsilon \cdot 10^{-3}$ $M^{-1} \cdot cm^{-1}$	Φ	Brightness $\varepsilon \cdot \Phi \cdot 10^{-3}$	Reference
UV-Vis pH indicators					
Naphthalimides	410-450	15-18	0.6-0.8	9-15	[100,101,113]
Fluoresceins	480-520	80	0.8	64	[114]
HPTS	450	20	0.9	18	[114]
BODIPY	500-580	80	0.9	72	[78,79]
red and far-red pH indicators					
Porphyrins	640-685	5-15 (Q bands)	0.18	N.A.	[115]
Perylenes	630-660	15-20	0.13-0.26	2-5	[42]
BODIPYs	630-670	70-100	0.1-0.7	7-70	[70,116]
aza-BODIPYs	650-710	80	0.2-0.3	16-24	[117]
Cyanine dyes	600-750	100-200	0.03-0.3	3-60	[118,119]
pH-insensitive red and far-red dyes					
Keyo fluors	600-720	190-320	0.6-1.0	114-320	[69,120]
NIR perylenes	600-650	92	1.0	92	[49]
NIR DPP dyes	720-750	100-135	0.6-0.75	60-100	[121]

HPTS and its derivatives belong to the class of fluorophores undergoing a photoinduced proton transfer (p. 20) in the excited state. 8-Hydroxypyrene-1,3,6-trisulfonate (R=O^-Na^+) is a triply charged indicator, which is highly soluble in water with a pK_a value around 7.3 in aqueous solution. Due to the PPT mechanism only the emission of the deprotonated form can be observed. Whereas, the absorption bands of the protonated and deprotonated form at around 405 and 465 nm respectively enable referenced ratiometric measurements. For incorporation of the triple charged HPTS dye into sensing materials covalent immobilization or derivatization are required.[11,109]

1,8-Naphthalimide dyes are a highly versatile class of pH indicators. Most commonly pH sensitive functionalization is realized by introduction of a PET group in imide position or at the naphthalene core. Due to the position of functionalization, the PET efficiency varies remarkably.[103,122] However, there have been also dyes reported bearing an electron-donating amino group in 4' position of the core, where an ICT excited state is obtained, resulting in increasing molar absorption coefficients and bathochromic shifts of absorption and emission spectra.[123] Covalent immobilization is easy accessible via copolymerization of functional groups in imide position, amide bond formation or direct bonding via the imide position.[8,102,124] Nevertheless, naphthalimide dyes suffer from low luminescent brightness due to moderate molar absorption coefficients.

At this point, it should be mentioned that indicators featuring long-wavelength (red and far-red: 600-780 nm, NIR: 780–900 nm) excitation and emission profiles are highly desirable due to reduction of sample photodamage, cellular autofluorescence and lower fluorescence background of biological samples. Moreover, dramatically reduced Rayleigh and Raman scattering of NIR light allows this radiation to penetrate deeply into biological cells and tissues. Additionally, availability of low-cost excitation sources and photodetectors are advantageous features. However, the photophysical properties are of high importance especially for *in vivo* measurements. Importantly, far-red and NIR fluorophores such as aza-BODIPYs, perylenes or other dyes (e.g. cyanines) possess poor to moderate brightness (**Table 2-1**). The brightness of these dyes is significantly lower than that of the more conventional UV-Vis probes. High fluorescence brightness is crucial for many important applications of pH sensors: (i) fast-responding sensors; (ii) measurements in tissues and other highly absorbing and scattering media; (iii) extra- and intracellular imaging with help of the nanoparticles. Bright probes enable lower nanoparticle loading which causes far less stress to the biological systems; (iv) microfluidic applications of the nanoparticles. This very fast growing field requires bright probes to accumulate sufficient signal in the tiny microfluidic channels; (v) low cost optical sensors which are particularly crucial e.g. for environmental monitoring. Therefore, indicators should provide an adequate luminescence brightness resulting from preferable molar absorption coefficients above 80000 M^{-1} cm^{-1} and quantum yields exceeding 30%. Naturally long-wavelength dyes have lowered quantum yields, due to more efficient non-radiative deactivation of the excited state. Another property which is of particular importance for long-term measurements is high photostability of the dye. Generally it can be considered that the photostability is strongly dependent on the dye class. Particularly, indicators with conjugated aromatic systems such as porphyrins or aza-BODIPYs are more photostable than dyes with extended conjugated polymethine groups like cyanine dyes.[64,68]

In summary, development of far red/NIR fluorophore based optical sensors meets many requirements and tremendous research efforts have been invested into design of new long-wavelength emitting dyes with requested photophysical and sensing properties. An overview of pH sensitive NIR-emitting chromophores will be given in the next section and comparison of some photophysical properties can be seen in **Table 2-1**.

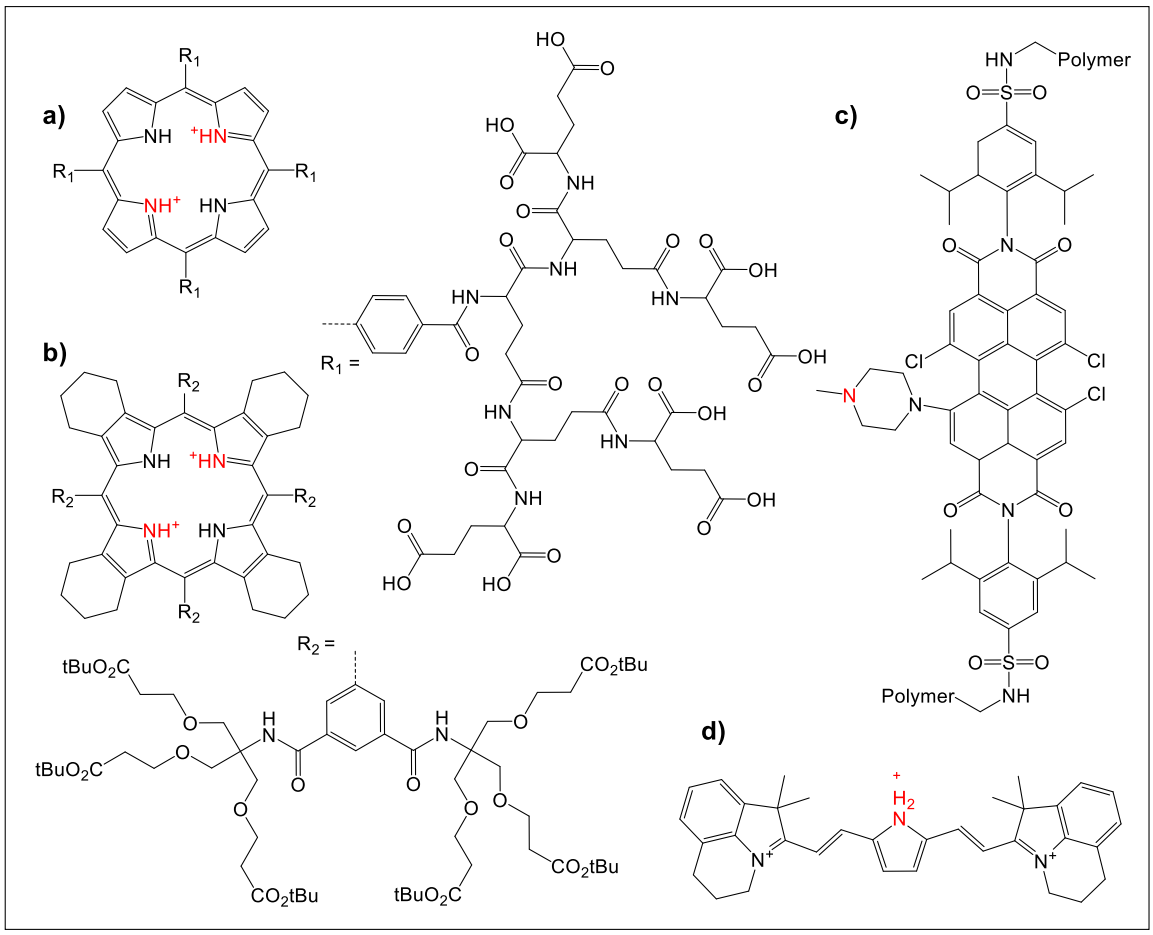

Figure 2-14 Chemical structures of long-wavelength emitting pH sensitive dyes. a) polyglutamic dendrimer based on a metal-free porphyrin. b) weakly emissive dendrimer based on a highly non-planar porphyrin. c) perylene bisimide with N-methylpiperazine functionalization in bay position. d) cyanine based dye with a pyrrole core, rendering the dye pH sensitive in two different pH ranges.

Metal-free *porphyrin dyes* are known for their protonable nitrogen atoms of the pyrrole under acidic conditions resulting in a dication formation. Generally, the pK_a value of such porphyrins is limited to the acidic range. There have been several attempts reported to shift this intrinsically low pK_a into the physiological range such as electrostatic stabilization of the porphyrin core by peripheral negative charges (e.g. polyglutamic dendrimers)[115] or substitution of dendrimers into the core[125] (**Figure 2-14a** and **b**), though this modifications dramatically increase the cross sensitivity to ionic strength. However, metal-free porphyrins represent interesting candidates for design of NIR pH sensitive chromophores, due to the absorption and emission profiles in the red/NIR part of the electromagnetic spectrum.[12]

Perylene bisimide dyes (PBI) are naturally π-extended analogs of naphthalenediimides. Usually, core-unsubstituted dyes absorb very efficiently in the green part of the spectrum and emit green-yellow light with QYs close to unity.[37] Their excellent photophysical properties and the versatility of chemical modifications make perylene bisimide dyes highly attractive as indicators for optical sensors and (bio)labels.[38–42,36] Unfortunately, perylene dyes which are strongly emissive in the red part of the spectrum are seldom.[36,42,48,49] *Aigner et al.* reported a NIR pH sensor based on a novel 1-aminoperylene, where absorption/emission is bathochromically shifted into the red/NIR part of the electromagnetic spectrum. pH sensitivity was introduced by substitution with a piperazine group in bay position, which is also the origin for the bathochromic shift. Furthermore, covalent immobilization into cross-linked poly(acryloylmorpholine) prevents dye leaching out of the sensor material and dye aggregation (**Figure 2-14c**). It should be mentioned that the modification in bay position results in a decrease of ε (to around 20000 M^{-1} cm^{-1}) and Φ (to about 26%).[42] More detailed description of perylene bisimide dyes and their modifications is given in **Section 2.2.1** (p. 9).

Cyanine dyes are interesting candidates for designing new pH sensitive dyes caused by their efficient long-wavelength absorption and emission, which can be used for ratiometric two-wavelength measurements and imaging. Moreover, the dye platform including cyanine, hemicyanine and squaraine feature extraordinary biocompatibility and low toxicity to living cells. But cyanine dyes are also known for their photolability, limiting their use in optical sensors, especially for long-term applications.[13,14] Nevertheless, recently highly promising chromophores for pH measurements for intracellular imaging and *in vivo* imaging in small animals have been developed. *Li et al.* presented a set of dyes featuring high fluorescence brightness for both forms (protonated and deprotonated), covering a broad range of pK_a values (6.2 -7.4) making them interesting for ratiometric measurements in medical and biotechnological applications.[126] Another group presented a cyanine based dye bearing a pyrrole core (**Figure 2-14d**), rendering the dye pH sensitive in two different pH ranges. The chromophore shows bathochromic shifts of absorption and emission with increasing pH. The authors demonstrated the applicability in ratiometric imaging in living cells and real-time pH sensing of enzymatic reaction.[127]

Boron-dipyrromethene (*BODIPY*) *dyes* feature high luminescence brightness and high versatility to structural modifications in consideration of their spectral properties as well as functionalization with analyte sensitive groups.[17] However, conventional BODIPYs absorb in the range of 500-600 nm, but various modifications have been performed to shift absorption and emission to the red/NIR part of the electromagnetic spectrum.[74,128] Despite high modularity, comparably few pH sensitive indicators based on BODIPYs have been reported. Several initial attempts to render BODIPY dyes pH sensitive have been demonstrated via introduction of PET receptors in *meso*-position of the core such as dimethylaniline group (pH range 0.5-2.5, **Figure 2-15b**)[70] or phenol groups for the alkaline region.[78,79] *Zhang et al.* synthesized a variation of pH sensitive π-extended BODIPYs by introduction of piperazine groups in 3,5'-position of the core. To avoid aggregation in aqueous media and provide sufficient hydrophilicity oligoethylene chains were introduced in *meso*-position of the core (**Figure 2-15a**). The surprisingly low pK_a values (2.9-3.6) enable monitoring of

lysosomal pH.[116] Another group presented the high versatility of pH PET receptors in *meso*-position of BODIPY dyes combined with read-out via a simple smartphone app. They synthesized a palette of pH responsive probes, embedded them in hydrogel together with selected reference dyes to cover the whole pH range from 0-14. The combination of the not reusable pH sensitive sensor strips with a smartphone allows autonomous operation for field measurements.[129]

In this thesis BODIPY dyes for use in optical sensors have been designed and further information about this class of dyes is given in **Section 2.3** (p. 14).

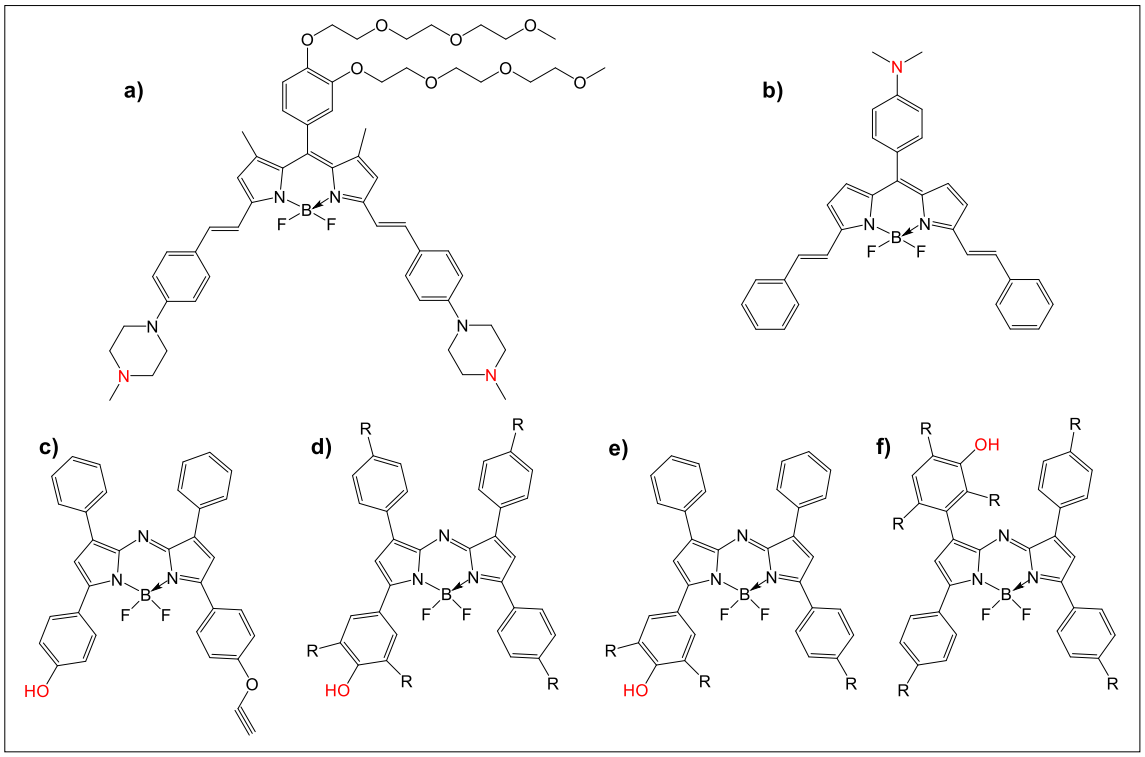

Figure 2-15 Chemical structures of pH sensitive (aza-)BODIPY indicators.

BF_2-chelated tetraarylazadipyrromethene (*aza-BODIPY*) *dyes* are particularly attractive for designing NIR pH sensitive chromophores due to excellent photostability and the bathochromically shifted absorption and emission spectra compared to classical BODIPY dyes.[130,131] Most commonly, phenol groups have been introduced in 3,5'-postions of both pyrrole rings acting as PET receptors.[132] Relatively simple synthesis of asymmetric aza-BODIPYs enables introduction of substituents for improvement of solubility or covalent immobilization. *Murtagh et al.* presented a aza-BODIPY dye bearing a phenolate receptor, where the fluorescence is virtually "switched off" upon deprotonation, with a concomitant shift of the absorption from 700 to 775 nm upon deprotonation (**Figure 2-15c**).[133] *Jokic et al.* demonstrated the systematical tuning of the pK_a value by introduction of electron-donating (alkyl, alkoxy-moieties) or electron-withdrawing (chlorine) groups and the outstanding photostability of all the dyes (**Figure 2-15d**).[117] *Strobl et al.* presented a palette of novel aza-BODIPYs covering the pH range from 1.5-13 featuring high photostability and almost identical spectral and photophysical properties. Combination of four

different dyes in a polyurethane hydrogel results in a broad-band pH sensor with an extended pH range from 2-9 (**Figure 2-15e**).[88] In a more recent work synthesis of an aza-BODIPY only based on PET with complete elimination of intramolecular charge transfer by breaking conjugation of the pH receptor to the fluorophore was reported by *Staudinger et al.* (**Figure 2-15f**).[134]

It should also be mentioned here, optical chemosensors for acidic (CO_2) and basic (NH_3) gases also rely on pH indicator dyes. Another important part of this thesis is dedicated to development of optical carbon dioxide sensors. Evidently, bright NIR indicators can also significantly improve the performance of these gas sensors. In the following section state-of-the-art sensor materials for optical carbon dioxide sensors will be described.

2.5.2 State-of-the-Art Optical Carbon Dioxide Sensors

This thesis is also focused on the development of optical carbon dioxide sensors, especially on so called *dry sensors* or *'plastic'-type sensors*. In this section state-of-the-art sensor compositions, including suitable indicator dyes and matrices as well as their fields of application will be discussed. A brief overview on routine detection techniques will be given.

Undoubtedly, carbon dioxide is one of the most significant analytes in the world, at a same importance level as oxygen or pH. Quantification of this metabolite is of highest interest in medical diagnostics, biology and photosynthesis research. It is used as indication for the existence of life or to measure the health status. Carbon dioxide represents a crucial component in modern food and beverage industry such as modified atmosphere packaging (MAP) or in the production of beer and soft drinks. Moreover, monitoring of carbon dioxide levels in environment is evidently essential due to the decisive role of anthropogenic factor in climate change. The closely related monitoring of ocean acidification is an important part of marine science.[10]

There are classical analytical, well established techniques such as gas chromatography, infrared spectroscopy, potentiometry (Severinghaus electrode) or spectrophotometry used for the quantification of carbon dioxide. All of them have their different advantages and limitations, hence optical chemical CO_2 sensors represent a promising alternative for specific applications e.g. if continuous monitoring of the analyte in gaseous or aqueous media is required.

Gas chromatography is a popular detection method for carbon dioxide and other greenhouse gases, with a high sensitivity and sample throughput of gaseous samples. However, the instrumentation is expensive, requires a trained operating personal and measurements of dissolved carbon dioxide in aqueous media are difficult to realize.[10,135]

The *Severinghaus electrode*, consisting of a pH electrode, placed in contact with a thin layer of an aqueous sodium bicarbonate solution, trapped behind a gas-permeable, ion-impermeable membrane – separating the sample and the electrode was developed in the late 1950's by Severinghaus and Bradley and has dominated the measurement of dissolved carbon dioxide in aqueous media especially in blood for more than 50 years. Carbon dioxide can diffuse through the

gas-permeable membrane causing a change in pH of the entrapped bicarbonate buffer layer that is measured by the pH electrode. This potentiometric device provides excellent selectivity but is prone to electrical interferences, can be affected by acidic or basic gases, and exhibits slow response and recovery times.[136,137]

Infrared spectroscopy is a direct measurement method using characteristic molecular vibrations induced by absorption of infrared radiation. It is often utilized as method of choice e.g. in medical diagnostics and is an advantageous method concerning fastness and non-destructiveness. On the other hand, this method is mostly suitable for gaseous samples due to noticeable interferences to water vapour and requires long path lengths, bulky and expensive equipment which lacks mechanical stability.[10,138]

Innovative developments in the field of *non-dispersive infrared (NDIR) gas detection sensors* made them to one of the most widely used optical gas detection techniques.[139] It gained attention as a very useful tool even for rather challenging measurements in aqueous media such as river water or marine environment. However, due to an inseparable unit consisting of probe compartment and read-out element measurements in small sample volumes are virtually impossible.[140]

Thus, optical chemical sensors represent a promissing alternative since fiber-optic sensors with very small diameters of a few dozens of microns can be fabricated, to enable point measurements in small volumes. Furthermore, the optoelectronic reader and the comparably small sensing component (millimeters in diameter and microns in thickness) can be separated in space and providing read-out performed through a transparent wall. Therefore, integration of sensing spots in a great variety of devices (flow-through cells, (microfluidic) chips, microplates etc.) combined with necessary treatments (e.g. sterilization) becomes possible. Finally, manufactured planar optical sensing formats allow mapping of the analyte distribution on surface.

In general, CO_2 sensors relying on pH transducers (pH sensitive indicators) allow for the highest flexibility of spectral properties and sensitivities. Due to its pK_a, high stability and large Stokes shift, commercially available 8-hydroxypyrene-1,3,6-trisulfonate (HPTS) is by far the most common dye used as fluorescent indicator in optical CO_2 sensors.[141–148] Unfortunately, absorption maxima at short wavelength and desired excitation in the blue part of the spectrum and green emission are not ideal for some applications. Furthermore, its pK_a of ~ 7.3 makes it challenging to prepare sensors resolving ambient carbon dioxide levels. Non-fluorescent indicators such as thymol-blue and *m*-cresol-purple are commonly used for colorimetric sensors but are known for their rather low photostability.[141] Several dyes of other classes including aza-BODIPYs[149–151], azaphthalocyanines[152], diketopyrrolopyrroles[153], α-naphtholphthalein[154,155] were prepared in the last years in attempt to overcome the above limitations, however tuneability of spectral and sensing properties still remains an issue. Structures and properties of several commonly used pH sensitive indicators for optical carbon dioxide sensors are shown in **Figure 2-17** and **Table 2-2**.

To achieve reliable measurements, addition of reference material is often required in sensor manufacturing. However, photobleaching of the used materials can cause a change in indicator/reference ratio, which strongly affects the sensor performance. Therefore, self-referencing (ratiometric) and highly photostable indicators are highly requested. Furthermore, for measurements in media with high autofluorescence and scattering, long-wavelength dyes are of high research interest.

Table 2-2 Properties of some absorption and fluorescence-based pH indicators used for carbon dioxide sensors. pK_a values, absorption and emission maxima for protonated and deprotonated (anionic) forms. Properties of HPTS, thymol-blue and m-cresol-purple determined in aqueous solution.

Dye	pK_a	λ_{Abs} prot/anionic form	λ_{Em} prot/anionic form
HPTS[156]	7.3-8.0	403/455 nm	435/512 nm
DPP (in THF)[153]	pK_{a2} <11.8	~530/ 630-655 nm	540-590/ 670-710 nm
aza-BODIPY (in EtOH/buffer) [150]	pK_{a2} 10.34	745[a]/ 805 nm [b]	non fluorescent
Thymol-blue[141]	pK_{a2} 8.9	432/590 nm	non fluorescent
m-cresol-purple[141]	pK_{a2} 8.3	428/571 nm	non fluorescent

[a] mono-anionic form; [b] di-anionic form

Recently, a carbon dioxide sensor based on a non-fluorescent aza-BODIPY indicator has been reported.[151] To obtain a referenced luminescence signal of the sensor they have to make use of a sophisticated inner-filter effect read-out. Thus, the sensor demands addition of two reference emitters in form of particles making sensor manufacturing more challenging particularly if other formats than planar optodes (e.g. fiber-optic microsensors) are considered. There are also carbon dioxide sensor systems reported based on FRET using phosphorescent porphyrin in combination with a colorimetric indicator, which are probably applicable for food packaging.[155]

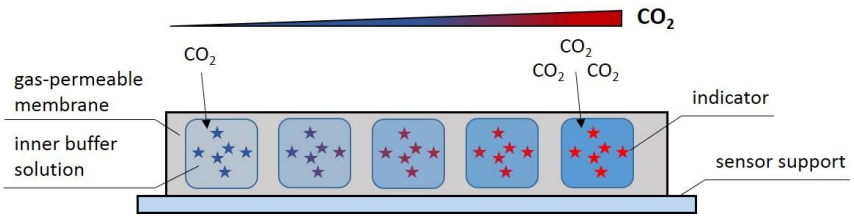

Figure 2-16 Schematic composition of a "Severinghaus"-type carbon dioxide sensor material.

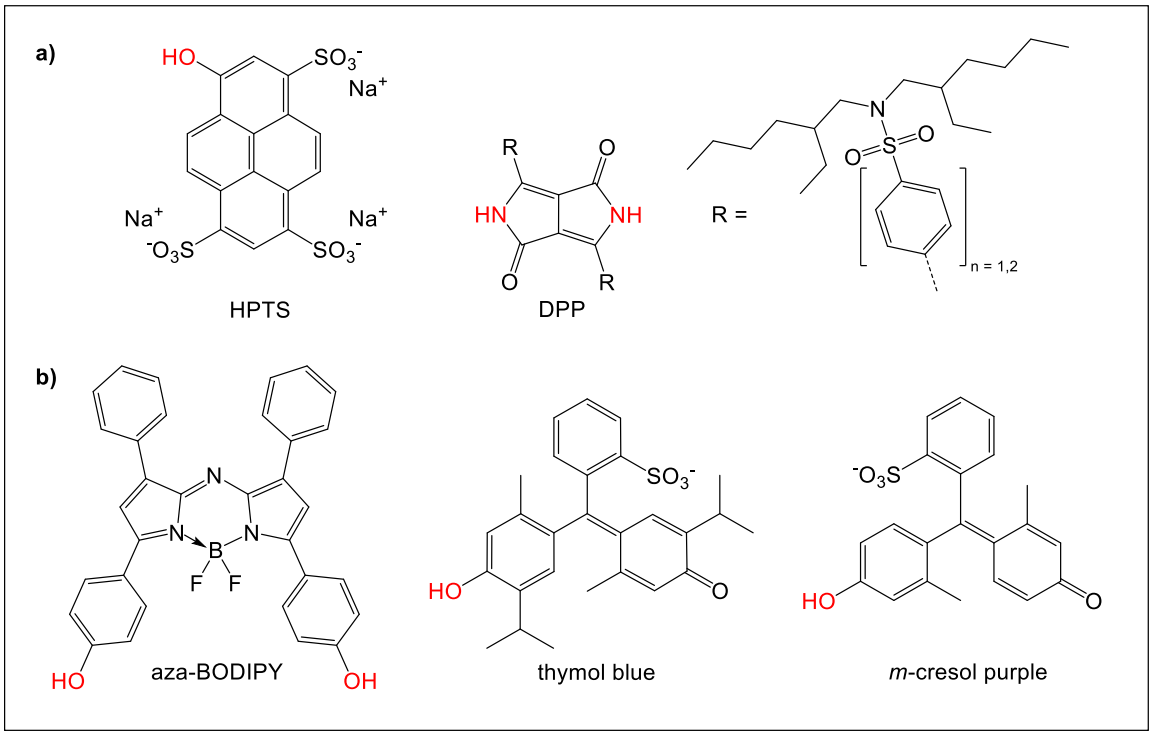

Figure 2-17 State-of-the-art a) fluorescent (HPTS and DPP); b) absorption-based (aza-BODIPY, thymol blue and m-cresol purple) pH indicators used for optical carbon dioxide sensors.

In general, optical carbon dioxide chemosensors mostly rely on colorimetric[141,157,158] or fluorescent[142,159–161] pH indicators that respond to CO_2 induced by pH changes correlated to the carbonic acid-water equilibrium, shown in **Equation 2.1**. There can be distinguished between two major categories: *wet sensors*, where the indicator is commonly dissolved in an aqueous buffer or *dry sensors* – here, the indicator is embedded in a polymeric matrix along with a lipophilic base.

$$CO_2 + H_2O \rightleftharpoons H_2CO_3 \rightleftharpoons HCO_3^- + H^+ \qquad \textbf{2.1}$$

First, in a so called *wet carbon dioxide optical sensor* the pH sensitive indicator stays in contact (dissolved or dispersed) with an aqueous encapsulation medium, containing buffer (commonly bicarbonate) which is covered with a hydrophobic gas-permeable but ion-impermeable membrane ('Severinghaus'-type).[107,162] The fundamental principles of operation of this sensor type are adapted from the Severinghaus electrode utilizing the diffusion of the carbon dioxide of the sample (gaseous or aqueous) through the covering gas-permeable membrane and balance an equilibrium with the entrapped aqueous sensor phase (**Figure 2-16**). However, these systems suffer from some drawbacks: Sensor behavior is strongly dependent on changes in the internal buffer caused by the cross-sensitivity of the pH indicator to ionic strength. Furthermore, defined storage conditions (humidity and carbon dioxide atmosphere) have to be fulfilled because dehydration of the sensor material can occur and would result in a long re-conditioning period. Additionally, the sensors exhibit long response times and are dependent on osmotic pressure.[10]

Hence, to accomplish the above mentioned drawbacks of a *wet sensor*, the development of *dry carbon dioxide sensors* gained more attention. These, also called 'plastic'-type sensors were developed by *Mills et al.*[163] Therefore, a pH sensitive dye is directly dissolved in a hydrophobic, polymeric/inorganic matrix along with a lipophilic, basic phase transfer agent, most commonly quaternary ammonium hydroxide (**Figure 2-18**).[141,142,157–160] Such a phase transfer agent most likely tetraoctyl ammonium hydroxide (TOAOH), tetrabutyl ammonium hydroxide (TBAOH) or hexadecyltrimethyl ammonium hydroxide (CTA) enables the solubility of the anionic (deprotonated) form of the indicator in hydrophobic solvents, which are compatible with even water-insoluble polymers like ethyl cellulose (EC). Furthermore, the lipophilic base cation forms an ion-pair with the indicator dye anion. Consequently, in presence of water molecules, the embedded indicator anion can interact with carbon dioxide – the equilibrium process is shown in **Equation 2.2**.

$$Ind^-TOA^+ + CO_2 + H_2O \rightleftharpoons \ HCO_3^-TOA^+ + Ind^-H^+ \qquad \textbf{2.2}$$

The polymer should be gas-permeable, but impermeable for charged species such as protons, to prevent cross-sensitivity to pH. Additionally, a separate protection layer, acting as proton barrier, such as silicone rubber can be used if the matrix itself not completely meet all requirements. Most commonly used polymers for optical carbon dioxide sensors are ethyl cellulose with various ethoxyl contents for entrapment of the indicator dye.

It is known that the sensitivity to carbon dioxide is well correlated to the pK_a value of the pH indicator.[10] Therefore, the choice of a suitable pH indicator is a key factor for the dynamic range of the sensor. In general, the higher the pK_a value of an indicator the less carbon dioxide is required to protonate the dye and the higher is the sensitivity, consequently.[141] Furthermore, utilization of plasticizers such as tributyl phosphate (TBP) can improve the diffusion of carbon dioxide through the polymer and enables fine-tuning of the sensor sensitivity.[158] The sensitivity can be slightly tuned by variation of the chain length of the lipophilic base. However, sufficient hydrophobicity (length of alkyl chains) of the base should be given to keep the base in the hydrophobic polymer environment.

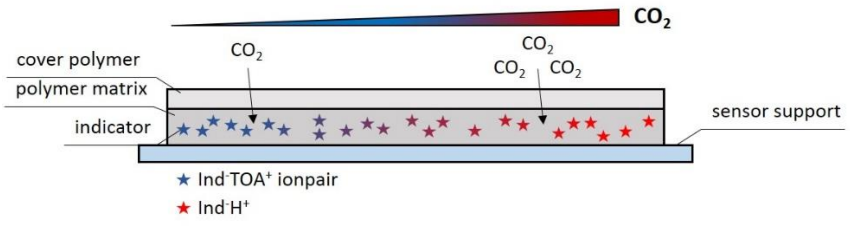

Figure 2-18 Schematic composition of a 'plastic'-type carbon dioxide sensor material.

One drawback of dry optical carbon dioxide sensors is the possibility of poisoning by other acidic gases such as hydrochloric acid, acetic acid, hydrogen sulfide, sulfur dioxide or nitrogen dioxide,

via diffusion through the gas-permeable membrane. One can distinguish between cross-sensitivities and poisoning of the sensor material. In contrast to the latter cross-sensitivity is a reversible phenomenon. However, both processes affecting the sensor in an overestimation of the carbon dioxide level, due to contribution of acidic gases to the overall pH change. Thus, the presence of such acidic gases can change the dye used in the sensor from its deprotonated form to its protonated form and consequently the sensor becomes insensitive to carbon dioxide. Unfortunately, almost every carbon dioxide sensor using a pH indicator (independent from the class of indicator) is prone to get poisoned, therefore strategies for prevention and deceleration of the effects are of high research interest.[10] The usage of perfluorinated polymers as protection layer turned out to slow down the poisoning significantly, originating from the lower gas permeability of the material. In a recent work the influence of different protective polymer materials have been systematically investigated.[151]

Classical fabrication of a plastic-type optical carbon dioxide sensor is achieved by preparation of a homogeneous cocktail containing polymer and indicator dye dissolved in an organic solvent, flushing it with pure carbon dioxide and adding the lipophilic base. Afterwards the cocktail can be knife- or spin coated on a transparent sensor support resulting a planar sensor foil after evaporation of the organic solvent. For aqueous samples and to prevent sensor poisoning a protective layer e.g. silicone rubber or perfluorinated polymers can be additionally coated on the sensor layer (**Figure 2-18**). Furthermore, additives such as referencing materials or light scattering materials can be added to the sensor layer or protective layer to manufacture referenced sensor materials or enhance signal intensity.

As mentioned above, there are classical detection methods dominating fields of application, but nevertheless optical carbon dioxide sensors are promising alternative tools for a palette of applications due to the flexibility of sensor formats. Optical carbon dioxide sensors are of particular importance due to their applications in environmental and marine science (monitoring of atmospheric carbon dioxide levels, monitoring of ocean acidification or in fish farming). In such fields fairly sensitive sensors with a high long-term stability are required due to the low atmospheric carbon dioxide level (~0.4 hPa) and its equilibrium with the upper layer of the oceans.[151] For instance, a modular platform for multi-parameter measurements with a single opto-electronic device has been recently reported.[164,165] Applications in medical diagnostics (e.g. capnography, blood gas analysis) and biotechnological industry (bioprocess monitoring, fermentation processes monitoring) have to deal with moderate pCO_2 levels and require less sensitive sensors, e.g. in blood gas analysis pCO_2 levels in the range of 40-60 hPa have to be detected or sensors used for fermentation monitoring have to be adjusted to be sensitive up to around 250 hPa.[143,166,167] The required dynamic ranges for applications in chemical industry (e.g. process controlling) and in food and beverage industry (e.g. modern food packaging – MAP, process monitoring) are spread over a wide range and the sensors have to be tuned in their properties specifically. On the one hand, MAP methods taking use of defined gas mixtures, most likely with exclusion of oxygen ranging from nitrogen/carbon dioxide mixtures up to pure carbon dioxide. On the other hand, measurements of high carbon dioxide levels above 1000 hPa are typical for the beverage industry.[155,168–171]

The challenging task of developing new optical carbon dioxide sensors and the necessary requirements which have to be fulfilled have been nicely described by *Mills et al.*:

"It is possibly surprising that there are no major lifetime-based optical sensors in the market, despite the fact that lifetime based optical sensors for oxygen already exist (e.g. OxySense™). However, it is most likely that the higher cost of such technologically advanced systems is still proving a major barrier to its market transition. The recent move towards cheaper, lower frequency, diode-based phase modulated systems, whether they be FRET- or DLR-based, may eventually lead to a relatively inexpensive, commercially viable product that challenges and widens the market for small intensity-based optical sensors for carbon dioxide. However, for this to happen a great deal more research is necessary. It remains to be seen, therefore, what the commercial future of optical sensors for carbon dioxide is which a slightly disappointing conclusion is given its history of initial rapid development and the importance of the area of analysis to life, industry and the environment."[10]

Part II

Results

3 Ultra-bright red-emitting photostable perylene bisimide dyes: new indicators for ratiometric sensing of high pH or carbon dioxide

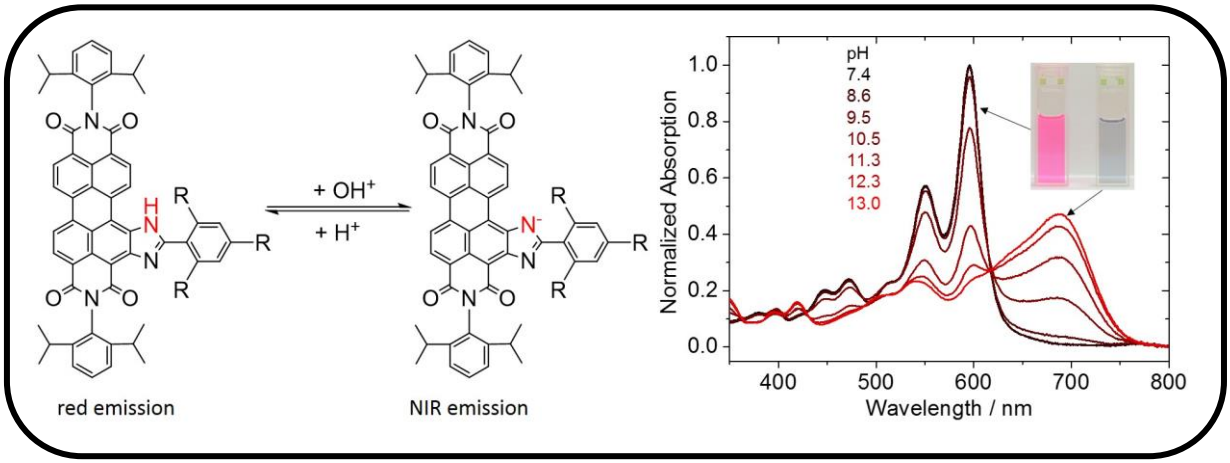

3.1 Preface for the Manuscript

This manuscript was published as Full Paper in *Chemistry – A European Journal* and is focused on the synthesis, characterization of the photophysical properties and the pH sensing properties of a palette of new core-extended perylene bisimide dyes.

Perylene bisimide dyes are known for their distinct absorption/emission bands, high photostability and excellent luminescence brightness. The aim of this study was to shift the characteristic absorption/emission bands bathochromically by bay-modification of the perylene structure (**Section 2.2.1**, p. 9) accompanied by a subsequent introduction of pH-sensitive functionalization. The highly photostable dyes show high molar absorption coefficients around 80 000 M^{-1} cm^{-1} and quantum yields close to unity.

In 2009 *Langhals et al.* [172] presented a simple one-step synthetic route of a perylene core-extension with a imidazole substituent which significantly shifts the absorption and emission bands of perylene dyes bathochromically. Depending on one or two imidazole substituents, the maxima of the spectra are shifted about 60 nm and 115 nm, respectively. By using this specific synthetic route starting from commercially available Lumogen Orange we observed pH dependency of perylene bisimide dyes showing strong bathochromic shift both in absorption and emission spectra upon deprotonation of imidazole nitrogen. This effect is driven by an intramolecular charge transfer and thus enables colorimetric as well as ratiometric sensing of pH (**Section 2.5.1**, p. 22). The pK_a' values were determined to be in the alkaline range, which make the indicators a promising candidate for several specific applications as well as the fabrication of optical carbon dioxide sensors for different dynamic ranges. For manufacturing of the pH sensitive sensor material the indicators were physically embedded in a polyurethane hydrogel. The corresponding pK_a' values in this matrix are in the range from 9.84-10.56. Obviously, the pH sensors with the response in the alkaline media are not suitable for conventional applications (e.g. biotechnology, biology and medicine) but interesting candidates for research on alkaliphilic bacteria and monitoring of pH in concrete. Thus, excellent chemical and photochemical stability of the new indicators is expected to be very valuable for long-term deployment of the sensors.

In this study plastic type optical carbon dioxide sensor materials were fabricated via immobilization of the pH indicator in a hydrophilic polymer (ethyl cellulose), along with a quaternary ammonium base (**Section 2.5.2**, p.30). The influence of plasticizer, different lipophilic bases and humidity on the sensitivity of the sensor material were systematically investigated. The sensitivity of the carbon dioxide sensor can be adjusted via variation of the dye, ratio of plasticizer to polymer and by varying the nature of the quaternary ammonium base. The di-substituted perylene shows unique behaviour with two protonation/deprotonation equilibria enabling sensing of carbon dioxide in unprecedentedly broad dynamic range. The new carbon dioxide sensors are likely to be promising for application in food packaging and beverage industry.

Ultra-bright red-emitting photostable perylene bisimide dyes: new indicators for ratiometric sensing of high pH or carbon dioxide

This manuscript was published as *Full Paper* in

Chemistry A European Journal, 2018, 24, 10711-10720.

doi: 10.1002/chem.201800867

Authors: David Pfeifer, Ingo Klimant and Sergey M. Borisov*

Institute of Analytical Chemistry and Food Chemistry, Graz University of Technology, Stremayrgasse 9, 8010 Graz, Austria

***Corresponding author:** sergey.borisov@tugraz.at

Keywords: Perylene, optical sensor, fluorescence, ratiometric, pH, carbon dioxide

3.2 Abstract

New pH sensitive perylene bisimide indicator dyes were synthesised and used for fabrication of optical sensors. The highly photostable dyes show absorption/emission bands in the red/near-infrared (NIR) region of the electromagnetic spectrum, high molar absorption coefficients (up to 100000 M^{-1} cm^{-1}) and fluorescence quantum yields close to unity. The absorption and emission spectra show strong bathochromic shift upon deprotonation of imidazole nitrogen which makes the dyes promising as ratiometric fluorescent indicators. Physical entrapment of the indicators into polyurethane hydrogel enables pH determination in alkaline pH. It is also shown that plastic carbon dioxide solid state sensor can be manufactured via immobilization of the pH indicator in a hydrophilic polymer, along with a quaternary ammonium base. The influence of plasticizer, different lipophilic bases and humidity on the sensitivity of the sensor material were systematically investigated. The disubstituted perylene, particularly, features two deprotonation equilibria enabling sensing over a very broad range from 0.5 to 1000 hPa pCO_2.

3.3 Introduction

pH determination is one of the most frequently performed analytical measurements in industry and numerous scientific disciplines, such as biotechnology[173–175], marine science[176,177], medical diagnostics[178,179] etc. to mention only a few. pH is most commonly measured with a glass electrode which provides information about the activity of hydronium ions in aqueous environment. Ion-sensitive field-effect transistors (ISFET) belong to other very common tools for pH measurement. The ease of use, fast response times, a broad working range and relatively low cost have been advantages of such methods. On the other hand, disadvantages include challenging miniaturization, electrical interferences, interferences due to the reference electrode (e.g. from variation in salinity) and rigid design allowing only point measurements.

In the last decades, optical pH sensors (optodes) have been intensively investigated. pH optodes do not suffer from electromagnetic interferences, do not require reference sensors, are easy to miniaturize and can be manufactured in a variety of formats which enable high versatility of application. Particularly, planar optodes proved to be excellent tools for imaging of pH distribution, fiber-optic sensors and microsensors enable higher mechanical flexibility, and nanoparticles are of high interest for extra- and intracellular imaging.[5,50,68,82,84–87,176,180]

In general, an optical pH sensor consists of a pH sensitive dye entrapped into a hydrophilic polymer matrix or a sol-gel. The protonated and deprotonated forms of the indicator dye feature different optical properties, most commonly either pH-dependent excitation and/or emission spectra[96,181,182] or fluorescence quenching via photoinduced electron transfer (PET) without change of the spectral properties.[6,88,117,128,133] The PET indicators can be prepared with virtually any class of chromophores[36] but require an additional luminescent reference for reliable measurement. On the contrary, ratiometric fluorescent indicators are essentially self-referenced but are limited only to several dye classes. The most frequently used representatives are fluorescein derivatives[97,98], hydroxycoumarins[105,106], 8-hydroxypyrene-1,3,6-trisulfonic acid (HPTS)[99,108], and seminaphthorhodafluors (SNARFs)[93]. Recently, several other representatives have been reported.[126,127,183–186]

The use of fluorescent dyes with absorption and emission in the red/NIR part of the spectrum has several advantages such as good light penetration in tissues essential for *in-vivo* measurements, lower auto-fluorescence and light scattering from biological samples and optical components, and lower energy demand for the excitation, which is useful for autonomous sensing. The number of reported red/NIR emitting indicators is rather limited and only a few of them show the ratiometric character.[12] Moreover, high fluorescence brightness and high photostability are also highly desirable properties of a pH indicator.

Perylene tetracarboxylic acid bisimide dyes (PBIs) and pigments gained substantial attention in academic and industrial research over the last decades. They are promising as n-type semiconductors for electronics applications and as indicators for optical sensors.[38,39,187,31,37,188,40,189,25,41,33,190] For sensing applications, excellent chemical and photochemical

stability of perylene dyes, their high molar absorption coefficients and quantum yields close to unity are particularly attractive. Unfortunately, perylene dyes which are strongly emissive in the red part of the spectrum are seldom. Often synthetic modifications resulting in bathochromic shift of absorption and emission are accompanied by strong decrease in fluorescence brightness.[23,24,42,46] Imidazole-substituted perylenes reported by Langhals et al. represent a notable exception.[49]

In this study, we present easily accessible core-extended perylene bisimide indicators that show efficient absorption in the orange-red part of the spectrum and strong red-NIR fluorescence. We will demonstrate that these dyes are intrinsically pH sensitive, showing strong bathochromic shift of the absorption and emission spectra upon deprotonation due to intramolecular charge transfer and thus enabling ratiometric sensing. The pK_a values in the alkaline range enable several specific applications as well as the preparation of optical carbon dioxide sensors for different dynamic ranges.

3.4 Materials and Methods

3.4.1 Chemicals and Materials

Anhydrous benzonitrile, 2,6-dichlorobenzonitrile, ethyl cellulose (EC49, ethoxyl content 49%), tetrabutylammonium hydroxide (TBAOH, 40% in water), tetraoctylammonium hydroxide (TOAOH, 20% in methanol) and tributyl phosphate (TBP) were purchased from Sigma Aldrich (www.sigmaaldrich.com). 4-Chlorobenzonitrile was obtained from TCI Europe (www.tcieurope.de). Lumogen Orange **1** was purchased from Kremer Pigmente (www.kremer-pigmente.de). Dichloromethane was received from Fisher scientific (www.fishersci.com). Cyclohexane, ethyl acetate, tetrahydrofuran and toluene (synthesis grade) and hydrochloric acid (37%) were purchased from VWR Chemicals (www.vwr.com). Polyurethane hydrogel (Hydromed D4) was obtained from AdvanSource biomaterials (www.advbiomaterials.com). Poly(ethylene terephthalate) (PET) support was received from Pütz (www.puetz-folien.com). Anhydrous sodium sulfate, anhydrous disodium phosphate and the buffer salts CAPS, MOPS and TRIS were obtained from Carl Roth (www.roth.de). Sodium amide (99%) was purchased from Acros (www.acros.com). Deuterated chloroform ($CDCl_3$) was purchased from Euriso-top (www.eurisotop.com). All purchased chemicals were used without further purification. Nitrogen, 0.2% carbon dioxide in nitrogen, 5% carbon dioxide in nitrogen, carbon dioxide (all of 99.999% purity) were received from Linde (www.linde-gas.at). Potassium chloride, silica-gel 60 (0.063-0.200 mm) were obtained from Merk (www.merck.at). PTFE hydrophobic membranes (45 µm) were obtained from Millipore Merck (www.merckmillipore.com).

Synthesis of compound 2a and 3a

Compound **1** (400 mg, 0.563 mmol) and $NaNH_2$ (99 %, 440 mg, 11.3 mmol) were dispersed in anhydrous benzonitrile (50 mL) under inert atmosphere and heated to 165 °C. The color changed from orange to green and afterwards to dark blue. Compressed air was bubbled through the reaction mixture for 30 minutes. The reaction was allowed to cool to RT, and 200 mL of a mixture of 1 M aqueous HCl/dichloromethane (1:1) were added. The organic phase was washed three times with 1 M aqueous HCl (100 mL) and dried over Na_2SO_4. The organic solvents were removed under reduced pressure. The purple crude products were purified by column chromatography using silica gel (35-70 µm) as stationary and cyclohexane/ethylacetate (93:7, v/v) as mobile phase to yield **2a** (220 mg, 47 %) and cyclohexane/ethylacetate (7:1, v/v) to elute **3a** (116 mg, 22 %).

^{1}H NMR (300 MHz, $CDCl_3$) of **2a**: 11.58 (s, 1H), 11.01 (d, J = 8.2 Hz, 1H), 8.98 (d, J = 8.2 Hz, 1H), 8.91-8.78 (m, 4H), 8.34 (dd, J = 6.6, 3.0 Hz, 2H), 7.70-7.62 (m, 3H), 7.53 (dt, J = 13.1, 7.9 Hz, 2H), 7.39 (dd, J = 12.6, 7.7 Hz, 4H), 2.82 (h, J = 6.9 Hz, 4H), 1.21 (dd, J = 6.9, 4.6 Hz, 24H)

^{13}C NMR (126 MHz, $CDCl_3$) of **2a**: δ 164.89, 163.84, 163.74, 163.68, 157.82, 145.82, 145.73, 144.18, 139.63, 136.00, 135.53, 135.41, 132.68, 132.36, 131.46, 131.37, 131.19, 130.79, 130.14, 129.86, 129.81, 129.59, 129.51, 128.12, 127.69, 127.21, 127.18, 125.83, 124.23, 124.08, 124.05, 123.29, 123.08, 122.70, 122.66, 121.59, 103.66, 29.29, 29.24, 24.09, 24.03, 24.02

MALDI-TOF-MS of **2a** m/z: [M^+] calc. for $C_{55}H_{46}N_4O_4$: 826.352; found: 826.458.

^{1}H NMR (300 MHz, $CDCl_3$) of **3a**: δ 11.69 (s, 2H), 11.24 (d, *J* = 8.2 Hz, 2H), 9.02 (d, *J* = 8.2 Hz, 2H), 8.36 (dd, *J* = 6.8, 2.9 Hz, 4H), 7.66 (m, *J* = 5.0, 2.1 Hz, 6H), 7.48 (m, 6H), 2.87 (h, *J* = 7.0 Hz, 4H), 1.09– 0.67 (m, 24H).

^{13}C NMR (126 MHz, $CDCl_3$) of **3a**: δ 164.79, 163.92, 156.51, 145.92, 142.95, 139.43, 135.58, 131.90, 131.33, 130.97, 129.76, 129.44, 129.28, 128.42, 127.55, 127.44, 124.65, 124.02, 122.67, 121.52, 103.04, 31.90, 29.63, 29.33, 29.22, 24.08, 24.00, 22.66, 14.07

MALDI-TOF-MS of **3a** m/z: [M^+] calc. for $C_{62}H_{50}N_6O_4$: 942.389; found: 942.485.

Synthesis of compound 2b

Compound **1** (105 mg, 0.148 mmol), $NaNH_2$ (99 %, 160 mg, 4.10 mmol) were quickly homogenised in a mortar and 4-chlorobenzonitrile (7.16 g) was added. The powder was transferred into a Schlenk flask and heated to 150 °C under inert atmosphere. The color changed from orange to purple/dark red. At 160 °C compressed air was bubbled through the reaction mixture and it was stirred for 3 hours under reflux conditions. The reaction was allowed to cool to RT, a 1:1 mixture of 1 M aqueous HCl/dichloromethane (150 mL) was added and the organic phase was washed three times with 1 M aqueous HCl (50 mL) (color change from green to purple) and dried over Na_2SO_4. The organic solvents were removed under reduced pressure. The crude product was purified by column

chromatography using silica gel (35-70 μm) as stationary and cyclohexane/ethyl acetate (94:6 v/v) as mobile phase to yield **2b** (47 mg, 37 %).

^{1}H NMR (300 MHz, $CDCl_3$) of **2b**: 11.56 (s, 1H), 10.96 (d, J = 8.2 Hz, 1H), 8.97 (d, J = 8.2Hz, 1H), 8.93-8.76 (m, 4H), 8.31-8.23 (m, 2H), 7.67-7.61 (m, 2H), 7.53 (dt, J = 12.6, 8.0 Hz, 2H), 7.39 (dd, J = 12.1, 7.7 Hz, 4H), 2.81 (m, 4H), 1.23-1.08 (m, 24H)

^{13}C NMR (126 MHz, $CDCl_3$) of **2b**: δ 164.88, 163.79, 163.70, 163.65, 156.66, 145.80, 145.72, 143.98, 139.55, 138.73, 136.06, 135.41, 135.35, 132.66, 131.61, 131.40, 130.75, 130.07, 129.86, 129.80, 129.61, 128.88, 127.26, 127.19, 126.63, 126.02, 124.24, 124.11, 124.09, 123.35, 123.18, 122.77, 122.70, 121.68, 103.71, 29.29, 29.24, 24.08, 24.03, 24.01

MALDI-TOF-MS of **2b** m/z: [M^+] calc. for $C_{55}H_{45}ClN_4O_4$: 860.313; found: 860.348.

Synthesis of compound 2c

2c was prepared analogously to **2b** 120 mg (0.169 mmol) of compound **1**, 500 mg (12.82 mmol) of $NaNH_2$ and 7.05 g of 2,6-dichlorobenzonitrile were used instead. The mixture was heated in a Schlenk flask at 160 °C under inert atmosphere. At 170 °C compressed air was bubbled through the reaction mixture and it was stirred for 1 hour under reflux conditions. Chromatographic purification of the crude product was performed using silica gel (35-70 μm) as stationary and dichloromethane as mobile phase to yield **2c** (101 mg, 67 %).

^{1}H NMR (300 MHz, $CDCl_3$) of **2c**: 11.40 (s, 1H), 10.89 (d, J = 8.2 Hz, 1H), 9.00-8.70 (m, 5H), 7.58 (d, J = 7.0 Hz, 2H), 7.54-7.45 (m, 3H), 7.37 (dd, J = 10.3, 7.7 Hz, 4H), 2.81 (m, 4H), 1.19 (m, 24H)

^{13}C NMR (126 MHz, $CDCl_3$) of **2c**: δ 164.49, 163.84, 163.70, 163.63, 152.69, 145.85, 145.71, 142.81, 138.24, 136.19, 135.90, 135.27, 135.20, 132.77, 132.40, 131.92, 131.58, 131.35, 130.74, 130.13, 129.80, 129.73, 129.58, 128.96, 128.35, 127.50, 127.16, 127.03, 124.18, 124.05, 123.97, 123.41, 123.30, 122.90, 122.78, 121.70, 104.43, 29.27, 29.23, 24.04, 24.00

MALDI-TOF-MS of **2c** m/z: [M^+] calc. for $C_{55}H_{44}Cl_2N_4O_4$: 894.2740; found: 894.2684.

Preparation of sensor foils

pH solid state sensor

A “cocktail” containing indicator dye (0.25 mg), hydrogel D4 (50 mg) in 500 µl THF was knife-coated on a dust-free, transparent PET support to obtain ~7.5 µm (for absorption measurements) and ~2.5 µm (for emission measurements) thick sensing layers after solvent evaporation.

Carbon dioxide solid state sensor

To prepare carbon dioxide solid state sensors, indicator dye (1 mg), ethyl cellulose 49% (100 mg) and optionally 200 µl or 50 µL tributyl phosphate (TBP) were dissolved in an ethanol:toluene mixture (2:3 v/v, 1.9 g). The "cocktail" was purged with carbon dioxide and 100 µl tetraoctylammonium hydroxide solution (20 % w/w TOAOH in MeOH) or tetrabutylammonium hydroxide solution (20 % w/w TBAOH in MeOH) were added. The "cocktails" were knife-coated on a PET support to obtain ~2.5 µm thick sensing layer after solvent evaporation. PTFE hydrophobic membrane was placed on each sensor layer before solvent evaporation. The exact composition of the sensing materials is shown in **Table 3-1**.

Table 3-1 Composition of carbon dioxide sensors.

Sensor	Dye	EC/TBP (w/w)	Base
CO2_1	2a	1:2	TOAOH
CO2_2	2b	1:2	TOAOH
CO2_3	2c	1:2	TOAOH
CO2_4	2c	2:1	TOAOH
CO2_5	2c	1:0	TOAOH
CO2_6	2c	1:0	TBAOH
CO2_7	2c	2:1	TBAOH
CO2_8	3a	1:2	TOAOH
CO2_9	3a	1:2	TBAOH

3.4.2 Methods

Mass spectroscopy was performed on Micromass TofSpec 2E Time-of-Flight Mass Spectrometer at the Institute for Chemistry and Technology of Materials, Graz University of Technology. ^{1}H NMR spectra were recorded on a 300 MHz Bruker Instrument (www.bruker.com) in $CDCl_3$ as a solvent and TMS as standard. ^{13}C NMR spectra were recorded on a 500 MHz Varian Inova 500 Instrument in $CDCl_3$ as a solvent and TMS as standard.

Absorption spectra were recorded on a Cary 50 UV-Vis spectrophotometer from Varian (www.agilent.com) using optical glass cuvettes from Hellma Analytics (www.hellma-analytics.com). Emission and excitation spectra were recorded on a FluoroLog 3 Spectrofluorometer from Horiba Scientific Jobin Yvon (www.horiba.com) equipped with a R2658 photomultiplier from Hamamatsu and corrected for detector response. Determination of absolute

fluorescence quantum yields Φ was carried out on the same Spectrofluorometer from Horiba equipped with an integrating sphere Quanta-phi.

Fluorescence decay times were measured via time correlated single photon counting (TCSPC) on a FluoroLog 3 Spectrofluorometer equipped with a DeltaHub module and NanoLEDs (λ = 435 nm and 635 nm, Horiba) as excitation sources. Data analysis was carried out with DAS6 software (www.horiba.com) using a mono-exponential fit.

The photostability of the dyes was accessed by irradiating water-free toluene solutions with an array of 12 green high power LEDs (λ = 528 nm, OSRAM Oslon SSL 80, www.led-tech.de) equipped with a cooling block and a focusing lens from Edmund optics (www.edmundoptics.de). The photostability of the deprotonated form of **2a** was accessed by irradiating water-free toluene solutions with an array of 12 red high power LEDs (λ = 635 nm, OSRAM Oslon SSL 80, www.led-tech.de) equipped with a cooling block and a focusing lens from Edmund optics (www.edmundoptics.de). The absorption spectra were acquired each 15-30 min. The photon flux was 15600 μmol s^{-1} m^{-2} for the green LEDs and 19999 μmol s^{-1} m^{-2} for the red LEDs, respectively as measured by a Li-250A light meter from Li-COR, (www.licor.com).

The pH of buffer solutions (CAPS, MOPS, TRIS and disodium phosphate) was adjusted with a pH meter (Education Line, Mettler Toledo, www.mt.com) using a glass electrode (InLab Routine Pro, Mettler Toledo, www.mt.com). The pH meter was calibrated at 25 °C with standard buffer solutions of pH 4.01, pH 7.01 and pH 10.01 (Hanna Instruments, www.hannainst.com). The ionic strength (0.15 M) of the buffers was adjusted with sodium chloride as background electrolyte.

For the leaching experiments, the sensor foil (hydrogel D4) was fixed in a home-made flow-through-cell. Buffer solutions (pH 6.6, pH 12.5, IS 0.15 M) were pumped through the cell at a constant flow and absorption spectra were recorded over 24 hours. A peristaltic pump equipped with a flexible tube from Ismatec (www.ismatec.com; purple/black, ID: 2.29 mm) was used.

For carbon dioxide measurements the sensor foil (CO2_1-9) was fixed in a home-made flow-through-cell connected to a gas mixing device. Gas calibration mixtures were produced with a gas mixing device from Voegtlin (www.voegtlin.com, red-y for gas flow) and a constant flow (200 mL/min) was controlled by LabView software. The flow-through-cell was filled with water which was purged with gas mixtures. In case of the measurement in the gas phase, relative humidity of 85% was adjusted via bubbling of the gas through saturated potassium chloride solution. Temperature was controlled with a cryostat Thermostat Thermo Haake K10.

3.5 Results and Discussion

3.5.1 Synthesis

Perylene bisimides are suitable for different synthetic modifications in the imide and bay regions of the chromophore.[15,25,187,188,191] Lateral extension of the conjugated system in the bay-region represents an interesting possibility to induce bathochromic shift of absorption and emission.[49] We chose fluorescent dye **1** as a starting compound due to high solubility rendered by diisopropylphenyl groups at the imide position and commercial availability. Strong electron-withdrawing character of the imide groups enables the reaction with a strongly nucleophilic sodium amide and a dipolar aprotic solvent benzonitrile to yield 2-phenyl-imidazole-substituated perylene bisimides (**Figure 3-1**). Mono-substituted derivatives **2a**, **2b** and **2c** were obtained from various benzonitriles as well as the doubly-substituted **3a** in case of benzonitrile. Notably, no doubly-substituted products were formed when 4-chlorobenzonitrile and 2,6-dichlorobenzonitrile were used. Although use of other benzonitriles is likely to be possible, we selected the chlorine-substituted derivatives due to the electron-withdrawing effect of the halogens and therefore expected lowering of the pK_a value (see below) of the perylene bisimide dyes. In case of doubly substituted perylene **3a** formation of different isomers is possible and indeed was observed during the reaction. The isomer **3a** can be isolated in a pure form with the position of the substituents confirmed by the ^{1}H and ^{13}C NMR spectra (**Figure S 3-9-25**, Supporting Information).

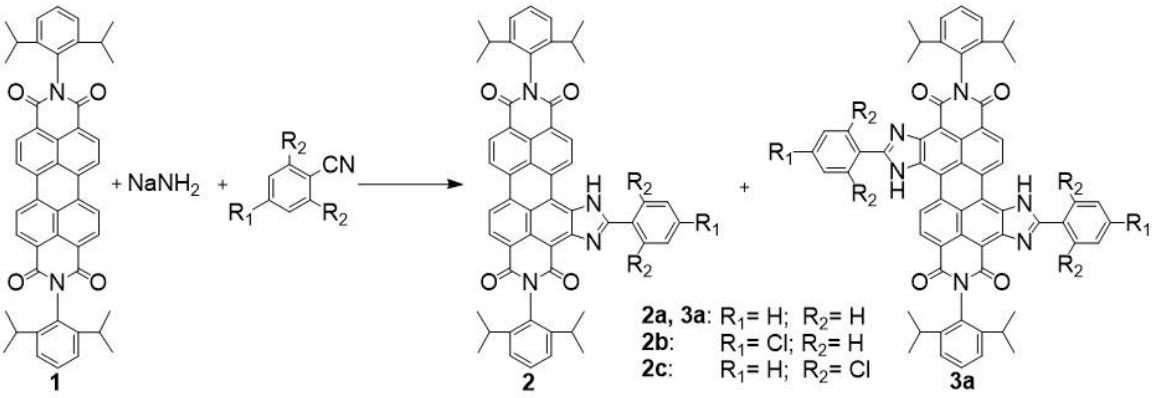

Figure 3-1 One-pot synthesis of laterally extended perylene bisimide dyes. Double substitution with 2-phenyl-imidazole-groups could only be observed for **3a.**

3.5.2 Photophysical Properties

Introduction of 2-phenyl-imidazole substituents in the bay position of the perylene chromophore results in strong bathochromic shift of the absorption and emission spectra (**Figure 3-2A**). Compared to **1,** the spectra of the mono-substituted dyes **2a**, **2b** and **2c** (neutral form) shift by ~ 55-65 nm, whereas the shift is as high as 115 nm for the di-substituted **3a** (**Table 3-2**). The absorption maximum of **2c** is hypsochromically shifted by ~ 12 nm compared to **2a** and **2b** may be

due to the electron-withdrawing character of the chlorine atoms and the decreased conjugation of the phenyl-substituent because of sterical hindrance. The molar absorption coefficients are rather high (**Table 3-2**) and are comparable to those of **1** (80 300 M^{-1} cm^{-1}).[192]

Table 3-2 Photophysical properties of perylene dyes in tetrahydrofuran. Absorption maxima (λ_{abs}), molar absorption coefficients (ε), emission maxima (λ_{em}), fluorescence quantum yields (Φ), fluorescence lifetimes (τ) for the acidic and the basic forms.

Dye	λ abs-acidic [nm]	λ abs-basic[a] [nm]	ε acidic [M^{-1} cm^{-1}]	ε basic [M^{-1} cm^{-1}]	λ em-acidic [nm]	λ em-basic[a] [nm]	Φ acidic	Φ basic[a]	τ acidic [ns]	τ basic[a] [ns]
2a	589	676	101300	55500	597	735	0.99	0.10	5.3	3.2
2b	590	673	71800	40300	597	736	0.99	0.10	5.3	3.1
2c	578	662	75900	47300	584	713	0.98	0.15	5.3	4
3a	635	736[b]	96600	48400[b]	646	776[b]	0.85	0.25[b]	6.4	2.8[b]
		789[c]		80400[c]		802[c]		0.05[c]		3.1[c]

[a] basic form is generated by addition of TOAOH to the solution
[b] mono-anionic form, generated by addition of TOAOH to the solution and bubbling with CO_2
[c] di-anionic form generated by addition of TOAOH to the solution

All the mono-substituted dyes in the neutral form show very strong fluorescence with quantum yields approaching unity (**Table 3-2**) and small Stokes shifts of ~ 8 nm. The fluorescence quantum yield of **3a** is only slightly lower (0.85). Overall, the brightness of the dyes (defined as a product of molar absorption coefficients and fluorescence quantum yields) is excellent. Additionally, an intense absorption band (ε ~ 40 000 M^{-1} cm^{-1}) which is located at ~50 nm shorter wavelength than the main band represents a very nice feature for practical applications since it efficiently enhances the effective Stokes shift and therefore enables collection of the full emission spectrum with a simple optical set-up.

Intrinsic pH sensitivity is the most striking property of the dyes. In basic media, deprotonation results in a strong bathochromic shift of the absorption and emission spectra of the mono-substituted dyes (**Figure 3-2B**) which is about 85 and 130 nm, respectively (**Table 3-2**). Such behaviour is typical for pH indicators based on a intramolecular charge transfer [93,98]. **3a**, bearing two imidazole groups, shows formation of the mono-anionic and the di-anionic forms which are bathochromically shifted by ~100 and 150 nm, respectively, compared to the neutral form of the dye (**Figure 3-2C**). Notably, absorption and emission spectra become significantly broader upon deprotonation. Broadening of the absorption spectra correlates well with decrease of the molar absorption coefficients. Interestingly, the di-anionic form of **3a** shows much smaller broadening and the molar absorption coefficients similar to those of the neutral form which may be due to symmetrical character of the formed species. The fluorescence quantum yields for the deprotonated form are about 10-fold lower than for the neutral form (**Table 3-2**). Overall, considering that the brightness of NIR dyes is generally significantly lower than that of the UV-Vis chromophores, the new dyes in the deprotonated form can be viewed as moderately strong NIR emitters.

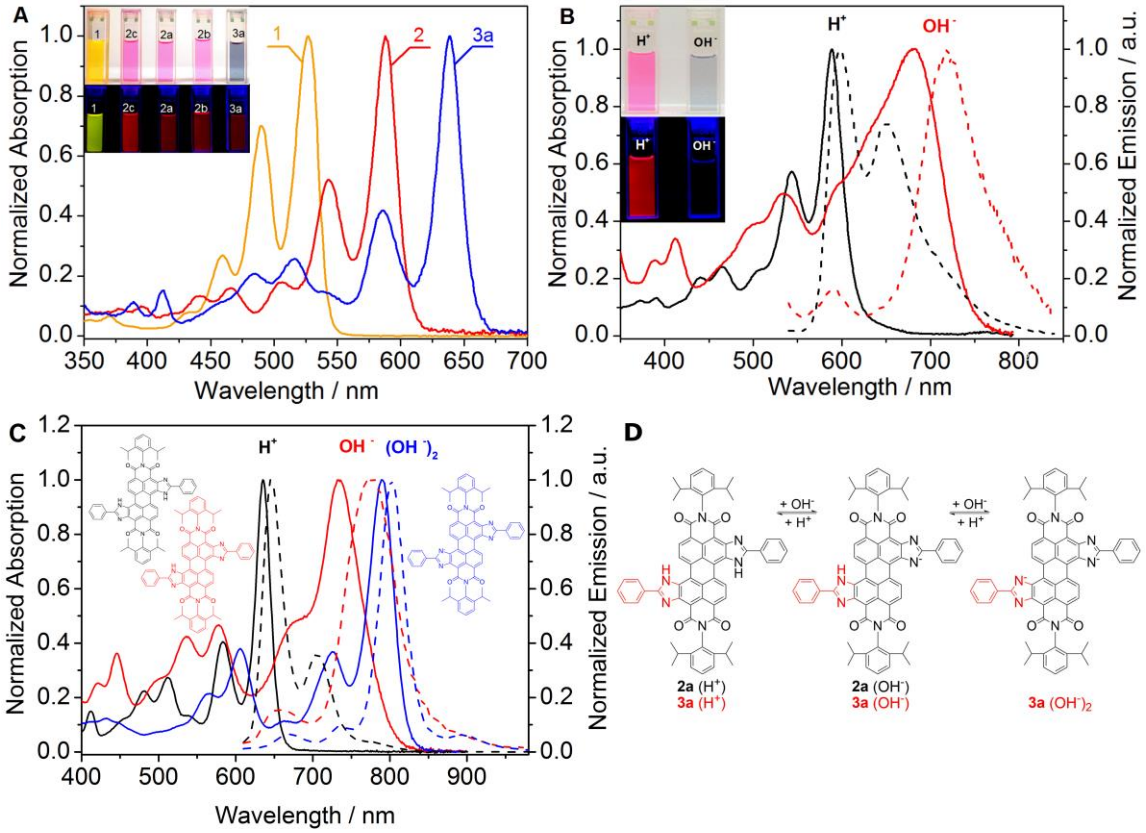

Figure 3-2 Spectral properties of the perylene dyes. A: absorption spectra of **1**, **2** and **3a** in tetrahydrofuran. B: representative absorption spectra (solid lines) and emission spectra (dashed lines) of neutral form (black) and of anionic form (red) of **2a** in tetrahydrofuran. The inserts show the photographic images of the dye solutions under daylight and UV illumination (365 nm), respectively. C: absorption spectra (solid lines) and emission spectra (dashed lines) of neutral form (black), mono-anionic form (red) and di-anionic form (blue) of **3a** in tetrahydrofuran. D: equilibrium of neutral and anionic forms of **2a** and **3a**.

The fluorescence lifetimes of the neutral forms are in a range of 5.3-6.4 ns (**Table 3-2**), which is typical for perylene fluorophores.[193] The lifetimes of the negatively charged forms are 1.3-3.6 ns shorter. The introduction of chlorine does not affect the lifetimes of the neutral forms. However, the enlargement of the conjugated system in **3a** results in a slight increase of the fluorescence lifetime. Perylene dyes are known for their extraordinary high photostability.[31] Irradiation of the neutral forms of the dyes in toluene solution with a green high power LED array (λ_{max} 528 nm, light intensity = 353 mW cm^{-2}) over 240 min did note result in any detectable bleaching (**Figure 3-3**). In contrast, irradiation of the basic form of **2a** in toluene solution with a red high power LED array (λ_{max} 635 nm) of comparable intensity (377 mW cm^{-2}) over 240 min showed degradation of about 6% of the dye (**Figure 3-3**). Lower photostability of the basic form may be due to the more electron-rich character of the core and therefore more favourable photo oxidation. Nevertheless, even in case of the anionic form the photostability is still sufficiently high considering very high light intensities used.

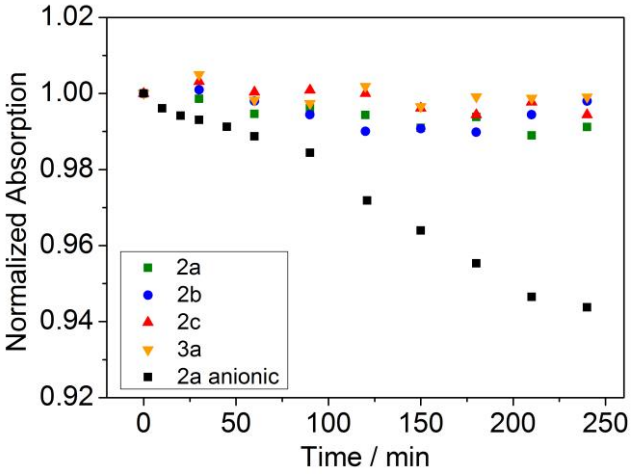

Figure 3-3 Photodegradation profiles of the neutral forms of **2a, 2b, 2c, 3a** and the anionic form of **2a** in toluene.

3.5.3 pH Sensing Properties

As was mentioned above, all the dyes show pH-dependent spectral properties. More detailed investigation conducted for THF/EtOH/aqueous buffered solution (3:2:2, v/v) revealed the pK_a values of 10.15-10.8. The values are slightly lower for **2b** compared to **2a**, **2c** and **3a** (**Table 3-3**). This effect can be explained by electron-withdrawing character of the chlorine atom in **2b** which enhances the acidity of imidazole. On the other hand, the sterical hindrance introduced by the two chlorine atoms in ortho-position in **2c** appears to compensate for the electron-withdrawing effect.

In order to enable continuous measurements of pH it is essential to immobilize an indicator dye into a proton-permeable polymer matrix. Two most common methods rely on covalent coupling of the dye to the polymer and noncovalent physical entrapment. Covalent coupling prevents leaching out of the matrix and migration, but further synthetic steps are necessary to introduce functional groups for coupling, which may also negatively affect the photophysical properties of the indicator. Moreover, noncovalent immobilization is a simple method to obtain pH sensors providing that the adequate combination of the indicator and the matrix is found. Planar solid state pH sensors were obtained by immobilization of the new perylenes into a commercially available polyurethane hydrogel (Hydromed D4) consisting of hydrophilic and hydrophobic domains and a water content in the swollen state of 50% of weight.[194]

As can be seen in **Table 3-1**, the pH-sensing behaviour of the immobilized dyes is very similar to that of the dyes in solution. Several isosbestic points are clearly visible in the absorption spectra, which indicates the equilibrium between two species (neutral and anionic) (**Figure 3-4A**). Thus, the new perylene dyes are suitable for colorimetric read-out.

Table 3-3 pH sensing properties of the perylene dyes in solutions and embedded in Hydrogel D4. Ionic strength (NaCl) 0.15 M, T = 25 °C

THF/EtOH/Buffer 3:2:2 (v/v)		Hydrogel D4			
Dye	**$pK_{a\ Abs}$**	**$\lambda_{abs\text{-}acidic}$ / $\lambda_{abs\text{-}mono\text{-}anionic}$ [nm]**	**$pK_{a}'_{Abs}$**	**$\lambda_{em\text{-}acidic}$ / $\lambda_{em\text{-}mono\text{-}anionic}$ [nm]**	**$pK_{a}'_{Em}$**
2a	10.63	596/689	10.88	608/728	10.14
2b	10.15	596/684	10.73	608/720	9.84
2c	10.78	586/664	11.45	595/708	10.56
3a	10.68	650/731	11.36	662/768	10.15

The apparent pK_a values determined from the absorption spectra are slightly higher for the immobilized dyes compared to the dissolved ones (**Table 3-3**). This may be due to localization of the indicators in the more hydrophobic domains of the hydrogel where deprotonation (resulting in formation of the charged form of the dye) is less favoured. Similarly to the absorption spectra, the fluorescence spectra show the existence of two forms (**Figure 3-4B**) which enables ratiometric read-out. The apparent pK_a' values in hydrogel D4 determined from the fluorescence spectra are 0.7-1.2 pH units lower than those obtained from absorption measurements (**Table 3-3**). This disparity of the pK_a' values can be explained by Förster resonance energy transfer (FRET) from the neutral to the deprotonated form of the dye. In fact, FRET is favoured by the good overlap between the absorption spectrum of the deprotonated form and the emission spectrum of the neutral form (**Figure 3-2B**) and by comparably high concentration of the dye in the polymer which results in a short distance between donor and acceptor molecules.

Evidently, because of the high pK_a' values, the new sensors are not suitable for conventional applications (biotechnology, biology and medicine). On the other hand, the new materials are promising for pH measurement under alkaline conditions. Potential applications include the measurement of pH on the surface of concrete, that is known for extremely alkaline conditions, which however change due to microbiological activity and interaction with acidic gases thus promoting corrosion of steel.[195,196] Here, optical pH sensors can be a promising alternative to pH electrodes because they do not suffer from alkali error, are easy to miniaturize and be also used for imaging of pH distribution. The new sensors may also be used in studies involving alkaliphilic microorganisms which are of great interest for many biotechnological applications as well as in detergent and textile industries.[197–199]

The response of the sensors to dynamic pH changes is reversible (**Figure S 3-4 and 3-5**, Supporting Information) but fairly slow (t_{90} ~ 77 s) considering comparably small thickness of the sensing layer (~2.5 µm). Some hysteresis in the response is also observed. This behaviour suggests localization of the dyes mostly in the hydrophobic domains of the hydrogel and some redistribution upon (de)protonation. Similar behaviour was previously observed for other hydrophobic perylene

dyes [41]. It may be overcome by covalent immobilization of the dyes in polymeric matrixes [42] or by increasing the hydrophilicity of the perylene (e.g. by employing other substituents in the imide position) and represents a room for future improvements.

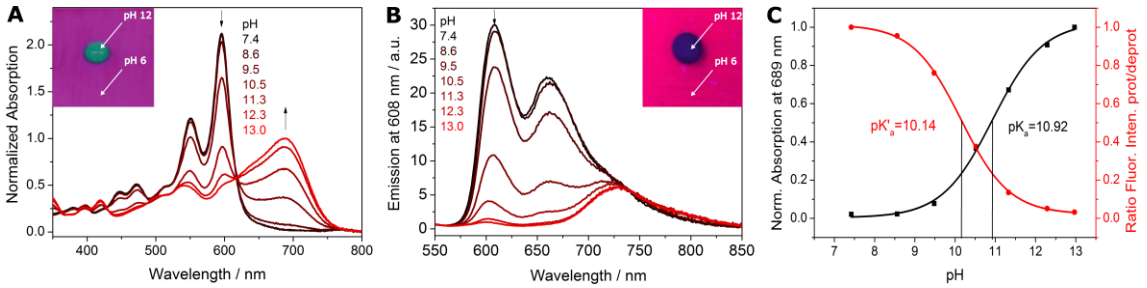

Figure 3-4 pH sensing properties of **2a** embedded into polyurethane hydrogel D4. A and B: pH dependence of absorption and fluorescence spectra, respectively. C: corresponding calibration curves. The inserts in A and B show photographic images of the sensor foils under daylight and UV illumination (365 nm), respectively.

3.5.4 Carbon Dioxide Sensors

High pK_a' values of the dyes imply their potential suitability for carbon dioxide sensing. Solid state or "plastic" optical carbon dioxide sensors rely on pH indicators embedded into polymers along with a lipophilic base, most commonly a quaternary ammonium base.[157,161,163,200] Several sensing materials based on ethylcellulose as a matrix have been manufactured to systematically investigate the influence of the indicator (**2a**, **2b**, **2c** and **3a**), base (tetraoctylammonium hydroxide and tetrabutylammonium hydroxide) and plasticizer (tributyl phosphate). The sensor composition is schematically shown in **Figure 3-5A**. A porous Teflon membrane was applied over the sensing layer to provide homogenous white background and to eliminate the influence of ionic species in case of solution measurements.

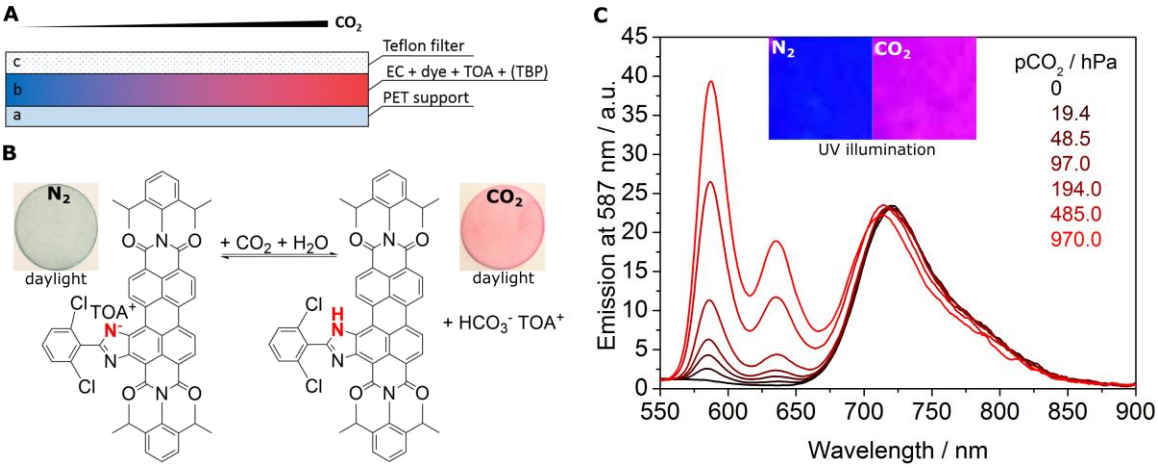

Figure 3-5 A: Cross-section of the optical carbon dioxide sensor. B: Sensing mechanism and photographic images of the planar sensor foil based on **2c** in ethyl cellulose with tributyl phosphate as plasticizer (1:2 w/w, material CO2_3) measured in water purged with nitrogen and 100% carbon dioxide, recorded under daylight. C: Corresponding emission spectra (λ_{exc} 493 nm) for CO2_3 sensor measured in water at different pCO_2 and photographic images of sensor under UV illumination (365nm).

As can be seen (**Figure 3-5B**) the sensors indeed respond to carbon dioxide. The color of the sensor changes from blue (in the absence of carbon dioxide) to red (in the presence of carbon dioxide), which enables colorimetric measurements of carbon dioxide. Increase in CO_2 concentration also results in appearance of the strong red fluorescence. The corresponding emission spectra (**Figure 3-5C**) show an increase of the fluorescence of the neutral form (λ_{max} 587 nm) in the presence of carbon dioxide. In contrast, the fluorescence intensity at 720 nm corresponding to the deprotonated form is nearly constant. The likely reason is a fairly efficient FRET from the neutral to the deprotonated form of the dye. Thus, a strong increase of the absorption of the neutral form at the excitation wavelength (λ_{exc} 493 nm) at high pCO_2 results in higher fluorescence intensity of the neutral form but also for the deprotonated form (via FRET), which compensates for the decrease in the concentration of the deprotonated form. Referenced ratiometric measurements at two emission wavelengths are clearly possible.

The sensitivity of carbon dioxide sensors is known to be governed by the pK_a value of the indicator and by many other reasons such as presence of a plasticizer.[141,158] **Figure 3-6A** shows that despite rather high pK_a values all the materials show comparably low sensitivity. All sensors operate in a dynamic range from 10 to 970 hPa pCO_2, which make them interesting candidates for Modified Atmosphere Packaging applications.[170] In good agreement with the pK_a values (**Table 3-3**), the sensitivity is the highest for **2c** (the highest pK_a) and the lowest for **2b** (the lowest pK_a) whereas **2a** occupies the intermediate position. Sensitivity of **3a** (first deprotonation step) is comparable to that of **2c**, however sterical reasons and lipophilicity of the dye might be additional contributing factors. The less sensitive sensors based on **2a** and **2b** (CO2_1 and CO2_2, respectively) are promising for measurements of carbon dioxide pressures >970 hPa, typical for beverage industry[168,171,201], because they show high residual protonation capability compared to the sensors based on **2c** and **3a** (CO2_3 and CO2_8, respectively) at 970 hPa pCO_2 (**Figure 3-6A**).

The sensitivity of the sensors is dramatically affected by presence and concentration of a plasticizer (**Figure 3-6B**). Whereas the sensor is almost insensitive in pure ethyl cellulose, the ratio of plasticizer to the polymer of 2:1 ensures the optimal response. The plasticizer is likely to influence the diffusion and solubility of carbon dioxide but also to alter polarity of the environment and water uptake. Thus, adjustment of the ratio of plasticizer to the polymer represents an excellent possibility for fine tuning of the sensor sensitivity. Further adjustment of the sensor sensitivity can be achieved by substitution of tetraoctylammonium hydroxide with tetrabutylammonium hydroxide. Shorter carbon chains of the latter are associated with higher sensitivity of the sensors most likely due to higher hydrophilicity of the dye environment (**Figure S 3-7-8** Supporting Information).

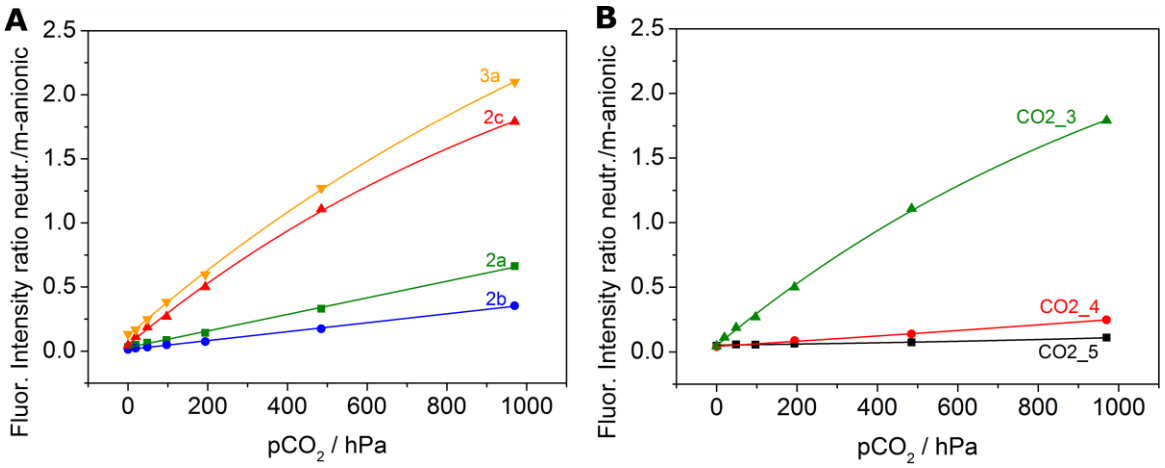

Figure 3-6 Carbon dioxide sensing properties of various materials measured in water at 25 °C A: Response of the sensors based on **2a, 2b, 2c** and **3a** in ethyl cellulose with tributyl phosphate as plasticizer (1:2 w/w, materials CO2_1, CO2_2, CO2_3 and CO2_8, respectively). B: Influence of plasticizer on the response of the sensor based on **2c**. Ethyl cellulose to tributyl phosphate ratio: 1:0 (CO2_5), 2:1 (CO2_4), 1:2 (CO2_3).

Humidity also plays an important role for response of the sensor material and it has to be adjusted accurately. Since the highest reproducibility of calibrations of fabricated sensor materials could be achieved by using a flow-through cell filled with water and bubbled with carbon dioxide, this setup was utilized for all measurements. Although the sensor shows response in the gas phase as well, the sensitivity at 85% relative humidity is significantly lower compared to water (**Figure S 3-8**, Supporting Information). Because of such a strong cross-talk application of the new sensors in the gas phase might be problematic.

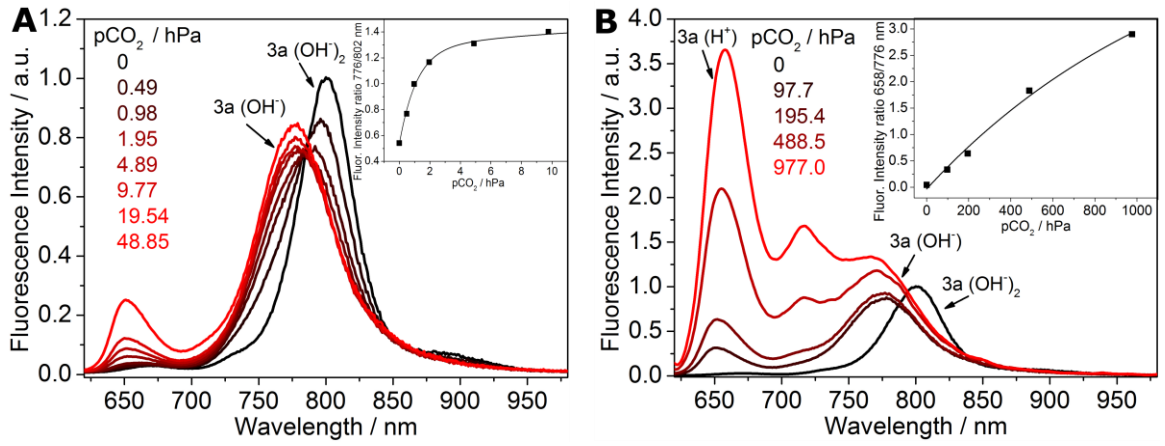

Figure 3-7 Response of the sensor based on **3a** (CO2_9, 25 °C, 85% relative humidity, λ_{exc} 590 nm) for the range from 0 to 49 hPa pCO_2 (A) and from 98 to1000 hPa pCO_2 (B). The inserts show the corresponding calibration curves. Equilibrium of neutral, mono-anionic and dianionic forms of **3a** is shown in Fig. 2D.

In contrast to mono-substituted dyes **2a-c**, di-substituted **3a** features two pH-sensitive groups. This results in unique behaviour which enables ratiometric sensing of carbon dioxide in two different dynamic ranges with a single indicator dye. Notably, all the three forms of the indicator (neutral, mono-anionic and dianionic) are fluorescent (λ_{max} 658, 776 and 802 nm, respectively) (**Figure 3-7**). The mono-anionic form is converted into the neutral form at comparably high pCO_2 (20-1000 hPa). In this dynamic range, the behaviour of the sensor is similar to that of the materials based on **2a-c.** In contrast, the dianionic form is stable only at very low pCO_2 (**Figure 3-7A**). It is completely converted into the mono-anionic form at ~ 2 hPa pCO_2. Remarkably, the pCO_2 well around atmospheric levels of 0.4 hPa can be resolved excellently. Thus, the sensor based on **3a** covers an extremely broad dynamic range from 0 to 1000 hPa pCO_2 which is unprecedented in the literature.

3.6 Conclusions

In summary, we introduced a new class of pH indicators based on bay-modified perylene dyes which can be utilized for optical pH sensors as well as for optical carbon dioxide sensors. The dyes show high luminescence brightness, extraordinary good photostability and versatility in respect to chemical modification. The indicators are accessible via a simple one-step reaction starting from commercially available Lumogen Orange. Characteristic perylene bisimide absorption and emission spectra for neutral and deprotonated forms enable colorimetric as well as ratiometric measurements of pH and carbon dioxide. The high pK_a values enable preparation of optical pH sensors for measurements in alkaline conditions. The sensitivity of the carbon dioxide sensor can be adjusted via variation of the dye, ratio of plasticizer to polymer and by varying the nature of the quaternary ammonium base. The di-substituted perylene shows unique behaviour with two protonation/deprotonation equilibria enabling sensing of carbon dioxide in unprecedentedly broad dynamic range. Whereas the new carbon dioxide sensors are likely to be promising for application in food packaging and beverage industry, the pH sensors with the response in the alkaline media are of interest for research on alkaliphilic bacteria and monitoring of pH in concrete. Here, excellent chemical and photochemical stability of the new indicators is expected to be very valuable for long-term deployment of the sensors.

Acknowledgements

Financial support by the Austrian Academy of Science (ÖAW) at the Institute of Analytical Chemistry and Food Chemistry, Graz University of Technology (DOC-Fellowship of David Pfeifer) is gratefully acknowledged. The authors also thank Prof. Hansjoerg Weber, Institute of Organic Chemistry, Graz University of Technology for the help in acquisition of the NMR spectra.

3.7 Supporting Information

3.7.1 pH Sensing Properties

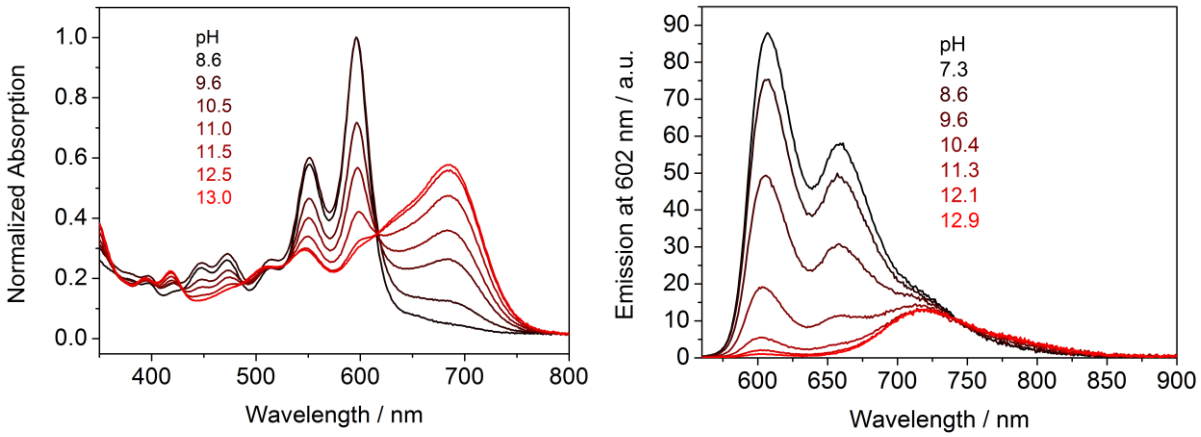

Figure S 3-1 pH dependence of absorption (left) and fluorescence (right) spectra of **2b** embedded in hydrogel D4, measured at 25 °C (λ_{exc} 528 nm).

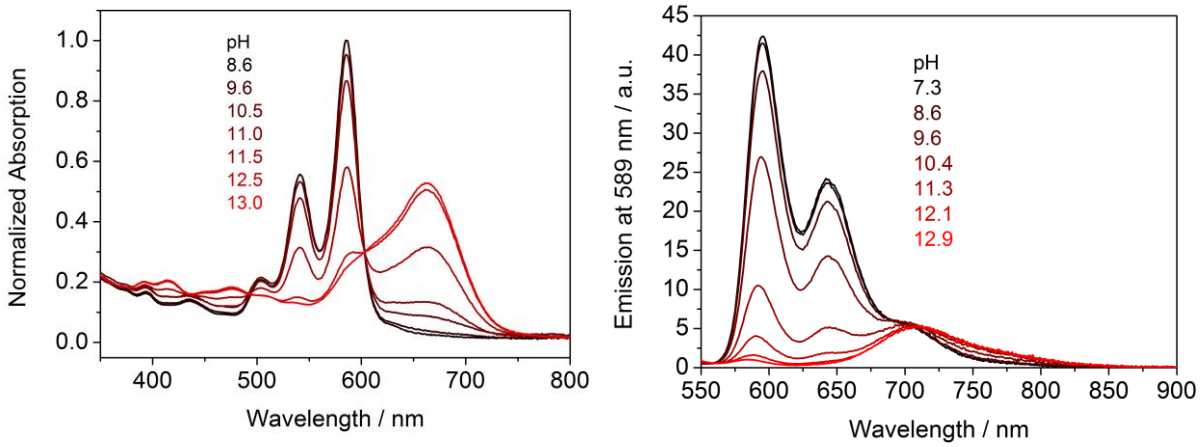

Figure S 3-2 pH dependence of absorption (left) and fluorescence (right) spectra of **2c** embedded in hydrogel D4, measured at 25 °C (λ_{exc} 493 nm).

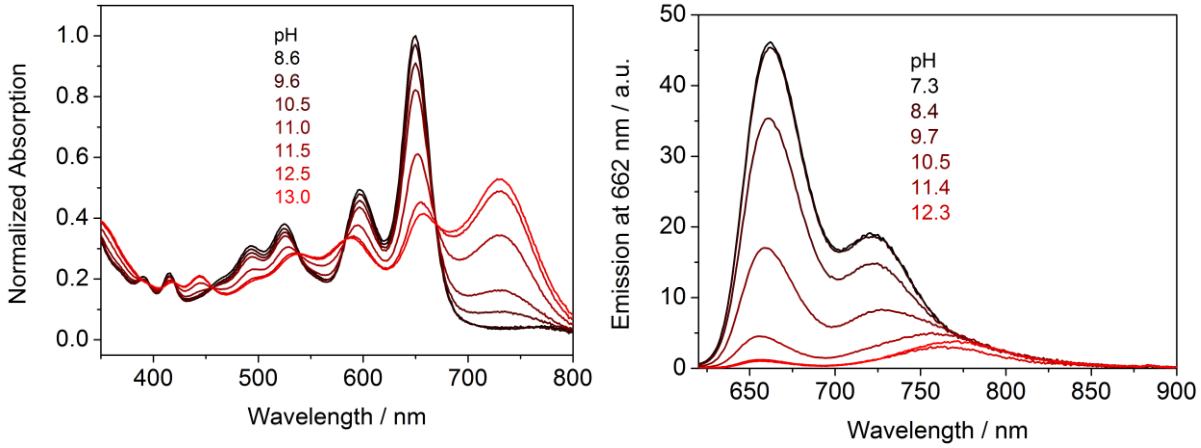

Figure S 3-3 pH dependence of absorption (left) and fluorescence (right) spectra of **3a** embedded in hydrogel D4, measured at 25 °C (λ_{exc} 590 nm).

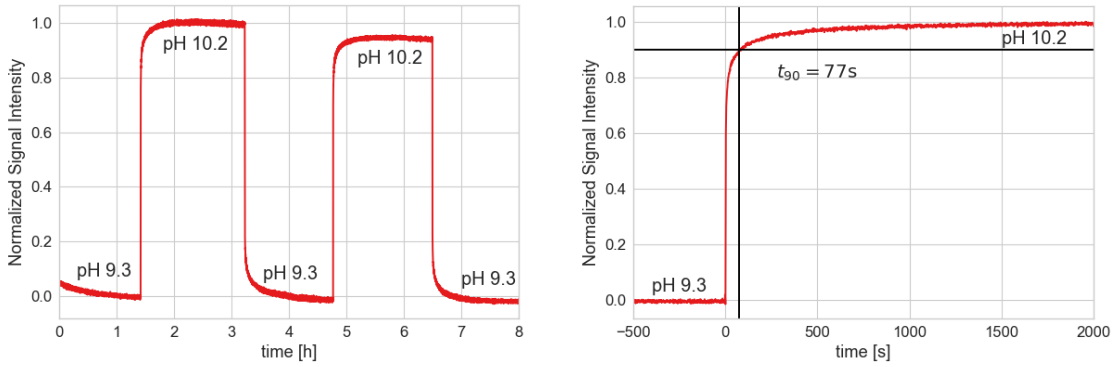

Figure S 3-4. Reversible sensor response to dynamic pH changes measured in buffer solutions at 25 °C (left). Measurement of t_{90} response time from pH 9.3-10.2 at 25 °C (right).

3.7.2 Carbon Dioxide Sensing Properties

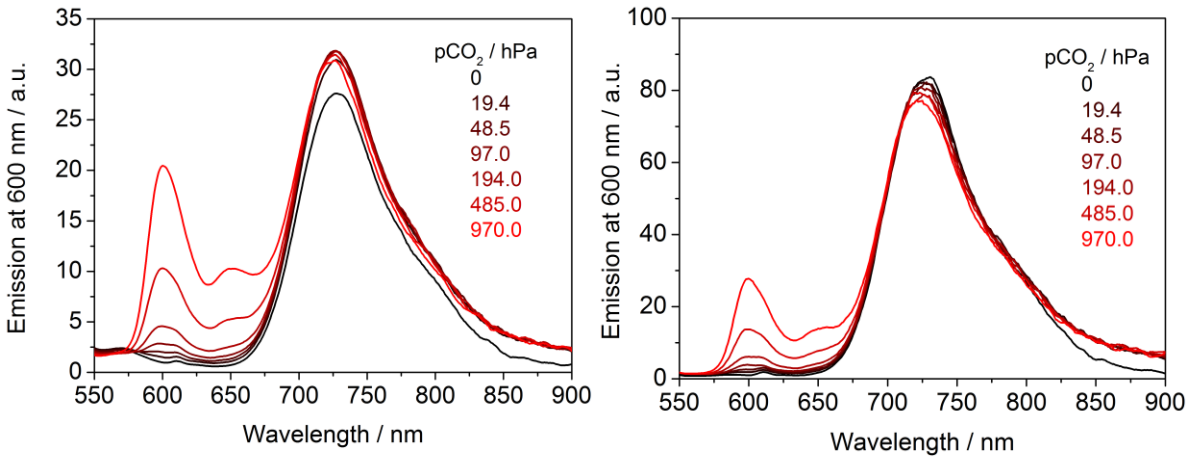

Figure S 3-5 Fluorescence spectra of CO2_1 (left) and CO2_2 (right) sensor foil measured in water at different pCO_2 (25 °C).

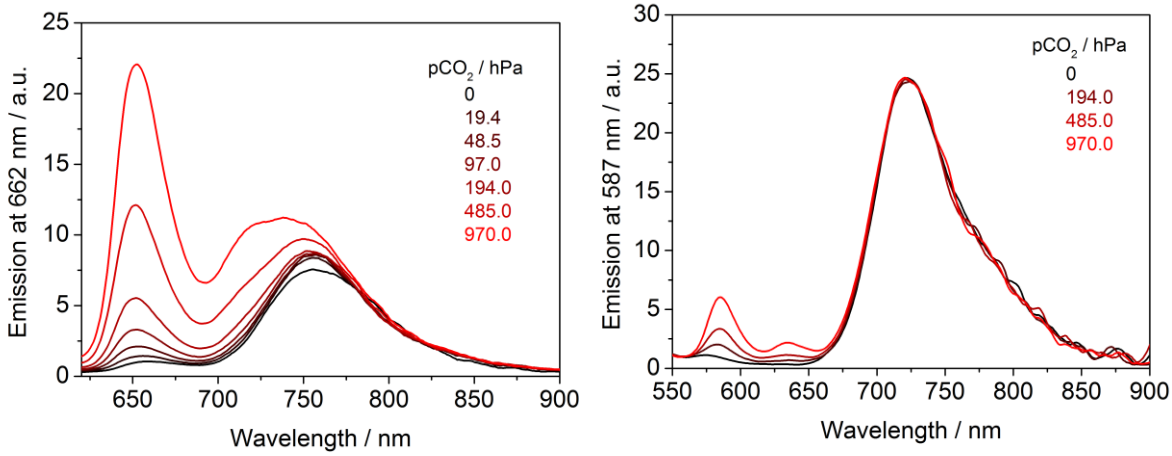

Figure S 3-6 Fluorescence spectra of CO2_8 (left) and CO2_4 (right) sensor foil measured in water at different pCO_2 (25 °C).

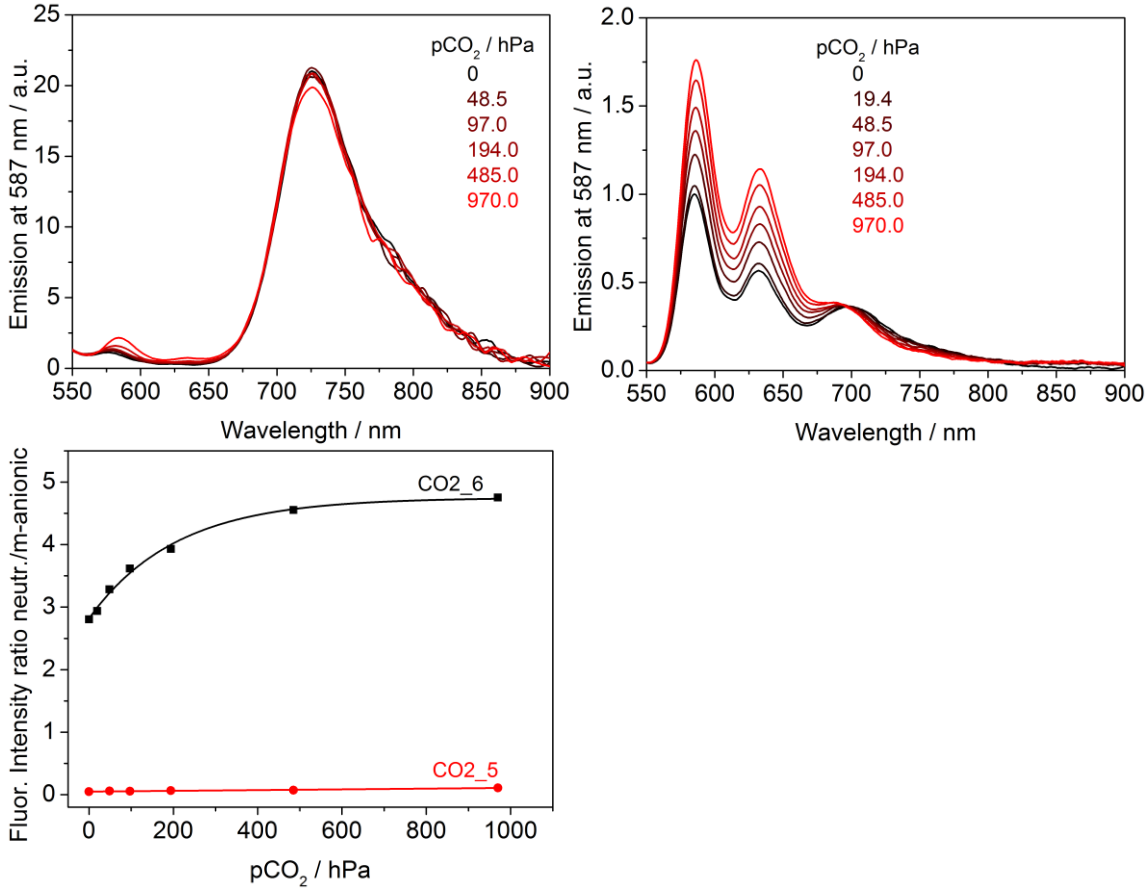

Figure S 3-7 Fluorescence spectra of CO2_5 (left) and CO2_6 (right) sensor foil measured in water at different pCO_2 (25 °C). Corresponding calibration curves of CO2_5 and CO2_6 (bottom).

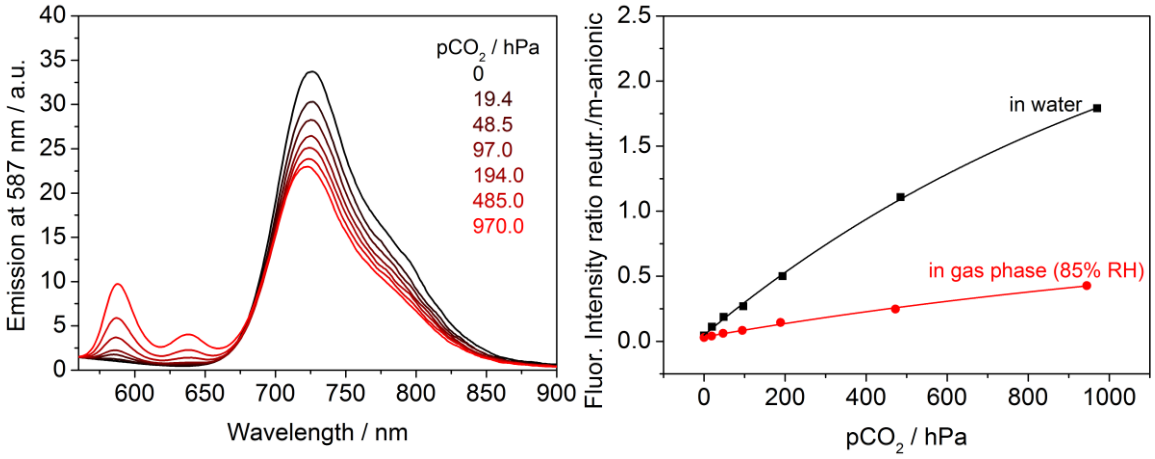

Figure S 3-8 Fluorescence spectra of CO2_3 sensor foil measured in gas phase at 85% relative humidity at different pCO_2, regulated by bubbling CO_2 through saturated KCl solution (25 °C) (left). Corresponding calibration curves of CO2_3 sensor foil calibrated in water and in gas phase at 85% relative humidity (right).

3.7.3 NMR Spectra

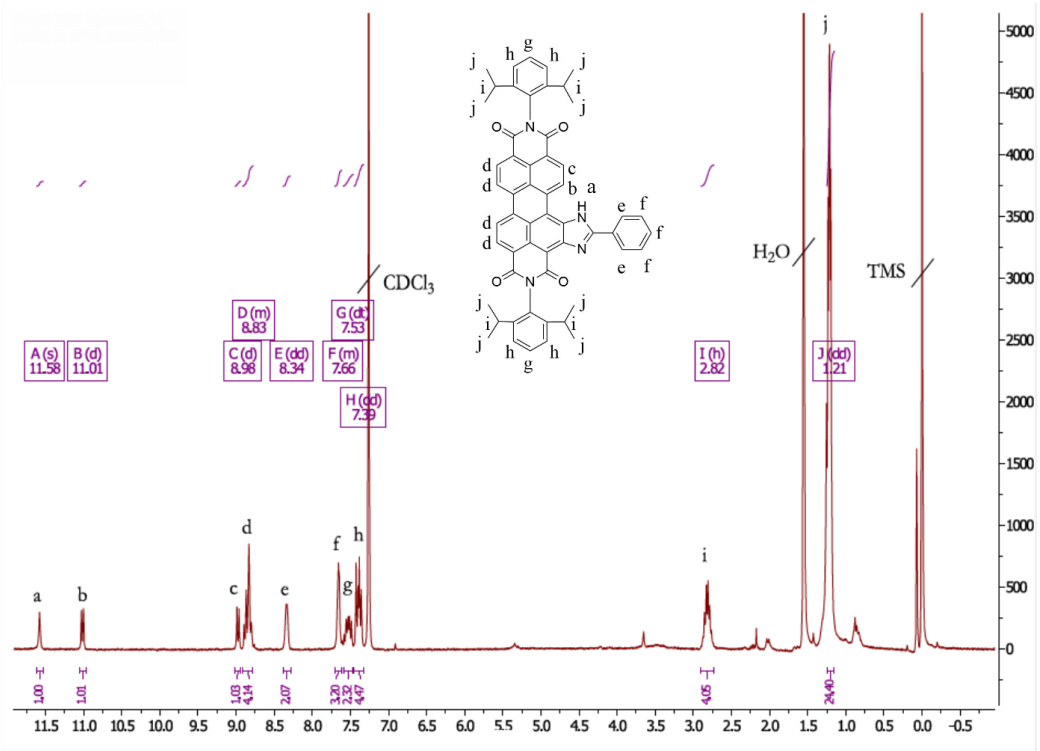

Figure S 3-9 ^{1}H NMR ($CDCl_3$, 300 MHz) of **2a**.

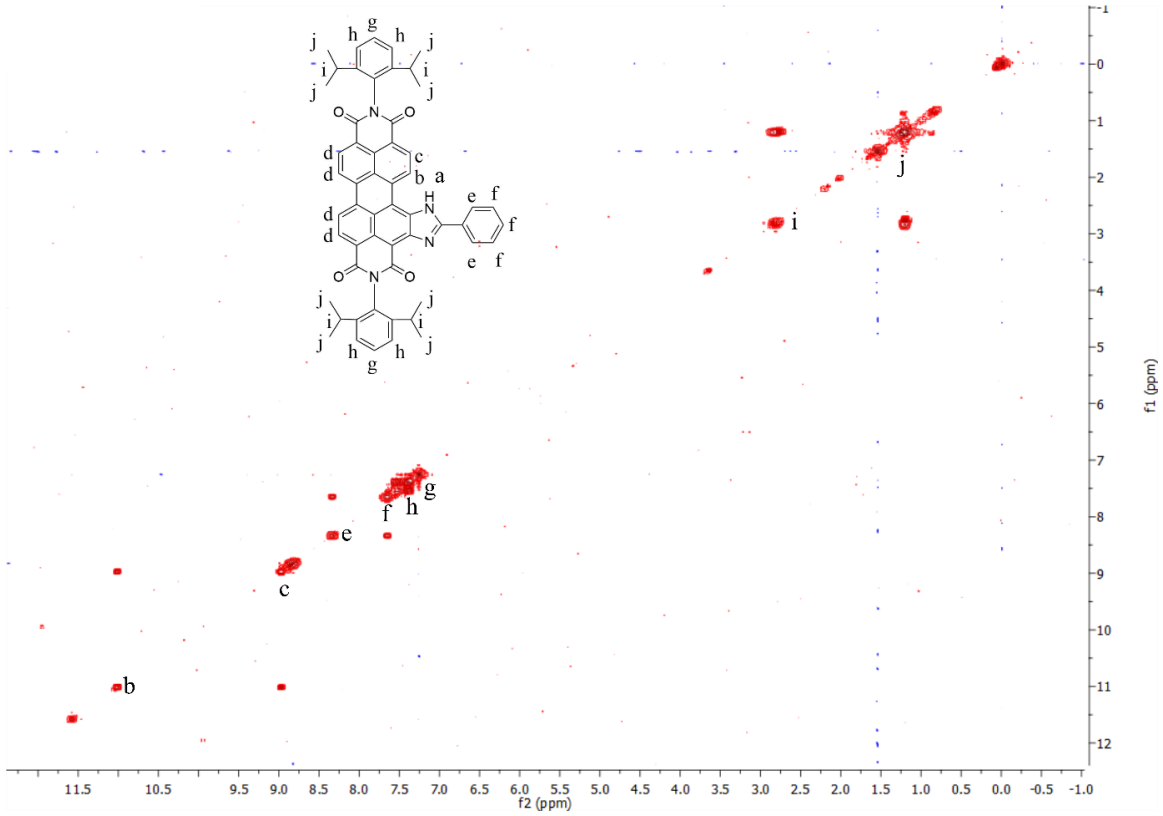

Figure S 3-10 ^{1}H-Cosy NMR ($CDCl_3$, 300 MHz) of **2a**.

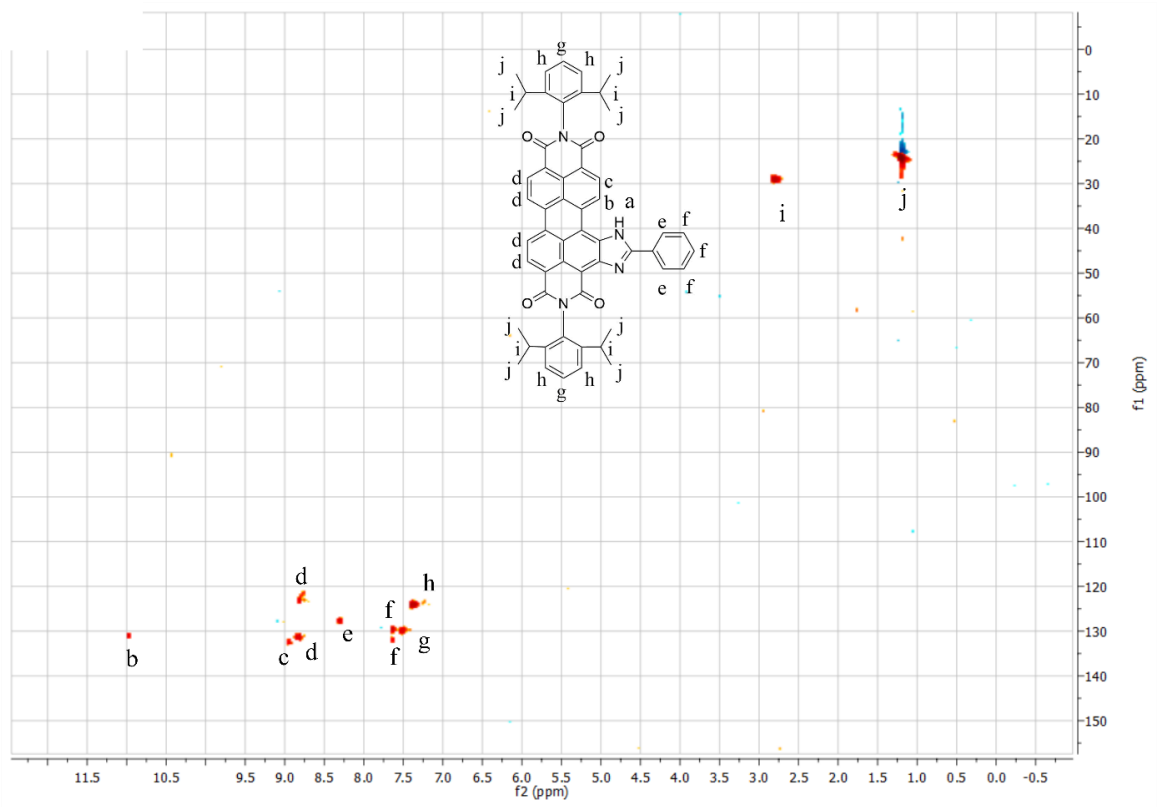

Figure S 3-11 HSQC NMR ($CDCl_3$, 500 MHz, 126 MHz) of **2a.**

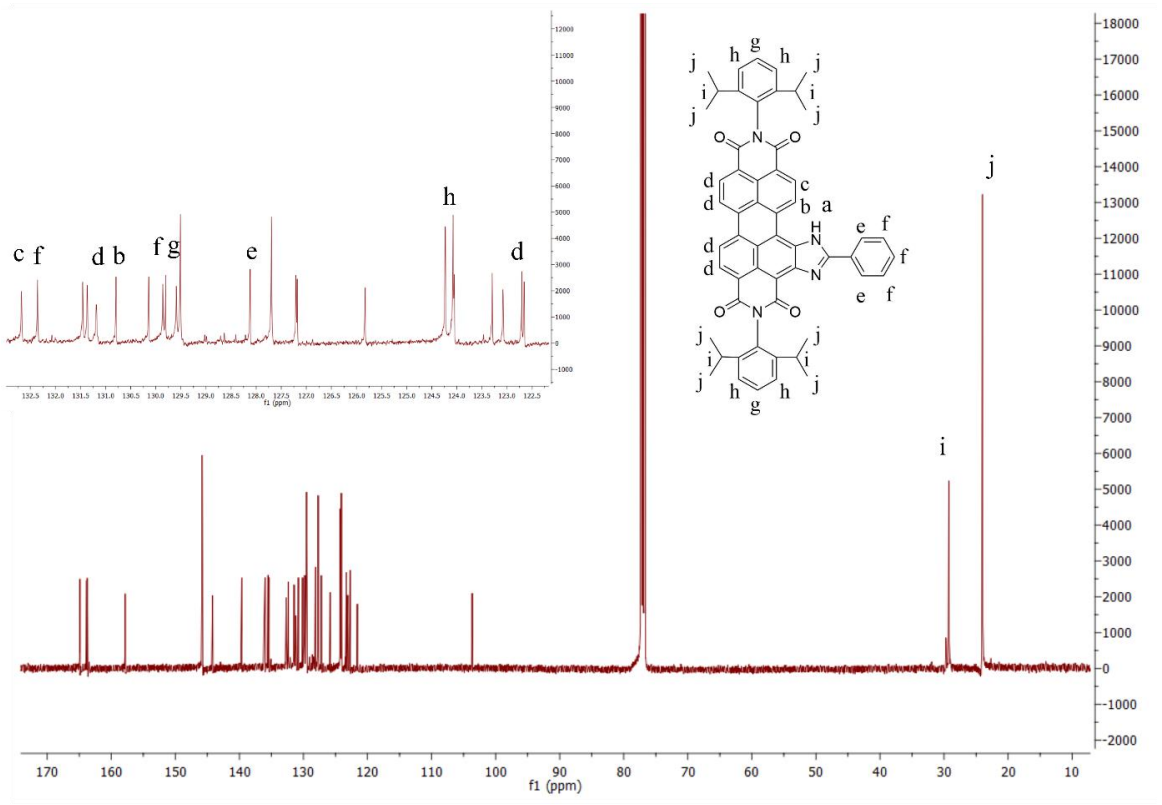

Figure S 3-12 ^{13}C NMR ($CDCl_3$, 126 MHz) of **2a**.

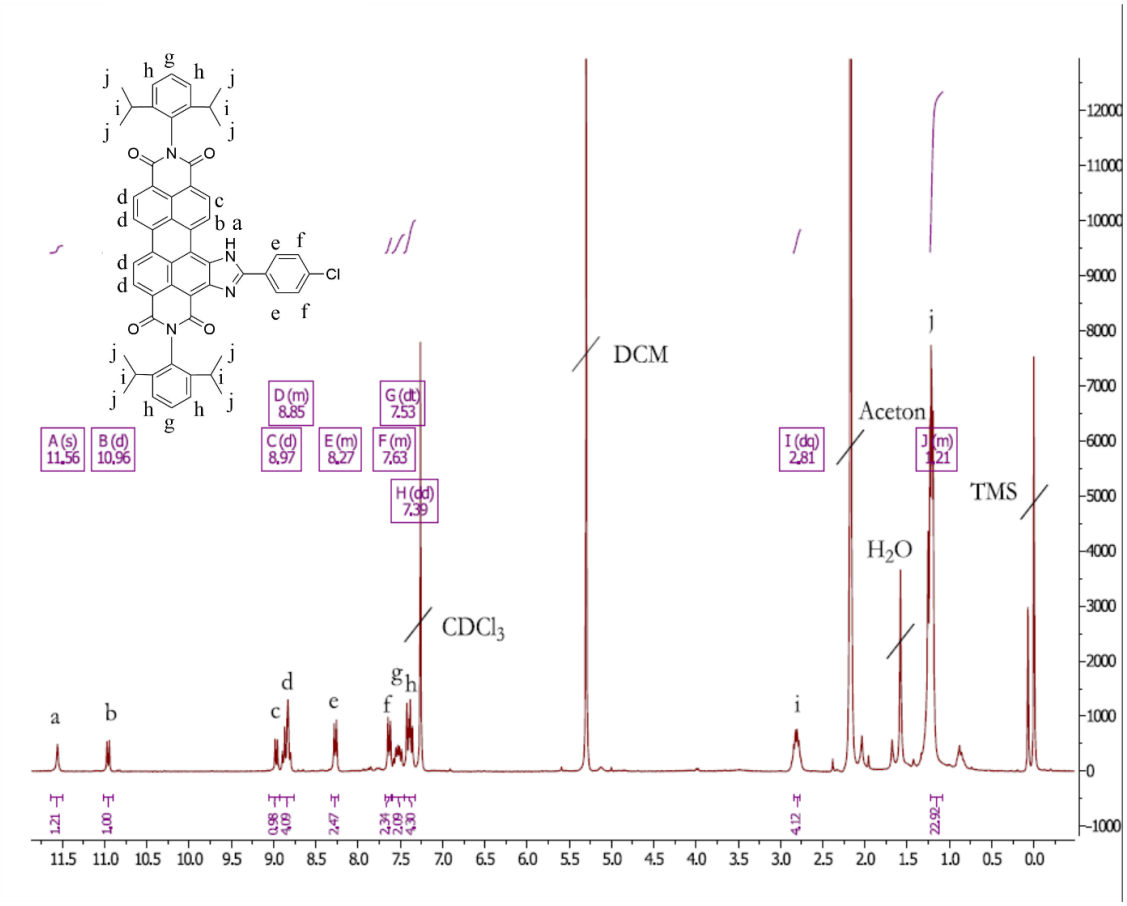

Figure S 3-13 ^{1}H NMR ($CDCl_3$, 300 MHz) of **2b.**

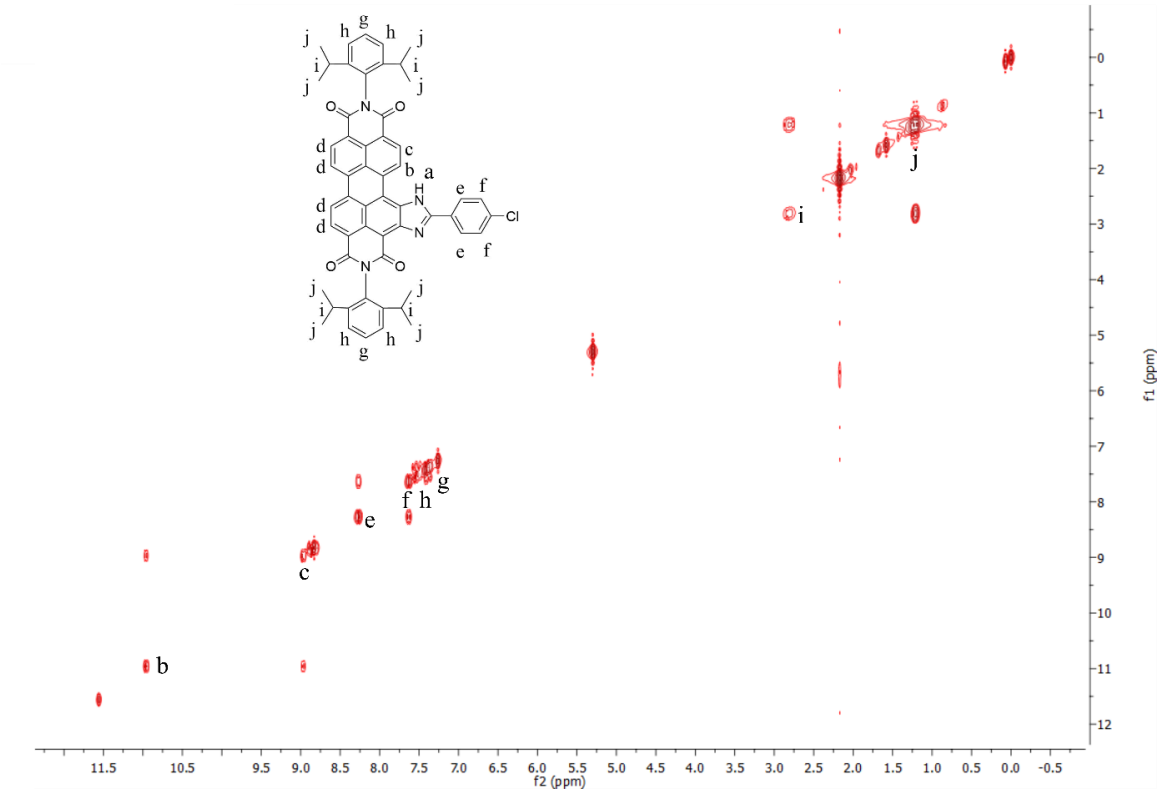

Figure S 3-14 ^{1}H-Cosy NMR ($CDCl_3$, 300 MHz) of **2b.**

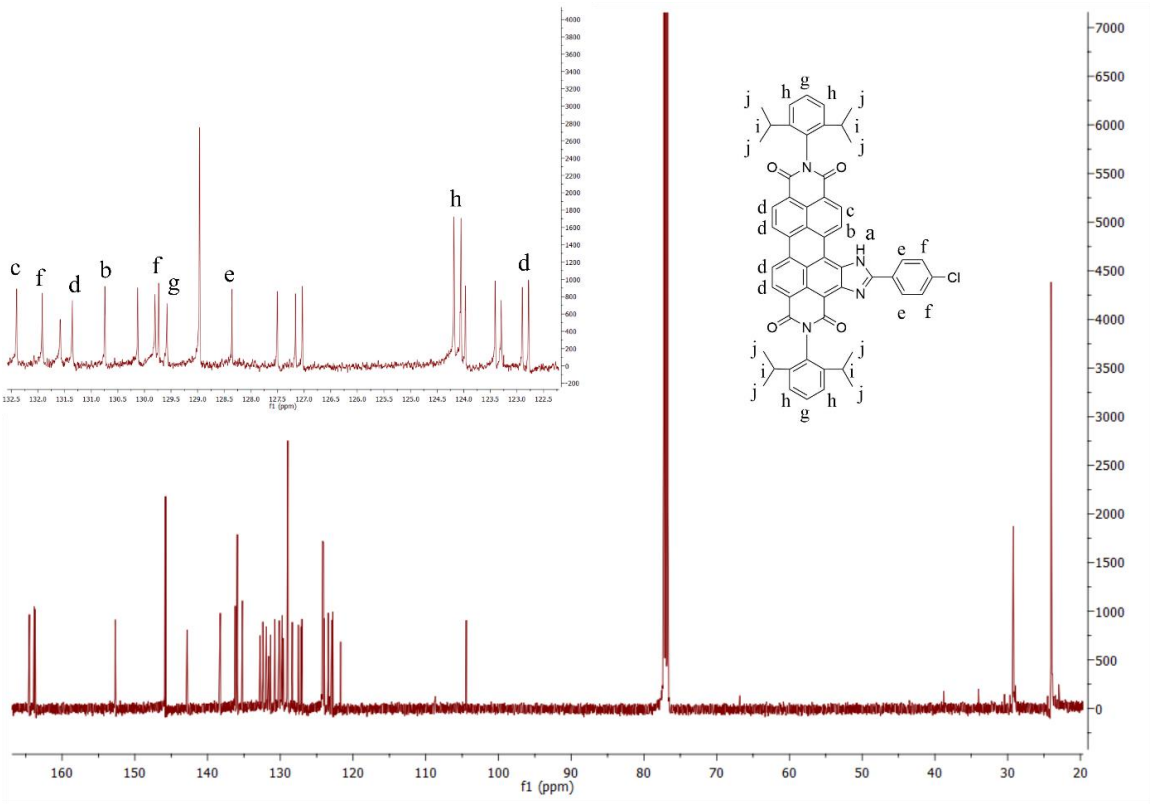

Figure S 3-15 ^{13}C NMR ($CDCl_3$, 126 MHz) of **2b.**

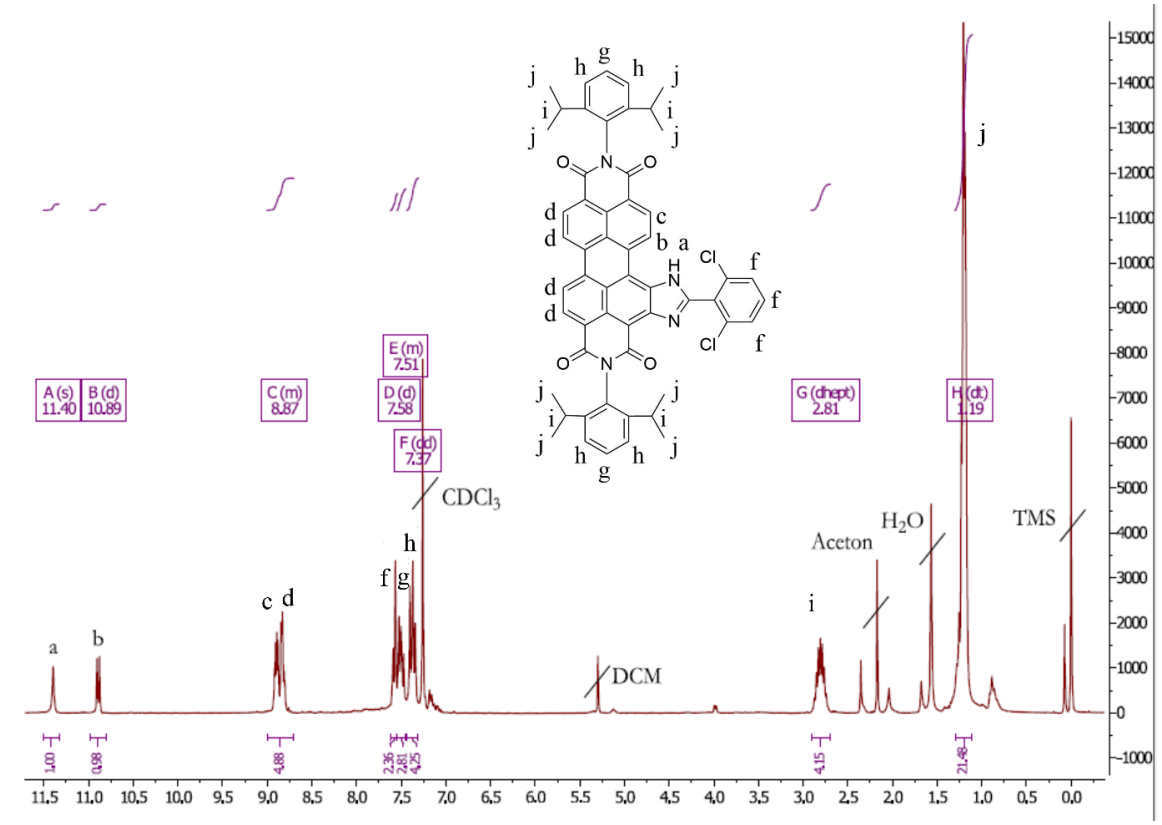

Figure S 3-16 ^{1}H NMR ($CDCl_3$, 300 MHz) of **2c**.

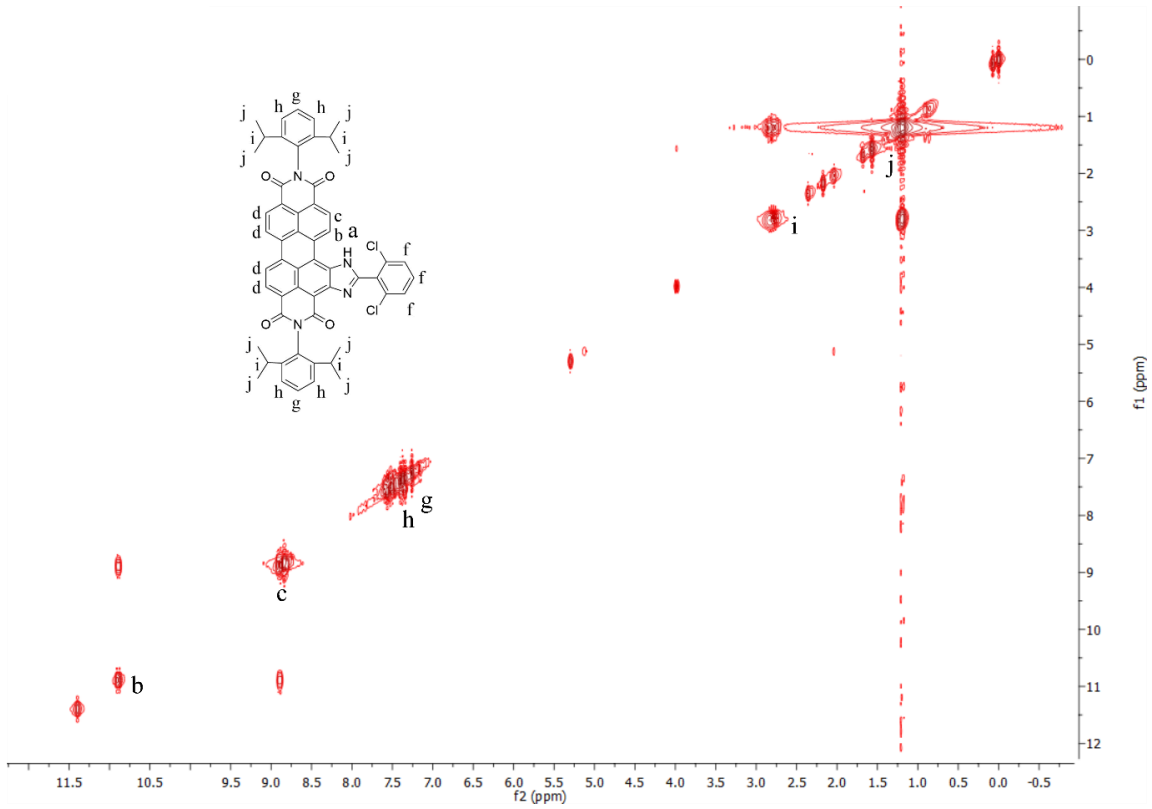

Figure S 3-17 ^{1}H-Cosy NMR ($CDCl_3$, 300 MHz) of **2c**.

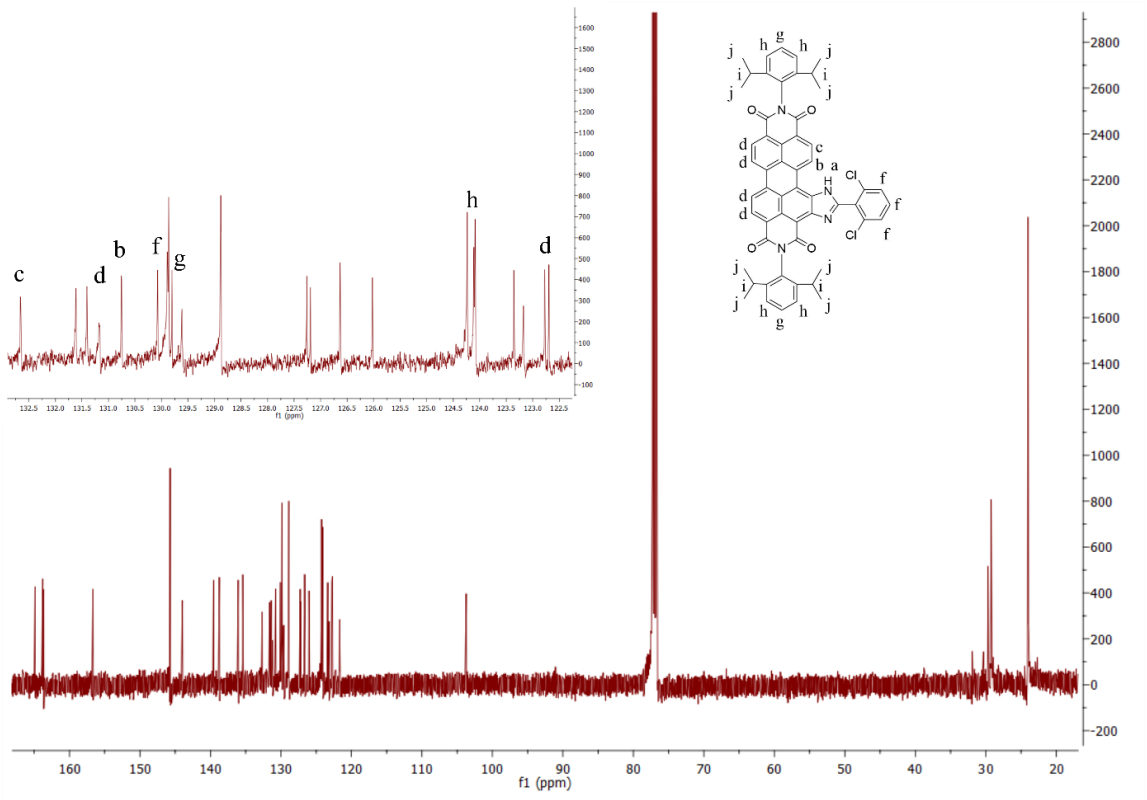

Figure S 3-18 ^{13}C NMR ($CDCl_3$, 126 MHz) of **2c.**

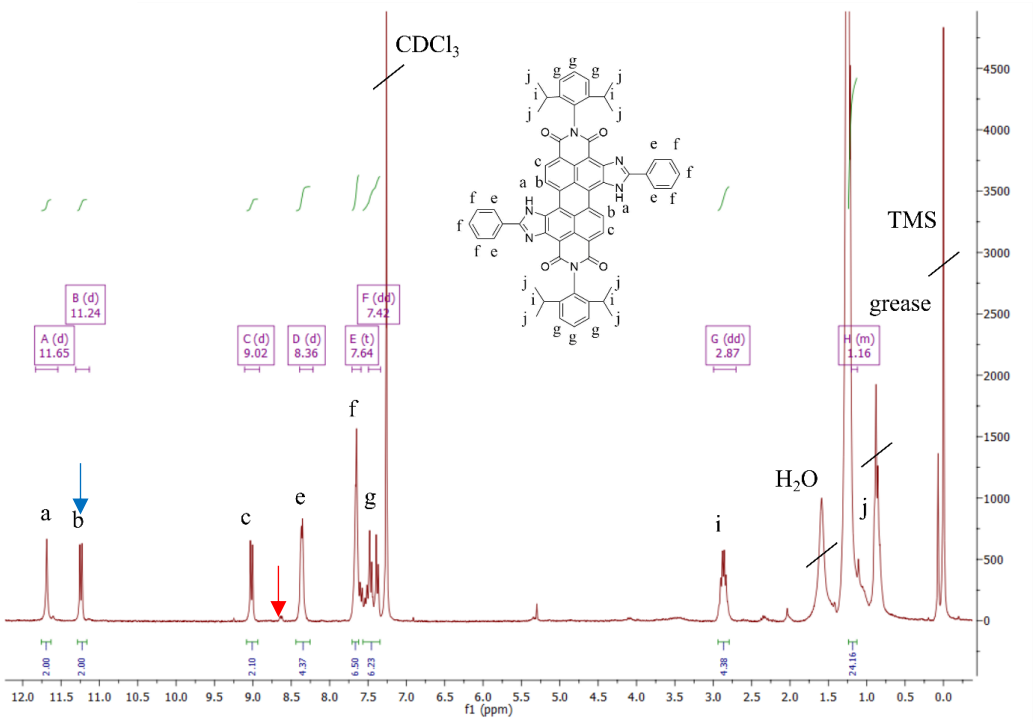

Figure S 3-19 ^{1}H NMR ($CDCl_3$, 300 MHz) of **3a**. The red arrow indicates the signals at around 8.85 ppm which would be expected for the H-atoms located on the opposite side of the perylene for the regioisomer bearing both phenyl-imidazole groups only on one side of the perylene (compare to the signals of *d*-protons in ^{1}H NMR of **2a**, **2b** and **2c** (Fig. S15, S19, S22)). Additionally, the signal from the protons (blue arrow) is located at about 11 ppm (similarly to the protons in **2a**, **2b** and **2c)** which is due to the proximity NH group. The regioisomer would not show protons with such a shift.

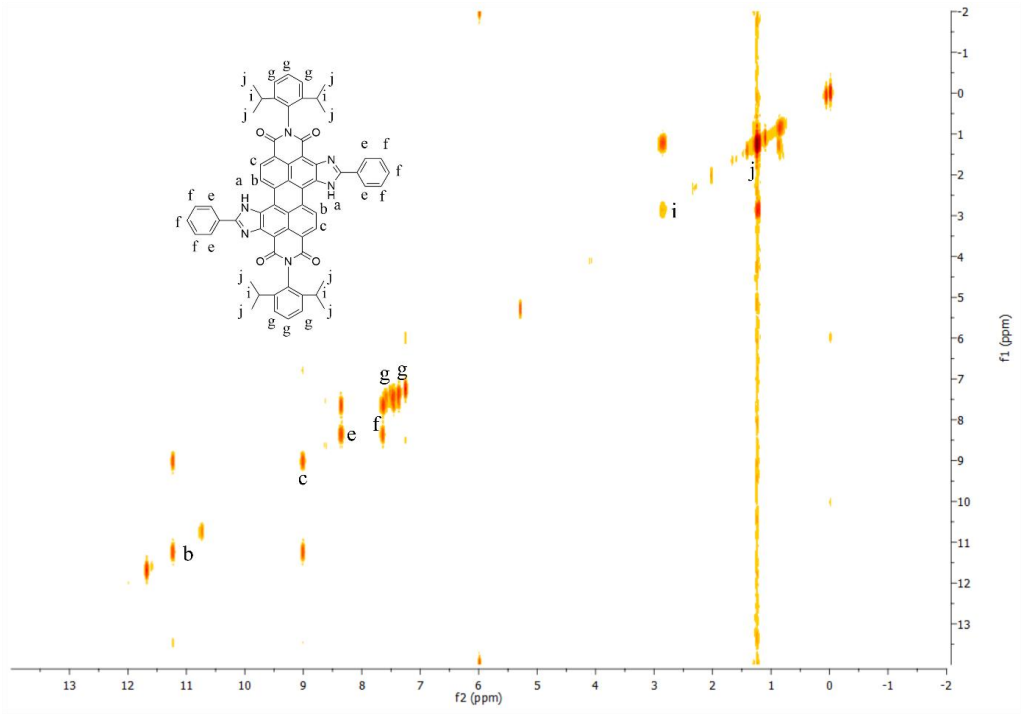

Figure S 3-20 ^{1}H-Cosy NMR ($CDCl_3$, 500 MHz) of **3a.**

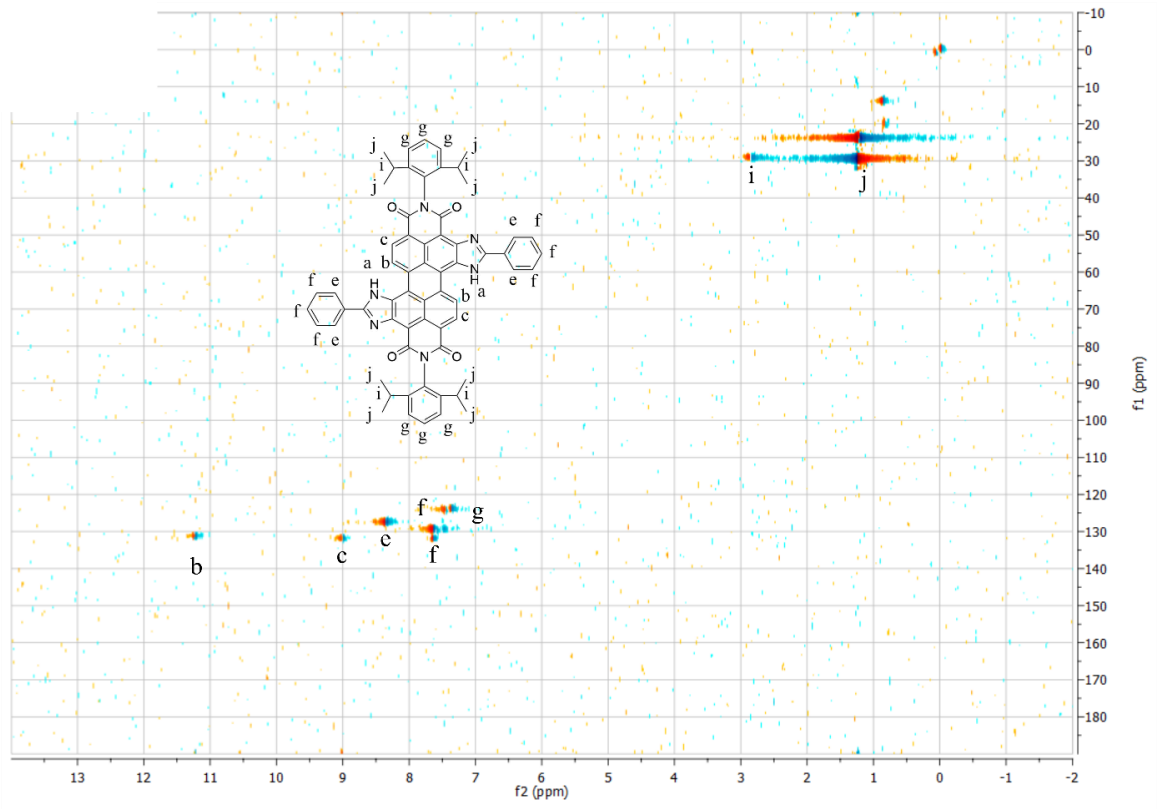

Figure S 3-21. HSQC NMR ($CDCl_3$, 500 MHz, 126 MHz) of **3a.**

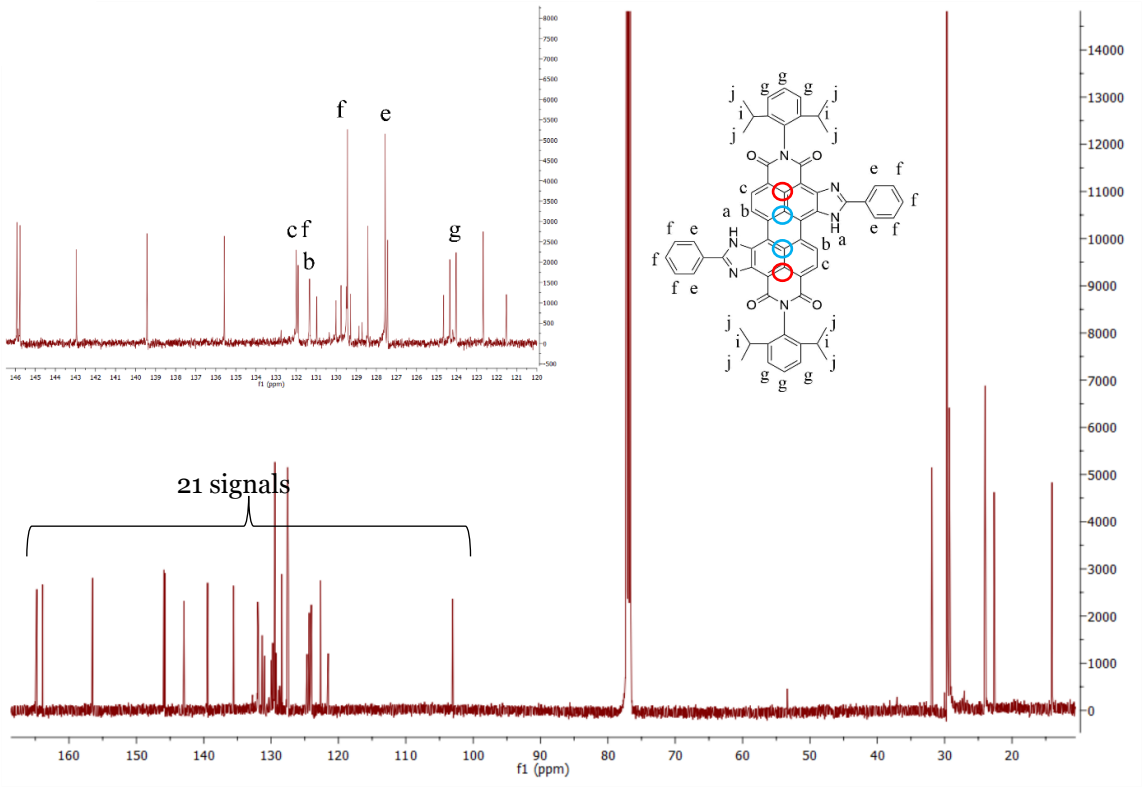

Figure S 3-22 ^{13}C NMR ($CDCl_3$, 126 MHz) of **3a** showing overall 21 signals in the aromatic region.

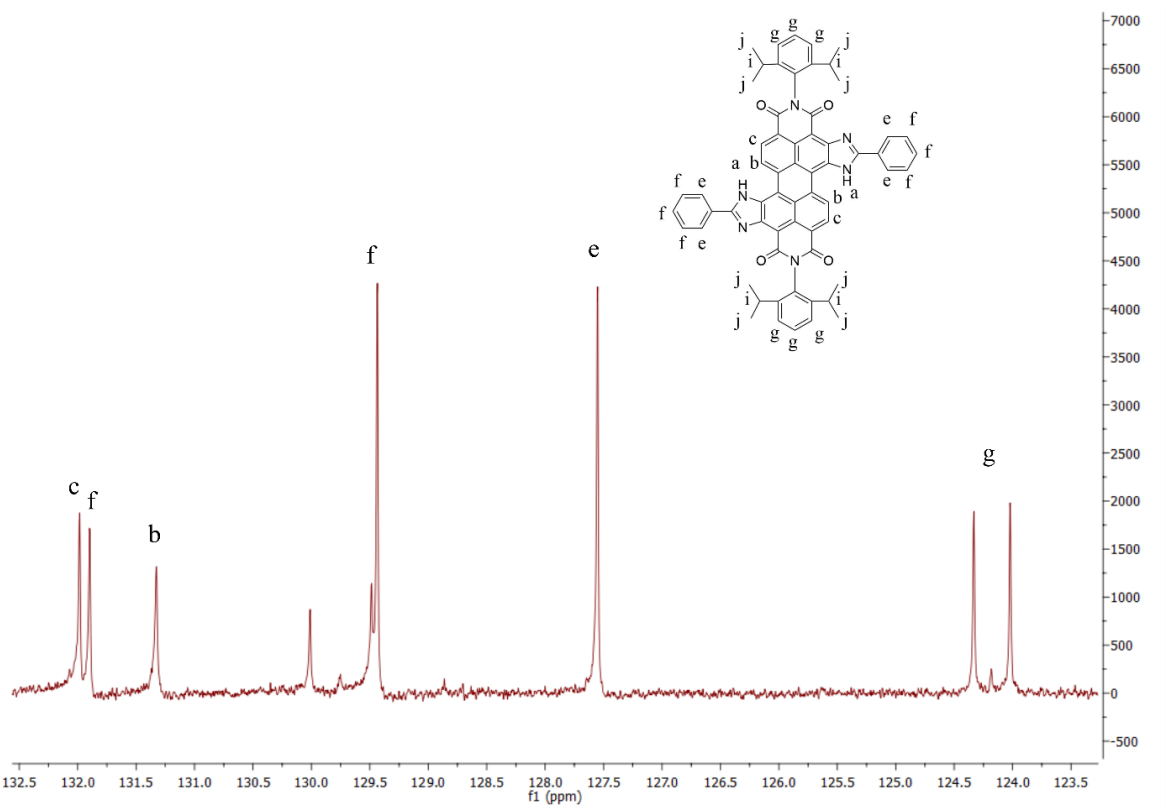

Figure S 3-23 ^{13}C-DEPT NMR ($CDCl_3$, 126 MHz) of **3a**.

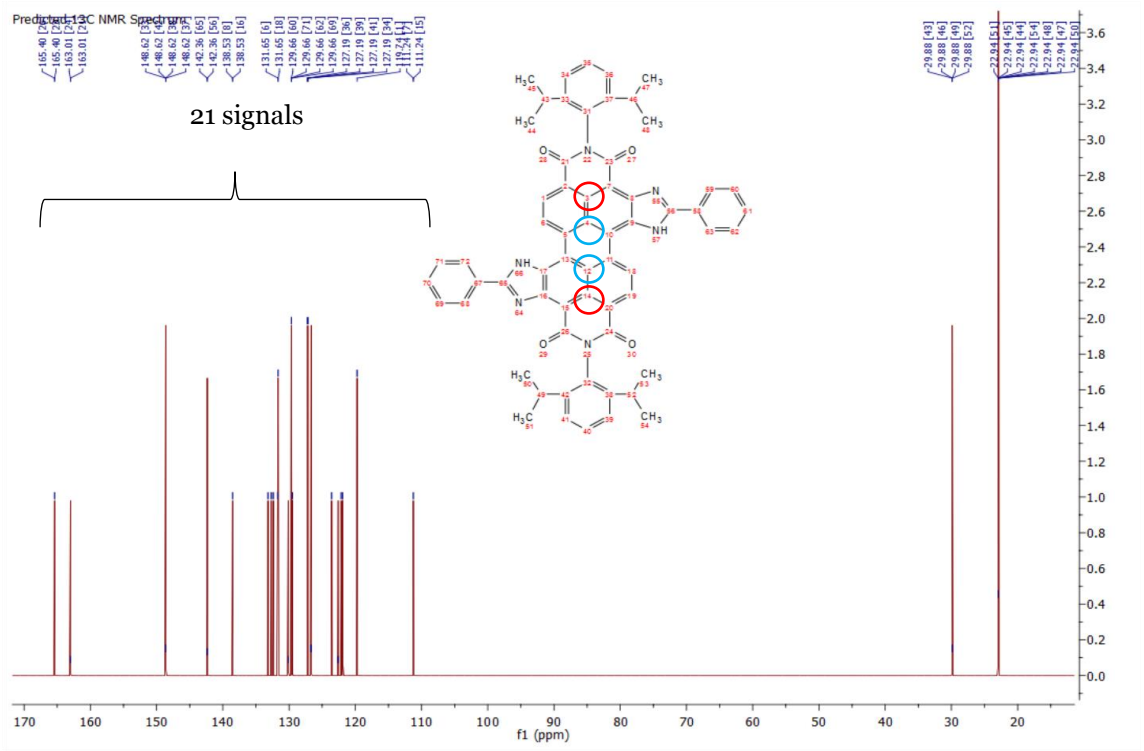

Figure S 3-24 ^{13}C NMR simulation for symmetric **3a** with 21 signals in the aromatic region. 4 C-atoms in the centre of the perylene system (marked with red and blue circles) deliver only 2 signals due to 2 different surroundings.

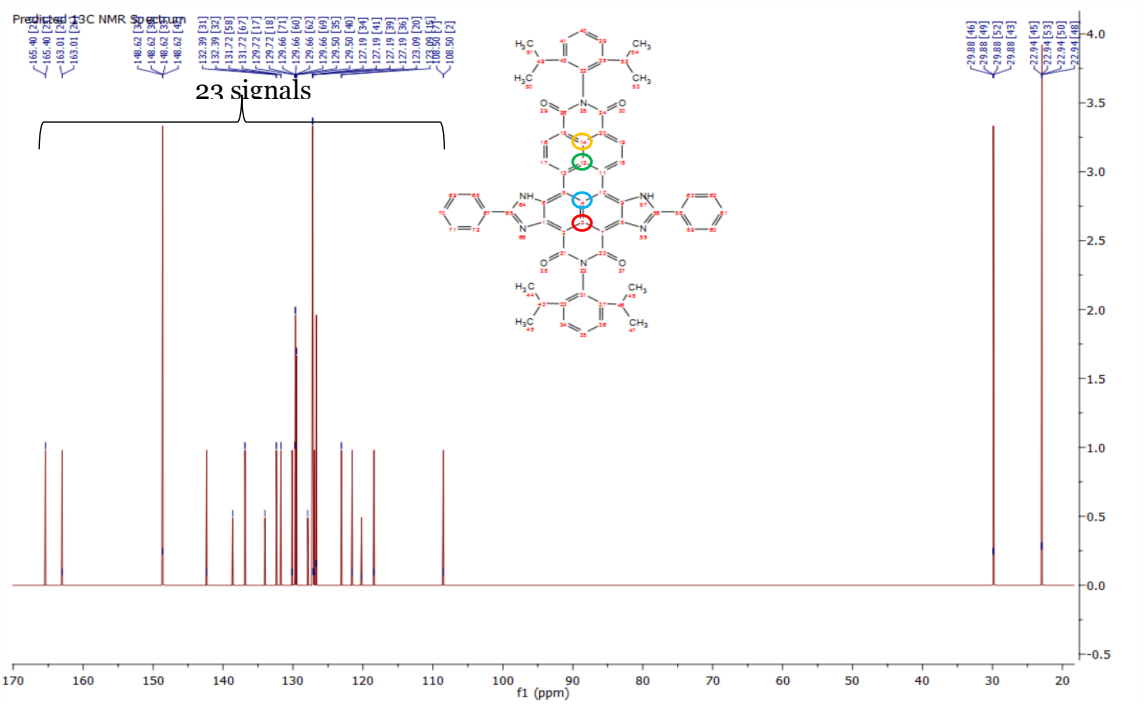

Figure S 3-25 ^{13}C NMR simulation of **3a** regioisomer with 23 signals in the aromatic region. 4 C-atoms in the centre of the perylene system (marked with red, blue, green and yellow circles) deliver 4 signals due to 4 different surroundings

.

3.7.4 MALDI-TOF-MS

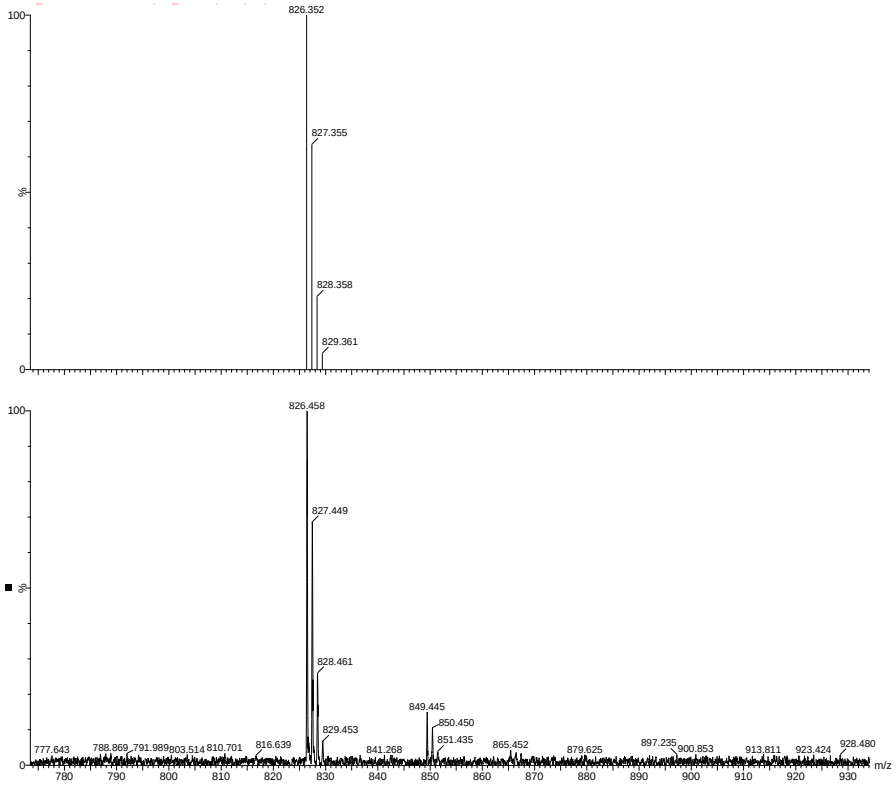

Figure S 3-26. Theoretical isotope pattern and experimental MALDI-TOF-Mass spectrum of **2a.**

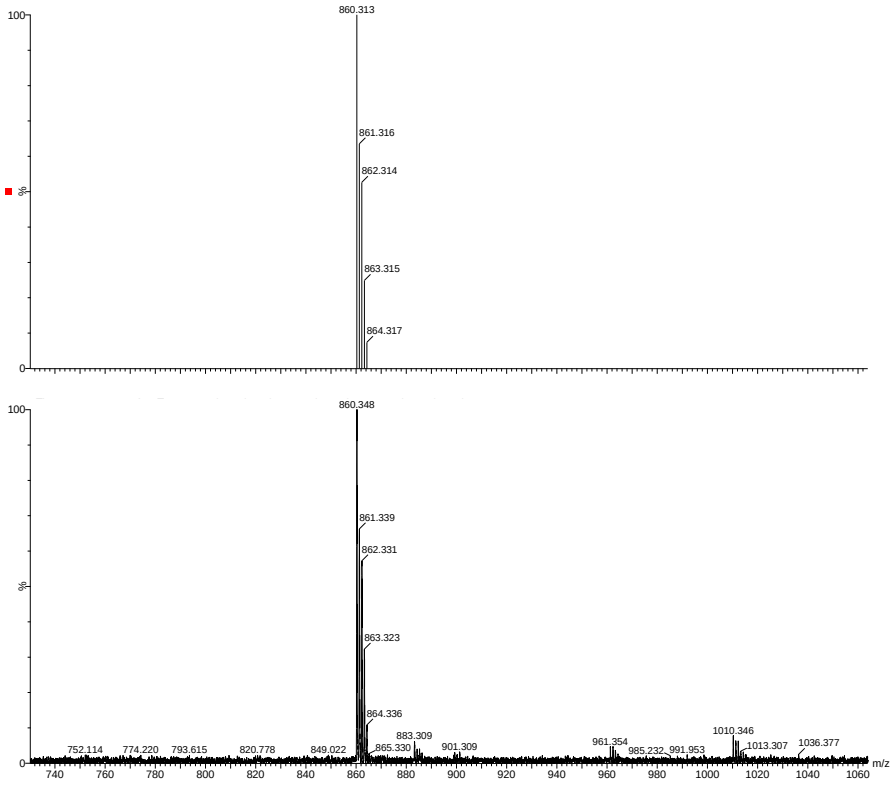

Figure S 3-27 Theoretical isotope pattern and experimental MALDI-TOF-Mass spectrum of **2b.**

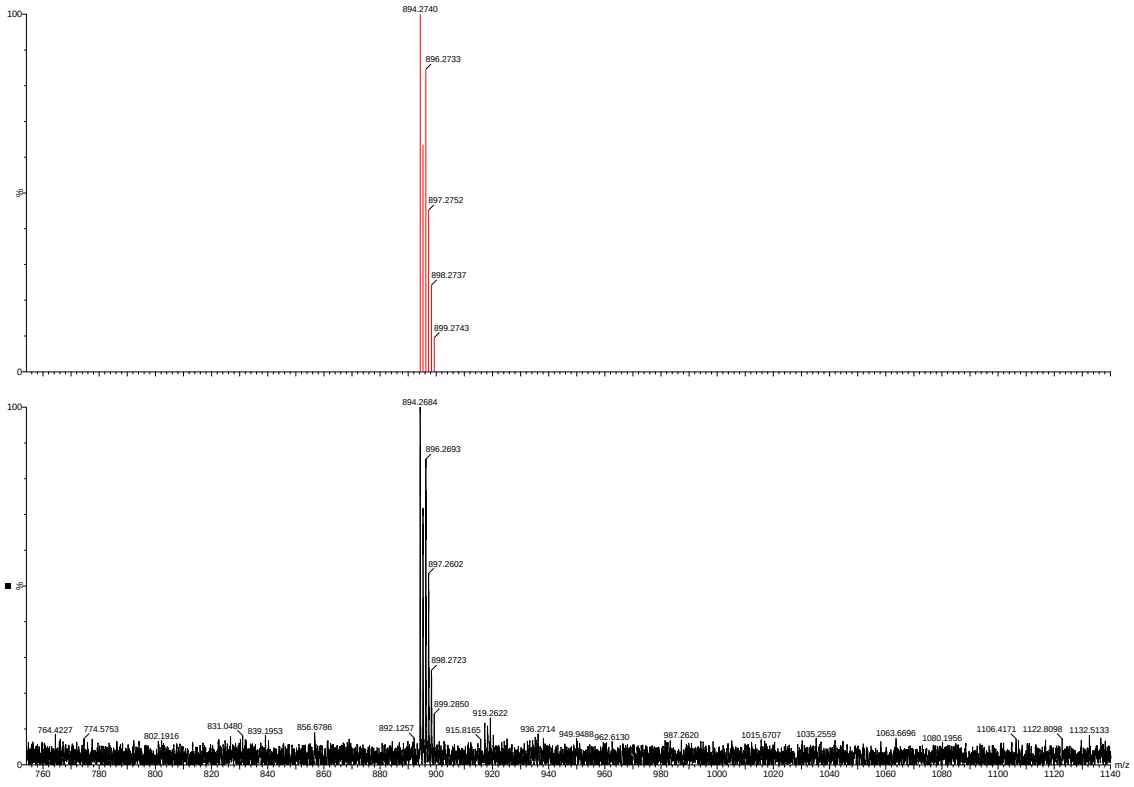

Figure S 3-28 Theoretical isotope pattern and experimental MALDI-TOF-Mass spectrum of **2c.**

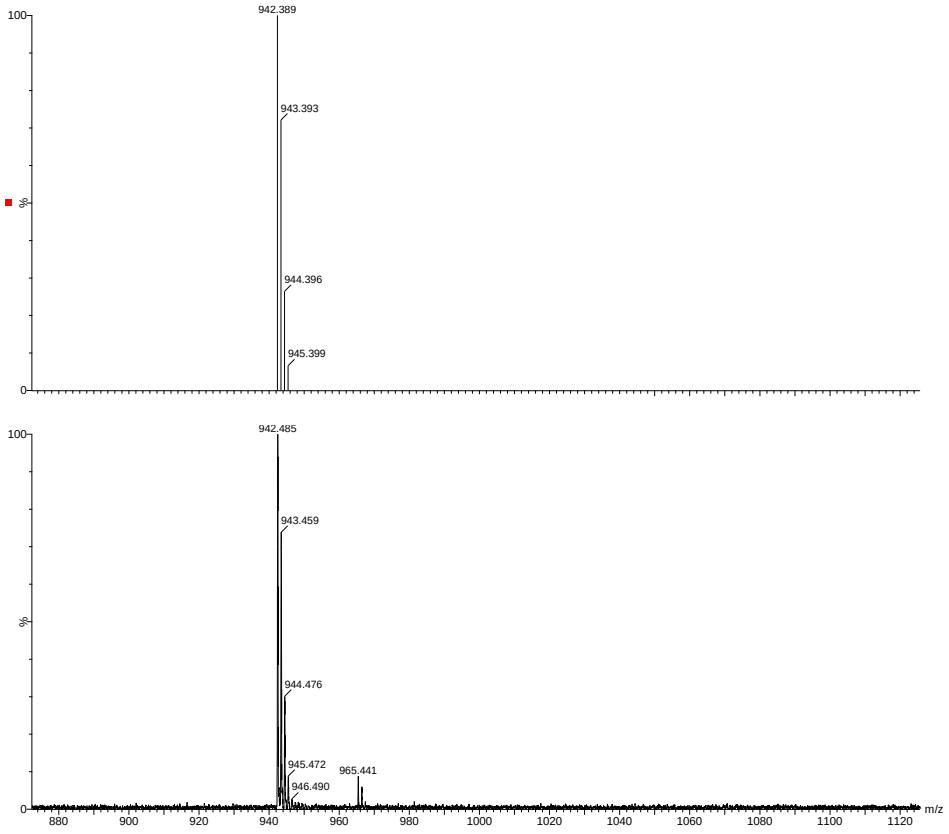

Figure S 3-29 Theoretical isotope pattern and experimental MALDI-TOF-Mass spectrum of **3a**.

4 Green to red emitting BODIPY dyes for fluorescent sensing and imaging of carbon dioxide

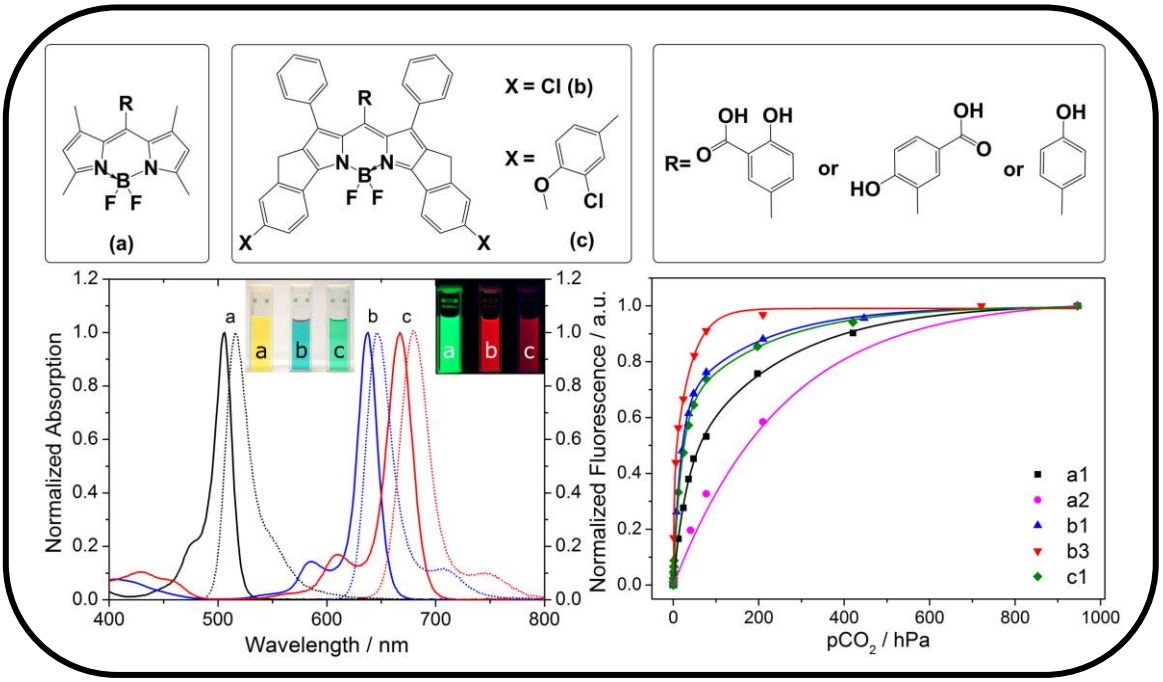

4.1 Preface for the Manuscript

This manuscript was published as Full Paper in *Sensors and Actuators B: Chemical* and is focused on novel pH sensitive BODIPY dyes used for sensing and imaging of carbon dioxide.

The aim of this publication was the synthesis of a palette of new pH indicator dyes spanning a broad emission range from green to far red of the electromagnetic spectrum utilizing different chromophore cores. BODIPY dyes belong to most popular chromophores because of their valuable photophysical properties. Furthermore, due to high versatility of chemical modifications extension of absorption and emission bands into NIR region of the electromagnetic spectrum is enabled, making BODIPYs even more attractive for sensing and (bio)imaging.

Apart from classical BODIPY chromophores with absorption maxima at around 505 nm, π-extended analogs absorbing around 635 and 665 nm have been prepared. All the dyes show excellent brightness, due to high absorption coefficients and high quantum yields. Additionally, the π-extended indicators feature unmatched photostability that make them particularly an attractive platform for optical sensing but also for other applications (e.g. fluorescence labels). Hitherto, such BODIPY-based sensor materials were not applied yet as plastic type carbon dioxide sensors and represent a promising alternative to state-of-the art sensors. For instance, a recently presented aza-BODIPY-based CO_2 sensor for marine application utilizes an absorption-based indicator combined with a sophisticated inner-filter effect read out. Additionally, the sensor requires two reference emitters, which make sensor manufacturing challenging, especially if other formats than planar optodes are considered (**Section 2.5.2**, p.30).

Different phenolic receptors were attached to the chromophores to render them pH sensitive, resulting in indicators for applications in optical CO_2 sensors covering all relevant sensitivity ranges. The motivation behind this work was combination of BODIPY fluorophores featuring excellent absorption coefficients and high fluorescence quantum yields with pH sensitive phenolic receptors due to simple modular synthetic pathways (**Section 2.3**, p.14).

Here we demonstrate the successful embedment of the indicator dyes in a polymer matrix along with a lipophilic organic base to get a plastic-type carbon dioxide sensor. It can be shown that fluorescence is virtually "switched on" in the presence of carbon dioxide and due to the origin of the chromophore as well as the receptor, the dyes show dynamics in different carbon dioxide concentration ranges.

Furthermore, we present the fabrication of sensor materials suitable for ratiometric imaging of carbon dioxide distribution using RGB camera equipment due to the almost ideal match of emission of the sensor materials to the maximum sensitivity of the green and red RGB channels. Finally, referenced sensor materials for phase fluorometry were prepared. The sensors show fully reversible behavior, very good resolution at pCO_2 below atmospheric levels and the estimated LOD of 0.009 hPa making the sensor one of the most sensitive fluorescent CO_2 sensors reported up to date.

Green to red emitting BODIPY dyes for fluorescent sensing and imaging of carbon dioxide

This manuscript was published as *Full Paper* in

Sensors and Actuators B: Chemical, 2020, 304, 127312.

doi: 10.1016/j.snb.2019.127312

Authors: David Pfeifer, Andreas Russegger, Ingo Klimant, Sergey M. Borisov*

Institute of Analytical Chemistry and Food Chemistry, Graz University of Technology, Stremayrgasse 9, 8010 Graz, Austria

***Corresponding author:** sergey.borisov@tugraz.at

Keywords: optical sensor, PET, fluorescence, near infrared, imaging, BODIPY

Highlights

- New fluorescent BODIPY dyes cover green to far red part of electromagnetic spectrum.
- The red emitting dyes feature unmatched photostability.
- Phenol receptors render dyes pH sensitive and suitable for sensing applications.
- Optical plastic carbon dioxide sensors are prepared upon immobilization of the indicators into ethyl cellulose.
- Tuneability of sensing properties and suitability for referenced ratiometric read-outs are demonstrated.

4.2 Abstract

Several new BODIPY pH indicators are prepared and tested as transducers in polymer-based optical carbon dioxide sensors. Apart from classical BODIPY chromophore absorbing at around 505 nm, π-extended analogs showing absorption maxima at around 635 and 665 nm are prepared. All the dyes possess excellent brightness due to combination of high molar absorption coefficients and fluorescence quantum yields. Additionally, the π-extended BODIPYs show unmatched photostability whereas the classical 1,3,5,7-tetramethyl-8-aryl-4,4-difluoroboradiazaindacene is found to be photolabile. The phenol receptors render BODIPY dyes pH sensitive inducing

fluorescence quenching in the phenolate form. Carbon dioxide sensors are prepared via immobilization of the dyes into ethyl cellulose along with tetraoctylammonium hydrogencarbonate. The sensitivity of these sensors is mainly guided by the nature of the receptor and to a smaller extent by the nature of the chromophore, and can be tuned over a very wide range covering all important applications. Introduction of the receptor bearing carboxylic group in the o-position towards OH group of the receptor enables highly sensitive sensors resolving ambient CO_2 levels (LOD 0.009 hPa). Sensors based on other indicators show optimal response from 0.2 to 60 hPa and from 20 to 400 hPa, making them attractive for medical and food packaging applications, respectively. Materials for referenced sensing with phase fluorometry and ratiometric imaging with RGB cameras have also been prepared.

4.3 Introduction

Carbon dioxide is undoubtedly one of the most important species to be detected. Quantification of this metabolite is of highest interest in medical diagnostics, biology and photosynthesis research. In food industry, carbon dioxide represents an essential component of Modified Atmosphere Packages, beer and soft drinks. Finally, monitoring of carbon dioxide levels in environment gains increasing attention due to the decisive role of its anthropogenic factor in climate change. In closely related carbon capture, utilization and storage (CCUS) detection of potential leaks is of utmost importance.

Although classical analytical techniques such as gas chromatography, potentiometry (Severinghaus electrode)[136,137], amperometry[202] and wet-chemical methods[203–205] are in principle suitable for CO_2 quantification, most of the above applications require compact and low cost instrumentation enabling continuous monitoring of the analyte in the gas phase or in aqueous solution. These requirements are fulfilled by nondispersive infrared sensors (NDIR)[139] which proved to be very useful even in the rather challenging marine environment.[206] The main limitation of the NDIR sensors is that the probe compartment and the read-out part represent an inseparable unit with possibility of miniaturization limited by the optical path necessary to achieve sufficient absorption. This makes measurements in small sample volumes virtually impossible. Here, optical chemical CO_2 sensors represent a promising alternative since comparably small sensing component (spot of several millimetres in diameter and a few microns in thickness) and the optoelectronic reader can be separated in space providing that the read-out is performed through a transparent wall. Such separation allows sensing spots to be integrated in a great variety of devices (microplates, (microfluidic) chips, flow-through cells etc.) and undergo necessary treatments (e.g. sterilization). Alternatively, fiber-optic sensors with diameters of a few dozens of microns can be manufactured to enable point measurement in small volume. Finally, optical chemosensors manufactured in a planar format allow mapping of the analyte distribution on surface.

Optical carbon dioxide chemosensors mostly rely on colorimetric[141,157,158] or fluorescent[142,159,160] pH indicators that (i) stay in contact with an aqueous buffer and are used in combination with a

hydrophobic gas-permeable membrane (Severinghaus type)[107,162] or (ii) are directly dissolved in a polymeric/inorganic matrix along with a hydrophobic base, most commonly quaternary ammonium hydrogen carbonate.[141,142,157–160] Although several other concepts have been reported[207,208], the CO_2 sensors relying on pH transducers allow for the highest flexibility of spectral properties and sensitivities. Among fluorescent indicators used in optical CO_2 sensors, commercially available 8-hydroxypyrene-1,3,6-trisulfonate (HPTS) is by far the most common dye.[141–148] Unfortunately, excitation in the blue part of the spectrum and green emission are not ideal for some applications, particularly in media with high autofluorescence and scattering. Moreover its pK_a of ~ 7.3 makes it challenging to prepare sensors resolving ambient carbon dioxide levels. Several dyes of other classes including diketopyrrolopyrroles[153], perylene bisimides[209], azaphthalocyanines[152] were prepared in the last years in attempt to overcome the above limitations, however tuneability of spectral and sensing properties still remains an issue.

BODIPY dyes belong to most popular fluorophores showing excellent molar absorption coefficients and high fluorescence quantum yields.[17,18] The absorption and emission spectra can be extended into NIR region[66] making the dyes even more attractive as fluorescent probes [64] for sensing and (bio)imaging.[67] To the best of our knowledge, these advantages have not been utilized yet in optical carbon dioxide sensors. It would be particularly desirable to combine the advanced photophysical properties of these dyes with the possibility of tuning the dynamic range of CO_2 sensors for a particular application. In fact, the relevant concentration range varies from well below 0.4 hPa (environmental monitoring) to almost 1000 hPa (food packaging) and above (soft drinks) and is not realistic to cover with a single indicator.

In this contribution we present a palette of new BODIPY-based pH indicators for application in optical CO_2 sensors which utilize different chromophores with emission spanning from green to far-red spectral range. The chromophores are combined with several phenolic receptors resulting in indicators covering all relevant sensitivity ranges and therefore making numerous important applications possible.

4.4 Materials and Methods

4.4.1 Materials

Boron trifluoride diethyl etherate (BF_3OEt_2), 2,3-dichloro-5,6-dicyano-p-benzoquinone (DDQ), 4-hydroxybenzaldehyde **3**, lithium diisoprpylamide, ethyl cellulose (EC49, ethoxyl content 49%), tetraoctylammonium hydroxide (TOAOH, 20% in methanol), potassium carbonate, PEPPSI-IPr catalyst, tetramethylrhodamine ethyl ester perchlorate (TMR), trifluoroacetic acid, trimethylchlorosilane and Fomblin Y were purchased from Sigma Aldrich (www.sigmaaldrich.com). 5-bromo-1-indanione, 3-chloro-4-methyoxyphenylboronic acid, 2,4-dimethylpyrrole **a**, methyl 5-formyl-2-hydroxybenzoate **1**, 4-*tert*-butylbenzaldehyde, N,N-diisopropylethylamine (DIPEA) were obtained from TCI Europe (www.tcieurope.de). Lumogen

Red and Daylight Fluorescent Green Pigment were purchased from Kremer Pigmente (www.kremer-pigmente.de). Methyl 3-formyl-4-hydroxybenzoate **2** was purchased from Fluorochem (www.fluorochem.co.uk). Dichloromethane (DCM) was received from Fisher scientific (www.fishersci.com). Cyclohexane (CH), ethanol (EtOH), ethyl acetate (EA), methanol (MeOH), tetrahydrofuran (THF) and toluene (synthesis grade), sodium chloride and hydrochloric acid (37%) were purchased from VWR Chemicals (www.vwr.com). Poly(ethylene terephthalate) (PET) and Teonex Q51/125 µm support was received from Pütz (www.puetz-folien.com). Poly(styrene-co-polydivinylbenzene) (PS/DVB) microbeads, anhydrous sodium sulfate, anhydrous disodium phosphate and the buffer salts CAPS and TRIS as well as microscope slides were obtained from Carl Roth (www.roth.de). Deuterated chloroform ($CDCl_3$) was purchased from Euriso-top (www.eurisotop.com). Titanium dioxide particles (TiO_2 P170) were received from Kemira (www.kemira.com). All purchased chemicals were used without further purification. Nitrogen, 0.2% carbon dioxide in nitrogen, 5% carbon dioxide in nitrogen and carbon dioxide (all of 99.999% purity) were received from Linde (www.linde-gas.at). Silica-gel 60 (0.063-0.200 mm) were obtained from Merk (www.merck.at). Silanized Egyptian blue particles (trimethylsilyl-modified), 3-phenyl-2H-azirene and 5-chloro-3-phenyl-1,4-dihydroindeno[1,2-b] pyrrole **b** were synthesized according to literature procedures.[210,211] Synthesis of 6-(3-chloro-4-methoxyphenyl)-3-phenyl-1,4-dihydroindeno[1,2-b]pyrrole **c** and reference dye **a-*t*Bu** for the photostability measurements is described in the Supporting information.

Synthesis of a1. The synthesis was carried out under water-free conditions, argon atmosphere and exclusion of light. Methyl 5-formyl-2-hydroxybenzoate **1** (94.8 mg, 0.526 mmol, 1 eq) and 1,4-dimethylpyrrole **a** (110 µL, 1.07 mmol, 2 eq) were dissolved in 12 mL of anhydrous DCM and 1 drop of trifluoroacetic acid was added. The mixture was stirred at RT for 2 h. DDQ (135.5 mg, 0.597 mmol, 1.1 eq) was added and the solution stirred for 60 min. N,N-diisopropylethylamine (0.90 mL, 5.29 mmol, 10 eq) was added, the solution stirred for 15 min following by addition of BF_3OEt_2 (1.00 mL, 7.89 mmol, 15 eq) and stirring for 30 min. The mixture was extracted 3 times with water, dried over Na_2SO_4 and the solvent removed under reduced pressure. The final product was purified by column chromatography (CH/EA gradient) and was obtained as yellow-reddish powder (100.5 mg, 48%).

NMR for the CH_3 ester: ^{1}H NMR (300 MHz, $CDCl_3$) δ 10.92 (s, 1H), 7.79 (s, 1H), 7.36 (d, J = 8.4, 1H), 7.13 (d, J = 8.5 Hz, 1H), 5.99 (s, 2H), 3.97 (d, J = 13.2 Hz, 3H), 2.55 (s, 6H), 1.46 (s, 6H). ^{13}C NMR (76 MHz, $CDCl_3$) δ 135.38, 129.72, 121.39, 121.25, 118.72, 52.62, 29.71, 14.97, 14.59.

MALDI-TOF-MS for the CH_3 ester: m/z: [M^+] calcd. for $C_{21}H_{21}BF_2N_2O_3$: 398.1617; found 398.0871.

Synthesis of a2. a2 was prepared analogously to **a1**, using methyl 3-formyl-4-hydroxybenzoate **2** (240.0 mg, 1.32 mmol, 1 eq), 1,4-dimethylpyrrole **a** (250 µL, 2.63 mmol, 2 eq), 20 mL of anhydrous DCM, DDQ (328.2 mg, 1.45 mmol, 1.1 eq), N,N-diisopropylethylamine (2.23 mL, 13.14

mmol, 10 eq) and BF_3OEt_2 (2.5 mL, 19.7 mmol, 15 eq) instead. The dye was purified by column chromatography (CH/EA gradient) and was obtained as a yellow-reddish powder (23 mg, 5%).

NMR for the CH_3 ester: ^{1}H NMR (300 MHz, $CDCl_3$) δ 8.08 (d, J = 8.5, 1.9 Hz, 1H), 7.88 (s, 1H), 7.07 (d, J = 8.6 Hz, 1H), 6.00 (s, 2H), 3.88 (s, 3H), 2.54 (s, 6H), 1.50 (s, 6H). ^{13}C NMR (76 MHz, $CDCl_3$) δ 143.12, 133.00, 131.52, 121.90, 121.88, 116.63, 52.13, 30.06, 14.71, 14.06.

MALDI-MS for the CH_3 ester: m/z: [M^+] calcd. for $C_{21}H_{21}BF_2N_2O_3$, 398.1617; found, 398.0738.

Synthesis of b1. b1 was prepared analogously to **a1**, using methyl 5-formyl-2-hydroxybenzoate **1** (51.0 mg, 0.283 mmol, 1 eq), 5-chloro-3-phenyl-1,4-dihydroindeno[1,2-b] pyrrole **b** (152.8 mg, 0.575 mmol, 2 eq), DDQ (69.8 mg, 0.307 mmol, 1.1 eq), N,N-diisopropylethylamine (0.48 mL, 2.82 mmol, 10 eq) and BF_3OEt_2 (0.52 mL, 4.21 mmol, 15 eq) instead. The product was purified by column chromatography (CH/EA gradient) and was obtained as a blue powder (34 mg, 16%).

NMR for the CH_3 ester: ^{1}H NMR (300 MHz, $CDCl_3$) δ 10.46 (s, 1H), 8.36 (d, J = 8.1 Hz, 2H), 7.49 (d, J = 8.4 Hz, 2H), 7.46 (s, 2H), 7.28 (s, 1H), 7.02 – 6.88 (m, 6H), 6.86 – 6.80 (m, 1H), 6.77 (d, J = 7.1 Hz, 4H), 6.07 (d, J = 8.6 Hz, 1H), 3.83 (s, 3H), 3.56 (s, 4H). ^{13}C NMR (76 MHz, $CDCl_3$) δ 161.67, 152.25, 138.25, 135.73, 134.49, 134.16, 131.21, 128.97, 128.47, 127.45, 126.38, 126.08, 125.44, 122.19, 116.01, 110.55, 52.01, 29.58.

MALDI-TOF-MS for the CH_3 ester: m/z: [M^+] calcd. for $C_{43}H_{27}BCl_2F_2N_2O_3$, 738.1467; found, 738.1410.

Synthesis of b3. b3 was prepared analogously to **a1**, using 4-hydroxybenzaldehyde **3** (34.6 mg, 0.283 mmol, 1 eq), 5-chloro-3-phenyl-1,4-dihydroindeno[1,2-b] pyrrole **b** (151.5 mg, 0.570 mmol, 2 eq), DDQ (69.8 mg, 0.307 mmol, 1.1 eq), N,N-diisopropylethylamine (0.48 mL, 2.82 mmol, 10 eq) and BF_3OEt_2 (0.52 mL, 4.21 mmol, 15 eq) instead. The product was purified by column chromatography (CH/EA gradient) and was obtained as a blue powder (40.5 mg, 21%).

NMR: ^{1}H NMR (300 MHz, $CDCl_3$) δ 8.36 (d, J = 8.1 Hz, 2H), 7.49 (d, J = 8.3 Hz, 2H), 7.45 (s, 2H), 6.94 (dd, J = 15.4, 7.8 Hz, 6H), 6.76 (d, J = 6.6 Hz, 4H), 6.66 (d, J = 8.4 Hz, 2H), 5.89 (d, J = 8.4 Hz, 2H), 3.55 (s, 4H). ^{13}C NMR (76 MHz, $CDCl_3$) δ 152.19, 144.35, 135.51, 134.80, 133.47, 128.80, 128.41, 127.46, 126.10, 126.02, 113.53, 29.66.

MALDI-TOF-MS: m/z: [M^+] calcd. for $C_{57}H_{39}BCl_2F_2N_2O_5$, 680.1412; found, 680.1971.

Synthesis of c1. c1 was prepared analogously to **a1**, using methyl 5-formyl-2-hydroxybenzoate **1** (32.1 mg, 0.178 mmol, 1 eq), 6-(3-chloro-4-methoxyphenyl)-3-phenyl-1,4-dihydroindeno[1,2-b]pyrrole **c** (130.*0* mg, 0.349 mmol, 2.1 eq), DDQ (80 mg, 0.350 mmol, 2.1 eq), N,N-diisopropylethylamine (0.28 mL, 1.66 mmol, 10 eq) and BF_3OEt_2 (0.32 mL, 2.5 mmol, 15 eq)

instead. The product was purified by column chromatography (CH/EA gradient) and was obtained as a green powder (24 mg, 15%).

NMR for the CH_3 ester: ^{1}H NMR (300 MHz, $CDCl_3$) δ 10.46 (s, 1H), 8.52 (d, J = 8.0 Hz, 2H), 7.75 – 7.68 (m, 4H), 7.64 (s, 2H), 7.60 – 7.50 (m, J = 8.5 Hz, 3H), 7.31 (d, J = 2.1 Hz, 1H), 7.04 (d, J = 8.6 Hz, 2H), 7.00 – 6.94 (m, 3H), 6.92 (s, 2H), 6.85 (s, 1H), 6.81 (s, 2H), 6.79 (s, 2H), 6.08 (d, J = 8.6 Hz, 1H), 3.97 (s, 6H), 3.84 (s, 3H), 3.62 (s, 4H). ^{13}C NMR (76 MHz, $CDCl_3$) δ 161.55, 151.65, 140.71, 138.40, 134.79, 134.29, 131.72, 129.06, 128.93, 127.40, 126.74, 126.53, 126.22, 124.97, 123.75, 123.02, 115.93, 112.40, 56.32, 52.01, 31.45, 30.22, 29.68.

MALDI-TOF-MS for the CH_3 ester: m/z: [M^+] calcd. for $C_{57}H_{39}BCl_2F_2N_2O_5$, 950.2307; found, 950.1091.

Preparation of Lumogen Red PS/DVB particles

1g PS/DVB particles were dispersed in 5 mL THF and 10 mg Lumogen Red dissolved in 1 mL THF was added and stirred for 1 hour. After addition of 100 mL dest. H_2O the colored particles were filtered, washed with 300 mL dest. H_2O and 200 mL EtOH and dried at 60 °C for 24 hours. Prior to usage the particles were grinded in a mortar.

Preparation of carbon dioxide sensors

40 µL of TOAOH solution in methanol were added to 0.25 mg of an indicator, purged with carbon dioxide and a solution of 50 mg EC49 in an ethanol:toluene mixture (2:3 v/v, 0.95 g) was added. After purging with carbon dioxide another 40 µL TOAOH solution in methanol was added. The homogenized "cocktail" was knife-coated on a glass support (treated with trimethylchlorosilane) to obtain an ~ 1.25 µm thick sensor layer after solvent evaporation. Afterwards, a solution of Hyflon AD60 in perfluordecalin (5% w/w) containing Fomblin Y as an additive (10% wt. in respect to the polymer) was knife-coated onto the dry sensor layer to obtain an overall sensor thickness of 2.55 µm.

Preparation of DLR-referenced sensors

DLR sensors were prepared analogously to unreferenced sensor materials, but with addition of silanized Egyptian blue particles (10% wt. in respect to the polymer) to the "cocktail". Lipophilic titanium dioxide particles (5% wt. in respect to the polymer) were added to the Hyflon layer.

Preparation of sensors for RGB imaging

Sensors for RGB imaging were prepared analogously to the unreferenced sensor materials. Homogenized "cocktails" based on **a1** or **b1** were knife-coated on a glass support (treated with trimethylchlorosilane) to obtain a ~3.75 µm thick sensor layers after solvent evaporation. Lipophilic titanium dioxide particles (20% wt. in respect to the polymer) and Lumogen Red PS/DVB particles (1% wt. in respect to the polymer) or Daylight Fluorescent Green Pigment (1% wt. in respect to the polymer) were added to the Hyflon layer for the sensors based on **a1** and **b1**, respectively. The overall sensor thickness was ~4.8 µm.

4.4.2 Methods

Mass spectroscopy was performed on Micromass TofSpec 2E Time-of-Flight Mass Spectrometer at the Institute for Chemistry and Technology of Materials, Graz University of Technology and on Advion expression CMS. ^{1}H and ^{13}C NMR spectra were recorded on a 300 MHz Bruker Instrument (www.bruker.com) in $CDCl_3$ as a solvent and TMS as standard.

Absorption spectra were recorded on a Cary 50 UV-Vis spectrophotometer from Varian (www.agilent.com) using optical glass cuvettes from Hellma Analytics (www.hellma-analytics.com). Emission and excitation spectra were recorded on a FluoroLog 3 Spectrofluorometer from Horiba Scientific Jobin Yvon (www.horiba.com) equipped with a R2658 photomultiplier from Hamamatsu and corrected for detector response. Determination of absolute fluorescence quantum yields Φ was carried out on the same Spectrofluorometer from Horiba equipped with an integrating sphere Quanta-phi.

Fluorescence decay times were measured via time correlated single photon counting (TCSPC) on a FluoroLog 3 Spectrofluorometer equipped with a DeltaHub module and NanoLEDs (λ = 435 nm and 635 nm, Horiba) as excitation sources. Data analysis was carried out with DAS6 software (www.horiba.com) using a mono-exponential fit.

The photostability of the dyes **a1**, **a2**, **b1**, **b3**, **c1**, **a-*t*Bu** and TMR was accessed by illumination with a Metal-Halogen-lamp (ConstantColor™ CMH Precise™, GE Lightening) with 14.000 nominal lumens. A heat protection filter (CALFLEX X; QIOPTIQ) and an UV blocking filter (UV-Blocking-Filters UV-B; QIOPTIQ) were used to narrow the spectrum of the lamp to 400 to 700 nm. The solution of the dye in THF (water in case of TMR) in a screw-capped quartz cuvette was stirred during the irradiation with help of a magnetic stirrer. The photon flux Φ_{out} transmitted through the cuvette was measured with a light-meter (LI-250A) equipped with a light sensor (LI-190 Quantum sensor; LI-COR Biosciences, www.licor.com). A Neutral-Density filter (25%; QIOPTIQ, www.qioptiq.de) was installed in front of the light sensor to avoid its saturation. The absorption spectra were acquired after irradiation periods of 5 min for the dyes **a1**, **a2** and **a-*t*Bu**, 10 min for TMR and 60 min for **b1**, **b3** and **c1**.

For carbon dioxide measurements the sensor foil was fixed in a custom-made flow-through cell connected to a gas mixing device. Gas calibration mixtures were produced with a gas mixing device from Voegtlin (www.voegtlin.com, red-y for gas flow) and a constant flow (400 mL/min) was controlled by LabView software. Relative humidity of 100% was adjusted via bubbling of the gases through deionized water. Temperature was controlled with a cryostat Thermostat Thermo Haake K10. A commercially available phase fluorometer (piccolo2 from Pyro Science, www.pyroscience.com) was used for the phase shift measurements that were carried out in a thermostatic chamber from Memmert (www.memmert.com). For the RGB imaging the combination of a Marlin F-201c camera from Allied vision technologies (www.alliedvision.com) and an array of 12 blue high power LEDs (λ = 455 nm, OSRAM Oslon SSL 80, www.led-tech.de) equipped with a cooling block, was used. A long-pass filter GG495 and a band-pass filter BG12 (both from Schott, www.schott.com) were used in front of the camera and the LED array, respectively.

4.5 Results and Discussion

4.5.1 Synthesis

The design of new pH-sensitive BODIPY dyes for application in optical CO_2 sensors was guided by following considerations. First, the synthesis should enable flexibility of spectral properties to make the dyes suitable for different sensing and imaging applications. The dyes should possess high luminescence brightness and good photostability and some representatives should absorb in the red part of electromagnetic spectrum in order to enable applications in environments with high levels of autofluorescence. Second, the dyes should possess good solubility in polymers such as ethyl cellulose. Finally, the receptor should allow for tuning the sensitivity of the sensors to carbon dioxide.

Generally, synthesis of pH sensitive BF_2-chelated dipyrromethenes is based on a modular combination of two building blocks – (i) the fluorophore core and (ii) the receptor (**Figure 4-1**) that define the spectral properties and pH sensitivity, respectively. The indicators are obtained via condensation of two pyrrole molecules and the aromatic aldehyde from the receptor, oxidation of the resulting intermediate with DDQ and subsequent complexation with BF_3-etherate. To establish structure-property relationships we used three different pyrroles and three different aromatic aldehydes. 2,4-Dimethylpyrrole **a** is commercially available, 5-chloro-3-phenyl-1,4-dihydroindeno[1,2-b]pyrrole **b** was prepared according to literature whereas 6-(3-chloro-4-methoxyphenyl)-3-phenyl-1,4-dihydroindeno[1,2-b]pyrrole **c** (Scheme S1, Supporting Information) was prepared from the respective ketone and 3-phenyl-2H-azirene.[210,212,213] Methyl 5-formyl-2-hydroxybenzoate **1**, methyl 3-formyl-4-hydroxybenzoate **2** and 4-hydroxybenzaldehyde **3** were used to introduce pH sensitivity and thus enable CO_2 sensing. It should be noted that in case of receptors **1** and **2** the synthesized dyes are prepared in the form of methyl ether. Deprotection of

the carboxy-groups occurs during addition of basic tetraoctylammonium hydroxide (TOAOH) prior to preparation of the CO_2 sensors.

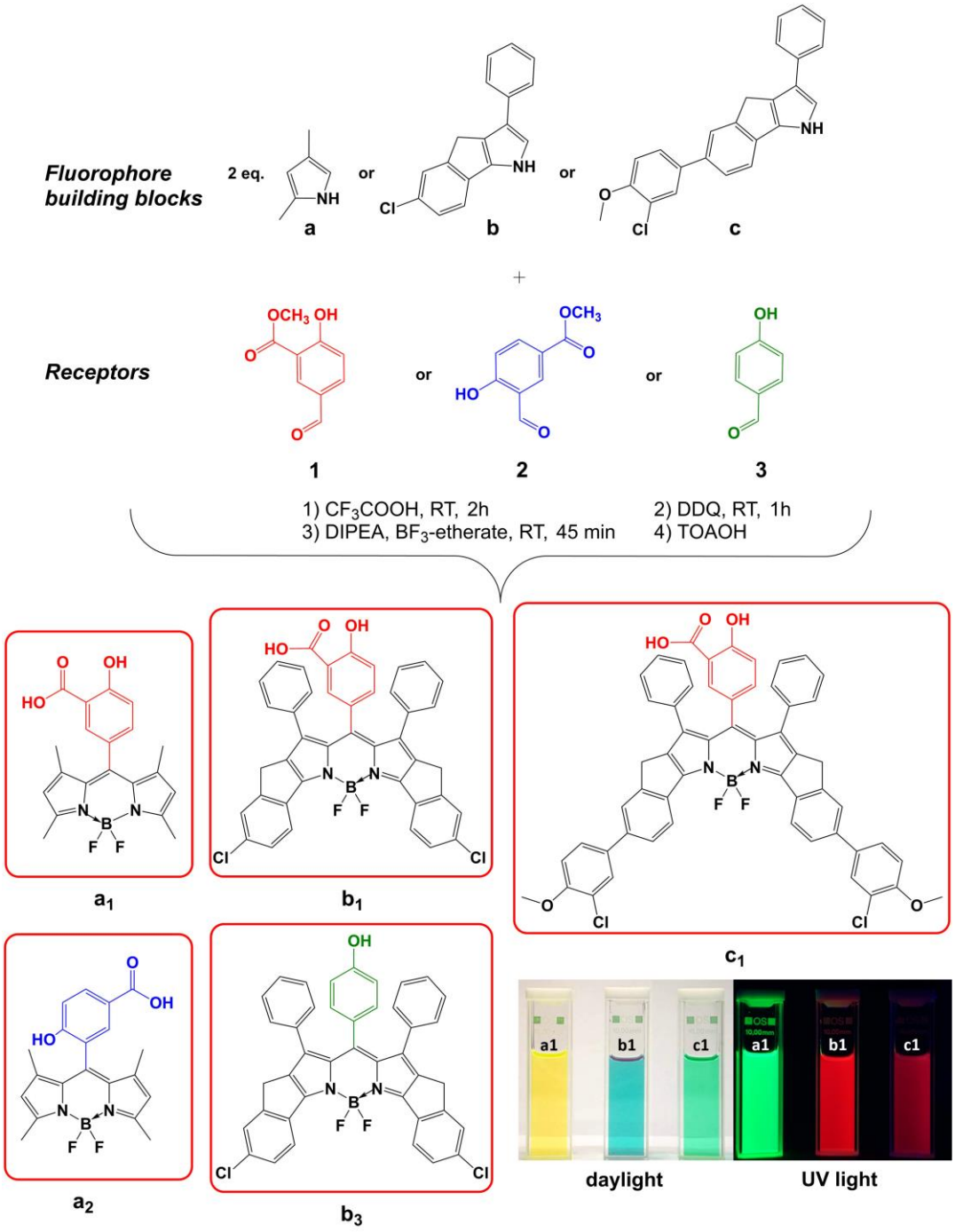

Figure 4-1 Synthesis and structures of BODIPY dyes and photographic images of fluorophores **a1**, **b1** and **c1** in toluene solution under daylight and under illumination with UV light (365 nm, bottom right).

4.5.2 Photophysical properties

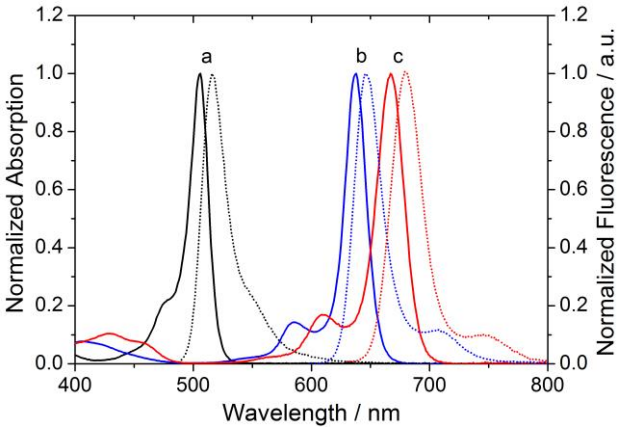

Figure 4-2 Normalized absorption spectra (lines) and emission spectra (dashed lines) of dyes a1 (black lines), b1 (blue lines) and **c1** (red lines) in toluene.

Absorption and emission spectra of the indicators bearing receptor **1** are shown in **Figure 4-2**. The spectra are typical for BODIPY dyes with relatively narrow absorption and emission bands and small Stokes shift of about 10 nm (**Table 4-1**). Dyes of the series **a** relying on the state-of-the-art chromophore absorb and emit in the green part of the spectrum. Extension of the π-system via rigidified phenyl substituents (series **b**) results in the bathochromic shift of about 120 nm. Finally, introduction of additional 3-chloro-4-methoxyphenyl substituents result in further bathochromic shift of about 30 nm (series **c**). The receptor is expected to show very little conjugation with the chromophore due to sterical hindrance from the neighboring methyl (series **a**) or phenyl (**b** and **c**) substituents and in fact only marginally affects the spectral properties (**Table 4-1**).

Table 4-1 Photophysical and sensing properties of the BODIPY dyes at 25 °C. Absorption maxima (λ_{abs}), molar absorption coefficients (ε), emission maxima (λ_{em}), fluorescence quantum yields (Φ) and fluorescence lifetimes (τ) for the dyes in toluene solution. Photobleaching quantum efficiency (Φ_{bl}) for the dyes in THF solution. Apparent pK_a' value for the dyes dissolved in THF/EtOH/buffer solution (ionic strength 100 mM).

Dye	λ_{abs} / nm	ε / M^{-1} cm^{-1}	λ_{em} / nm	Φ	τ / ns	Φ_{bl}	pK_a'
a1	506	60 000	516	0.86	3.90	1.9×10^{-5}	11.4
a2	510	74 000	522	0.92	5.20	2.1×10^{-5}	10.5
b1	635	146 000	646	0.78	5.20	3.9×10^{-8}	11.6
b3	637	108 000	646	0.83	5.23	1.0×10^{-7}	11.7
c1	667	102 000	680	0.49	4.57	5.7×10^{-8}	n. d.[a]

[a] Solubility of the dye in THF/EtOH/buffer solution is too poor.

Fluorescence quantum yields of almost all the dyes (protonated form) are very high and exceed 78% (**Table 4-1**). Dye **c1** has somewhat lower quantum yield (49%) which is nevertheless rather high for the dye emitting in the far red part of the electromagnetic spectrum. Considering high molar absorption coefficients it can be concluded that all the dyes show excellent fluorescent brightness (defined as a product of ε and Φ).

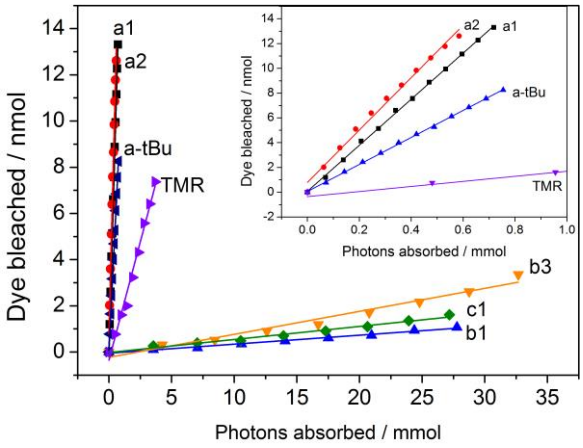

Figure 4-3 Photodegradation of indicators and reference dyes and corresponding linear fit.

Photostability is another parameter relevant for practical applications. In order to estimate the photostability, we irradiated the solutions of the dyes in THF (except for TMR which was dissolved in water) with a metal-halogen lamp and quantified the photodegradation via UV-Vis spectroscopy (**Figure S 4-2-8**, Supporting information). As reference dyes a BODIPY fluorophore **a-*t*Bu** and commercially available tetramethylrhodamine ethyl ester perchlorate (TMR) were chosen. **a-*t*Bu** represents analogue of dyes a1 and a2 but bears inert p-tert-butylphenyl substituent instead of a pH sensitive receptor. This dye is also almost identical to the commercially available [1-[(3,5-Dimethyl-1H-pyrrol-2-yl)(3,5-dimethyl-2H-pyrrol-2-ylidene)methyl]-4-iodobenzene](difluoroborane) (CAS: 250734-47-5) but bears no iodine atom that can potentially promote faster bleaching due to enhanced population of the triplet state. TMR is a typical representative of rhodamine dyes; the photostability of TMR and other rhodamine and coumarin dyes was studied by Eggerling and co-workers.[214]

As can be seen (**Figure 4-3**), dyes **a1**, **a2**, **a-*t*Bu** show much faster photodegradation compared to TMR, that in turn bleaches much faster than the π-extended BODIPYs **b1**, **b3** and **c1**. The quantitative parameter, the photobleaching quantum efficiency Φ_{bl} is calculated from the slope of the curve (number of bleached dye molecules vs. total number of absorbed photons) and is compared in **Table 4-1**. Φ_{bl} for **a-*t*Bu** is calculated to be 1.1×10^{-5}, which is comparable to that of **a1** and **a2**, indicating that the nature of receptor only minor affects the photobleaching rates. Φ_{bl} for TMR is ~10-fold lower (2.0×10^{-6}) than for **a1** and **a2**. Finally, indicators **b1**, **b3** and **c1** show Φ_{bl} of 3.9×10^{-8} – 1.0×10^{-7} and are thus more than two orders of magnitude more photostable than the dyes based on chromophore **a**. Such drastic improvement of the photostability compared to the dyes of series **a** might be due to electron-withdrawing effect of the aromatic substituents attached to the pyrrole rings or to saturation of all available positions in the pyrrole rings reducing their potential reactivity. It can be concluded that the π-extended BODIPYs represent a particularly attractive platform for design of optical sensors but also for application in other fields (e.g. fluorescent labels) combining the long-wavelength absorption and emission, excellent brightness and unmatched photostability.

4.5.3 Acid-base equilibrium

The investigated type of the optical CO_2 chemosensor relies on use of a pH indicator, therefore pH sensing properties of the new dyes are of utmost importance. As was shown by Mills and co-workers, the sensitivity of the sensors correlates fairly well with the pK_a value of the indicator (higher pK_a – higher sensitivity).[141] On the other hand, other factors such as sterical availability of the receptor and hydrophilicity of the microenvironment are expected to affect the sensitivity as well. Here we expected receptors **1** and **2** to show significantly different behaviour compared to the receptor **3** which is phenol without any substituents. In fact, receptors **1** and **2** bear additional carboxylic group from a permanent ion pair with bulky quaternary ammonium cation.

Figure 4-4 exemplifies the pH sensitivity of dye **a1** in tetrahydrofuran/ethanol/aqueous buffer (1:1:1 v/v/v); the response of other indicators can be found in Supporting Information (**Figure S 4-9-11**). pH sensitivity can also be observed in organic solvents such as dichloromethane and chloroform. As can be seen from **Figure 4-4** and **Figure S 4-12** (Supporting Information), fluorescence is virtually completely "switched off" upon deprotonation of the receptor. This can be attributed to efficient photoinduced electron transfer from phenolate to the chromophore.[36] This behaviour is in full agreement with the literature reports on phenol-modified BODIPY dyes.[79,129,215] Receptor **3** shows the highest apparent pK_a' value of 11.7 (**Table 4-1**). Receptors **1** and **2** attached to the chromophore **a** have lower pK_a' values (11.4 and 10.5, respectively) which is explained by the electron-withdrawing effect of the carboxy group. Proximity of phenol to the BODIPY core appears to be important as well with **a2** showing lower pK_a' than dye **a1**.

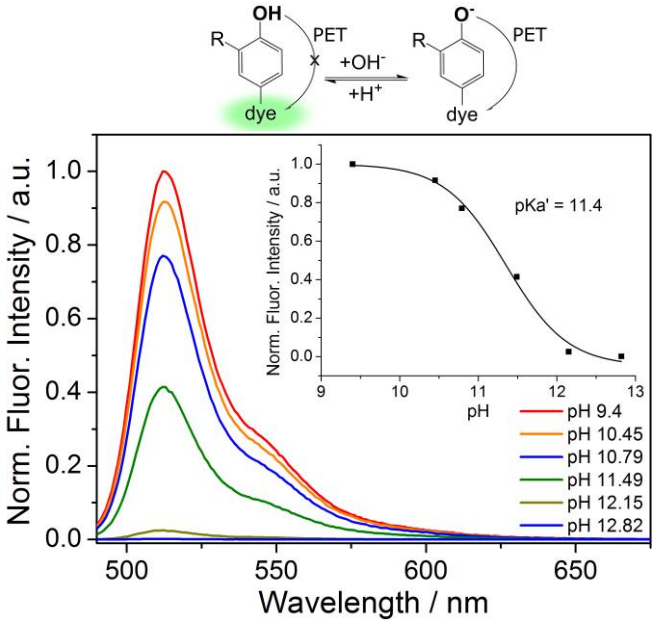

Figure 4-4 pH dependency of the emission spectra of **a1** in THF/EtOH/aqueous buffer (1:1:1 v/v/v) and the corresponding calibration curve with fit using Boltzmann sigmoid (inset).

4.5.4 Carbon dioxide sensing properties

Optical CO_2 chemosensors rely on the indicators dissolved in a polymeric matrix (ethyl cellulose) along with a lipophilic organic base (tetraoctylammonium hydrogencarbonate, $TOAHCO_3$). Importantly, the quaternary ammonium cation builds ion pairs with phenolate and, in case of all indicators except **b3,** also with carboxylate. Such ion pairing was expected to strongly affect the microenvironment of the dye. The 1.25 µm-thick sensor layers are additionally covered by a thin layer of CO_2 permeable perfluorinated Hyflon AD 60 polymer that acts as a barrier protecting the sensing layer from poisoning by acidic volatile species.[151] **Figure 4-5a** exemplary shows emission spectra of the sensor based on **c1**. As can be seen, fluorescence is "switched on" in presence of carbon dioxide, with most dynamics below ~50 hPa CO_2. Sensors based on other dyes show similar behavior (**Figure S 4-13-16**, Supporting Information). Response of sensors based on different indicators is compared in **Figure 4-5b-d**. The pCO_2 values corresponding to 50% of the fluorescence change (pCO_2 at S = ½) are compiled in **Table 4-2**. The sensor based on **a2** is the most insensitive among all showing the dynamics up to 945 hPa CO_2. This material may be interesting for food packaging applications since the CO_2 content in Modified Atmosphere Packaging is typically very high. Comparison of **a1** and **a2** reveals dramatically better sensitivity of the former probably due much higher pK_a' value (11.4 and 10.5 for **a1** and **a2**, respectively). Generally, all the indicators relying on receptor **1** show high sensitivity in the sensing materials (pCO_2 at S = ½ is 23-63 hPa). Sensitivity of the **b3** bearing simple phenol receptor is the highest among all the dyes which again correlates with the higher pK_a value of the dye **b3**. Although the sensor based on **b3** shows excellent dynamics up to ~ 50 hPa CO_2 making it potentially suitable for environmental monitoring, the lower brightness of the material (**Table 4-2**) should be considered as well. Comparison of the sensing properties of **a1**, **b1** and **c1**, all bearing the same receptor but based on different BODIPY chromophores, reveals the lowest sensitivity for the dye **a1**. This may be due to the lowest pK_a' value of the dye but also may correlate to the size of the dye. In fact, the sensitivity of the sensors utilizing bulky chromophores **c1** and **b1** is higher than for the **a1**-based sensor.

Apart from the sensitivity, brightness of a sensing material is another important parameter. The absolute fluorescence quantum yields (**Table 4-2**) were measured for the immobilized indicators in the fully protonated state which was achieved via poisoning of the sensor with gaseous HCl (Φ_{HCl}). In these conditions all the sensors with the exception of **b3**-based one show high Φ values of about 50%. In case of **b3**, the quantum yield is ~4-fold lower than for other sensors, which may indicate fairly efficient fluorescence quenching even by the protonated receptor.

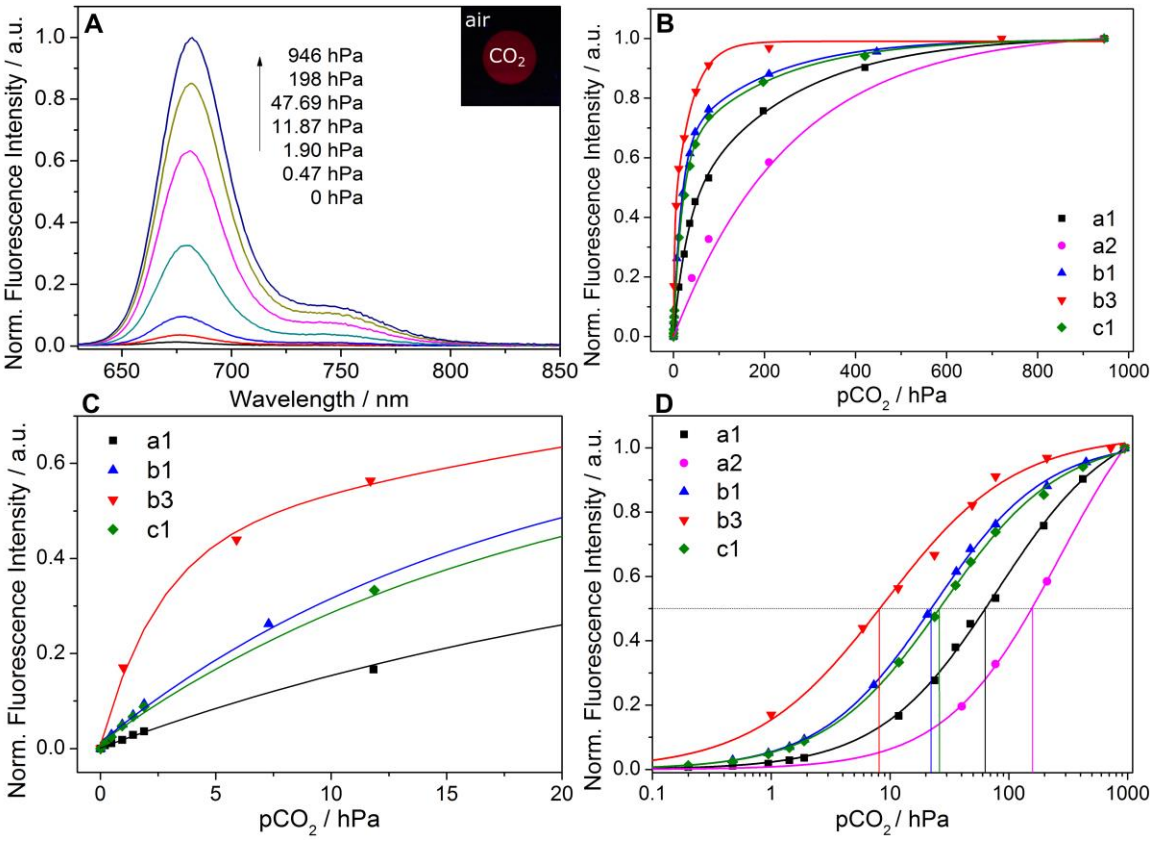

Figure 4-5. CO_2 sensing properties of the new materials. A: Fluorescence spectra of the sensor based on **c1** embedded into EC 49 along with $TOAHCO_3$. Photographic image showing fluorescence of the sensor in presence of 945 hPa pCO_2 under UV light illumination (365 nm, insert). B and C: response of the sensors to CO_2 in the range up to 945 hPa pCO_2 and 20 hPa pCO_2, respectively. D: response of the sensors to CO_2 in the range up to 945 hPa pCO_2, fit with Boltzmann sigmoid. All measurements are performed at 25 °C and 100% relative humidity.

Although all the sensors show saturation of the fluorescence intensity at 945 hPa pCO_2 (FI_{CO2}, **Table 4-2**), the brightness of the sensors in these conditions is not identical. Whereas the fluorescence intensity ratio FI_{CO2}/FI_{HCl} is high in case of the sensors based on **a1** and **c1** (> 0.5), it is much lower for **b1**, **b3** and particularly **a2**. In case of **b1** and **b3** such behavior can be explained by formation of H-aggregates evidenced by dramatic change in the absorption spectra (**Figure S 4-17-24**). In fact, the absorption spectra of **b1** and **b3** in ethyl cellulose along with tetraoctylammonium hydrogencarbonate show a strong decrease of the absorbance accompanied by the hypsochromic shift and significant broadening of the spectrum (**Figure S 4-19** and **S 4-21**, respectively). Change of the color from blue to rose is also observed (**Figure S 4-19** and **S 4-21** inset). The typical spectrum of the BODIPY is recovered after protonation with 945 hPa pCO_2 and poisoning of the sensor with HCl, respectively. Formation of such aggregates for BODIPY dyes was documented in literature and strongly depends on the chromophore-matrix interactions.[216,217] Variation of the base (tetraethylammonium hydrogencarbonate and tetrabutylammonium hydrogen carbonate instead of TOA) showed that aggregation effects decrease with increasing hydrophilicity of quaternary ammonium cation (TOA>TBA>TEA, **Figure S 4-19-23**, Supporting Information). Unfortunately, in case of TEA the sensitivity of the CO_2 sensors was dramatically affected as well and deprotonation of the indicators in the absence of CO_2 was not possible anymore.

Table 4-2: Characteristics of the CO_2 sensors. Sensitivity of the ethyl cellulose-based sensor expressed as pCO_2 corresponding to 50% of the fluorescence change (pCO_2 at S = ½), fluorescence quantum yields for the CO_2 sensors after poisoning with HCl (Φ_{HCl}) and fluorescence intensity ratio (FI_{CO2}/FI_{HCl}) for the sensors equilibrated at 945 hPa pCO_2 and after poisoning with HCl, respectively.

Dye	pCO_2 at S = ½ / hPa	Φ_{HCl}	FI_{CO2}/FI_{HCl}
a1	63	0.52	0.62
a2	156	0.66	0.03
b1	23	0.61	0.12
b3	8	0.15	0.15
c1	26	0.55	0.53

On the contrary, the absorption spectrum of **a1** (**Figure S 4-17**) shows only a slight hypsochromic shift explained by electronic effects of the receptor on the chromophore. The behavior of **c1** (**Figure S 4-22**) is similar to that of **a1** but some broadening of the absorption band is also visible which may indicate some degree of aggregation as well. Generally, the behavior of the sensors based on **a1** and **c1** (little change in the absorption spectrum but strong change in the fluorescence) is what one would expect for the dyes based on PET effect. Interestingly, the sensor based on **a2** does not show much change in the absorption spectrum (**Figure S 4-18**) but a very low FI_{CO2}/FI_{HCl} ratio is observed.

The above data indicate the importance of the chromophore structure on the photophysical properties of the material. The planar chromophores without bulky substituents show strong tendency to aggregate in ethyl cellulose under certain conditions. The introduction of alkoxyphenyl-substituent appears to be a promising strategy to overcome the aggregation but a simple alkyl substituent is likely to be sufficient as well. It should be noted here that variation of the matrix polymer and addition of plasticizers would not only affect the sensitivity of the CO_2 sensors but may also positively influence the aggregation behavior of the indicators.

4.5.5 Materials for RGB imaging of carbon dioxide

RGB imaging is an important analytical technique allowing mapping of analyte distribution on surfaces. The basic equipment needed is much simpler than in the set-ups utilizing bandpass filters with no moving parts (such as filter wheels) necessary. RGB imaging can be conveniently realized with a consumer RGB camera or a smartphone [129,177,218,219] and is also implemented in some commercial products (www.presens.de). Referenced imaging is performed by utilizing an analyte-sensitive luminescence in one of the channels and analyte-insensitive luminescence from a reference in another channel. However, since the three color channels show fairly strong overlap, selection of an indicator and a reference dye with appropriate spectral properties can be rather challenging (**Figure S 4-23**). The emission of the indicators of the series **a** and **b** almost ideally matches the maximum sensitivity of the green and red RGB channels, respectively (**Figure S**

4-23). As reference materials for the green- and red-emitting indicators we selected polystyrene microparticles doped with Lumogen Red and commercially available Daylight Fluorescent Green Pigment that emit in the red and green parts of the spectrum, respectively. These particles can be homogeneously dispersed in the protective Hyflon AD60 layer. **Figure 4-6** shows the response of the ratiometric materials which is generally similar to the response of the unreferenced sensors (**Figure 4-5**). At this point it should be mentioned that the sensor material based on **b1** serves only for demonstration purposes and further modification of the chromophore core is required to improve the sensor performance.

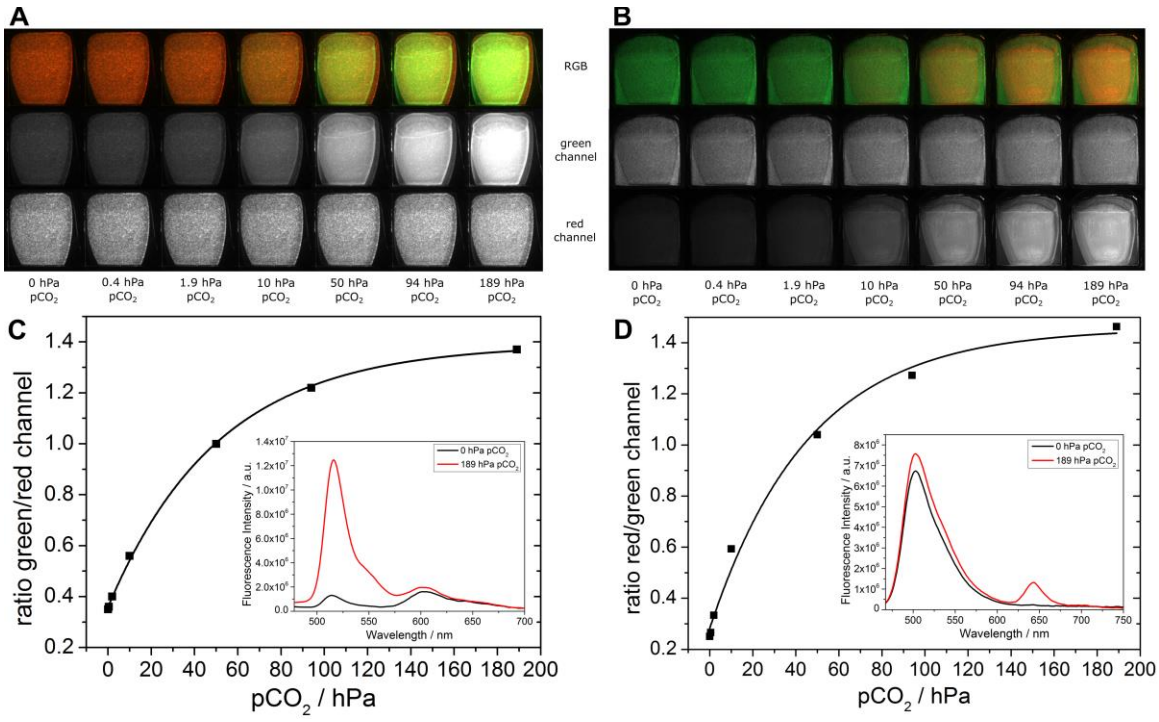

Figure 4-6 RGB imaging with sensor materials based on **a1** (left) and b1 (right). A and B: RGB, red and green channel images of sensors on **a1** and **b1**, respectively, at different pCO_2. C and D: Ratiometric response of the sensors; insets: emission spectra of the sensor materials in absence of CO_2 (black lines) and at 946 hPa pCO_2 (red lines). All measurements are performed at 25 °C and 100% relative humidity.

4.5.6 Referenced sensing materials for phase fluorometry

Recently we presented a modular platform which enables sensing of different vital parameters with a single opto-electronic set-up.[164,165] Such unification would allow reducing measurement costs and therefore spreading sensing technology into new fields. Whereas presented O_2 and pH sensors showed excellent compatibility to the reader, the CO_2 sensor utilized an absorption-based indicator and made use of a sophisticated inner-filter effect read-out to obtain referenced luminescence signal.[151] In fact, the reported sensor requires addition of two reference emitters in form of particles (**Figure S 4-24**, Supporting Information) that reduces homogeneity of the material and make sensor manufacture more challenging particularly if formats other than planar optodes (e.g. fiber-

optic microsensors) are considered. Among the indicators presented here, **c1** shows fairly good compatibility with the opto-electronic set-up of the reader. In fact, the 625-nm LED is suitable for the excitation of the indicator in the shoulder (**Figure 4-2**) and significant part of the NIR emission can be detected after passing the long pass-filter. In order to achieve referenced phase shift-based read-out, we added Egyptian blue microcrystalline powder in the Hyflon layer. Egyptian blue[211] is an inert inorganic phosphor with long emission lifetime (~150 µs) thus enabling referenced read-out of fluorescent indicator with help of a dual lifetime referencing technique (DLR).[92,220] **Figure 4-7** shows that this read-out scheme works very well and the sensor shows fully reversible behaviour in the pCO_2 range from 0 to 1.9 hPa. The phase shifts values of the two sensors are not identical due to not fully homogeneous distribution of reference material and indicator dye in the solid sensor layer. The sensor shows very good resolution at pCO_2 well below atmospheric levels (**Figure 4-7b**). The LOD was estimated to be 0.009 hPa making the sensor one of the most sensitive fluorescent CO_2 sensors reported up to date. The response times t_{90} (0.5-1.0 hPa pCO_2) of 220 s and recovery times t_{90} (1.0-0.5 hPa pCO_2) of 210 s at 25 °C are acceptable for most applications.

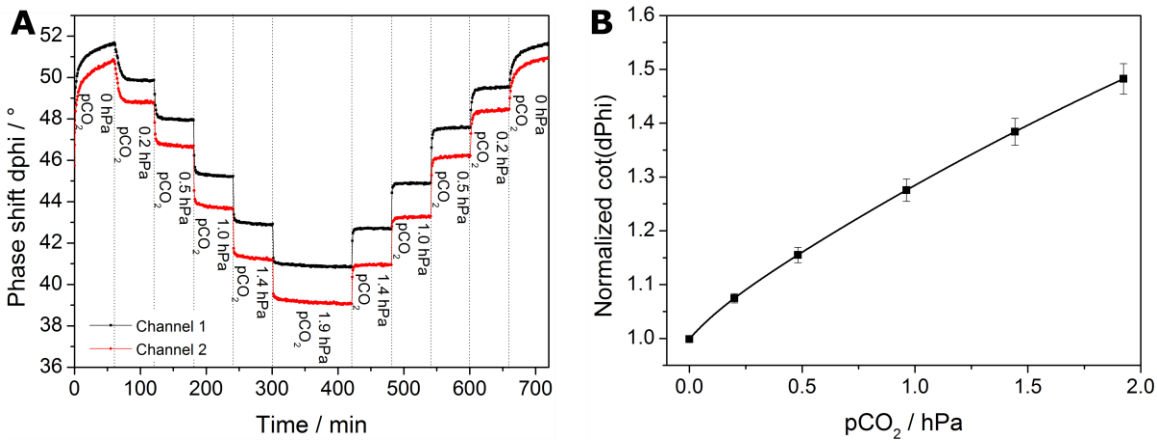

Figure 4-7 A: Response of two DLR-referenced sensors (black and red line) based on **c1** at 25 °C and 100% relative humidity. B: corresponding calibration curve.

4.6 Conclusions

In conclusion, we prepared a series of new BODIPY pH indicators for application in optical carbon dioxide sensors. The spectral properties of the indicators are determined by the chromophore with the absorption and emission of the dyes spanning from the green to far-red part of the spectrum. All the dyes feature high molar absorption coefficients and fluorescence quantum yields resulting in excellent brightness in solution. Photodegradation studies reveal unmatched photostability of the π-extended dyes with bleaching rates more than 2 orders of magnitude lower than for the dyes based on conventional BODIPY chromophore. These degraded significantly faster than tetramethylrhodamine used as a reference. In agreement with previous literature reports, the BODIPY chromophores are rendered pH sensitive via modification with a phenolic receptor. We

have demonstrated that such modification makes them particularly suitable for application in polymer-based CO_2 sensors. The sensitivity of the sensors is mostly governed by the nature of the receptor, and to the less extent by the nature of chromophore. Importantly, the pK_a' of the indicator is not the only factor contributing to the sensitivity. The sensor performance is significantly improved by introduction of the carboxylic group in the o-position to the OH group probably due to formation of additional ion pair with the quaternary ammonium cation. Furthermore, some of the indicators show high tendency to form aggregates in ethyl cellulose which does not influence the sensitivity but significantly reduces the sensor brightness and applicability. Introduction of a bulky alkoxy-phenyl substituent not only results in the further bathochromic shift of the absorption and emission spectra but also minimizes the undesired aggregation effects. The sensors prepared from the dyes based on combination of 3-carboxy-4-hydroxyphenyl receptor and π-extended chromophores show unmatched sensitivity, resolving ambient CO_2 levels which is particularly interesting for environmental applications. Although 2-hydroxy-5-carboxyphenyl receptor induces response at much higher pCO_2 levels, the indicator prepared with this receptor showed low brightness in ethyl cellulose indicating necessity of further modifications. Finally, we also designed several sensing materials for ratiometric imaging of CO_2 distribution with RGB cameras and a referenced material for phase fluorometric read-out. The latter shows good spectral compatibility with the compact devices presented previously.

Acknowledgments

Financial support by the Austrian Academy of Science (ÖAW) at the Institute of Analytical Chemistry and Food Chemistry, Graz University of Technology (DOC-Fellowship of David Pfeifer) is gratefully acknowledged. The authors also thank Lukas Tribuser (synthesis), Lukas Troi and Loretta Eggenreich (photostability set-up and measurements) for their support.

4.7 Supporting Information

4.7.1 Synthesis

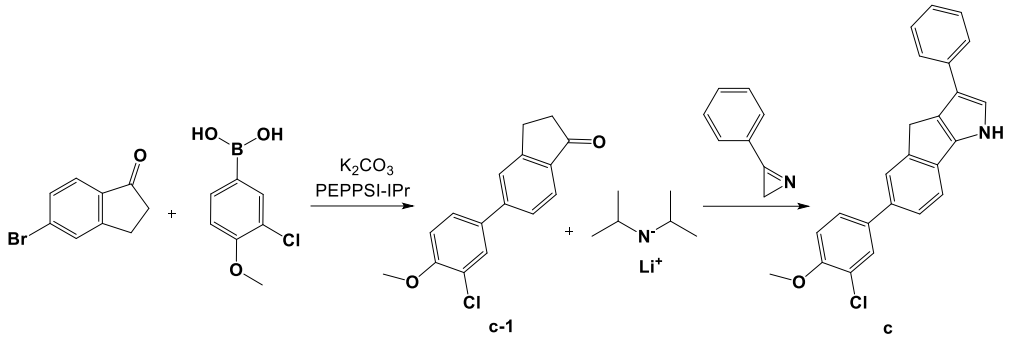

Figure S 4-1 Synthesis of 6-(3-chloro-4-methoxyphenyl)-3-phenyl-1,4-dihydroindeno[1,2-b]pyrrole **c**.

5-Bromo-1-indanone (573.7 mg, 2.72 mmol, 1 eq), 3-chloro-4-methoxyphenylboronic acid (565.2 mg, 3.03 mmol, 1.1 eq) and K_2CO_3 (1.13 g, 8.18 mmol, 3 eq.) were dissolved in 40 mL THF, 40 mL toluene and 20 mL H_2O. The mixture was degassed for 30 min by vigorously stirring under heavy Argon flow. After addition of the catalyst [1,3-Bis(2,6-Diisopropyl-phenyl)imidazol-2-ylidene](3-chloropyridyl)palladium(II) dichloride (PEPPSI-IPr) (4.5 mg, 0.24 mol%) the reaction mixture was heated up to 40 °C and stirred for 20 h under inert atmosphere. After cooling, the organic phase was washed with water and brine, dried over Na_2SO_4 and evaporated. The resulting residue was purified by column chromatography (silica gel, eluent: CH + EA from pure CH to 4 + 1) to obtain 5-(3-chloro-4-methoxyphenyl)-2,3-dihydro-1H-inden-1-one **c-1** as a yellow solid (661.7 mg, 90%).

^{1}H-NMR (300 MHz, $CDCl_3$): δ 7.80 (d, J = 8.0 Hz, 1H), 7.67 (d, J = 2.0 Hz, 1H), 7.62 (s, 1H), 7.51 (dd, J = 14.4, 5.6 Hz, 2H), 7.02 (d, J = 8.5 Hz, 1H), 3.96 (s, 3H), 3.24 – 3.14 (m, 2H), 2.80 – 2.69 (m, 2H).

c-1 (500.1 mg, 1.83 mmol, 1 eq) was dissolved in 25 mL dry THF, cooled down to –78 °C and LDA (2 M in THF, 0.95 mL, 1.01 eq) was added. After 10 min stirring 3-phenyl-2H-azirene (0.23 mL, 2.16 mmol, 1.2 eq) were added dropwise. The mixture was stirred at –78 °C for 20 min, warmed up to RT, quenched with water and neutralized with diluted HCl to a pH of about 7. THF was removed under vacuum and the mixture was extracted with DCM, dried over Na_2SO_4 and filtered through a short silica column. After removal of the solvent under vacuum, the residue was recrystallized from CH/EA to obtain the product **c** as greenish crystals.

^{1}H-NMR (300 MHz, $CDCl_3$): δ 8.64 (s, 1H), 7.75 – 7.34 (m, 10H), 7.30 – 7.17 (m, 2H), 7.04 (d, J = 8.6 Hz, 1H), 3.94 (s, 3H), 3.83 (s, 2H).

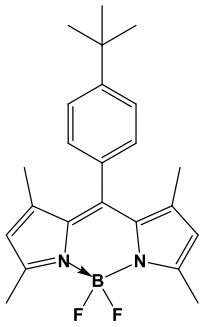

a-*t*Bu

Synthesis of a-*t*Bu. a-*t*Bu was prepared analogously to **a1**, using 4-*tert*-butylbenzaldehyde (85.3 mg, 0.53 mmol, 1 eq), 1,4-dimethylpyrrole **a** (100 µL, 2.63 mmol, 2 eq), 10 mL of anhydrous DCM, DDQ (131.1 mg, 0.58 mmol, 1.1 eq), DIPEA (0.89 mL, 5.26 mmol, 10 eq) and BF_3OEt_2 (1 mL, 7.9 mmol, 15 eq) instead. The dye was purified by column chromatography (CH/EA gradient) and was obtained as a yellow-reddish powder (80 mg, 40%).

^{1}H NMR (300 MHz, $CDCl_3$): δ 7.49 (d, J = 8.3 Hz, 2H), 7.18 (d, J = 8.3 Hz, 2H), 5.97 (s, 2H), 2.55 (s, 6H), 1.36 (s, 15H).

MS: m/z: [M^-] calcd. for $C_{23}H_{27}BF_2N_2$, 380.29; found, 379.8.

4.7.2 Photophysical properties

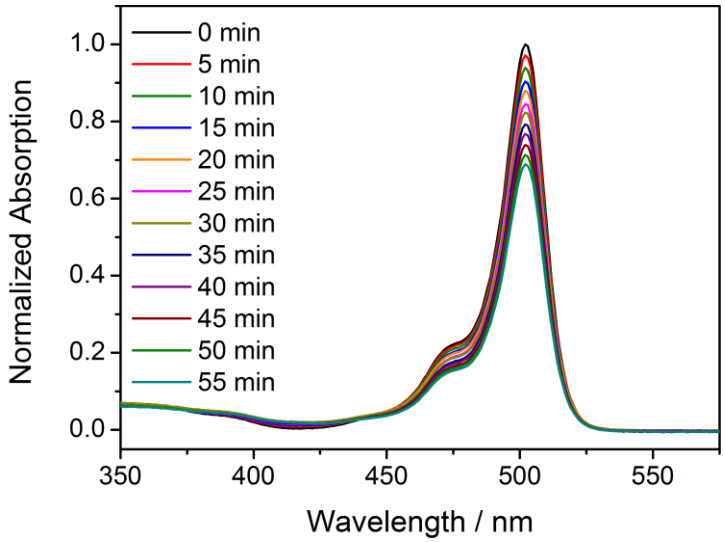

Figure S 4-2 Absorption spectra of **a1** in THF upon irradiation with a metal-halogen lamp.

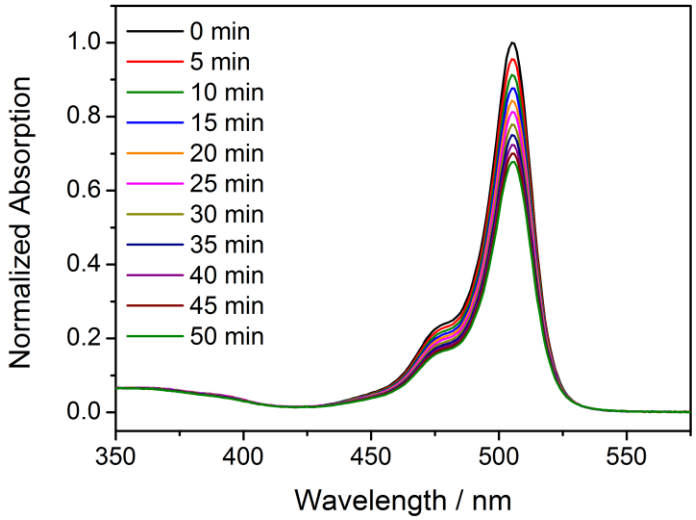

Figure S 4-3 Absorption spectra of **a2** in THF upon irradiation with a metal-halogen lamp.

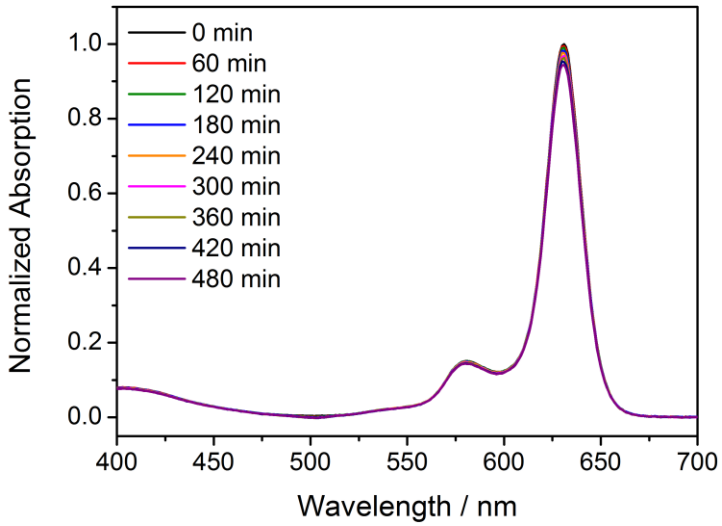

Figure S 4-4 Absorption spectra of **b1** in THF upon irradiation with a metal-halogen lamp.

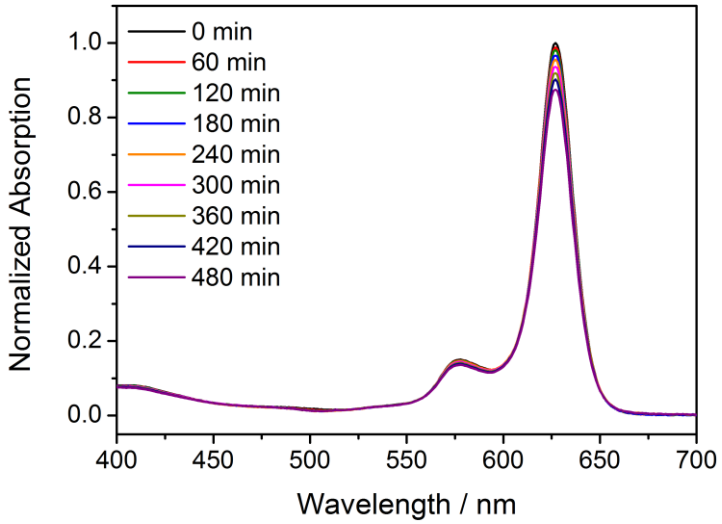

Figure S 4-5 Absorption spectra of **b3** in THF upon irradiation with a metal-halogen lamp.

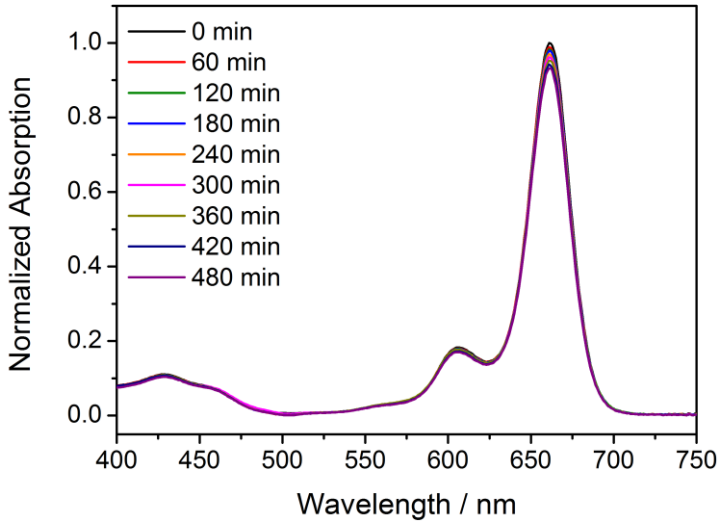

Figure S 4-6 Absorption spectra of **c1** in THF upon irradiation with a metal-halogen lamp.

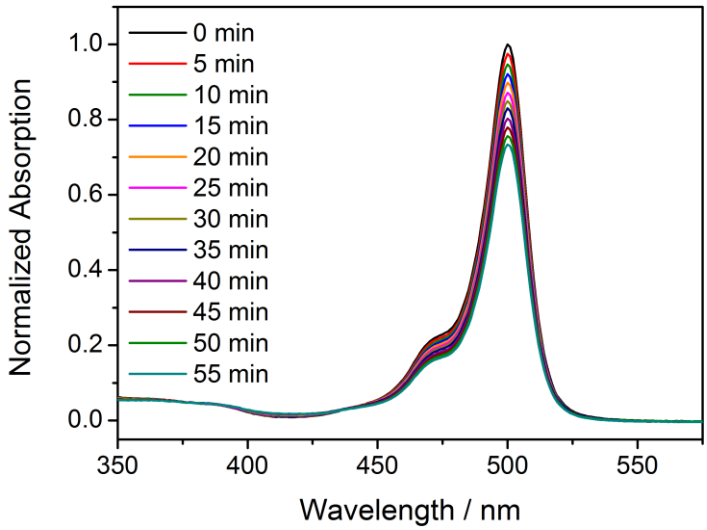

Figure S 4-7 Absorption spectra of **a-*t*Bu** in THF upon irradiation with a metal-halogen lamp.

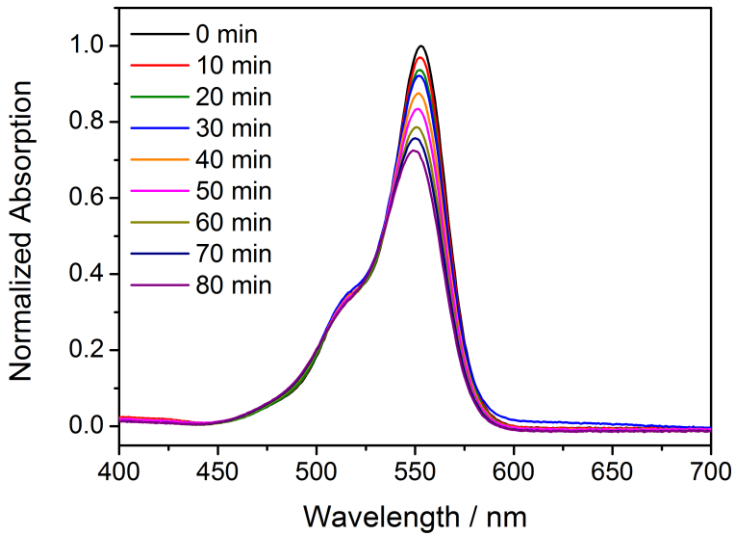

Figure S 4-8 Absorption spectra of **TMR** in water upon irradiation with a metal-halogen lamp.

4.7.3 Acid-base equilibrium

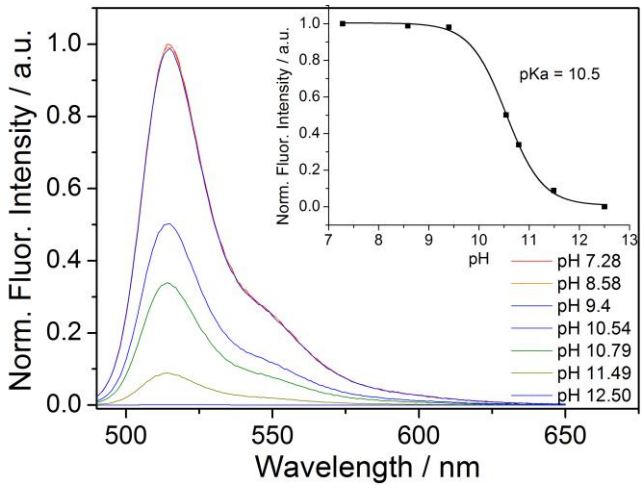

Figure S 4-9 pH dependency of the emission spectra of **a2** in THF/EtOH/aqueous buffer (1:1:1 v/v/v) and the corresponding calibration curve fit with Boltzmann sigmoid.

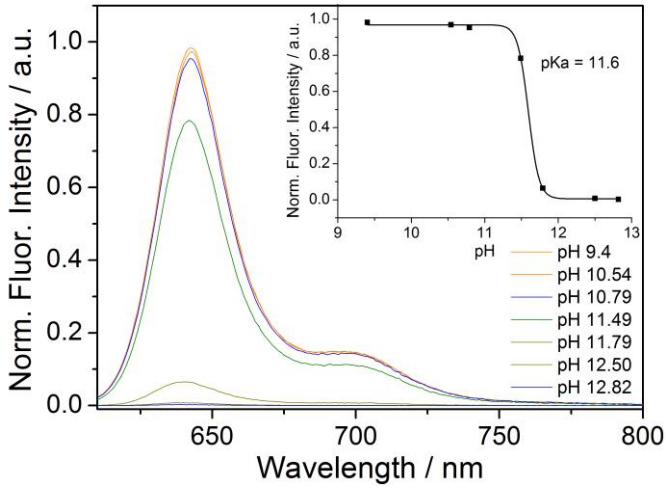

Figure S 4-10 pH dependency of the emission spectra of **b1** in THF/EtOH/aqueous buffer (1:1:1 v/v/v) and the corresponding calibration curve fit with Boltzmann sigmoid.

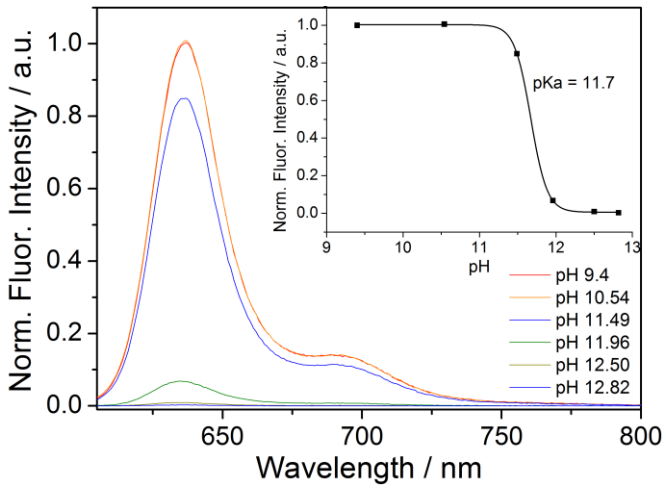

Figure S 4-11 pH dependency of the emission spectra of **b3** in THF/EtOH/aqueous buffer (1:1:1 v/v/v) and the corresponding calibration curve fit with Boltzmann sigmoid.

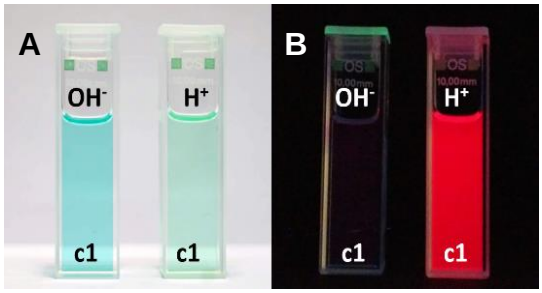

Figure S 4-12 A: Photographic image of indicator **c1** dissolved in dichloromethane in basic (addition of basic tetraoctylammonium hydroxide) and neutral conditions under daylight. B: Photographic image of indicator **c1** dissolved in dichloromethane in basic and neutral conditions under illumination with UV light (365 nm).

4.7.4 Carbon dioxide sensing properties

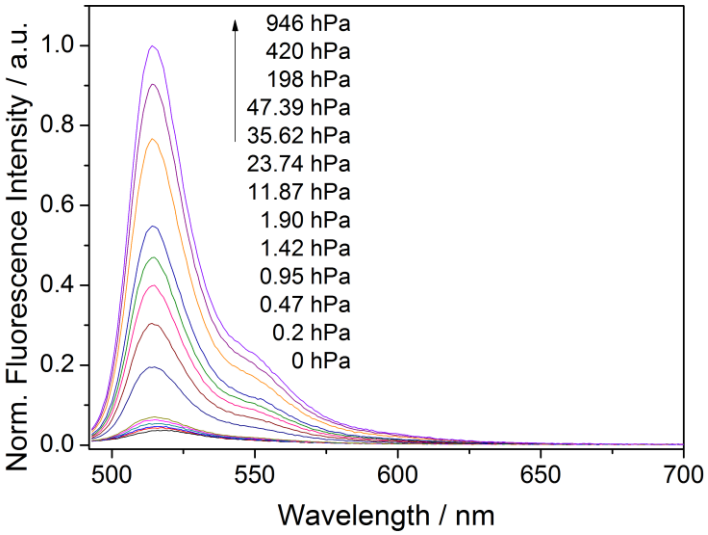

Figure S 4-13 Fluorescence spectra of the sensor based on **a1** embedded into EC 49 along with $TOAHCO_3$. All measurements are performed at 25 °C and 100% relative humidity.

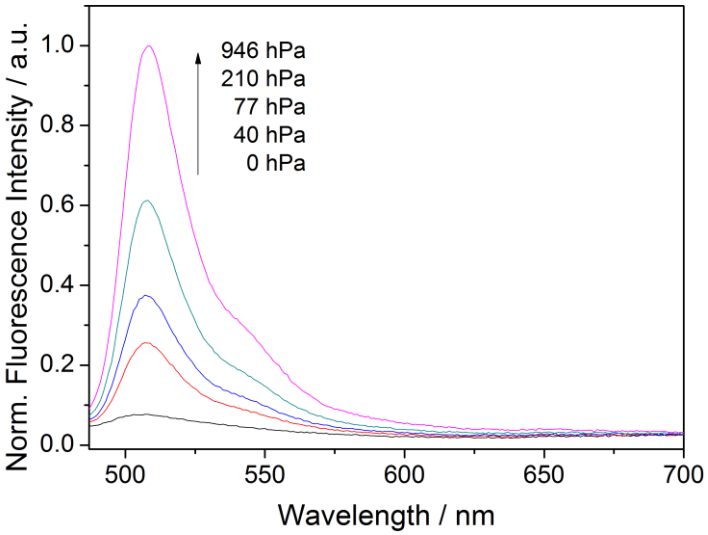

Figure S 4-14 Fluorescence spectra of the sensor based on **a2** embedded into EC 49 along with $TOAHCO_3$. All measurements are performed at 25 °C and 100% relative humidity.

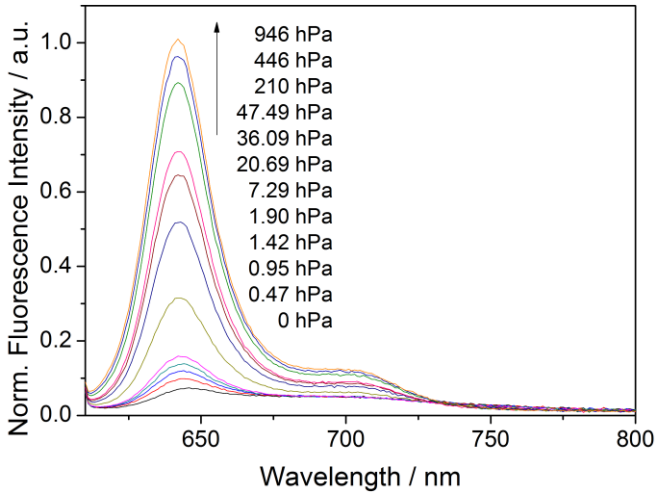

Figure S 4-15 Fluorescence spectra of the sensor based on **b1** embedded into EC 49 along with $TOAHCO_3$. All measurements are performed at 25 °C and 100% relative humidity.

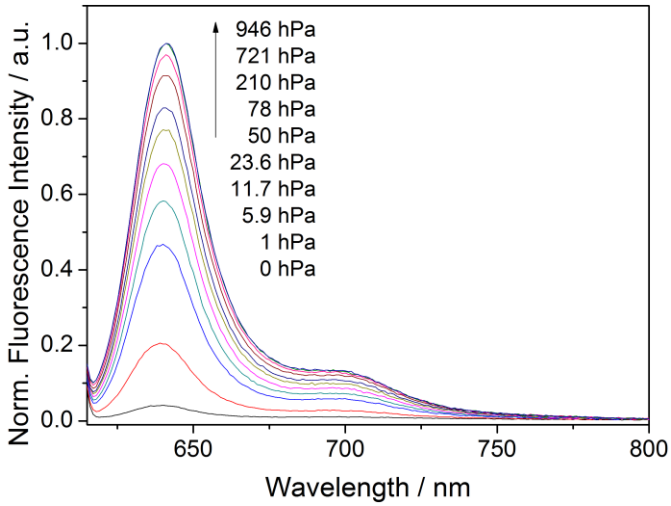

Figure S 4-16 Fluorescence spectra of the sensor based on **b3** embedded into EC 49 along with $TOAHCO_3$. All measurements are performed at 25 °C and 100% relative humidity.

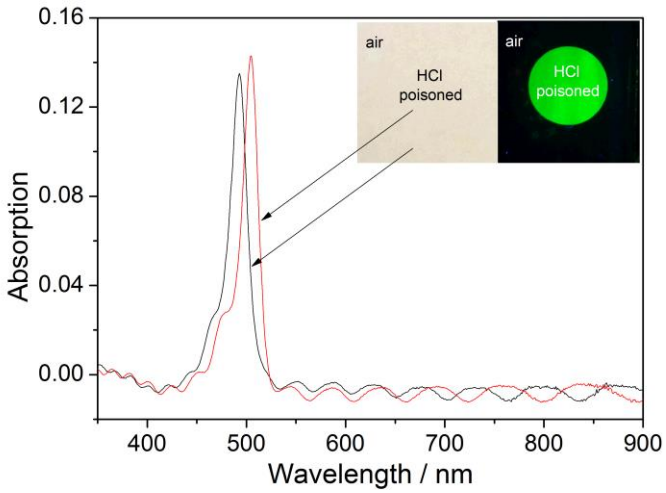

Figure S 4-17 Absorption spectra of the sensor based on **a1** embedded into EC 49 along with $TOAHCO_3$ under atmospheric conditions (~0.4 hPa pCO_2, black line) and fully protonated (treated with gaseous HCl, red line). Photographic images of sensor material with fully protonated spot under daylight (left) and under illumination with UV light (365 nm, right).

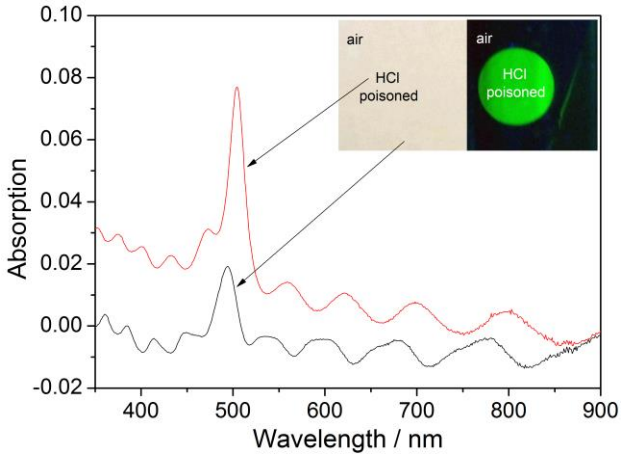

Figure S 4-18 Absorption spectra of the sensor based on **a2** embedded into EC 49 along with $TOAHCO_3$ under atmospheric conditions (~0.4 hPa pCO_2, black line) and fully protonated (treated with gaseous HCl, red line). Photographic images of sensor material with fully protonated spot under daylight (left) and under illumination with UV light (365 nm, right).

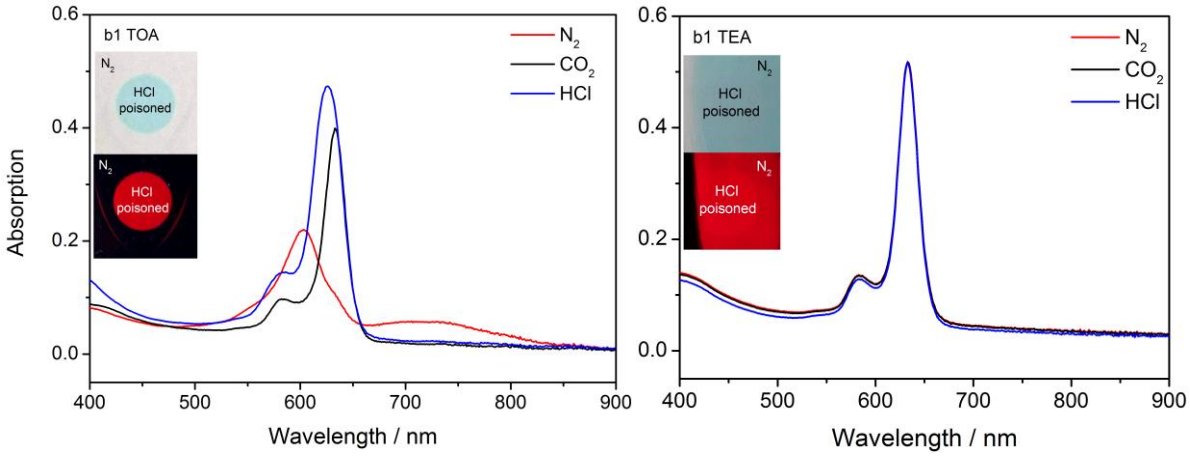

Figure S 4-19 Absorption spectra of the sensor based on **b1** embedded into EC 49 along with $TOAHCO_3$ (left) and $TEAHCO_3$ (right) under N_2 (red line), under 945 hPa pCO_2 (black line) and fully protonated (treated with gaseous HCl, blue line). Photographic images of sensor material with fully protonated spot under daylight (top) and under illumination with UV light (365 nm, bottom).

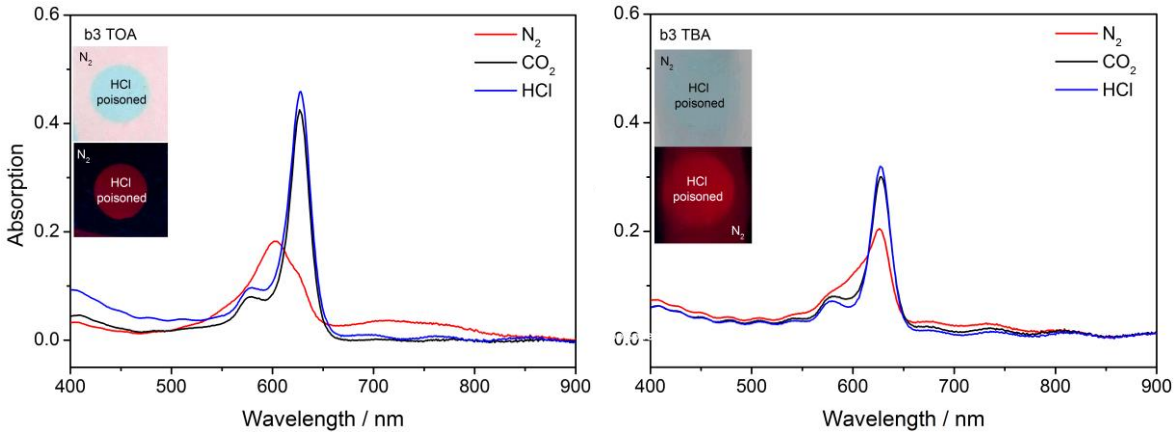

Figure S 4-20 Absorption spectra of the sensor based on **b3** embedded into EC 49 along with $TOAHCO_3$ (left) and $TBAHCO_3$ (right) under N_2 (red line), under 945 hPa pCO_2 (black line) and fully protonated (treated with gaseous HCl, blue line). Photographic images of sensor material with fully protonated spot under daylight (top) and under illumination with UV light (365 nm, bottom).

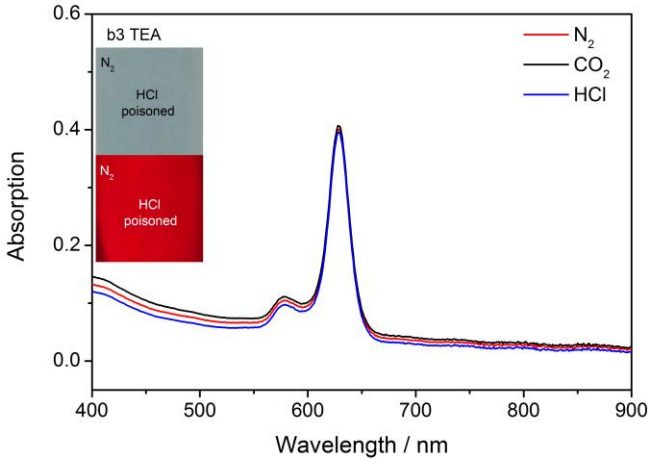

Figure S 4-21 Absorption spectra of the sensor based on **b3** embedded into EC 49 along with $TEAHCO_3$ under N_2 (red line), under 945 hPa pCO_2 (black line) and fully protonated (treated with gaseous HCl, blue line). Photographic images of sensor material with fully protonated spot under daylight (top) and under illumination with UV light (365 nm, bottom).

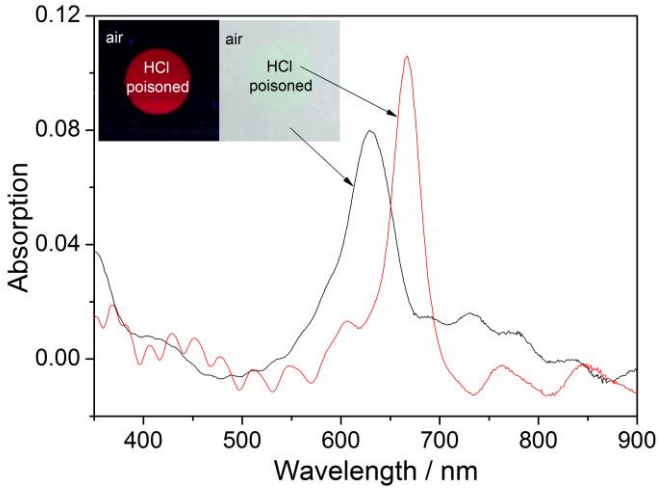

Figure S 4-22 Absorption spectra of the sensor based on **c1** embedded into EC 49 along with $TOAHCO_3$ under atmospheric conditions (~0.4 hPa pCO_2, black line) and fully protonated (treated with gaseous HCl, red line). Photographic images of sensor material with fully protonated spot under daylight (right) and under illumination with UV light (365 nm, left).

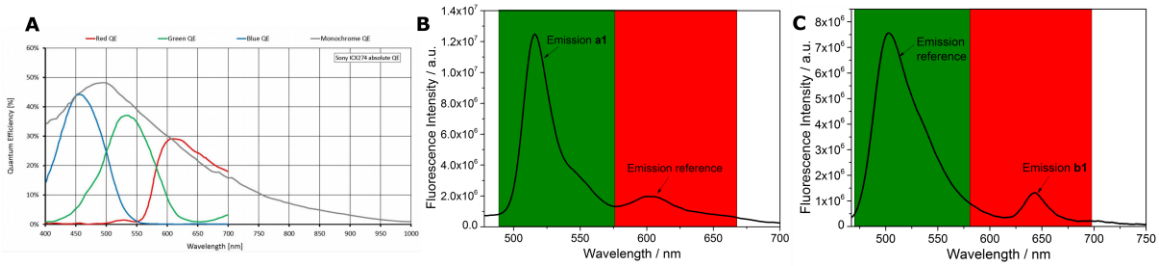

Figure S 4-23 A: Maximum sensitivity and quantum efficiency of blue (blue line), green (green line) and red (red line) channel of Sony ICX274 CCD sensor used in Marlin F-201 camera.[221] B and C: Emission spectra of sensor material based on **a1** with red reference and **b1** with green reference, respectively.

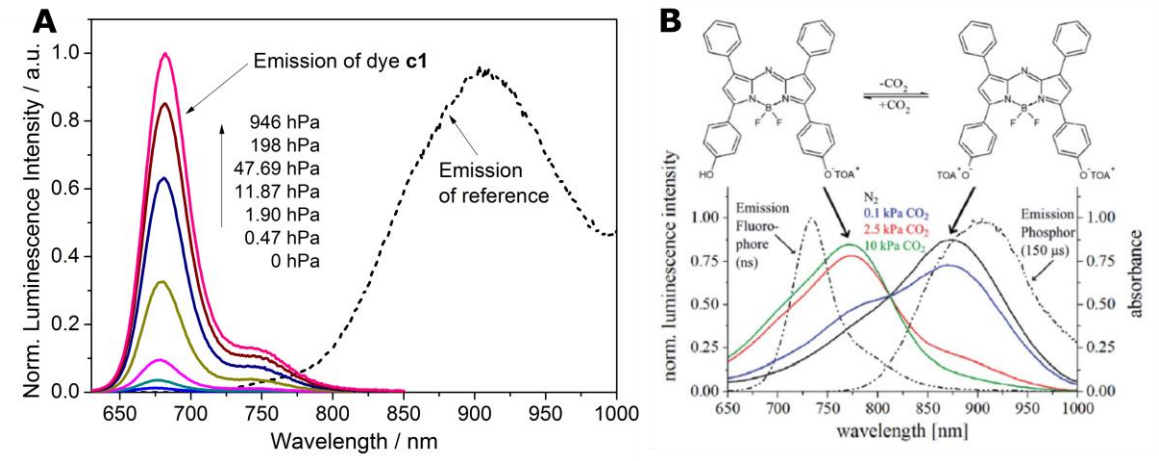

Figure S 4-24 A: Emission spectra of referenced sensor material based on **c1** at different pCO_2 pressures and emission spectrum of reference particles (dashed lines). B: Absorption and emission spectra of the CO_2 sensor based on colorimetric aza-BODIPY pH indicator, an inert chromophore and phosphorescent reference particles and a gas-permeable protection layer.[151]

4.7.5 Mass spectra

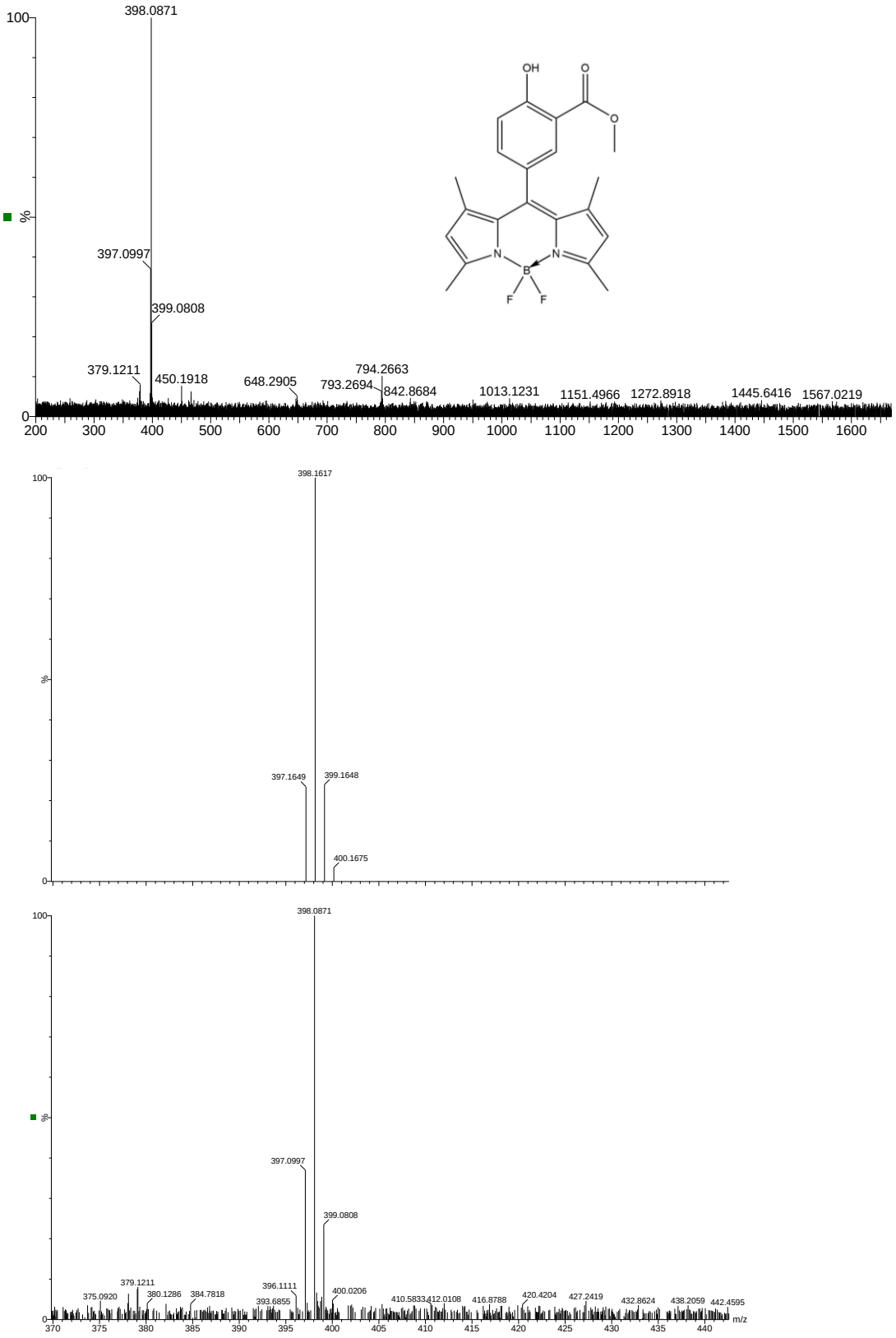

Figure S 4-25 Experimental MALDI-TOF Mass spectrum (upper part); mass relevant range for theoretical isotope pattern (middle) and experimental MALDI-TOF-Mass spectrum (lower part) of **a1** in the methyl ester form**.**

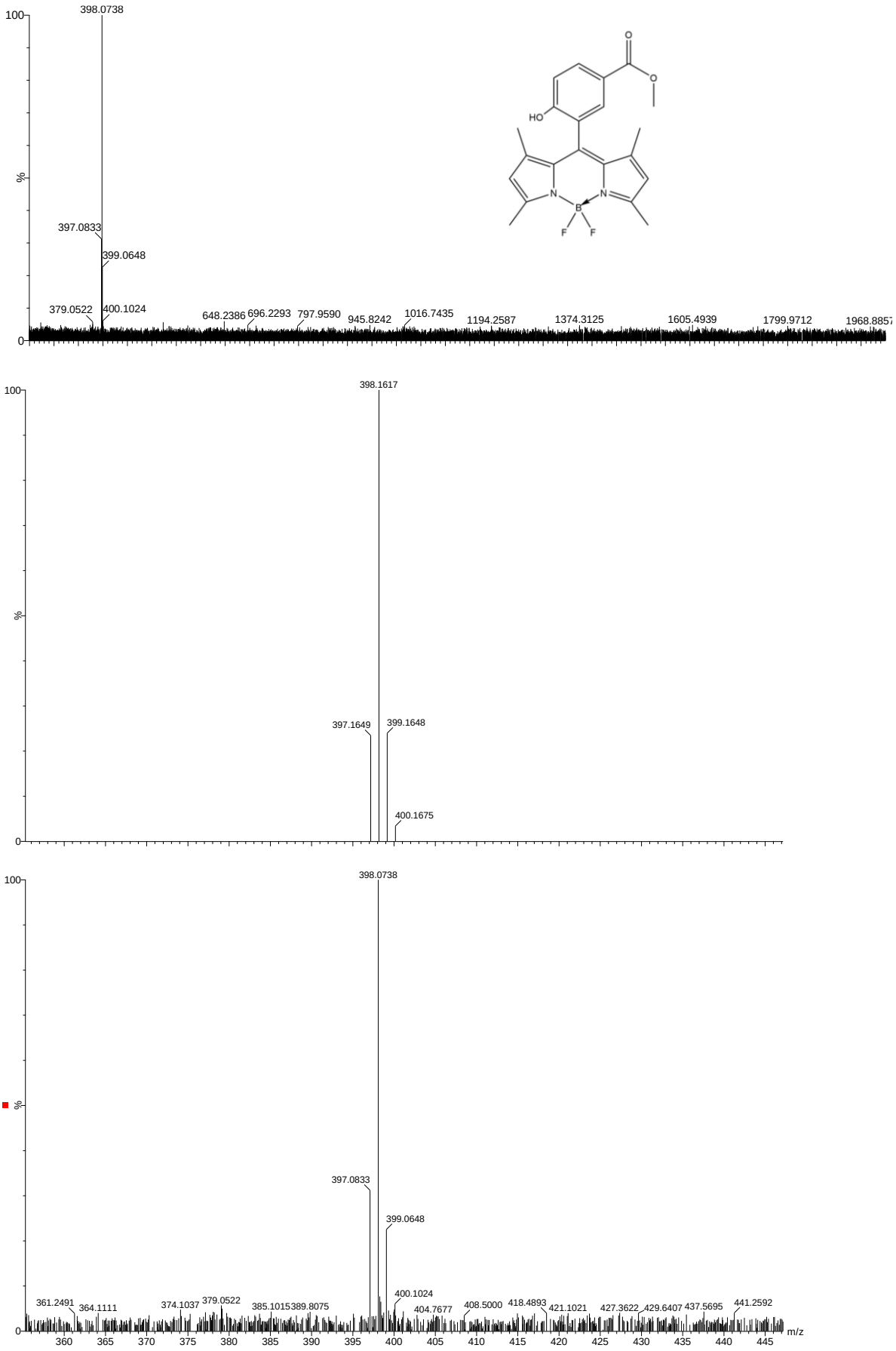

Figure S 4-26 Experimental MALDI-TOF Mass spectrum (upper part); mass relevant range for theoretical isotope pattern (middle) and experimental MALDI-TOF-Mass spectrum (lower part) of **a2** in the methyl ester form.

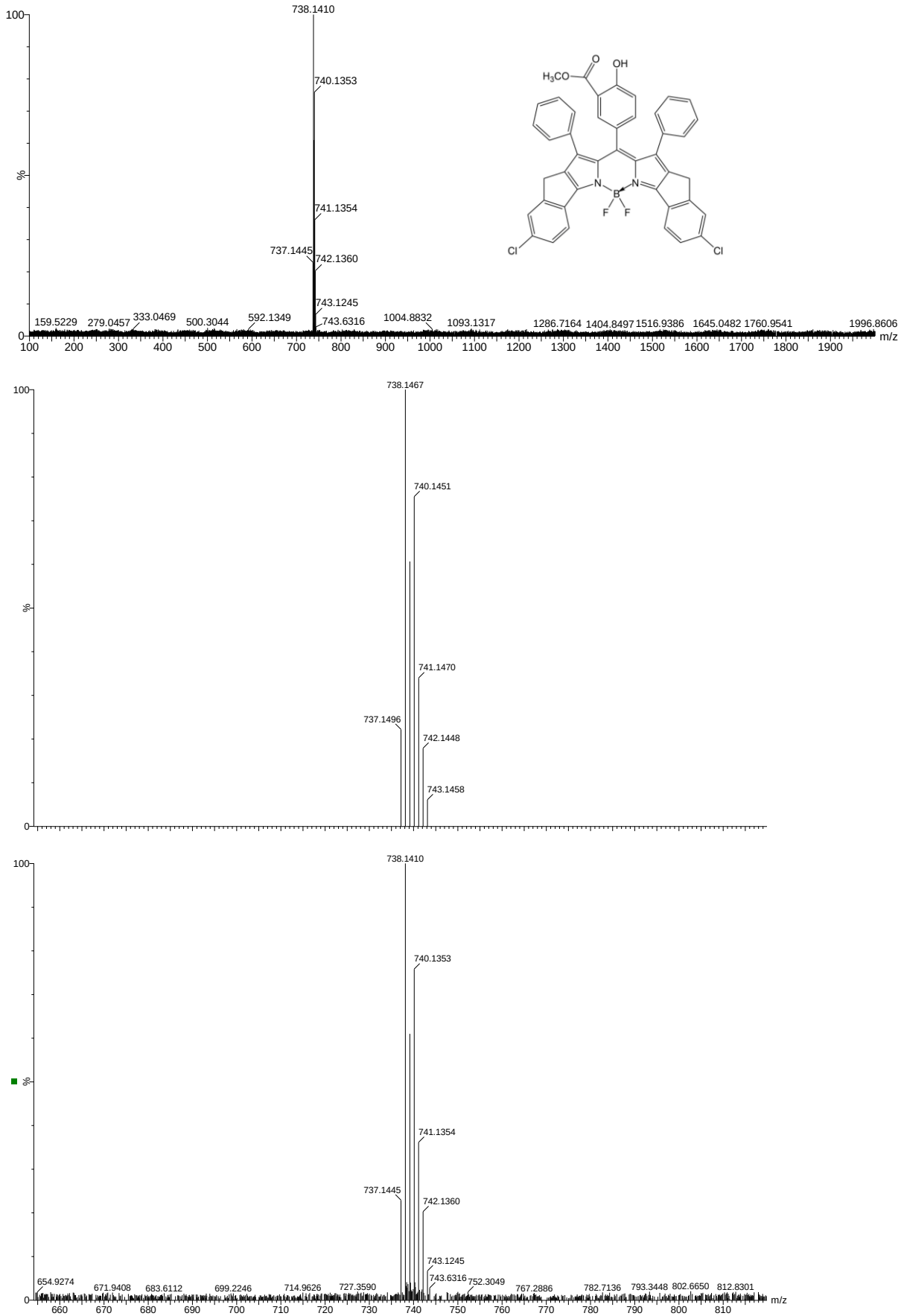

Figure S 4-27 Experimental MALDI-TOF Mass spectrum (upper part); mass relevant range for theoretical isotope pattern (middle) and experimental MALDI-TOF-Mass spectrum (lower part) of **b1** in the methyl ester form**.**

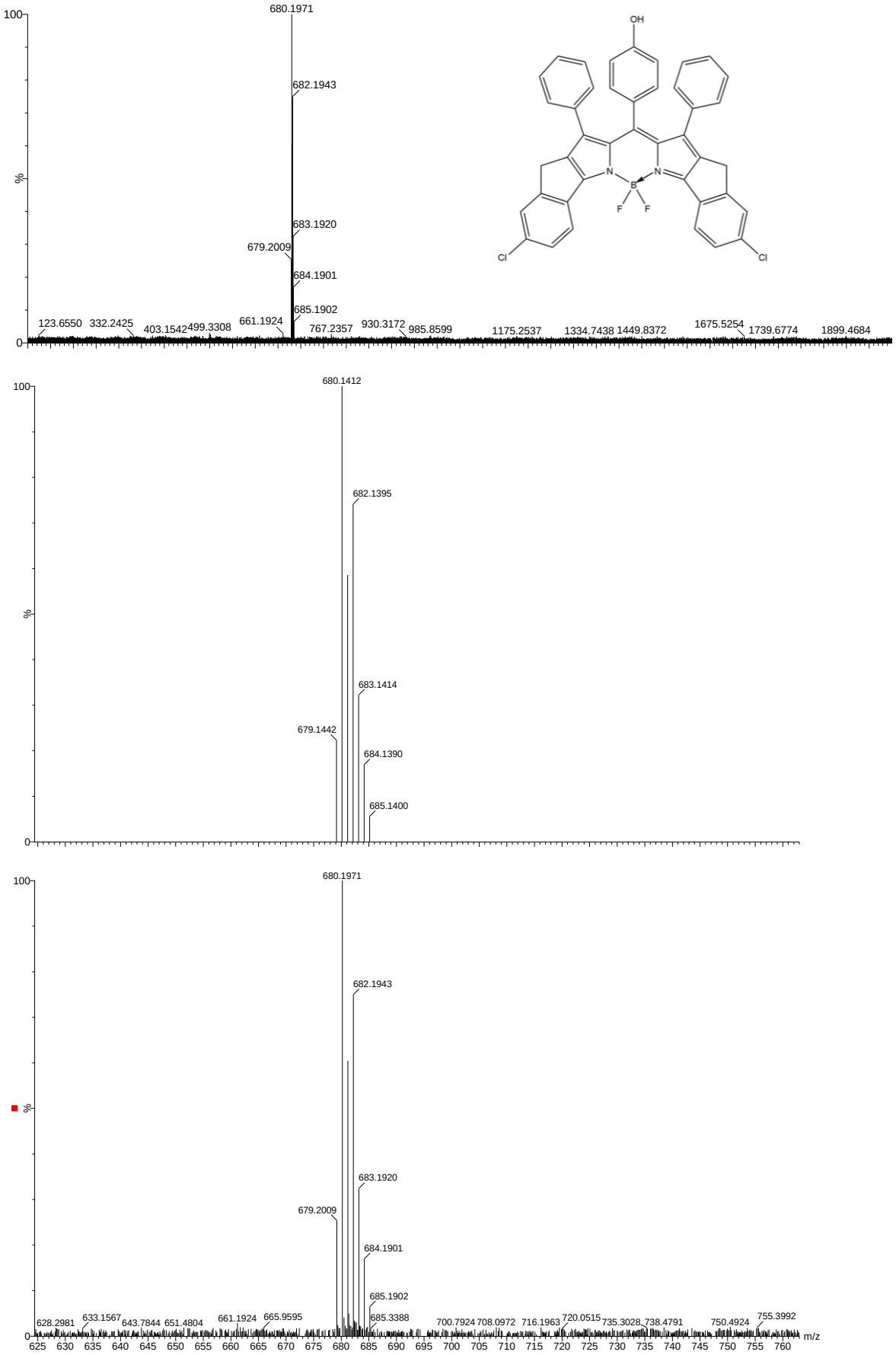

Figure S 4-28 Experimental MALDI-TOF Mass spectrum (upper part); mass relevant range for theoretical isotope pattern (middle) and experimental MALDI-TOF-Mass spectrum (lower part) of **b3.**

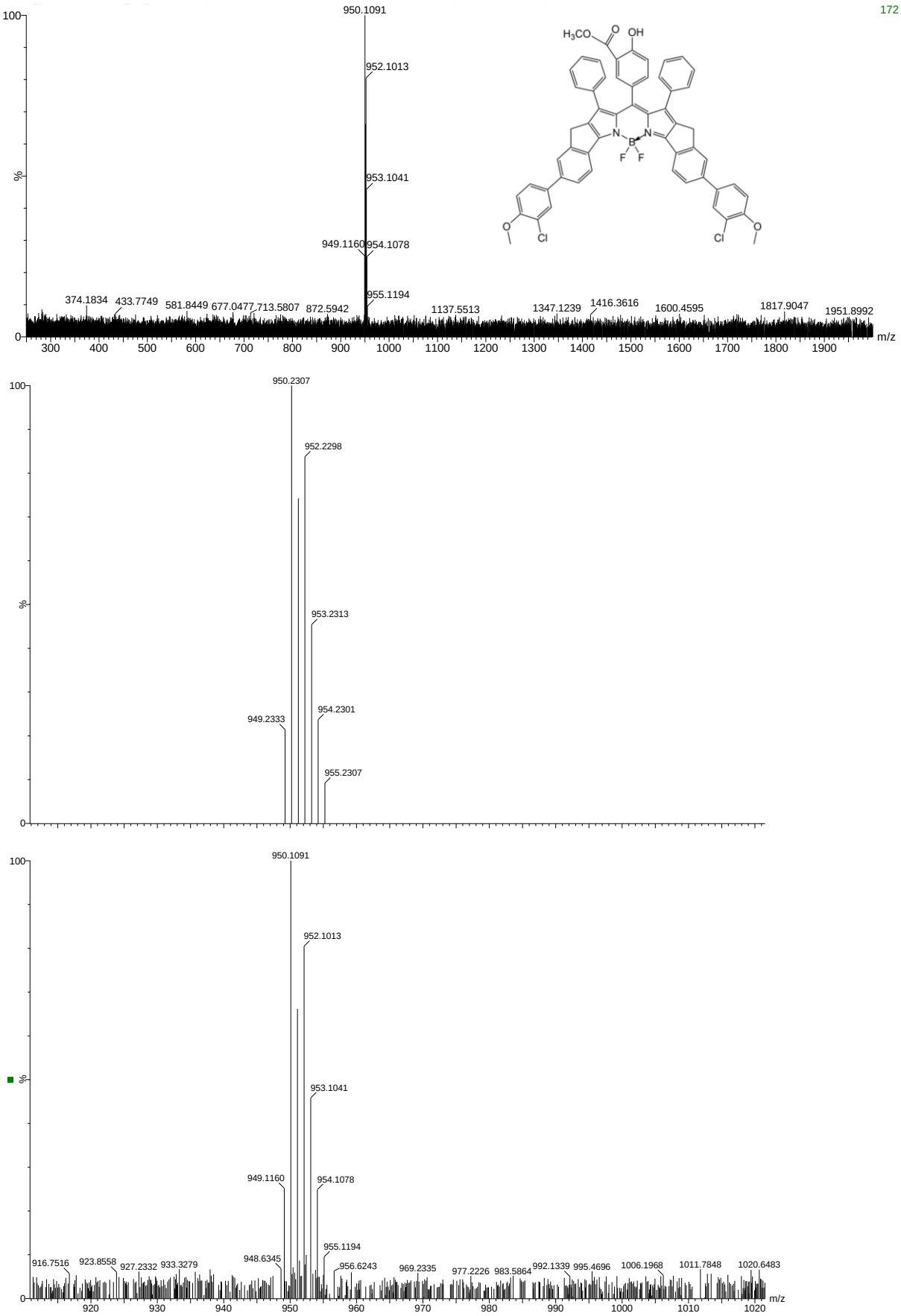

Figure S 4-29 Experimental MALDI-TOF Mass spectrum (upper part); mass relevant range for theoretical isotope pattern (middle) and experimental MALDI-TOF-Mass spectrum (lower part) of **c1** in the methyl ester form.

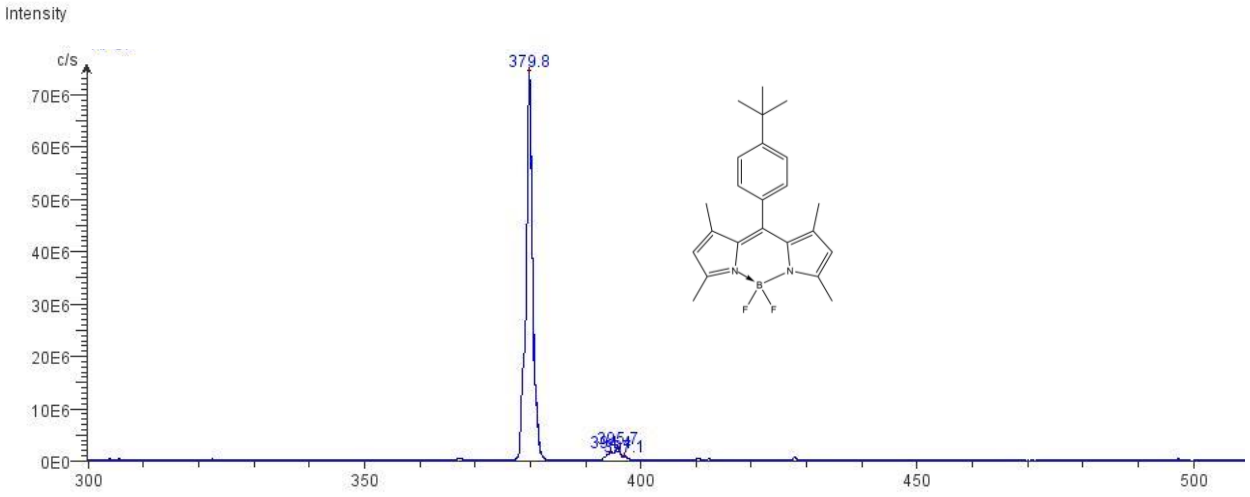

Figure S 4-30 Mass spectrum of **a-*t*Bu** recorded on Advion expression CMS.

4.7.6 NMR spectra

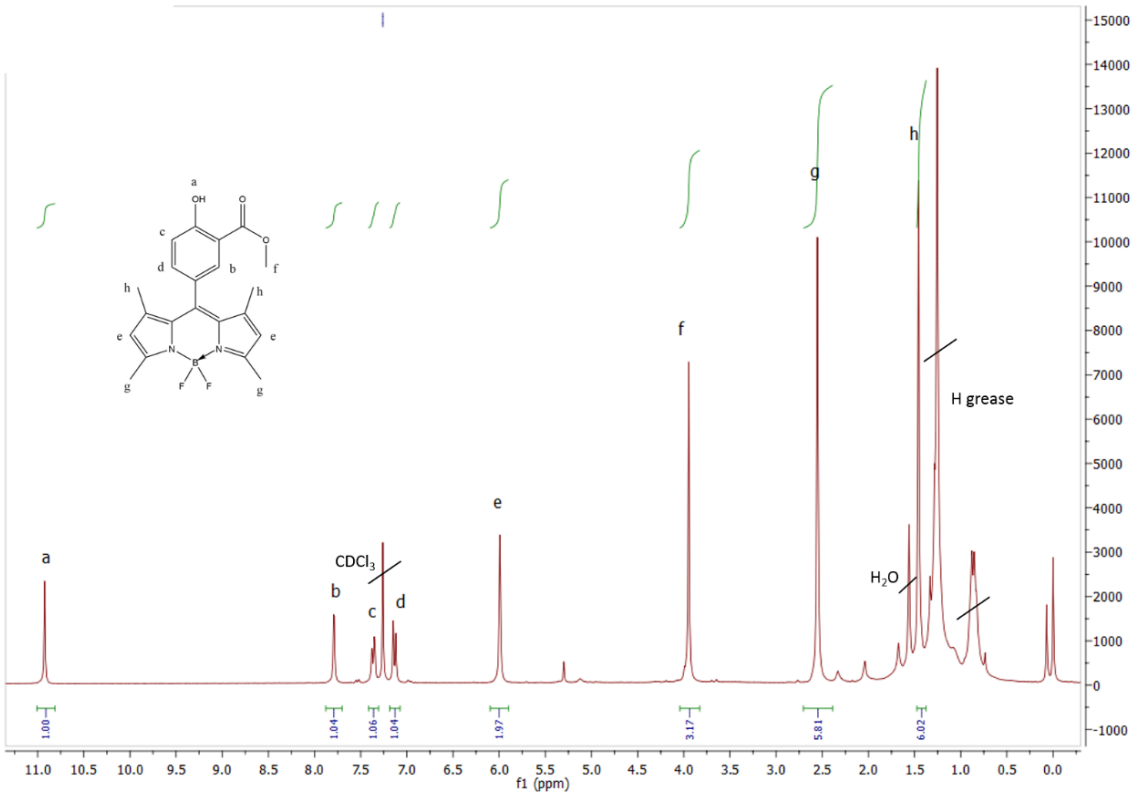

Figure S 4-31 ^{1}H NMR (300Hz, in $CDCl_3$) of **a1**.

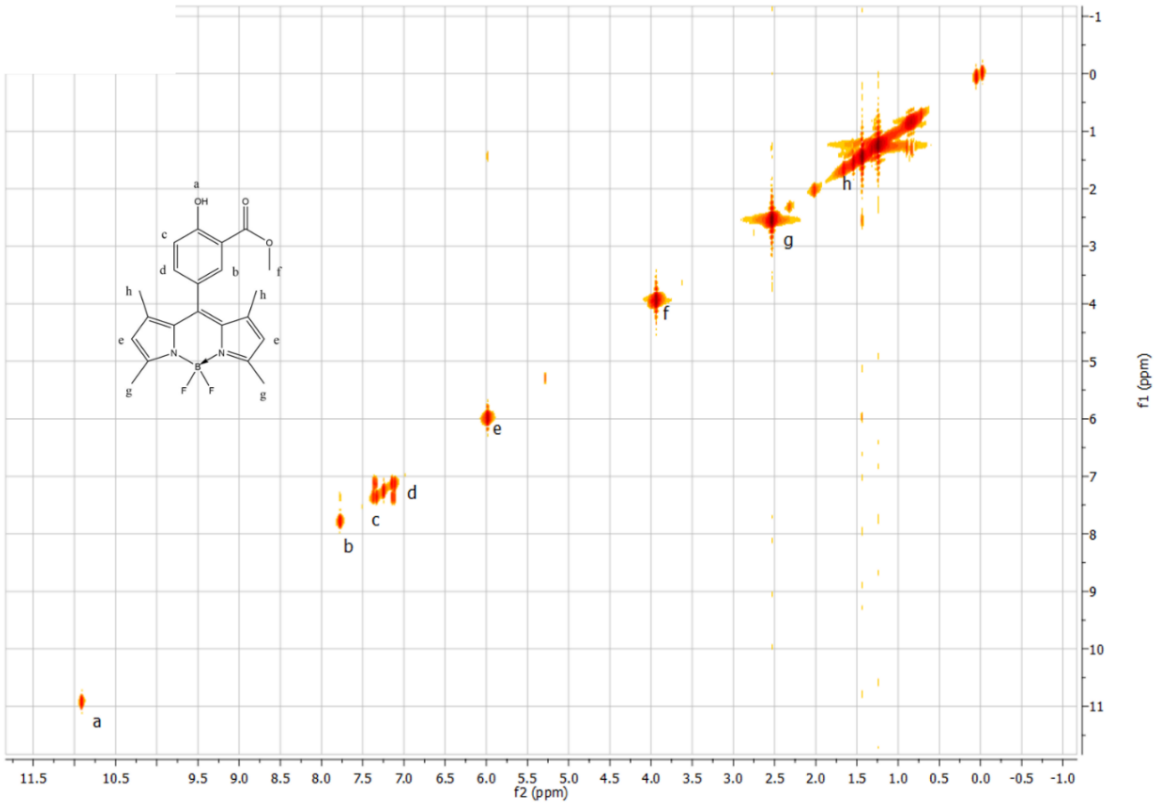

Figure S 4-32 ^{1}H-Cosy NMR (300Hz, in $CDCl_3$) of **a1**.

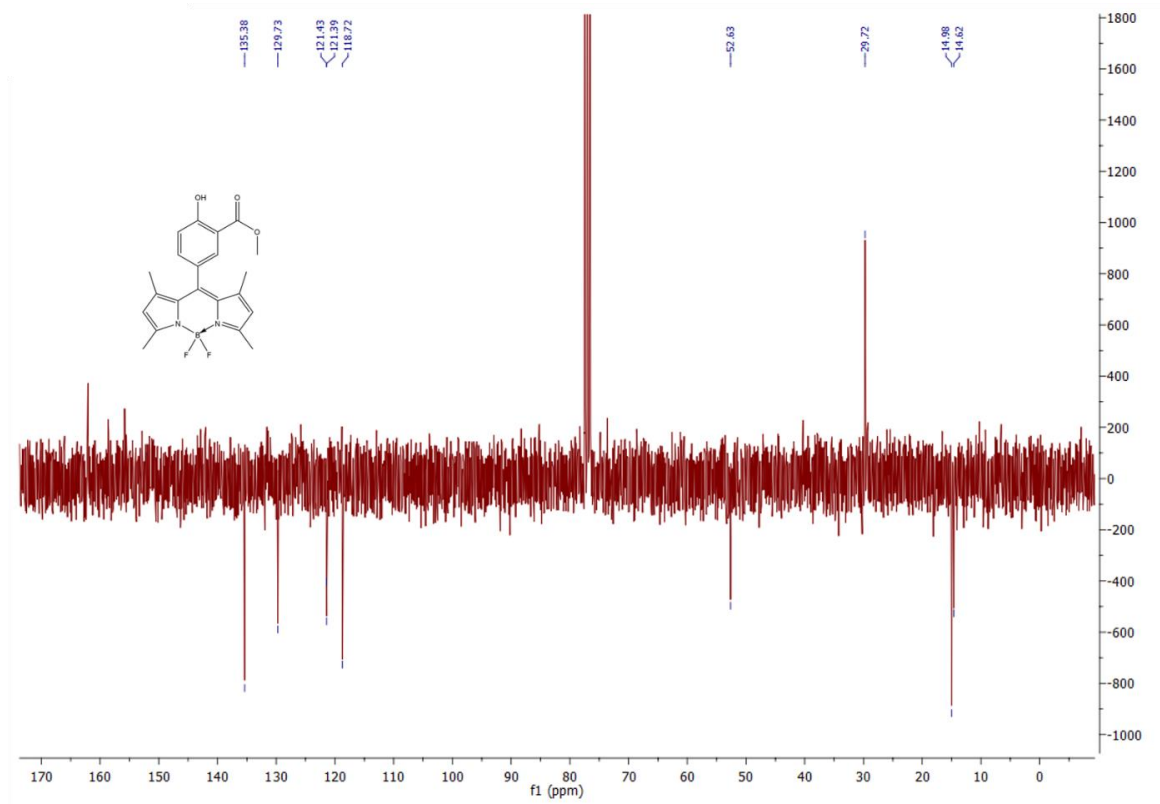

Figure S 4-33 ^{13}C-APT NMR (76Hz, in $CDCl_3$) of **a1**.

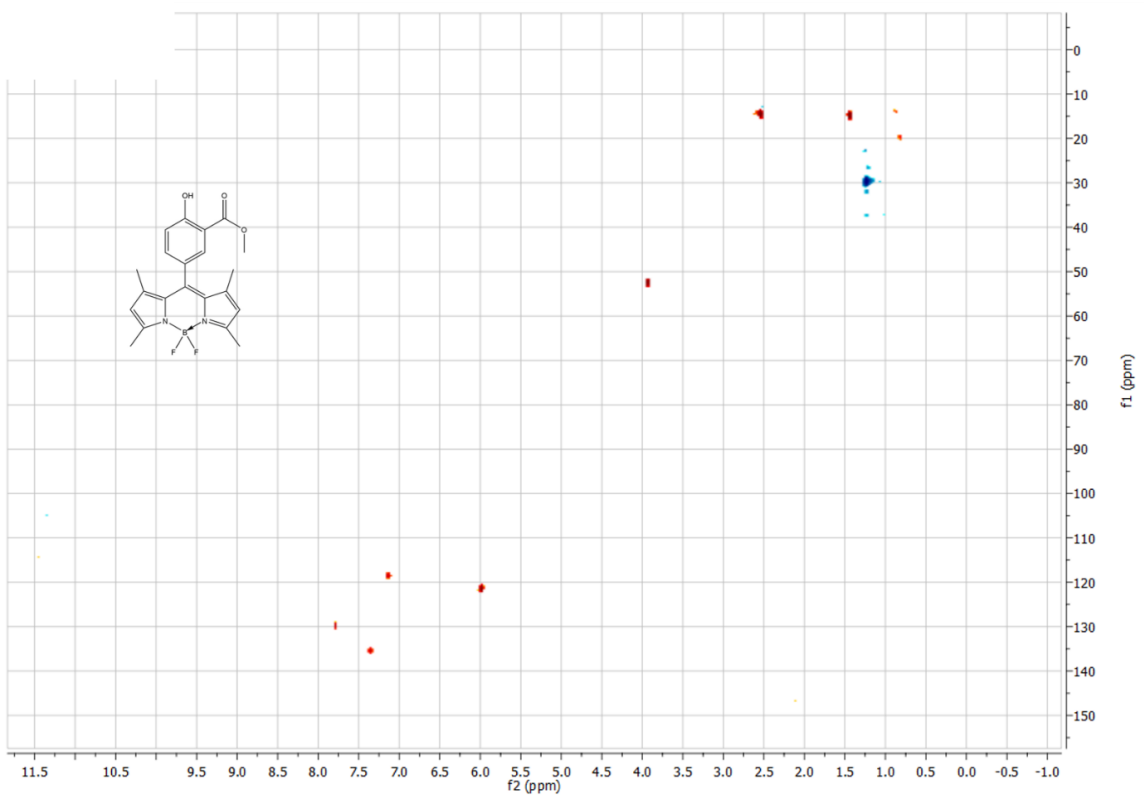

Figure S 4-34 HSQC NMR (76Hz, 300Hz in $CDCl_3$) of **a1**.

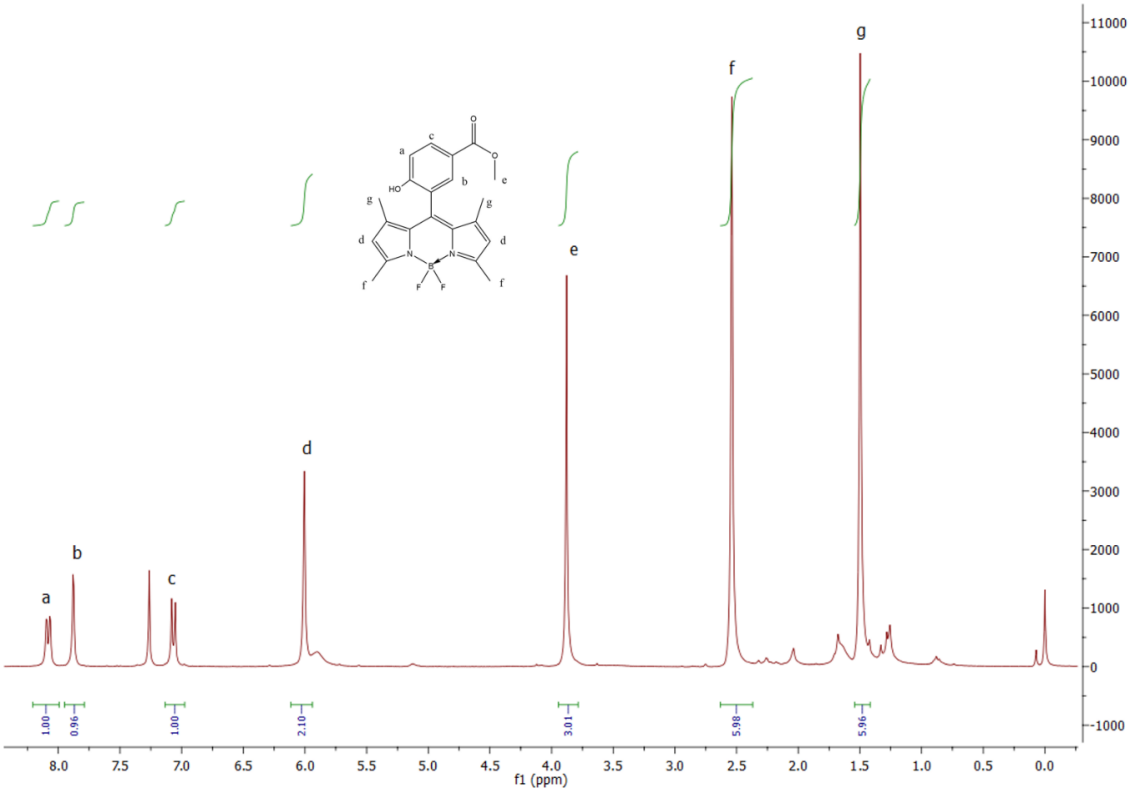

Figure S 4-35 ^1H NMR (300Hz, in $CDCl_3$) of **a2.**

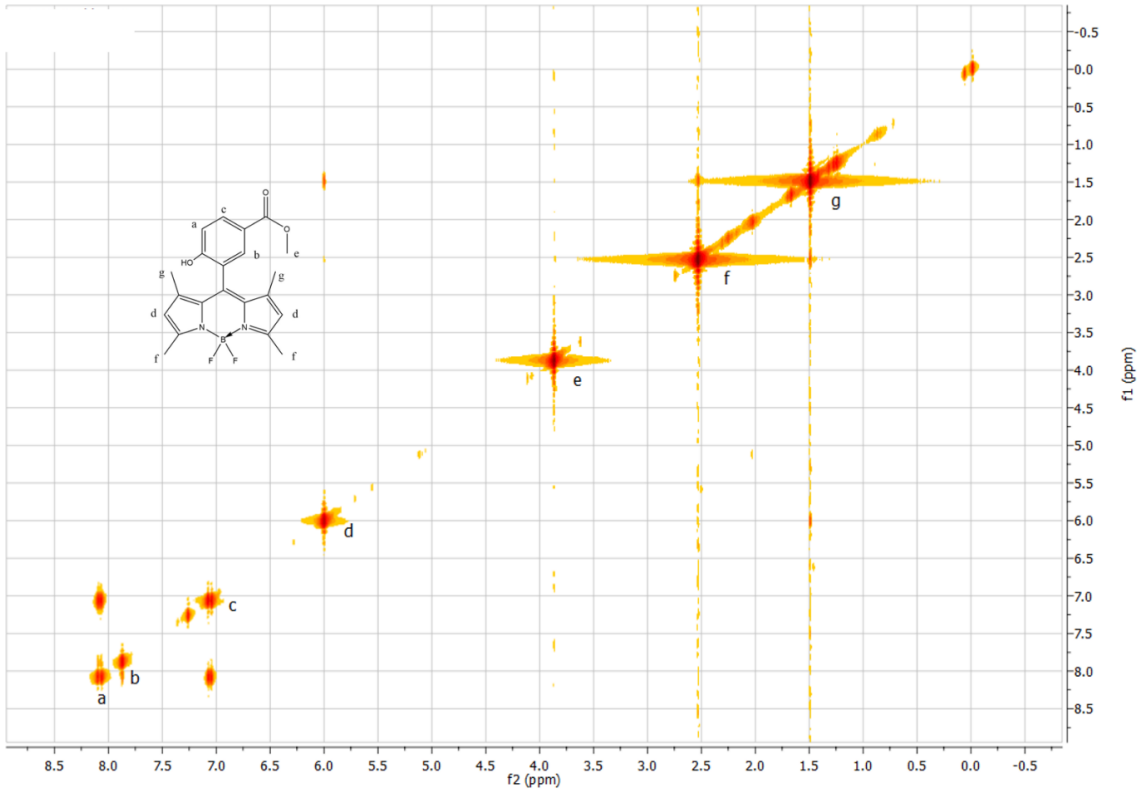

Figure S 4-36 ^{1}H-Cosy NMR (300Hz, in $CDCl_3$) of **a2**.

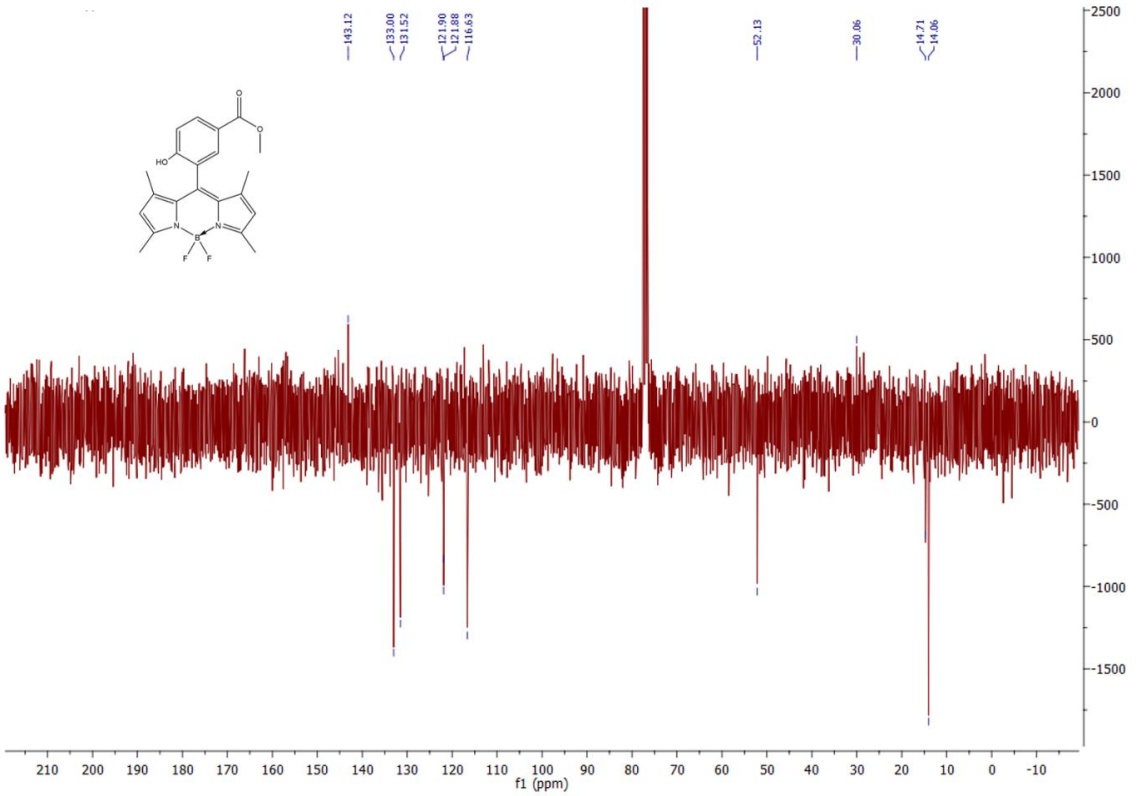

Figure S 4-37 ^{13}C-APT NMR (76Hz, in $CDCl_3$) of **a2.**

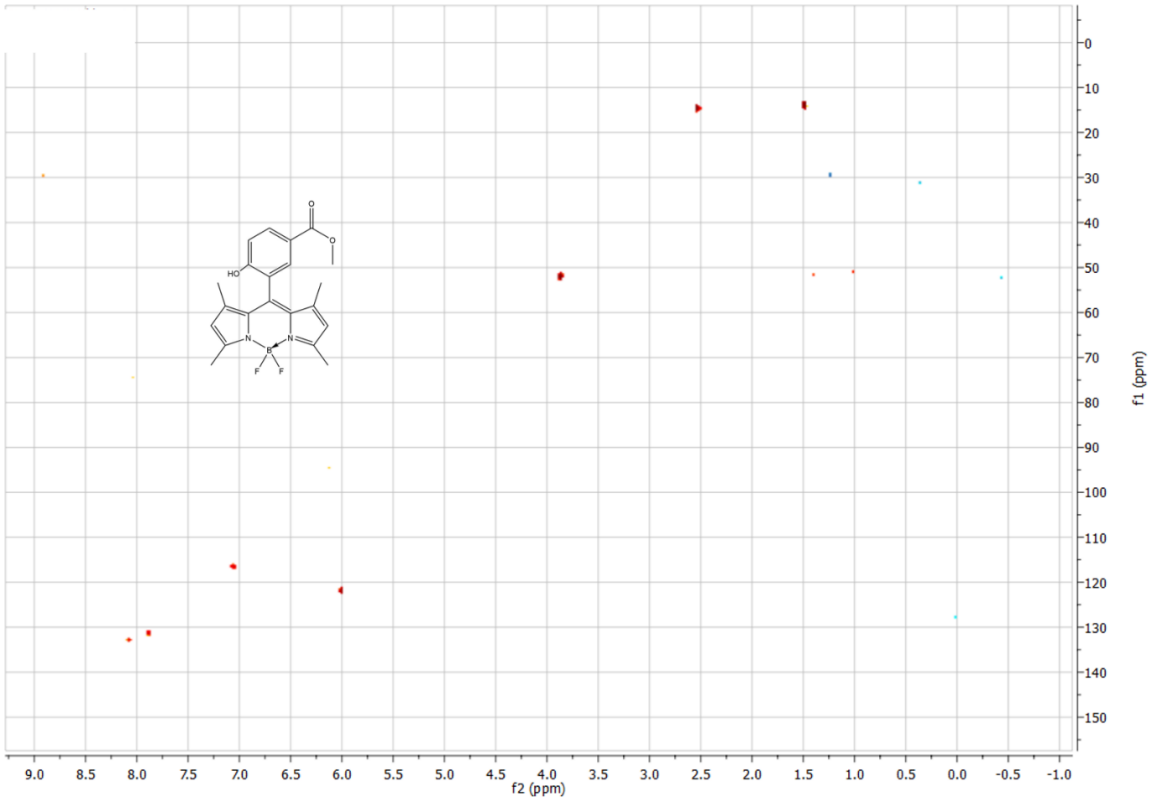

Figure S 4-38 HSQC NMR (76Hz, 300Hz in $CDCl_3$) of **a2**.

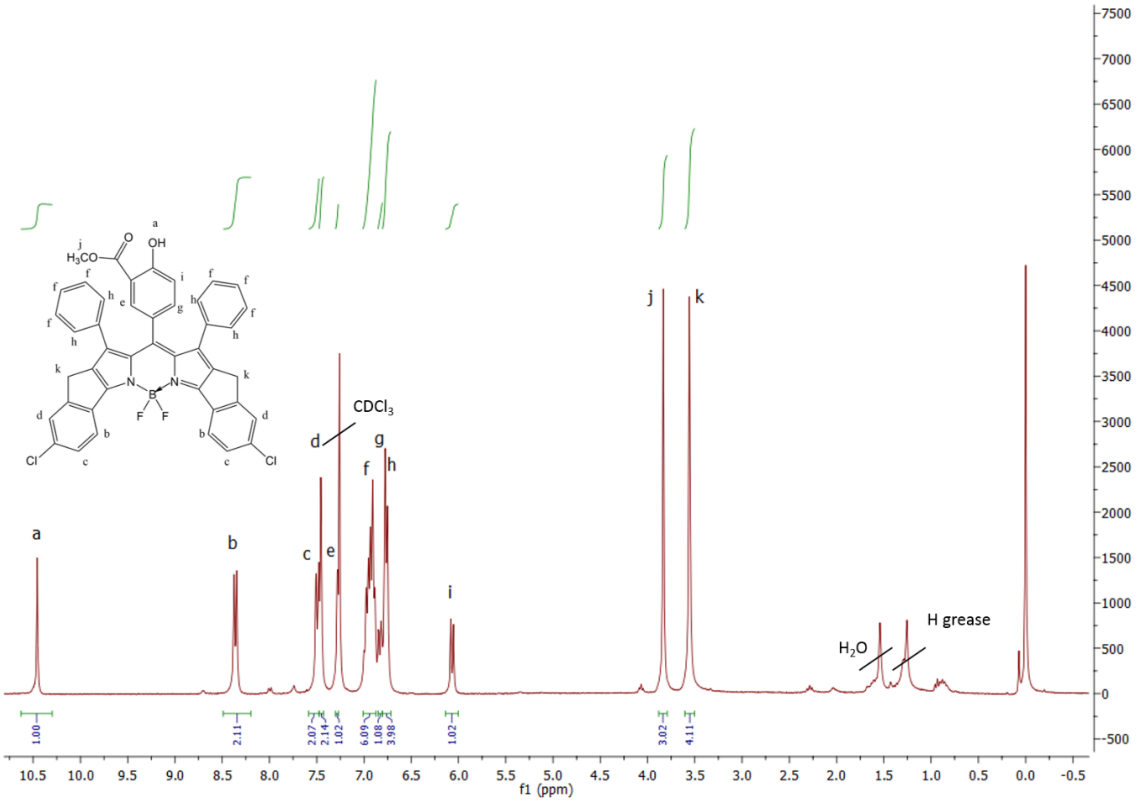

Figure S 4-39 ^1H NMR (300Hz, in $CDCl_3$) of **b1**

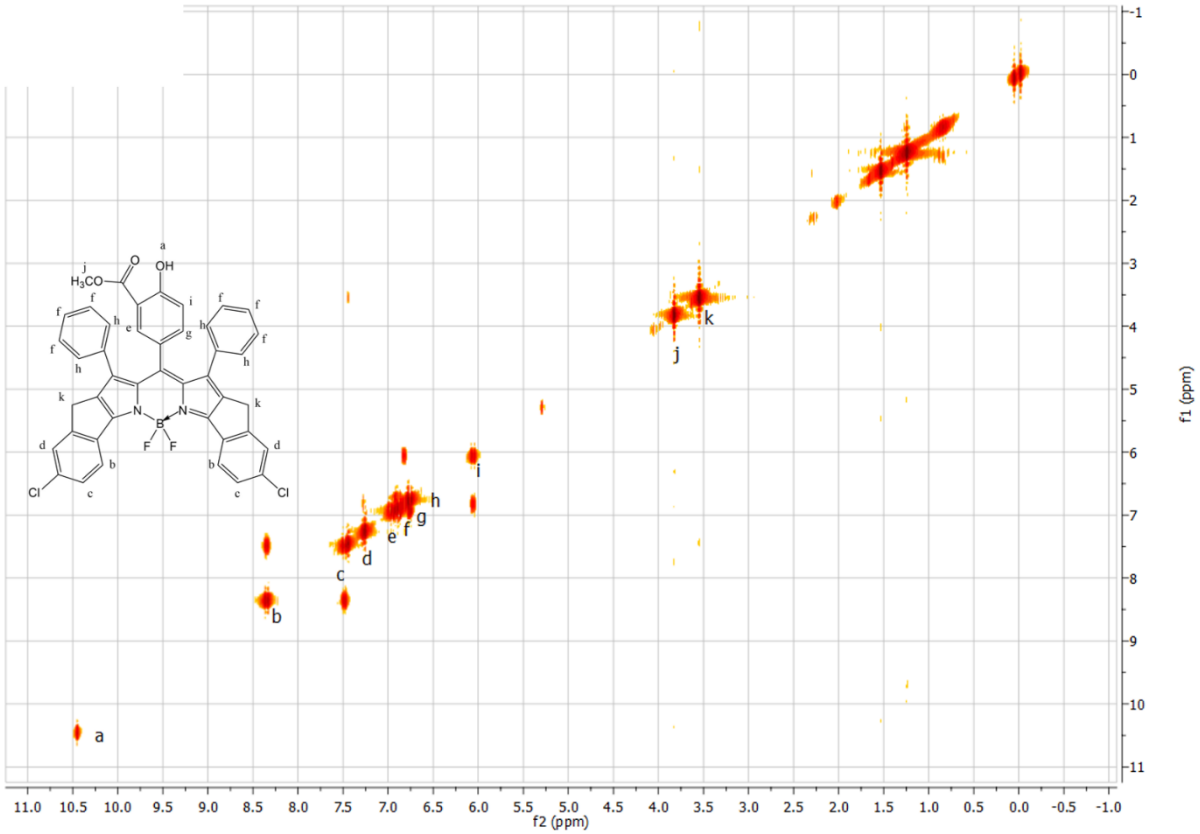

Figure S 4-40 ^{1}H-Cosy NMR (300Hz, in $CDCl_3$) of **b1**.

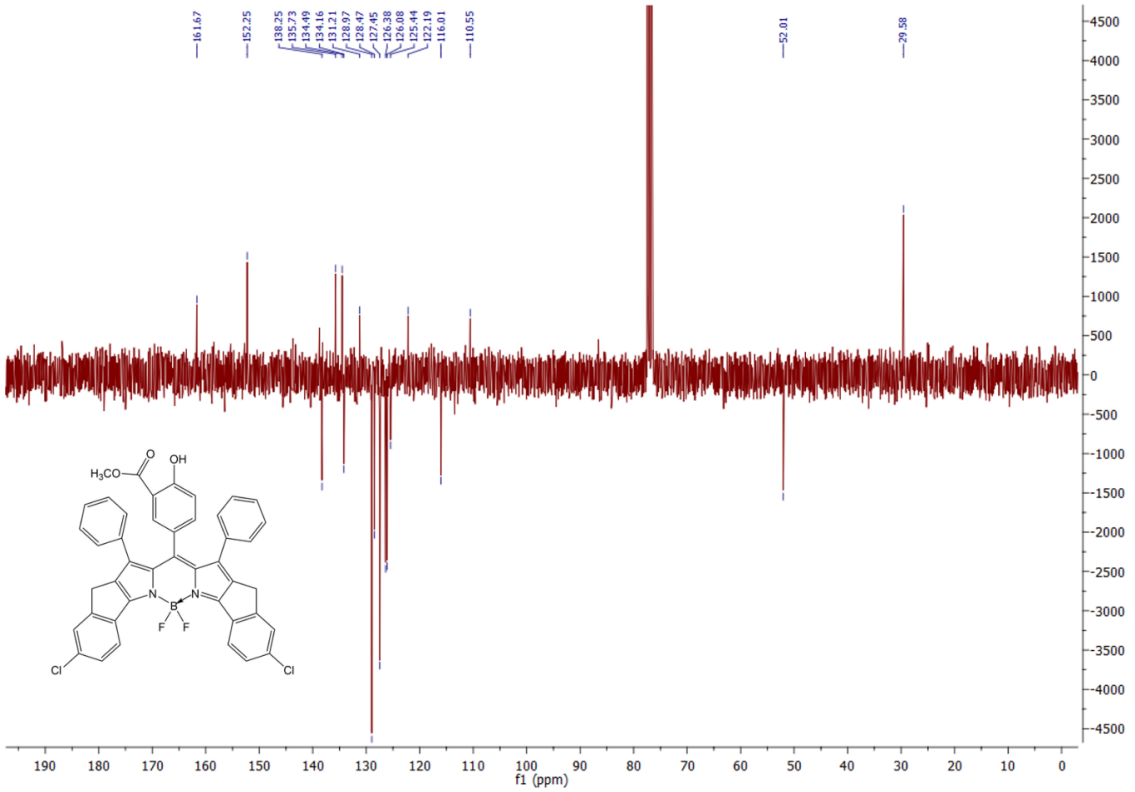

Figure S 4-41 ^{13}C-APT NMR (76Hz, in $CDCl_3$) of **b1.**

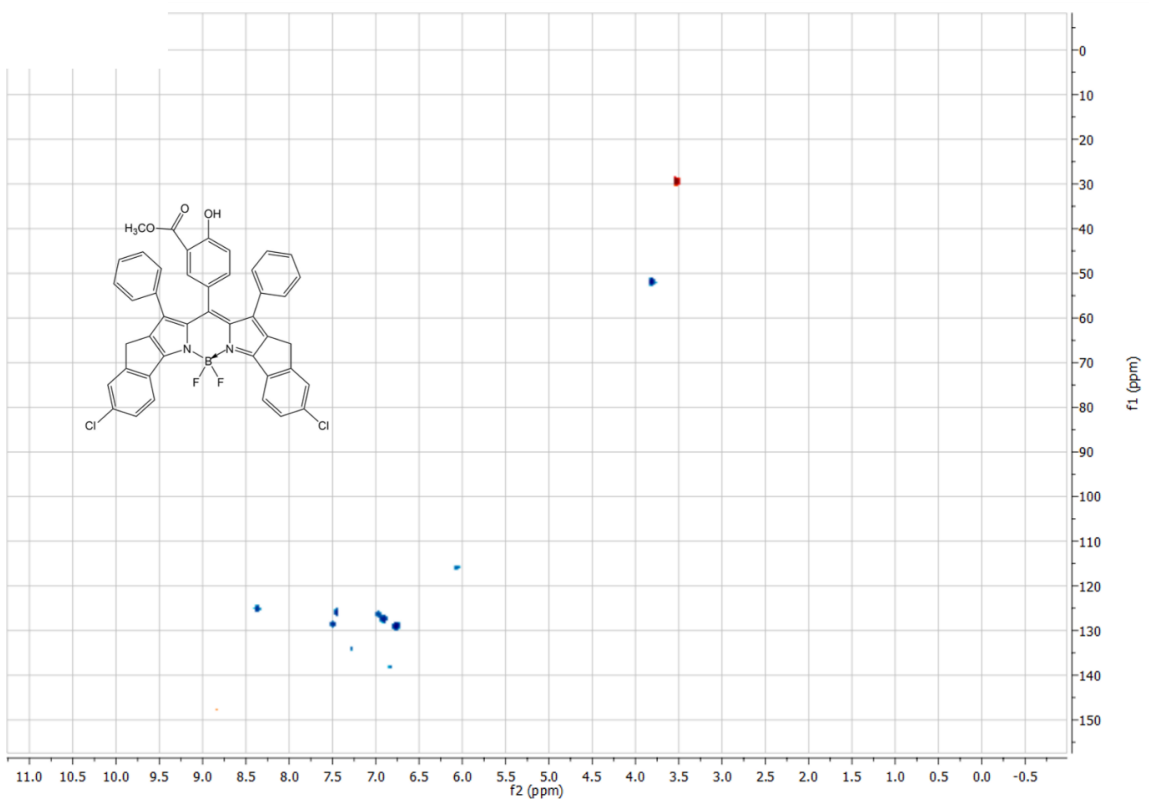

Figure S 4-42 HSQC NMR (76Hz, 300Hz in $CDCl_3$) of **b1**.

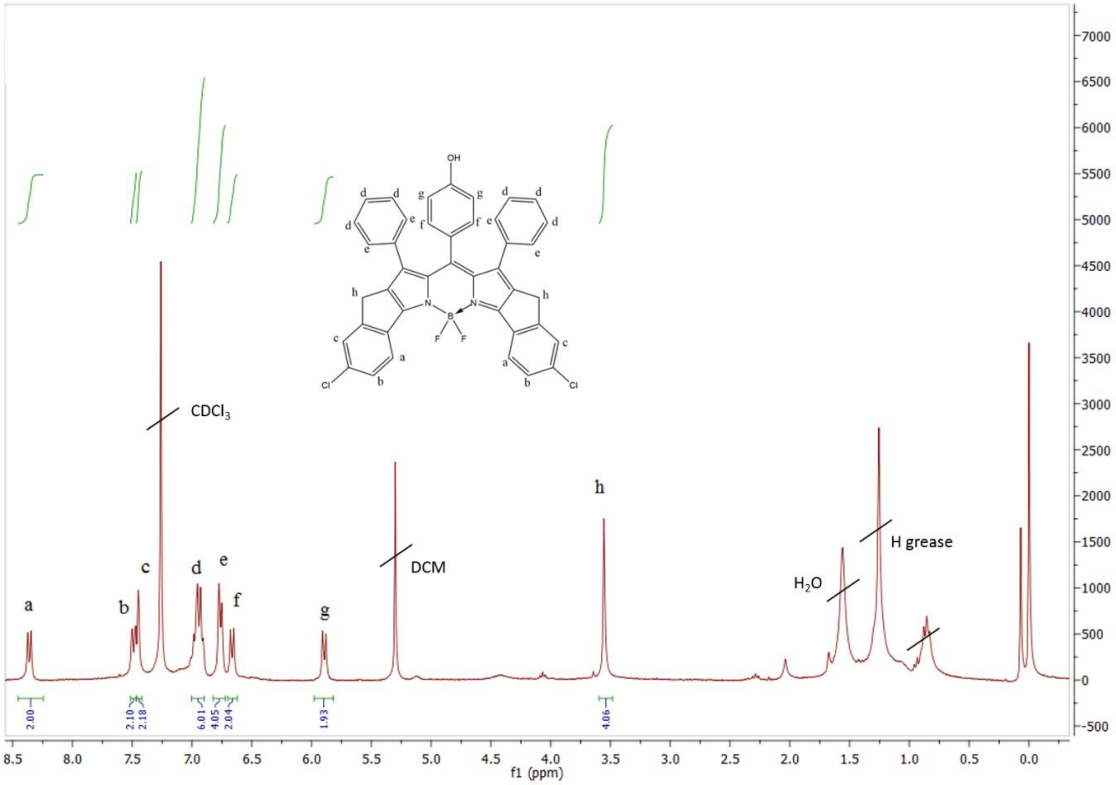

Figure S 4-43 ^1H NMR (300Hz, in $CDCl_3$) of **b3**.

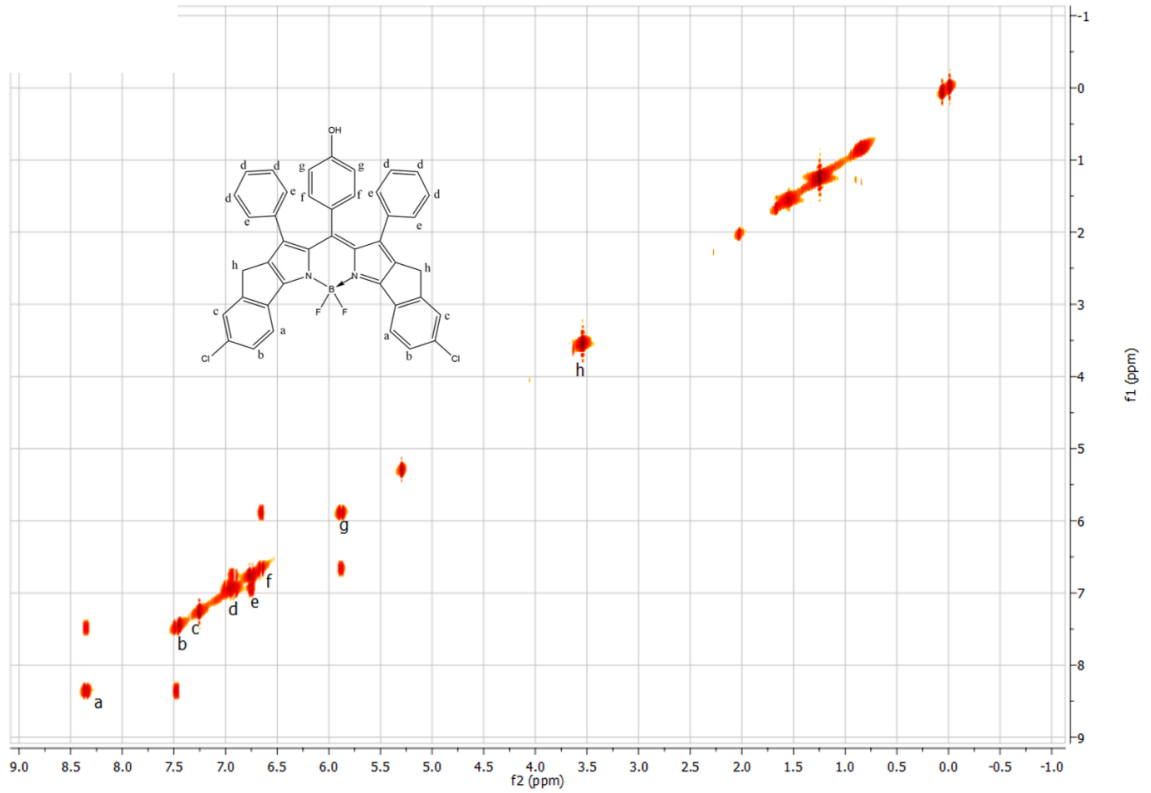

Figure S 4-44 ^{1}H-Cosy NMR (300Hz, in $CDCl_3$) of **b3**.

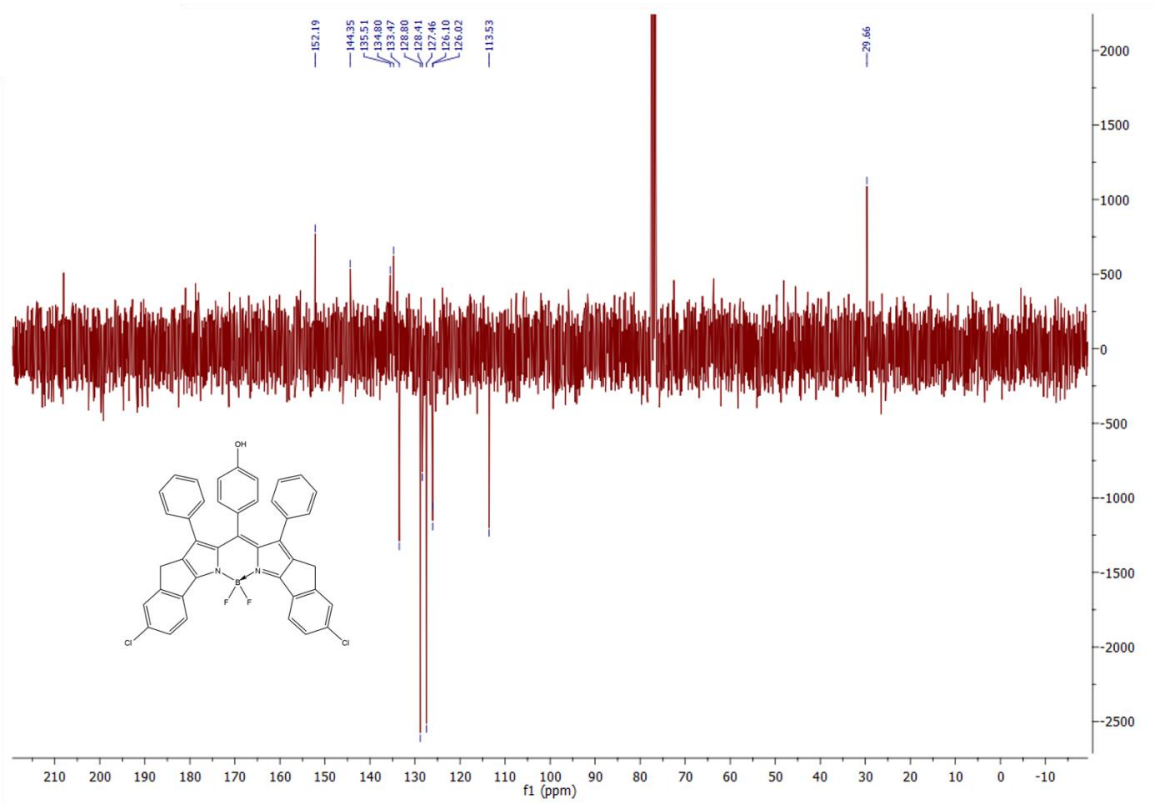

Figure S 4-45 ^{13}C-APT NMR (76Hz, in $CDCl_3$) of **b3.**

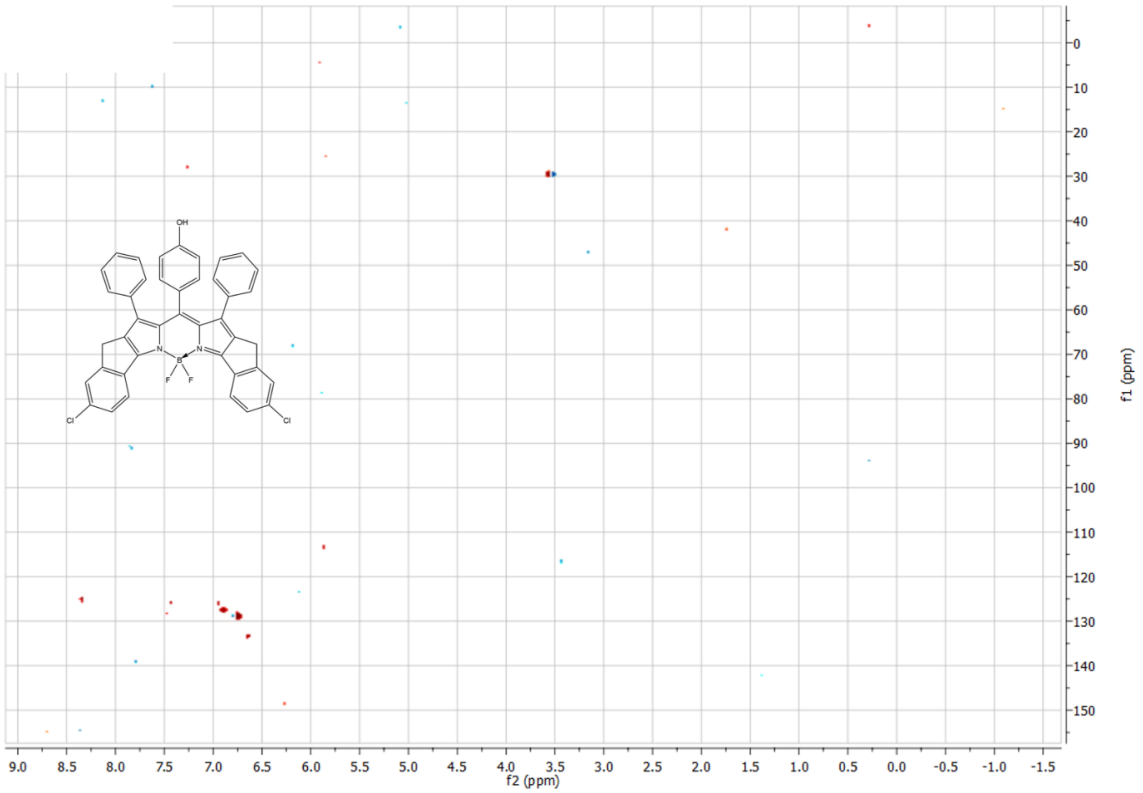

Figure S 4-46 HSQC NMR (76Hz, 300Hz in $CDCl_3$) of **b3**.

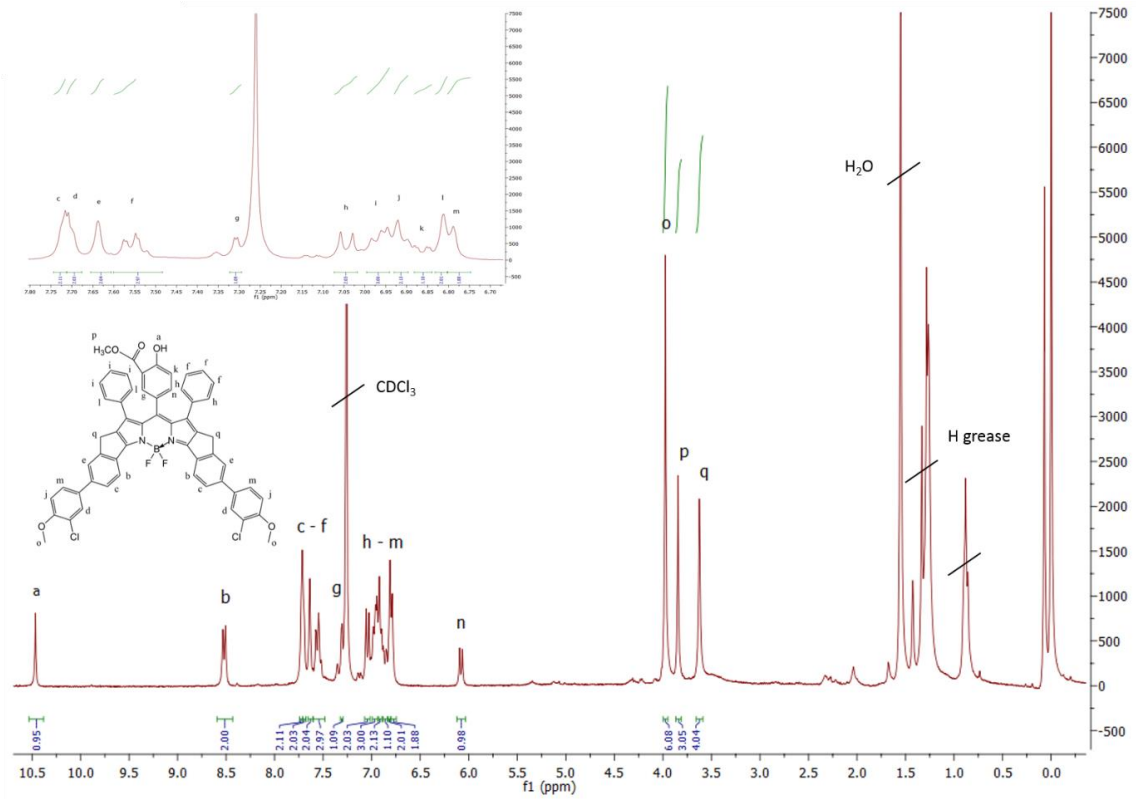

Figure S 4-47 ^1H NMR (300Hz, in $CDCl_3$) of **c1.**

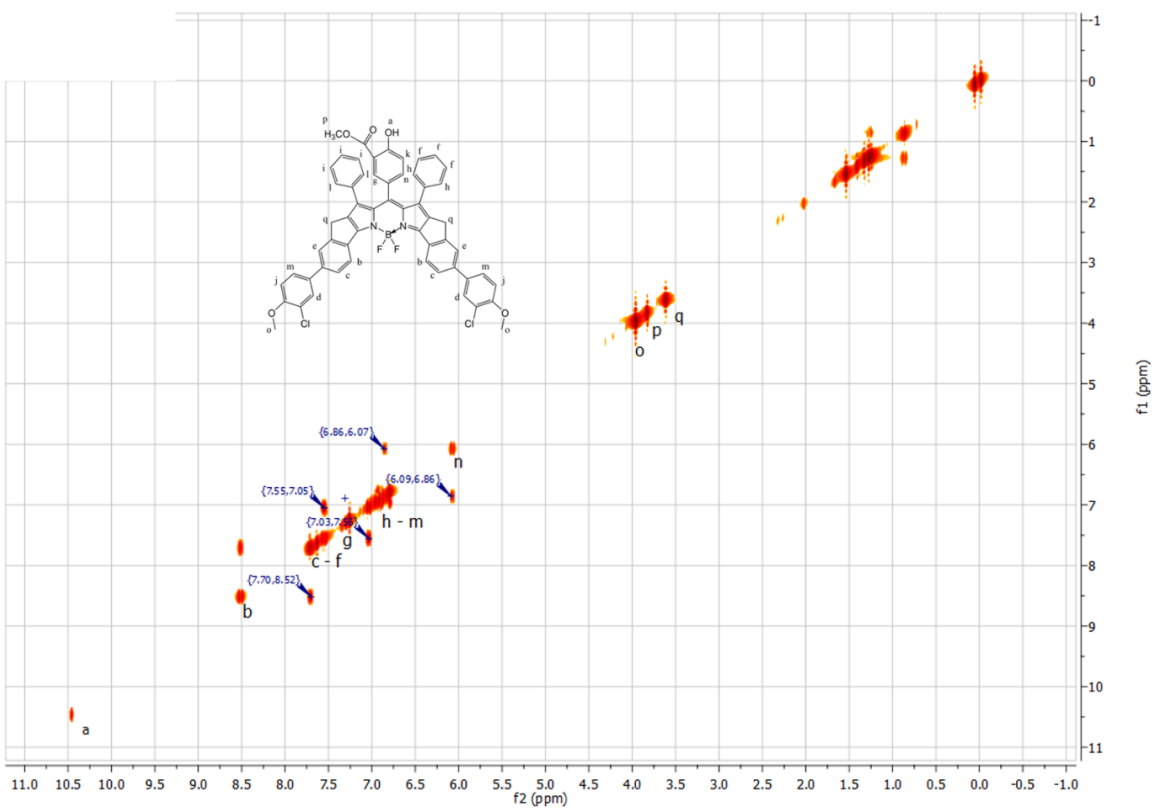

Figure S 4-48 ^{1}H-Cosy NMR (300Hz, in $CDCl_3$) of **c1**.

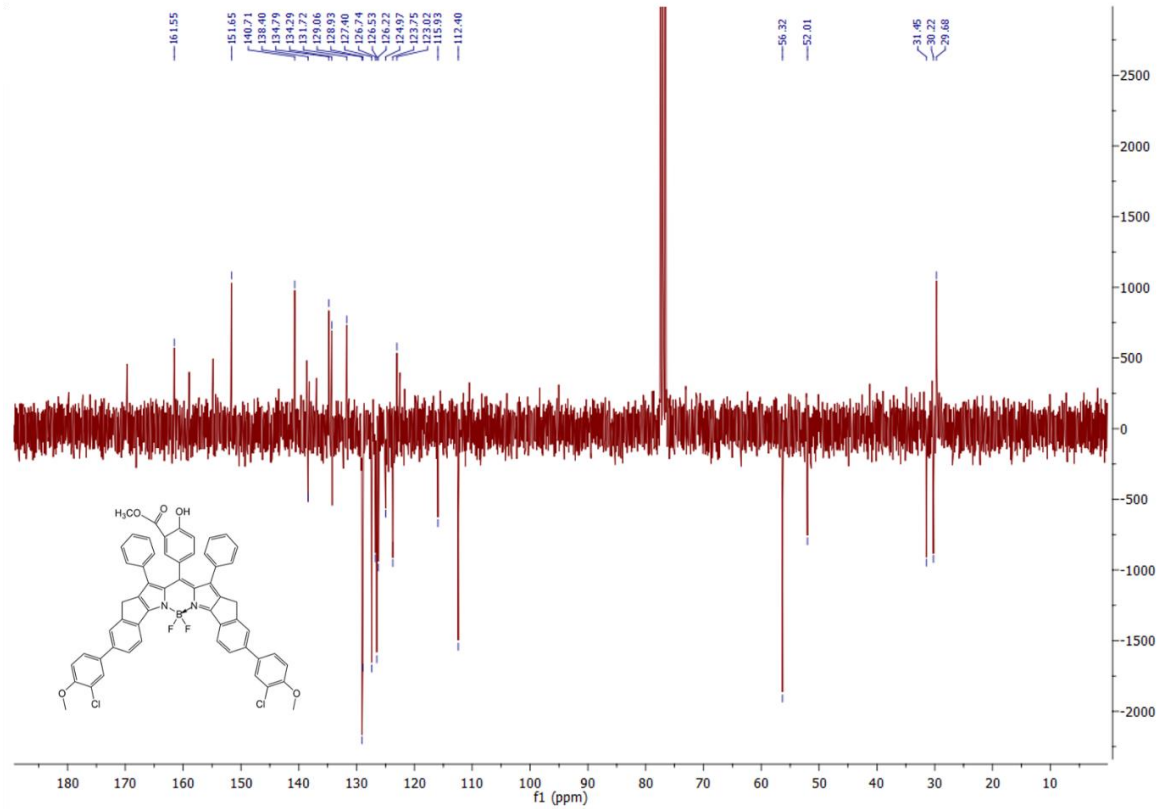

Figure S 4-49 ^{13}C-APT NMR (76Hz, in $CDCl_3$) of **c1**

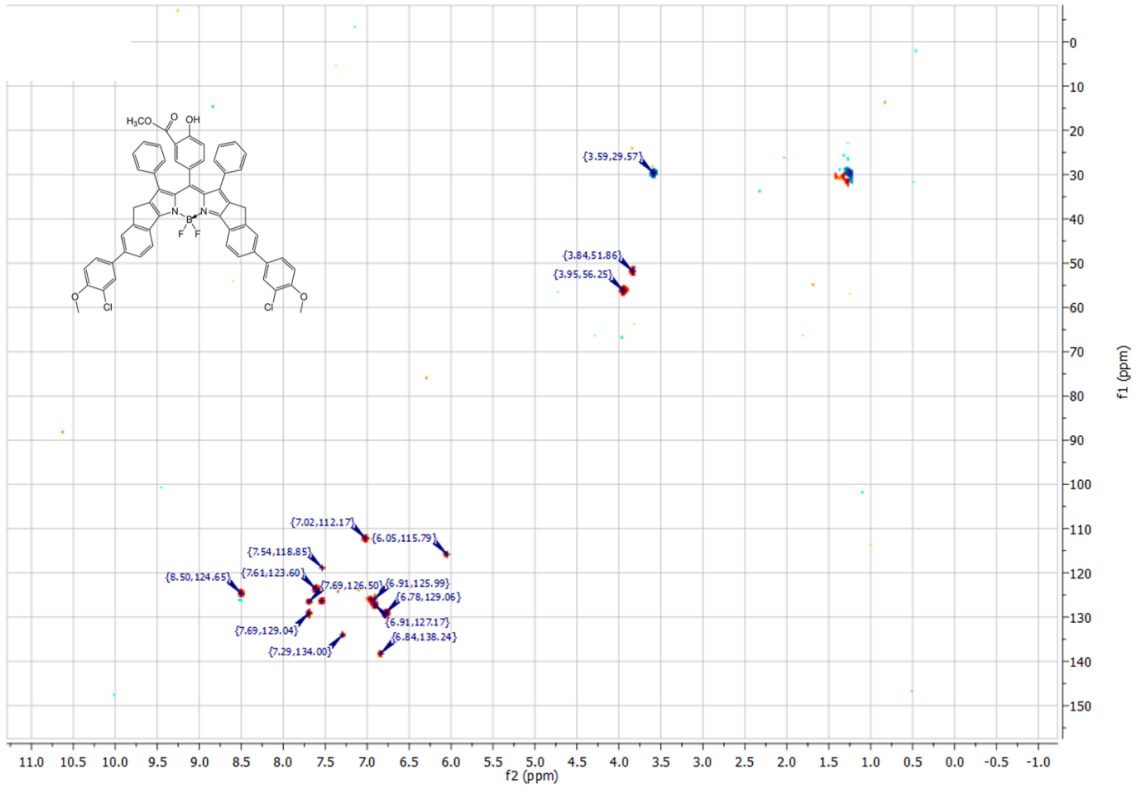

Figure S 4-50 HSQC NMR (76Hz, 300Hz in $CDCl_3$) of **c1**.

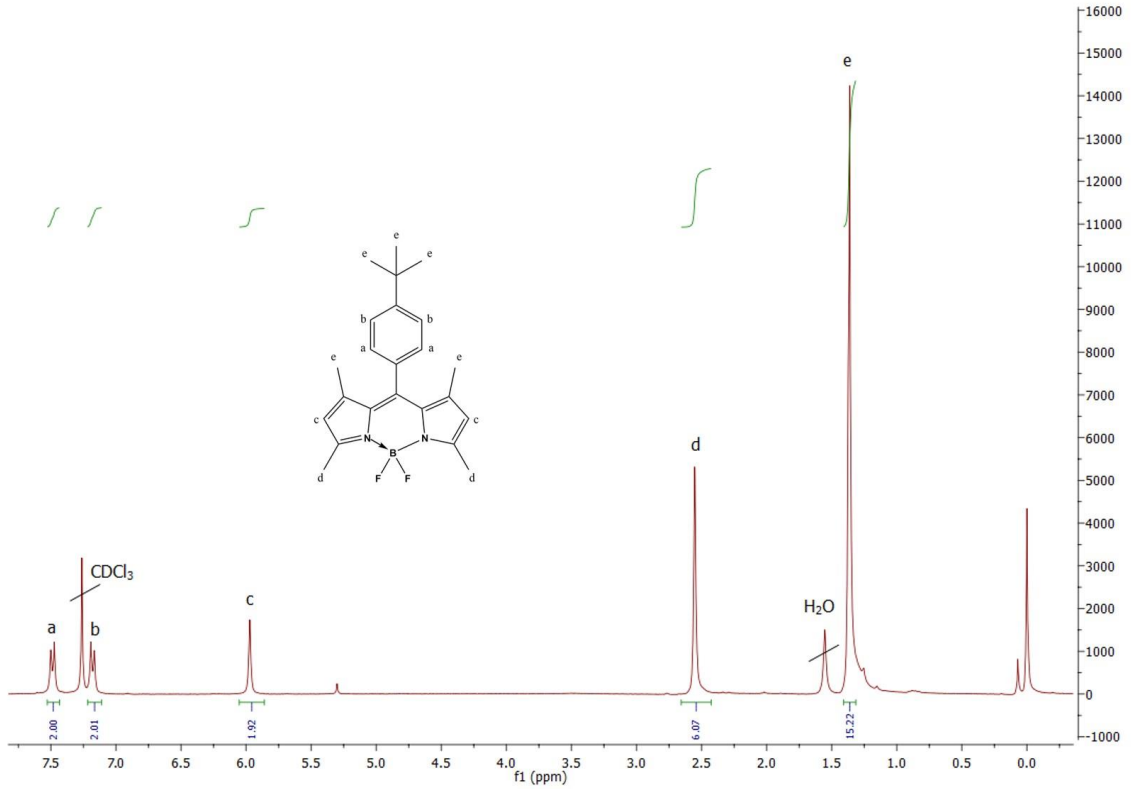

Figure S 4-51 ^{1}H-NMR (300Hz, in $CDCl_3$) of **a-*t*Bu**.

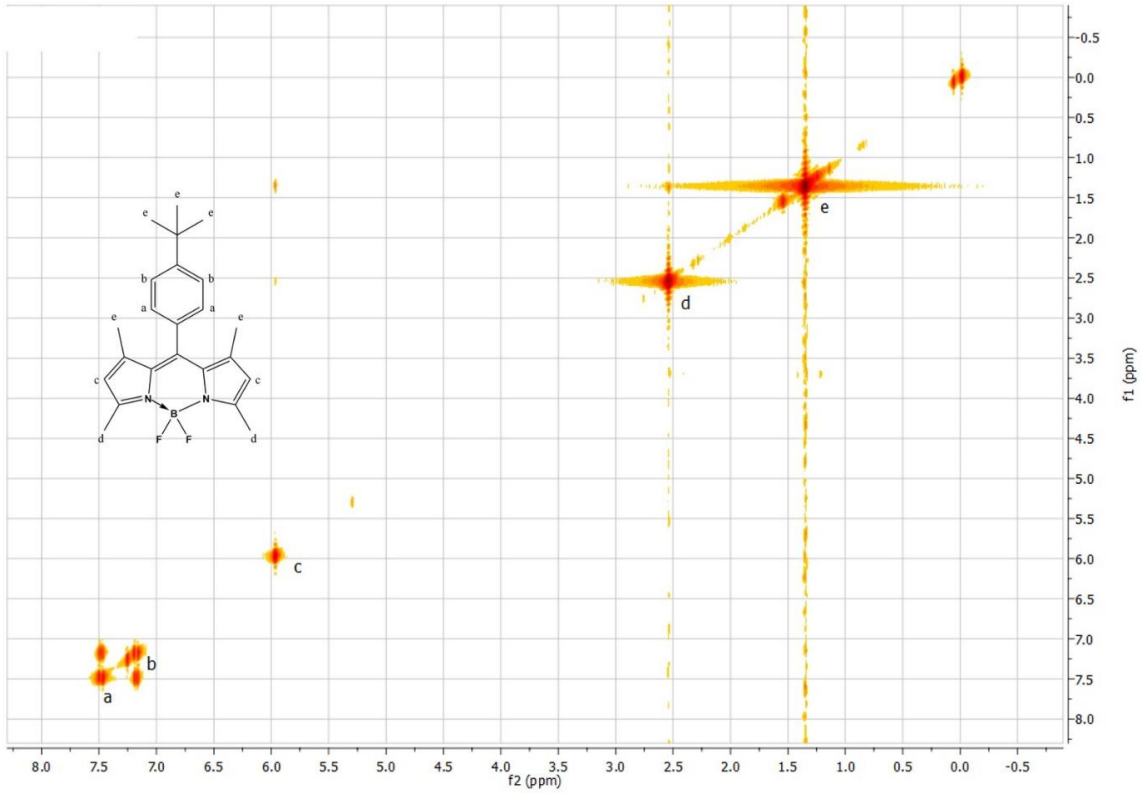

Figure S 4-52 ^{1}H-Cosy-NMR (300Hz, in CDCl3) of **a-*t*Bu**

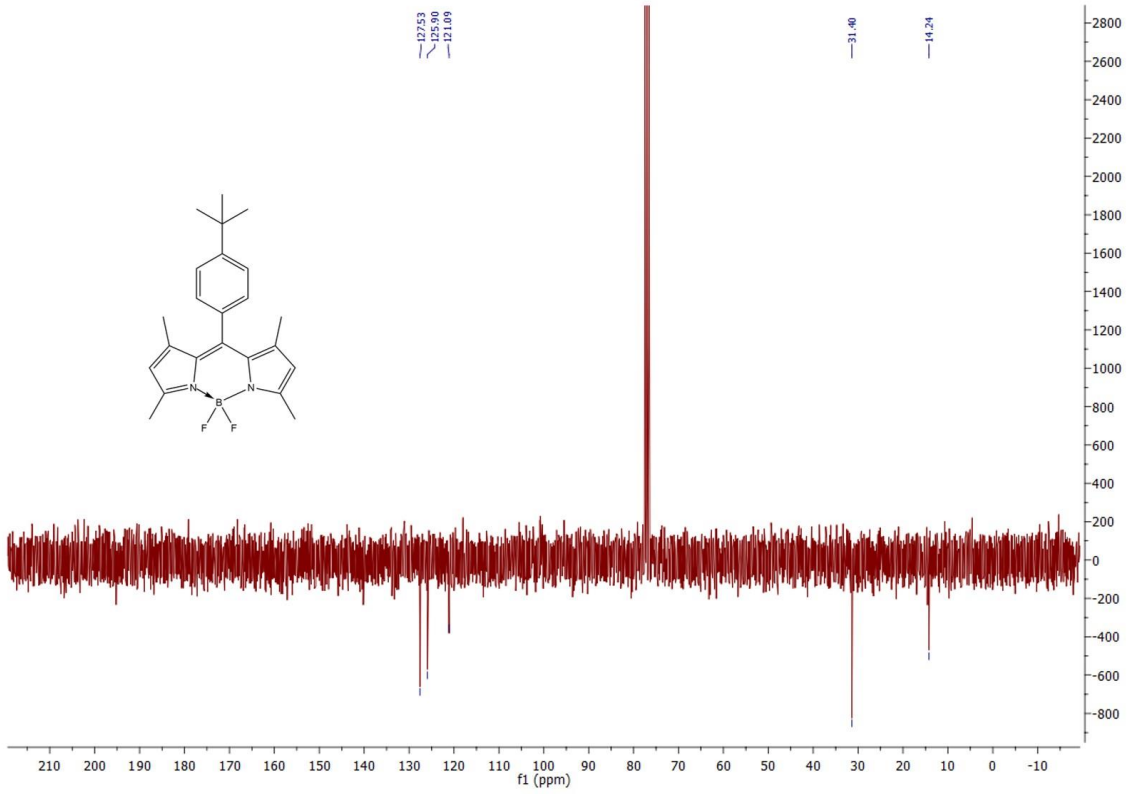

Figure S 4-53 ^{13}C-APT NMR (76Hz, in $CDCl_3$) of **a-*t*Bu**.

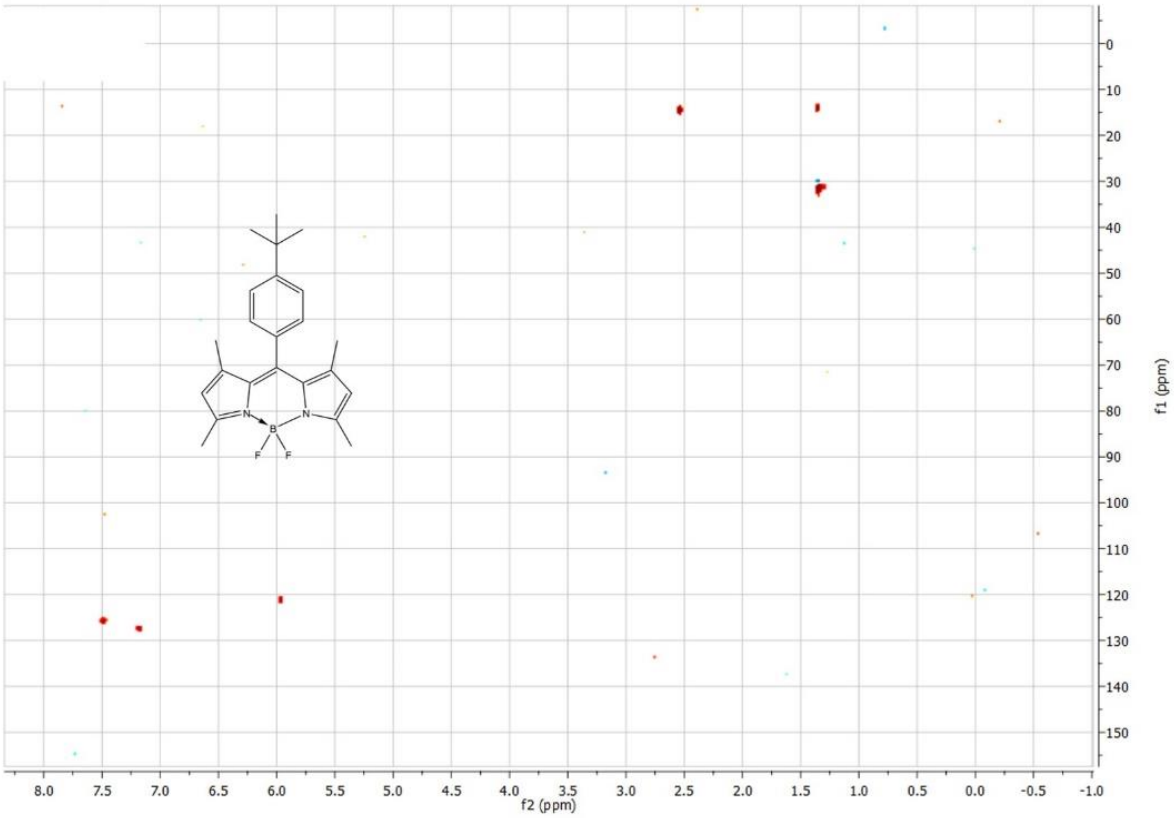

Figure S 4-54 HSQC NMR (76Hz, in CDCl3) of **a-*t*Bu**.

5 Highly photostable far-red emissive terrylene diimide dyes

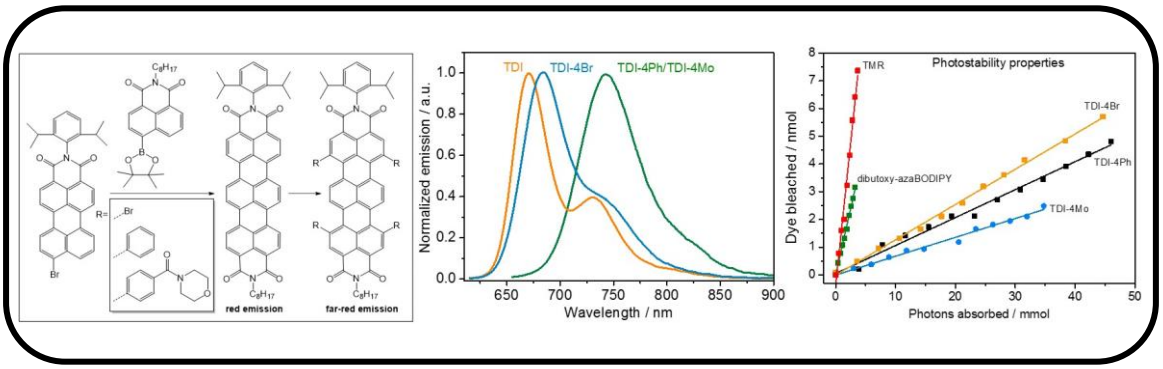

5.1 Preface for the Manuscript

This manuscript is focused on the synthesis and the characterization of the photophysical properties of bay-modified terrylene diimide dyes.

Terrylene diimides are built up by a conjugated framework of three naphthalene units connected to each other in *peri*-position belonging to the class of rylene dyes. The first red emitting TDI was synthesized by *Holtrup et al.* in 1997, driven by the motivation to close the gap between yellow to red emissive perylene bisimides and NIR emitting quaterrylene bisimides.[23] In general, terrylene diimide dyes feature high luminescence brightness, extraordinary high photostability, and bathochromically shifted absorption/emission bands (about 100 nm per additional naphthalene unit compared to classical perylene bisimide) in the far red to NIR region of the spectrum, but due to their structural properties they are rather hydrophobic and prone to aggregation. In recent years functionalized rylene derivatives have been successfully implemented in several challenging applications.[16,25,51,222] Particularly, terrylene derivatives have only be investigated for academic research and not for industrial applications yet, most probably due to the difficult and time-consuming synthesis (**Section 2.2.2**, p. 11).

The overall aim of this work was the synthesis of pH sensitive, far-red emitting, hydrophilic terrylene diimide dyes, featuring high luminescence brightness and high photostability. Hence, to provide suitable indicators for the use in optical pH sensors. The synthesis aim was divided in different parts: i) a straightforward multistep synthesis of terrylene diimide derivatives; ii) making use of structural modifications in bay-position affecting the photophysical properties displayed in form of bathochromically shifted characteristic absorption and emission bands; iii) introduction of pH sensitive PET-receptors by substitution either in imide-position or in bay-position.

As presented previously, synthesis of terrylene diimide is a challenging and time-consuming task, due to laborious purification procedures, limited yields of various synthetical steps and indeed poor solubility of several compounds lowers the accessibility of more modified terrylene derivatives. Although, monofunctionalized perylene diimides have been described in literature[36,41], monofunctionalization methods for TDIs are rather limited.[51,53]

In this study asymmetric core-enlarged dyes have been synthesized bearing phenyl-groups or 4-benzoyl-morpholino-groups in bay-region to increase solubility, enhance the hydrophilic character of the structure, built up by naphthalene building blocks and prevent aggregation. The presented terrylene diimides exhibit rather high molar absorption coefficients, bright red to far-red fluorescence emission, and extraordinary high photostability. Nevertheless, it was not possible to introduce pH sensitivity via PET receptors to the terrylene structure neither in imide-position nor in bay-position.

Highly photostable, far-red emissive terrylene diimide dyes

Authors: David Pfeifer, Anna Knaus, Ingo Klimant, Sergey M. Borisov

Institute of Analytical Chemistry and Food Chemistry, Graz University of Technology, Stremayrgasse 9, 8010 Graz, Austria

Keywords: terrylene diimide, fluorescence, far-red emitting, highly photostable

5.2 Abstract

Here, a multistep synthesis and characterization of core-extended terrylene diimide dyes is presented. The synthesis includes a cascade of Pd-catalyzed Suzuki couplings, bromination of the terrylene core, and further functionalization. Terrylene diimides are a relatively young part of the large class of rylene dyes, closing the gap between perylene- and quaterrylene diimides. Terrylene diimides usually feature absorption and emission bands in the red/far red region of the spectrum, but due to their structural properties they are rather hydrophobic and prone to aggregation. Novel asymmetric core-enlarged dyes have been synthesized bearing phenyl-groups or 4-benzoyl-morpholino-groups in bay-position to increase solubility, enhance the hydrophilic character of the structure built up by naphthalene building blocks and prevent aggregation. The synthesized dyes exhibit high molar absorption coefficients, bright red to far-red fluorescence emission, and extraordinary high photostability. Furthermore, several synthetic attempts have been carried out to introduce a pH sensitive PET receptor by adapting previously applied procedures used for perylene and terrylene diimide dyes but without the expected success to get pH sensitive, far-red emitting, hydrophilic terrylene diimide indicators, which can be applied for optical sensors.

5.3 Introduction

Terrylene bisimide or terrylene diimide (TBI or TDI) dyes, are a relatively young member in the class of rylene dyes. In recent years functionalized rylene derivatives have been successfully implemented in several challenging applications such as optoelectronics[26,27] and photovoltaic devices[28], light emitting diodes[29] and energy transfer cascades[30] to mention only a few. The first red emitting TDI was synthesized by *Holtrup et al.* in 1997, driven by the motivation to close the gap between yellow to red emissive perylene bisimides and NIR emitting quaterrylene bisimides.[23]

Terrylene diimides are built up by a conjugated framework of three naphthalene units connected to each other in *peri*-position. In general, this dyes feature high luminescence brightness, extraordinary good photostability, and bathochromically shifted absorption/emission bands (about 100 nm per additional naphthalene unit compared to classical perylene bisimide) in the far red to NIR region of the spectrum and additionally versatility in respect to chemical modification.[16,25,51,222] Structural modifications in bay-position affect the photophysical properties noticeably, whereas substitution in imide-position is reasonable for functionalization and enhancement of solubility. Although, monofunctionalized perylene diimides have been described in literature[36,41], monofunctionalization methods for TDIs are rather limited.[51,53] None of those dyes has yet been used for optical pH sensors.

5.4 Results and Discussion

5.4.1 Synthesis

The motivation of this study was tuning of the intrinsic properties by structural modifications of terrylene diimide dyes, which in general feature high luminescence brightness, extraordinary good photostability, and bathochromically shifted absorption/emission bands in the far red to NIR region of the spectrum (absorption maxima of classical unsubstituted terrylene bisimide dyes are usually located at around 650 nm). Nevertheless, TDIs have only be investigated for academic research but not gained industrial attention yet, due to challenging and time-consuming synthesis procedures.[16,52–54] In respect to synthesis, tuning of the photophysical properties of terrylene bisimide dyes is commonly achieved by substitution in bay-region of the terrylene core. Furthermore, introduction of substituents should prevent aggregation in hydrophilic environment such as polyurethane based hydrogels, which are commonly used for optical pH sensors. In this study several synthetic strategies have been investigated to introduce a pH sensitive PET receptor either in the bay-position or in imide-position, though without the desired result affording a pH sensitive terrylene diimide, which could be applied in optical sensors. However, a series of terrylene diimides without pH sensitive functionality have been prepared to investigate their optical properties and the general applicability of these dyes in optical sensors.

Overall can be said, that the synthetic pathways even to an unsubstituted asymmetric terrylene diimide proved to be challenging and time-consuming tasks. A scheme for the synthetic pathways is shown in **Figure 5-1**. The synthetic pathway starting from 4-bromo-naphthalic anhydride **1** were adapted from a procedure published previously.[223] Here, it was possible to convert **1** in a two-step synthesis first into the 4-bromonaphthalenecarboximide **3** and afterwards by reaction with bis(pinacolato)diboron and $Pd(PPh_3)_4$ to the corresponding boronic ester **5** in 35 % yield. The synthesis of the second building block 9-bromoperylenedicarboximide **8** could also be accomplished via two synthetic steps according to literature.[223,224] Terrylene diimide precursor **10** ccould be synthesized via Pd-catalyzed Suzuki reaction using the boronic ester **5** and 9-

bromoperylenedicarboximide **8**. This naphthylperylene derivative **10** was cyclized with K_2CO_3 in ethanolamine affording the formation of **TDI** in good yield (84 %) after several washing steps, because unsubstituted **TDI** suffers from moderate solubility in organic solvents. The procedures were adapted from protocols published previously.[51,223]

The next step, introduction of four bromine atoms in bay-region opens the door for further functionalization at the terrylene core.[58] Bromination of **TDI** was carried out in chloroform with elemental bromine under exclusion of light to gave the tetrabrominated **TDI-4Br**, which led to a noticeable increase in solubility, due to the distortion of the terrylene skeletal structure. As can be seen in the reaction scheme (**Figure 5-1**) **TDI-4Br** was used as precursor for several modifications including bay-substitution as well as attempts to introduce a PET receptor to render the dye pH sensitive. Introduction of substituents in bay-region reduces planarity of the fluorophoric system and results in a significant increase of solubility in organic solvents. Furthermore, extension of the chromophoric core with aromatic substituents causes a noticeable bathochromic shift of absorption and emission bands.[51,225]

Substitution of the bromine atoms with four phenyl groups was accomplished via Pd-catalyzed Suzuki coupling reaction[54], using an excess of phenylboronic acid in toluene/EtOH mixture for 24 h at 70 °C giving green tetraphenyl-substituted **TDI-4Ph** in 52 % yield.

To enhance both the hydrophilic character of terrylene diimide and the solubility, introduction of four morpholino(phenyl)methanone substituents in bay-position was conducted, again via a Pd-catalyzed Suzuki coupling of boronic ester **12** with **TDI-4Br** yielding greenish **TDI-4Mo** in good yield (67 %) after purification via column chromatography. Reaction conditions were adapted from procedures published previously.[48,51,58] Photophysical properties of **TDI-4Br**, **TDI-4Ph** and **TDI-4Mo** are described in the next **Section 5.4.2**.

Since **TDI-4Mo** shows a significant bathochromic shift in absorption and emission bands, further synthetic pathways are focused on the introduction of pH functionality into the molecule. For that reason, several synthetic routes have been considered to render the terrylene pH sensitive. This attempts include (see **Figure 5-1**), (a) an introduction of a PET-receptor in imide-position via two step synthesis consisting of a saponification of the imide followed by condensation with an amine bearing a phenol such as 4-amino-2,6-dichlorophenol - see *synthesis pathway v)* using **TDI-4Mo** as starting material and *vii)* using **TDI-4Br** as starting material; (b) starting from **TDI-4Br** affording a chlorsulfonation at the 2,6-diisopropylphenyl group in the imide structure followed by reaction with an amino group such as 4-amino-2,6-dichlorophenol (see *synthesis pathway vii)*); (c) a Pd-catalyzed Suzuki coupling of a phenol based boronic acid or boronic ester to afford an asymmetric bay-substituted terrylene diimide derivative **16a** or **16b** (see *synthesis pathway viii)*).

Thus, two different conditions for saponification reaction were tested. First, according to a procedure reported previously used for partial saponification of perylene bisimides[48] with 50-fold excess of KOH, in a 6:1 mixture 2-propanol-water under reflux no conversion of terrylene bisimide **TDI-4Mo** was obtained. Second, according to the literature[53], **TDI-4Mo** was dissolved in *t*-

butanol at 80 °C and a mixture of hot *t*-butanol, potassium fluoride and potassium hydroxide was added and stirred for 45 min. After addition of acetic acid, the mixture was stirred for another hour. After aqueous workup no conversion of **TDI-4Mo** was observed. Due to the unsuccessful attempts of (partial) saponification the final step, no condensation of terrylene monoimide with the PET receptor (4-amino-2,6-dichlorophenol) was conducted.

The second promising synthetic pathway was adapted from a procedure applied for perylene bisimides.[42] Therefore, **TDI-4Br** was heated to 60 °C in chlorosulfonic acid for 3 h. After cooling to RT, the mixture was added dropwise onto crushed ice, transferred into a separation funnel, washed with ice water and dried with a rotary vane pump. The resulting blue precipitate was dissolved in N,N-dimethylformamide, together with 4-amino-2,6-dichlorophenol and triethylamine, the mixture was stirred overnight at RT under exclusion of light. The aqueous workup was followed by separation of the precipitate via centrifugation. The greenish blue residue was only soluble in dimethyl sulfoxide and N,N-dimethylformamide, thus purification with conventional chromatography was not possible and conversion to **14** could not be confirmed with NMR spectroscopy or mass spectrometry.

Finally, in the third synthetic route, a Pd-catalyzed Suzuki reaction[61], coupling of **TDI-4Br** with 0.9 equivalents of 3-chloro-4-hydroxyphenyl boronic acid was expected to give the functionalized terrylene diimide **16a**. The reaction was carried out in THF/toluene mixture under argon atmosphere at 80 °C for 3 days. After purification via column chromatography a high amount of unconverted **TDI-4Br** and different undefined side products were identified and the expected product could not be obtained as pure regioisomer in acceptable yields (>5 %). Due to the disappointing result, another Pd-catalyzed Suzuki coupling with a different 3,5-dichloro-4-hydroxyphenyl boronic acid pinacol ester was performed, using similar reaction conditions as mentioned above, but at 70 °C for 5 days. Unfortunately, neither regioisomers nor multiple substituted product could be isolated. During the workup a dark oil was obtained in the aqueous phase, emphasizing that most probably, the boronic acid pinacol ester is not suitable for such Suzuki-reaction conditions.

Summarizing it can be said, that even the synthesis to the terrylene diimide is challenging and time-consuming. The yields of all steps do not enable the gram scale synthesis of terrylene diimide, which is of course a limiting factor for further synthetic pathways. Nevertheless, different starting materials may simplify the syntheses in consideration of different synthetic routes published recently. Perhaps, it will be possible to introduce the pH sensitivity in imide-position in an earlier stage of synthesis, right before cyclodehydrogenation to terrylene diimide[51] or alternatively, designing terrylene structures from readily available naphthalene building blocks such as 4,5-dibromo-functionalized naphthalene diester and 1,4-naphthalenediboronic acid pinacol ester.[62]

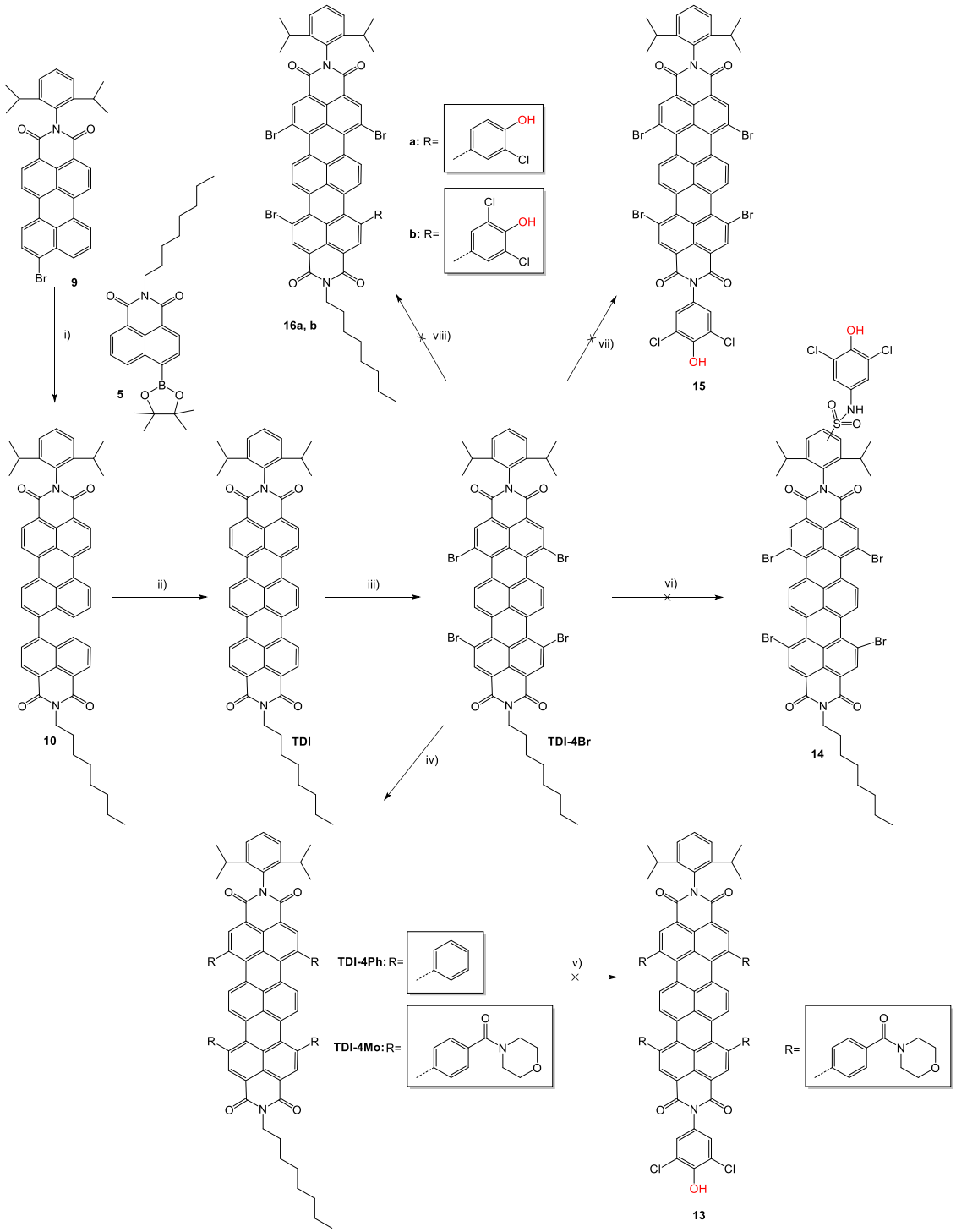

Figure 5-1 Reaction scheme – reagents and conditions i) $Pd(PPh_3)_4$, Na_2CO_3, toluene/EtOH, 32%; ii) K_2CO_3, ethanolamine, 84%; iii) Br_2, chloroform, light exclusion, 65%; iv) **TDI-4Ph**: phenyl boronic acid, $Pd(amphos)Cl_2$, toluene/EtOH, 52%; **TDI-4Mo**: Morpholino(4-(4,4,5,5-tetramethyl-1,3,2-dioxaborolan-2-yl)phenyl)methanone, $Pd(amphos)Cl_2$, THF/toluene, 67%; v) a) KOH, 2-propanol/H_2O 6:1 b) (1) KOH, KF, t-butanol (2) acetic acid; vi) (1) HSO_3Cl, (2) H_2O/ice, (3) 4-amino-2,6-dichlorophenol, DMF, triethylamine; vii) KOH, 2-propanol/H_2O 6:1; viii) **16a**) 3-chloro-4-hydroxyphenyl boronic acid, $Pd(amphos)Cl_2$, Na_2CO_3, THF/toluene; **16b**) (1) 3,5-dichloro-4-hydroxyphenyl boronic acid pinacol ester, $Pd(amphos)Cl_2$, Na_2CO_3, THF/toluene.

5.4.2 Photophysical Properties

Due to invincible challenges in synthesis of pH sensitive terrylene bisimide dyes, three bay-substituted TDIs (**TDI-4Br**, **TDI-4Ph** and **TDI-4Mo**) are chosen to investigate the photophysical properties in respect to their applicability in different solvent environments. Absorption spectra of building blocks (compounds **5** and **9**), the precursor of terrylene diimide **10**, the conjugated **TDI** and of the tetrabromo terrylene derivative (**TDI-4Br**) are shown in **Figure 5-2**. **TDI** exhibits a brilliant deep blue color, its absorption maximum in chloroform solution is located at 652 nm and its emission maximum at 670 nm, respectively.

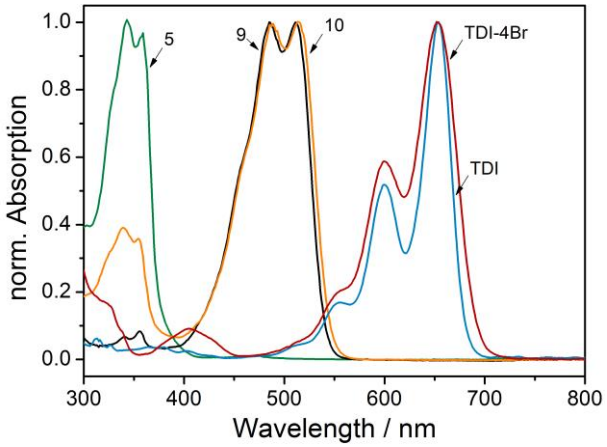

Figure 5-2 Normalized absorption spectra of compounds **5**, **9**, **10**, **TDI** and **TDI-4Br** in chloroform.

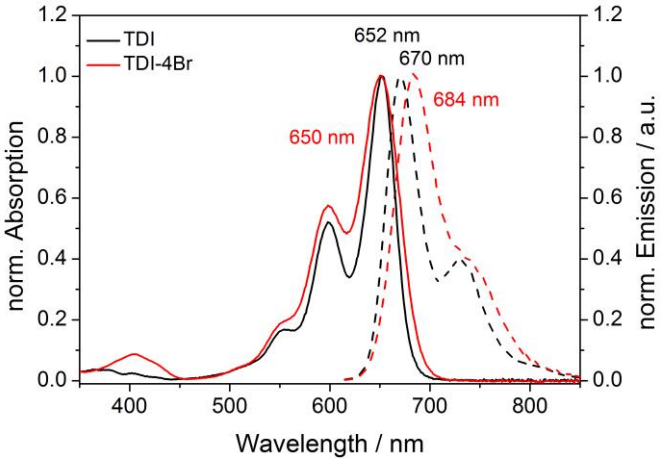

Figure 5-3 Normalized absorption (solid lines) and emission (dashed lines) spectra of **TDI** (black lines) and **TDI-4Br** (red) in chloroform.

The spectra are typical for rylene dyes with relatively narrow absorption and emission bands and Stokes shifts of about 20 nm. As can be seen (**Figure 5-3**) introduction of four bromine atoms at the bay-position changes the spectral properties, while the absorption spectrum is only affected in

its shape and no shift of the maximum is obtained the emission band is bathochromically shifted to 684 nm, and the Stokes shift is enlarged up to about 35 nm, respectively. Further substitution by introduction of four phenyl groups (**TDI-4Ph**) or morpholino(phenyl)methanone groups (**TDI-4Mo**) cause a significant bathochromic shift of both absorption and emission maxima to around λ_{abs} 700 nm and λ_{em} 743 nm due to extension of the π-system (**Figure 5-4**). The products show greenish-blue color compared to the blue unsubstituted **TDI**. The fluorescence quantum yields were determined relative to dibutoxy-aza-BODIPY (Φ = 0.36 in chloroform), which also exhibit emission in the deep red region of the spectrum.

Table 5-1 Photophysical properties of synthesized bay-substituted terrylene dyes at 25 °C. Absorption maxima (λ_{Abs}), molar absorption coefficients (ε) emission maxima (λ_{Em}), fluorescence quantum yields (Φ) and fluorescence lifetimes (τ) for the dyes in chloroform solution. Photobleaching quantum efficiency (Φ_{bl}) for the dyes in THF solution.

Dye	λ_{abs} [nm]	ε [M^{-1} cm^{-1}]	λ_{em} [nm]	Φ	Φ_{bl}	τ [ns]
TDI-4Br	653	82000	683	0.43	1.0 x 10 $^{-7}$	3.5
TDI-4Ph	702	44000	748	0.18	1.3 x 10 $^{-7}$	2.6
TDI-4Mo	700	76000	743	0.18	6.8 x 10 $^{-8}$	2.9

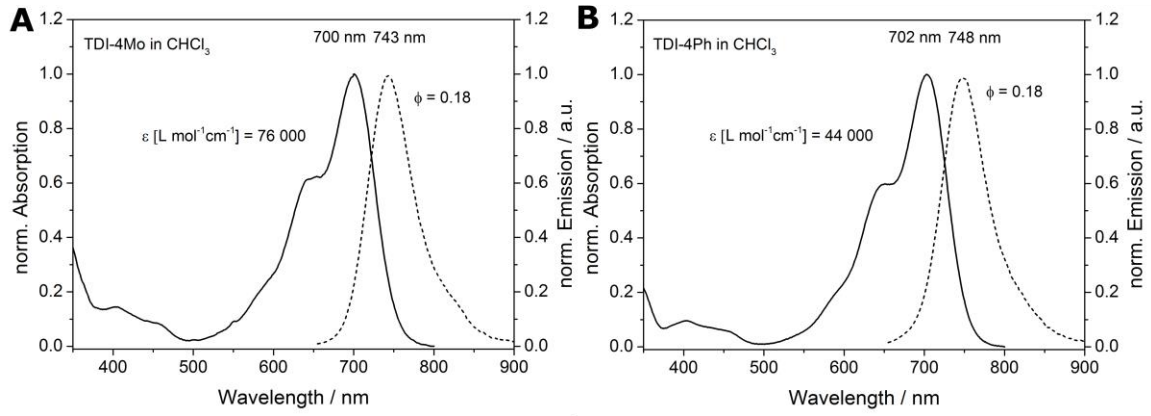

Figure 5-4 Normalized absorption (solid lines) and emission (dashed lines) spectra of **TDI-4Mo** (left) and **TDI-4Ph** (right) in chloroform.

The influence of the solvent environment on the photophysical properties were systematically investigated, summarized in **Table 5-2-5-4**. The highest molar absorption coefficient for **TDI-4Br** was obtained in THF, whereas the highest luminescence brightness was determined in $CHCl_3$. Due to high polarity of EtOH and precipitation of the tetrabrominated derivative measurements could not be performed in this solvent.

Table 5-2 Photophysical properties of **TDI-4Br** in organic solvents at 25 °C.

Solvent	λ_{abs} [nm]	ε [M^{-1} cm^{-1}]	λ_{em} [nm]	Φ	τ [ns]
toluene	651	68000	680	0.43	3.6
THF	644	94000	676	0.35	3.1
$CHCl_3$	653	82000	683	0.43	3.5

TDI-4Ph showed the highest molar absorption coefficient and the highest fluorescence quantum yield in toluene. Moreover, molar absorption coefficients were determined to be in the same range while remarkable differences in fluorescence quantum yields (15-fold higher in toluene compared to EtOH) were obtained. A similar trend concerning the fluorescence quantum yields was observed for **TDI-4Mo**, whereas the highest molar absorption coefficient was determined in $CHCl_3$. Fluorescence lifetimes were calculated to be in a typical range for rylene dyes of around 2.4 -3.6 ns. An exception was detected in EtOH solution for both **TDI-4Ph** and **TDI-4Mo** (τ<0.6 ns). This correlates well with the lowest quantum yields and is likely to be due to efficient radiativeless deactivation in polar solvent.

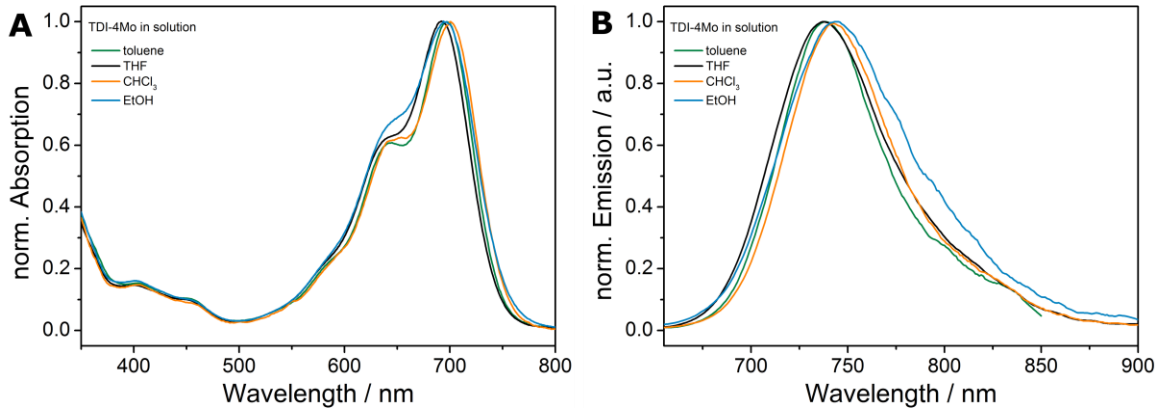

Figure 5-5 Normalized absorption (left) and emission (right) spectra of **TDI-4Mo** in different organic solvents.

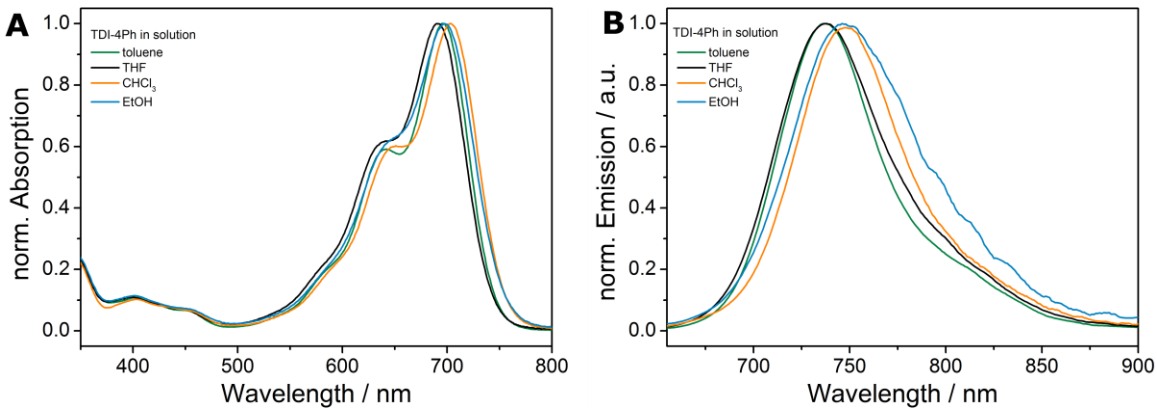

Figure 5-6 Normalized absorption (left) and emission (right) spectra of **TDI-4Ph** in different organic solvents.

By introduction of morpholino(phenyl)methanone groups in bay-position the hydrophilic character could be enhanced. As can be seen from the absorption and emission spectra in

Figure 5-5 and **Figure 5-6** neither detectable aggregation nor strong solvatochromic effects in polar solvents are visible, whereas terrylene diimides are usually prone to aggregation.[16,23] This could make **TDI-4Mo** derivatives promising candidates for embedment in hydrophilic hydrogels commonly used for optical pH sensors. On the other hand, significant decrease of QY in these conditions should be considered as well.

Table 5-3 Photophysical properties of **TDI-4Ph** in organic solvents at 25 °C.

Solvent	λ_{abs} [nm]	ε [M^{-1} cm^{-1}]	λ_{em} [nm]	Φ	τ [ns]
toluene	696	52000	738	0.30	3.8
THF	689	40000	738	0.17	2.4
$CHCl_3$	702	44000	748	0.18	2.6
EtOH	697	42000	748	0.019	0.5

Table 5-4 Photophysical properties of **TDI-4Mo** in organic solvents at 25 °C.

Solvent	λ_{abs} [nm]	ε [M^{-1} cm^{-1}]	λ_{em} [nm]	Φ	τ [ns]
toluene	697	61000	739	0.27	3.7
THF	693	70000	738	0.14	2.5
$CHCl_3$	700	76000	743	0.18	2.9
EtOH	694	68000	746	0.019	0.6

Photostability is another parameter relevant for practical applications. In order to estimate the photostability, we irradiated the solutions of the dyes in THF (except for TMR which was dissolved in water) with a metal-halogen lamp and quantified the photodegradation via UV-Vis spectroscopy. As reference dyes an aza-BODIPY fluorophore and commercially available tetramethylrhodamine ethyl ester perchlorate (TMR) were chosen. Dibutoxy-aza-BODIPY represents a highly photostable, far red emitting aza-BODIPY dye without functionality but bearing two butoxy groups.[150] TMR is a typical representative of rhodamine dyes; the photostability of TMR and other rhodamine and coumarin dyes was studied by Eggerling and co-workers.[214]

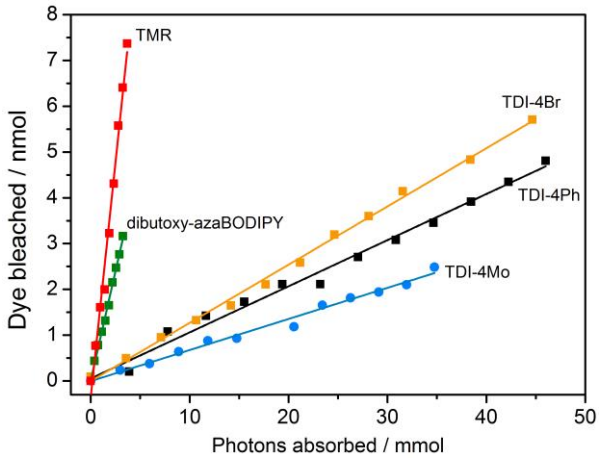

Figure 5-7 Photodegradation of terrylene diimides and reference dyes and corresponding linear fit.

As can be seen (**Figure 5-7**) that TMR and dibutoxy-aza-BODIPY bleaches faster than the terrylene dyes **TDI-4Br**, **TDI-4Ph** and **TDI-4Mo**. The quantitative parameter, the photobleaching quantum efficiency Φ_{bl} is calculated from the slope of the curve (number of bleached dye molecules vs. total number of absorbed photons) and is compared in **Table 5-1**. Φ_{bl} for dibutoxy-aza-BODIPY is calculated to be 9.5 x 10^{-7}, which is comparable to that of TMR, which is ~2-fold higher (2.0 x 10^{-6}). Finally, terrylene dyes **TDI-4Br**, **TDI-4Ph** and **TDI-4Mo** show Φ_{bl} of 6.8 x 10^{-8} – 1.0 x 10^{-7} and are thus more than one orders of magnitude more photostable than the reference chromophores. It can be concluded that the terrylene dyes feature extraordinary high photostability combined with the long-wavelength absorption and emission, and high brightness. Due to the dramatic decrease in brightness in polar environment, they are only particularly attractive for applications in non hydrophilic environments.

5.5 Materials and Methods

5.5.1 Materials

Bromine, potassium acetate, potassium hydroxide, potassium fluoride, 1,4-dioxane, 2,6-diisopropylaniline, tetramethylrhodamine ethyl ester perchlorate (TMR), n-octylamine, 3,3-diethylthiadicarbocyanin iodide zinc acetate dihydrate and 4-amino-2,6-dichlorophenol were purchased from Sigma Aldrich (www.sigmaaldrich.com). Bis(pinacolato)diboron, tetrakis(triphenylphosphine)palladium ($Pd(PPh_3)_4$), 4-bromo-naphthalic anhydride, phenyl boronic acid, 3-chloro-4-hydroxyphenyl boronic acid and 3,5-dichloro-4-hydroxyphenyl boronic acid pinacol ester were obtained from TCI Europe (www.tcieurope.de). Imidazole, perylene-3,4,9,10-tetracarboxylic dianhydride, morpholino(4-(4,4,5,5-tetramethyl-1,3,2-dioxaborolan-2-yl)phenyl)methanone were purchased from Fluorochem (www.fluorochem.co.uk). Chlorosulfonic acid and $Pd(amphos)Cl_2$ were received from acros organics (www.acros.com). Dichloromethane

(DCM) was received from Fisher scientific (www.fishersci.com). Cyclohexane (CH), ethanol (EtOH), ethyl acetate (EA), methanol (MeOH), tetrahydrofuran (THF) and toluene (synthesis grade), sodium chloride, potassium carbonate and hydrochloric acid (37%) were purchased from VWR Chemicals (www.vwr.com). Poly(styrene-co-polydivinylbenzene) (PS/DVB) microbeads, anhydrous sodium sulfate, acetic acid, N,N-dimethylformamide, dimethyl sulfoxide and 2-propanol were obtained from Carl Roth (www.roth.de). Deuterated chloroform ($CDCl_3$) and methylene chloride (CD_2Cl_2) was purchased from Euriso-top (www.eurisotop.com). All purchased chemicals were used without further purification. Silica-gel 60 (0.063-0.200 mm) was obtained from Merk (www.merck.at). Reference compound BF2 chelate of [5-(4-buthoxyphenyl)-3-phenyl-1Hpyrrol-2-yl][5-(4-buthoxyphenyl)-3-phenylpyrrol-2-ylidene]amine ("dibutoxy-aza-BODIPY") was prepared according to a literature procedure.[150]

5.5.2 Methods

Mass spectroscopy was performed on Micromass TofSpec 2E Time-of-Flight Mass Spectrometer at the Institute for Chemistry and Technology of Materials, Graz University of Technology and on Advion expression CMS benchtop MS. ^{1}H and ^{13}C NMR spectra were recorded on a 300 MHz Bruker Instrument (www.bruker.com) in CD_2Cl_2 or $CDCl_3$ as a solvent and TMS as standard.

Absorption spectra were recorded on a Cary 50 UV-Vis spectrophotometer from Varian (www.agilent.com) using optical glass cuvettes from Hellma Analytics (www.hellma-analytics.com). Emission and excitation spectra were recorded on a FluoroLog 3 spectrofluorometer from Horiba Scientific Jobin Yvon (www.horiba.com) equipped with a R2658 photomultiplier from Hamamatsu and corrected for detector response. Determination of relative fluorescence quantum yields Φ were carried out in chloroform, EtOH, THF and toluene solutions on the above mentioned spectrofluorometer from Horiba with "dibutoxy-aza-BODIPY" solution in chloroform (Φ = 0.36)[226] and 3,3-diethylthiadicarbocyanin iodide solution in EtOH (Φ = 0.35)[227] as reference material according to Crosby and Demas.[228]

Fluorescence decay times were determined via time correlated single photon counting (TCSPC) on a FluoroLog 3 spectrofluorometer equipped with a DeltaHub module and NanoLED (λ = 635 nm, Horiba) as excitation sources. Data analysis was carried out with DAS6 software (www.horiba.com) using a mono-exponential fit.

The photostability of the dyes **TDI-4Br**, **TDI-4Ph, TDI-4Mo**, dibutoxy-aza-BODIPY and TMR was accessed by illumination with a Metal-Halogen-lamp (ConstantColor™ CMH Precise™, GE Lightening) with 14.000 nominal lumens. A heat protection filter (CALFLEX X; QIOPTIQ) and an UV blocking filter (UV-Blocking-Filters UV-B; QIOPTIQ) were used to narrow the spectrum of the lamp to 400 to 700 nm. The solution of the dye in THF (water in case of TMR) in a screw-capped quartz cuvette was stirred during the irradiation with help of a magnetic stirrer. The photon flux Φ_{out} transmitted through the cuvette was measured with a light-meter (LI-250A) equipped with a light sensor (LI-190 Quantum sensor; LI-COR Biosciences, www.licor.com). A Neutral-Density

filter (25%; QIOPTIQ, www.qioptiq.de) was installed in front of the light sensor to avoid its saturation. The absorption spectra were acquired after irradiation periods of 30 min for the dyes **TDI-4Br**, **TDI-4Ph**, **TDI-4Mo**, 10 min for TMR and 5 min for dibutoxy-aza-BODIPY.

5.5.3 Synthesis

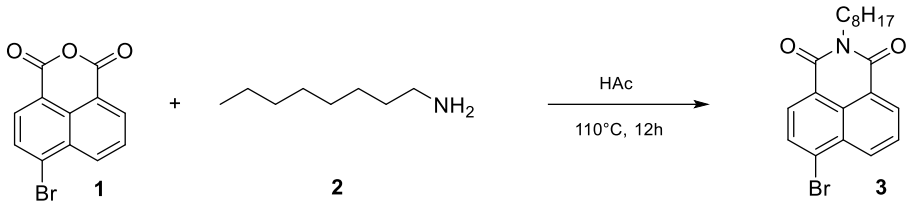

6-Bromo-2-octyl-1*H*-benzo[de]isoquinoline-1,3(2*H*)-dione (3). The synthetic pathway was adapted from a procedure published previously.[223] A Schlenk flask was charged with 4-bromo-naphtalic anhydride **1** (2.03 g, 1.00 eq.) in 50 mL acetic acid. After the anhydride was dissolved, n-octylamine **2** (3.8 mL, 3.20 eq.) was added. The mixture was heated to reflux for 16 h. The reaction mixture was allowed to cool down to room temperature, acetic acid was removed under reduced pressure, and the residue was redissolved in DCM and dried over Na_2SO_4. The crude product was purified via column chromatography (silica gel, cyclohexane/DCM) resulting in a white solid **3** (2.63 g, 92 %). ^{1}H NMR (300 MHz, Chloroform-*d*) δ 8.65 (s, 1H), 8.56 (s, 1H), 8.41 (s, 1H), 8.06 (s, 1H), 7.85 (s, 1H), 4.16 (s, 2H), 1.73 (s, 2H), 1.27 (s, 10H), 0.87 (s, 3H).

MS of **3** m/z: [M$^+$] calc. for $C_{20}H_{22}BrNO_2$: 387.08; found: 388.0.

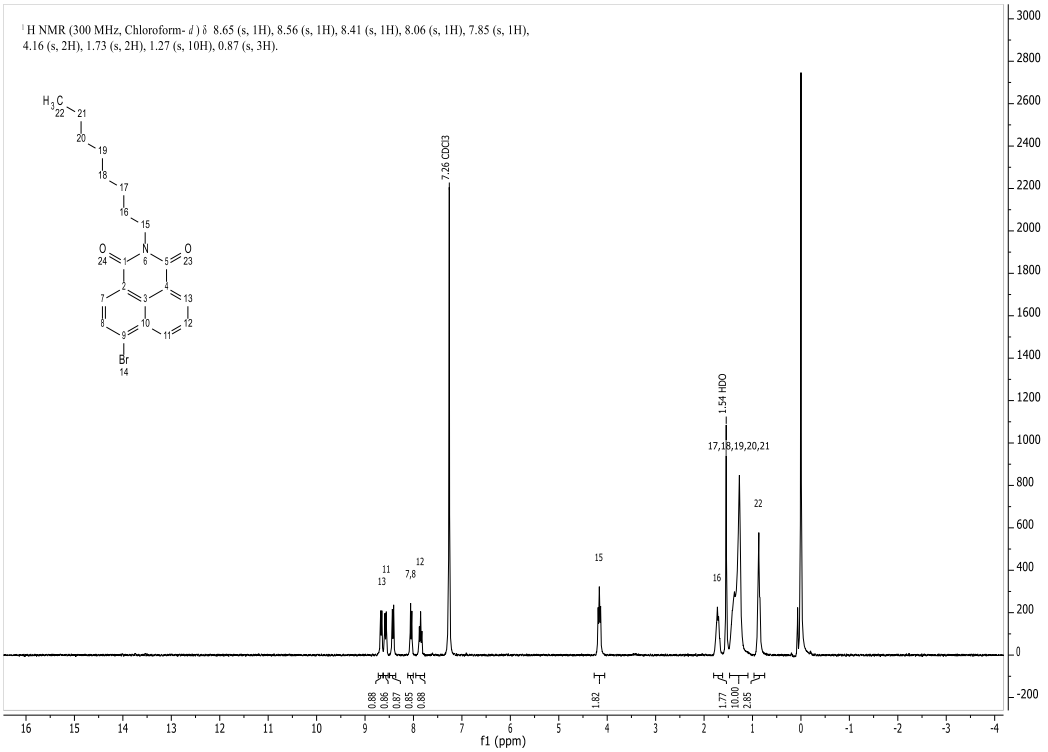

Figure 5-8 ^{1}H-NMR spectrum of **3** in chloroform-d at room temperature (300 MHz).

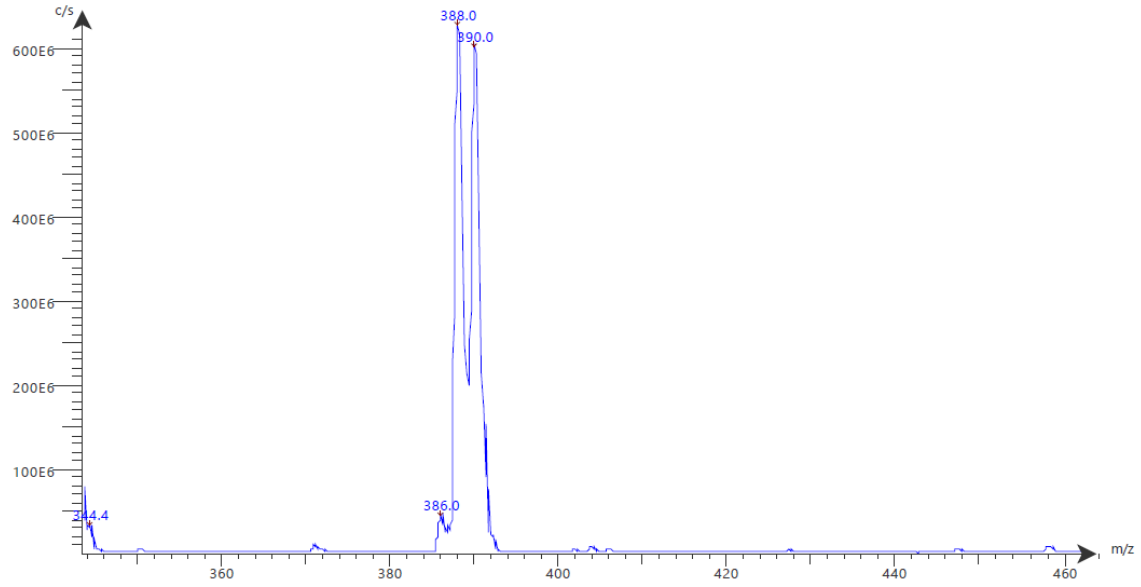

Figure 5-9 Mass spectrum of **3** recorded on Advion expression CMS.

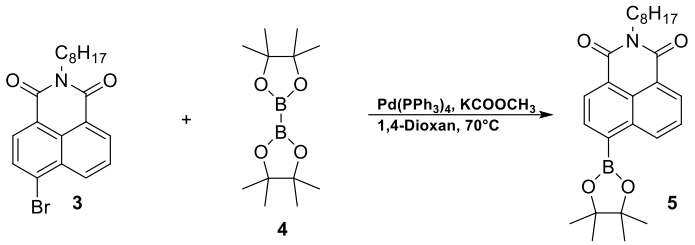

2-octyl-6-(4,4,5,5-tetramethyl-1,3,2-dioxaborolane-2-yl)-1*H*-benzo[de]isoquinoline-1,3(2*H*)-dione (5). The reaction was carried out under argon atmosphere and dry conditions according to literature.[223] Bis(pinacolato)diboron **4** (72.0 mg, 1.10 eq.), **3** (103 mg, 1.00 eq.) and potassium acetate (78.9 mg, 3.10 eq.) were homogenized in a dry 10 mL Schlenk tube and 2 mL of semidry 1,4-dioxane were added. Prior to addition of a catalytic amount of $Pd(PPh_3)_4$ the reaction mixture was bubbled with argon for 15 minutes and then it was heated to 70 °C. After stirring for 22 h, reaction control was accomplished by TLC and 64.6 mg of bis(pinacolato)diboron **4** were added additionally. The mixture was stirred for another 72 h at 70 °C. The reaction mixture was allowed to cool to room temperature and washed with water. Extraction was done with DCM and the organic phase was dried over Na_2SO_4. The solvent was evaporated under reduced pressure and a yellow oil was obtained. The crude product was purified by column chromatography (silica gel, cyclohexane/DCM; 6:4 to 2:8) yielding 40.1 mg (35 %) of a yellowish oil. The oil crystallized after several days at ambient conditions. ^{1}H NMR (300 MHz, Chloroform-*d*) δ 8.76 (s, 1H), 8.66 (s, 1H), 7.79 (s, 1H), 7.67 (s, 2H), 4.23 (s, 2H), 2.04 (s, 1H), 1.78 (s, 2H), 1.27 (d, J = 9.2 Hz, 20H), 0.88 (s, 5H).

MS of **5** m/z: [MH$^+$] calc. for $C_{26}H_{34}BNO_4$: 435.4; found: 436.3.

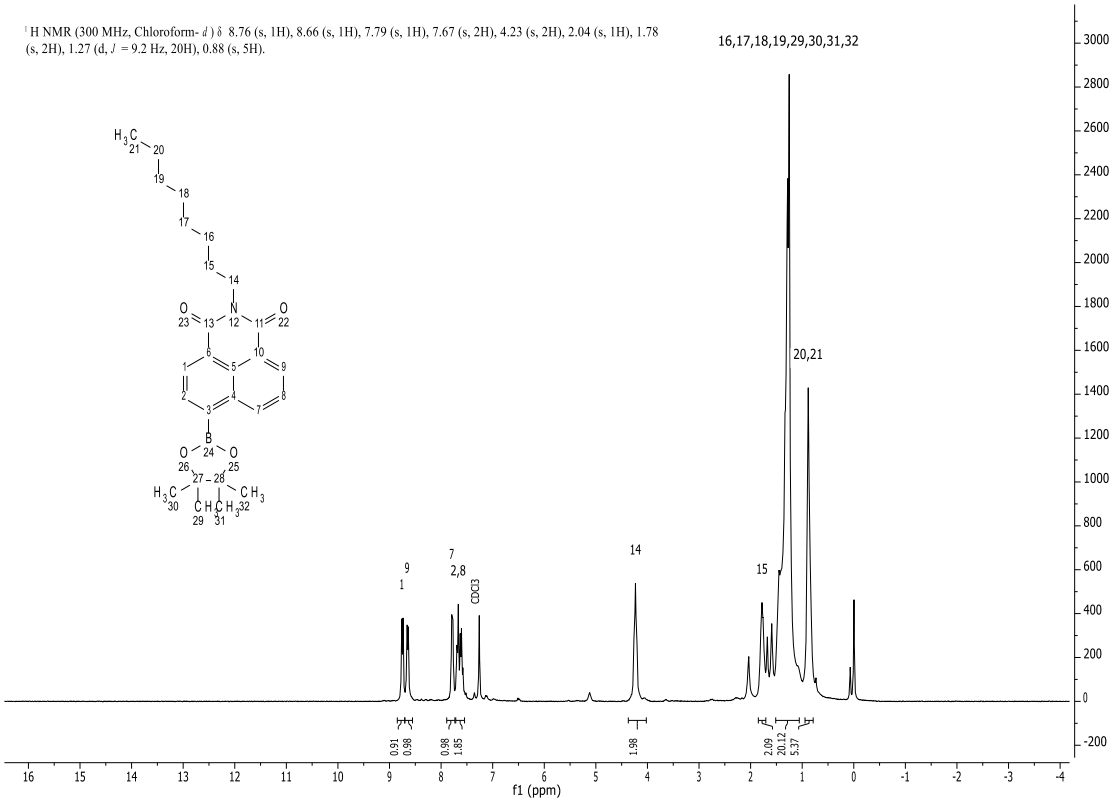

Figure 5-10 ^{1}H-NMR spectrum of **5** in chloroform-d at room temperature (300 MHz).

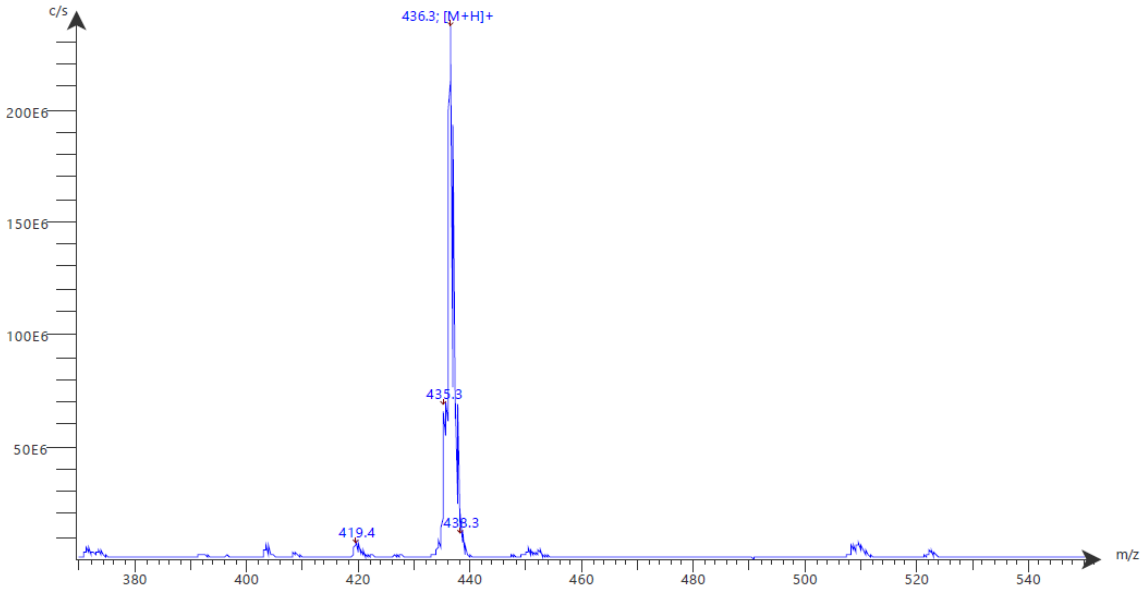

Figure 5-11 Mass spectrum of **5** recorded on Advion expression CMS.

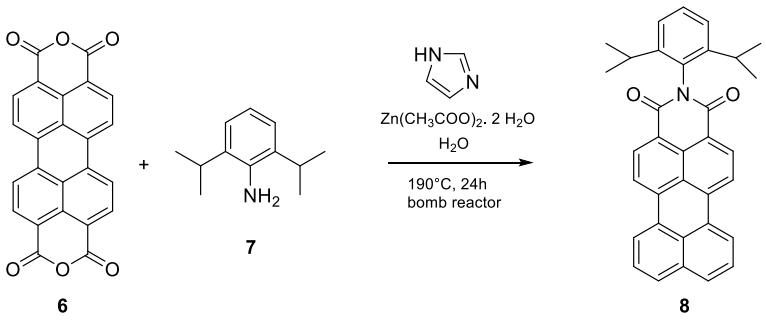

2-(2,6-diisopropylphenyl)-1*H*-benzo[10,5]anthra[2,1,9-*def*]isoquinoline-1,3(2*H*)-dione (8). The synthetic pathway was adapted from a procedure published previously.[224] The reaction was carried out according to literature, in a bomb reactor with a volume of 23 mL. Diisopropylaniline **7** (0.254 g, 1.00 eq.), perylene-3,4,9,10-tetracarboxylic dianhydride **6** (1.18 g, 2.00 eq.), imidazole (5.68 g, 55,6 eq.), zinc acetate dihydrate (0.346 g, 1.36 eq.) and 2.5 mL deionized water, were mixed in the bomb reactor. The bomb was screwed tightly and heated to 190 °C for 24 h. It was allowed to cool down to room temperature and 1.8 mL HCl conc. were added to the mixture. The mixture was filtered, washed with water and dried in the vacuum drying oven at 60 °C. The reaction was performed three times. To isolate the crude product out of the filter cake, Soxhlet extraction was performed using chloroform as solvent. The dry filter cakes received from the three reactions were combined and dispersed in 200 mL $CHCl_3$. Before extraction, an ultrasonic bath was used to ensure homogeneous particle sizes. Soxhlet extraction was carried out for 17 h. The crude product was purified by column chromatography (silica gel, cyclohexane/DCM, 7+3, 6+4) yielding a red solid (1.93 g, 93 %). ^{1}H NMR (300 MHz, Chloroform-*d*) δ 8.66 (s, 2H), 8.49 (s, 4H), 7.92 (s, 2H), 7.67 (s, 2H), 7.48 (s, 1H), 7.35 (s, 2H), 2.77 (s, 2H), 1.18 (d, J = 6.8 Hz, 12H).

MS of **8** m/z: [MH$^+$] calc. for $C_{34}H_{27}NO_2$: 481.6; found: 482.0.

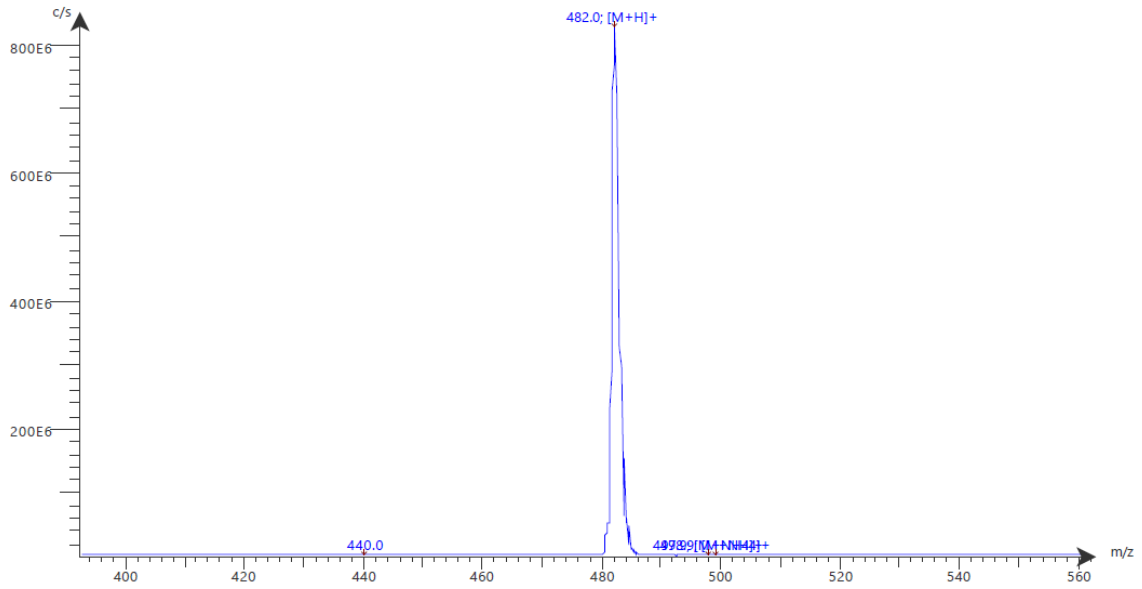

Figure 5-12 Mass spectrum of **8** recorded on Advion expression CMS.

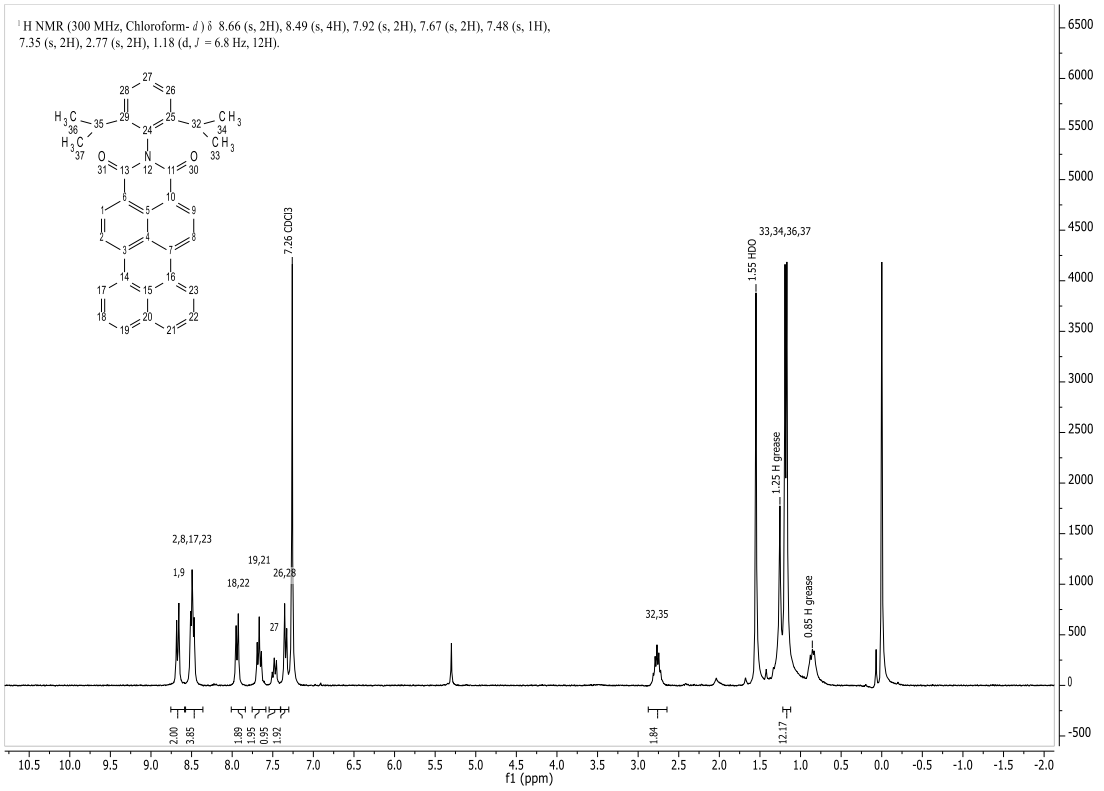

Figure 5-13 ¹H-NMR spectrum of **8** in chloroform-d at room temperature (300 MHz).

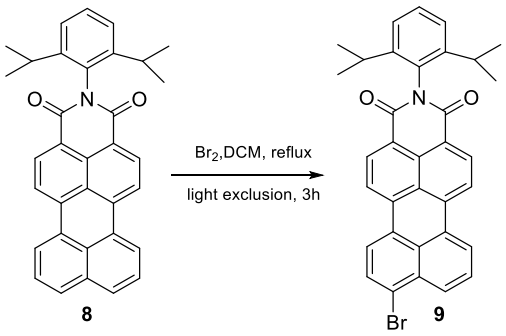

8-Bromo-2-(2,6-diisopropylphenyl)-1*H*-benzo[5,10]anthra[2,1,9-def]isoquinoline-1,2(2*H*)dione (9). The reaction was carried out under argon atmosphere according to literature.[223] 498.1 mg of perylene monoimide **8** (1.00 eq.) and 65 mL DCM were added in a dry 250 mL 2-neck-flask which was adjusted with a reflux condenser and a bubbler. After the solid was dissolved, bromine (0.07 mL, 1.00 eq.) was added in one portion. The reaction mixture was heated to reflux for 3 h and then cooled to room temperature. The solvent was removed under reduced pressure. The crude product was redissolved in DCM and was dried over Na_2SO_4. The resulting residue was purified by column chromatography (silica gel, cyclohexane/DCM, 7:3, 6:1) to obtain the product as a red solid with a yield of 441 mg (76 %). Due to poor solubility, only mass spectrometry was used for analytical characterization.

MS of **9** m/z: [MH^+] calc. for $C_{34}H_{26}BrNO_2$: 560.5; found: 560.0.

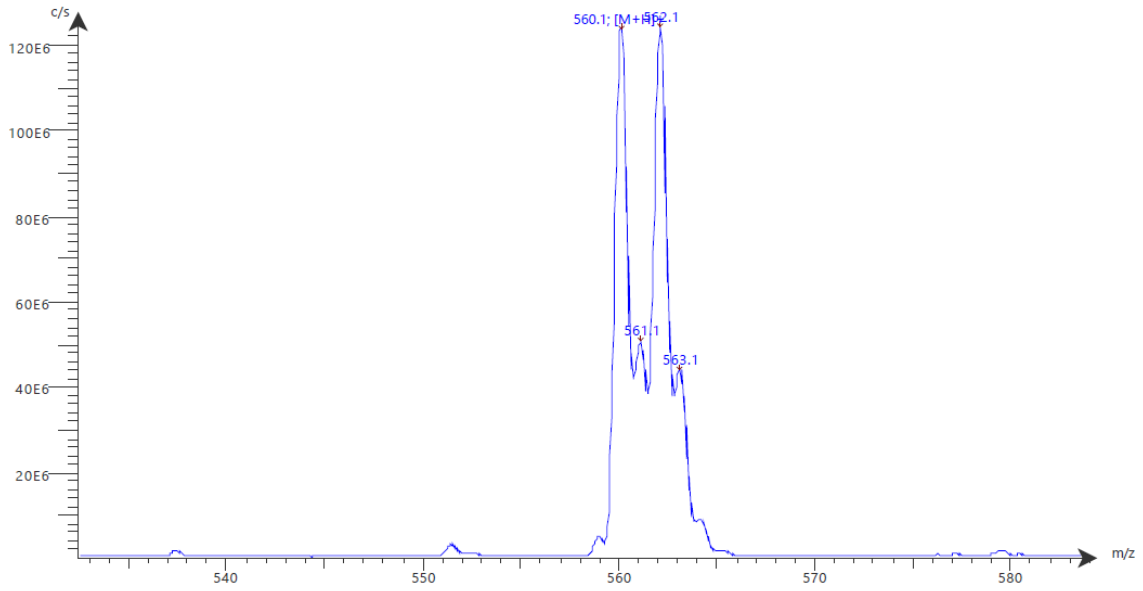

Figure 5-14 Mass spectrum of **9** recorded on Advion expression CMS.

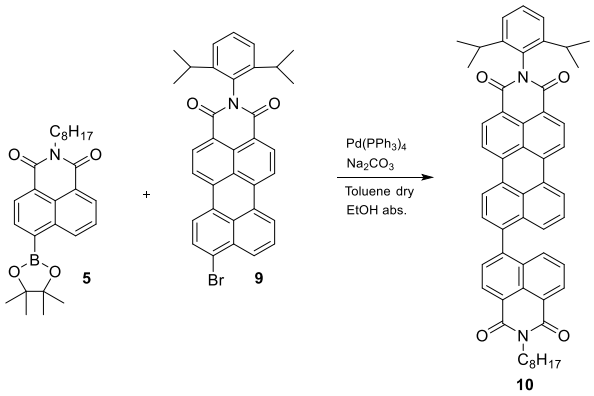

2-(2,6-diisopropylphenyl)-8-(2-octyl-1,3-dioxo-2,3-dihydro-1*H*-benzo[de]isoquinolin-6-yl)-1H-benzo[10,5]anthra[2,1,9-def]isoquinoline-1,3(2*H*)-dione (10). The reaction was carried out under argon atmosphere according to literature.[223] A 10 mL Schlenk tube was charged with 4-naphthaldicarboximide boronic ester **5** (400.0 mg, 2.30 eq.) and 9-bromoperylenedicarboximide **9** (226.5 mg, 1.00 eq.) and 2 mL of dry toluene. In addition, 0.2 mL of 0.5 M Na_2CO_3 and 0.1 mL of ethanol abs. were added to the suspension. The reaction mixture was bubbled with argon for 20 min, before a catalytic amount of air sensitive catalyst $Pd(PPh_3)_4$ was added. The suspension was heated to 80 °C for 42 h. Then, the reaction was cooled down to room temperature, washed with H_2O and extracted with DCM and was dried over Na_2SO_4. The solvent was removed under reduced pressure and the residue purified by column chromatography (silica gel, cyclohexane/DCM, 2:3 to DCM + 1% MeOH) to obtain 102 mg (32 %) of the orange product. ^{1}H NMR (300 MHz, Chloroform-*d*) δ 8.57 (s, 8H), 7.78 (s, 2H), 7.59 (s, 2H), 7.41 (s, 3H), 7.29 (s, 1H), 7.18 (s, 1H), 4.17 (s, 2H), 2.70 (s, 2H), 1.71 (s, 2H), 1.16 (d, J = 33.2 Hz, 25H).

MALDI-TOF-MS of **10** m/z: [M$^+$] calc. for $C_{54}H_{48}N2O_4$: 788.3614; found: 788.3293.

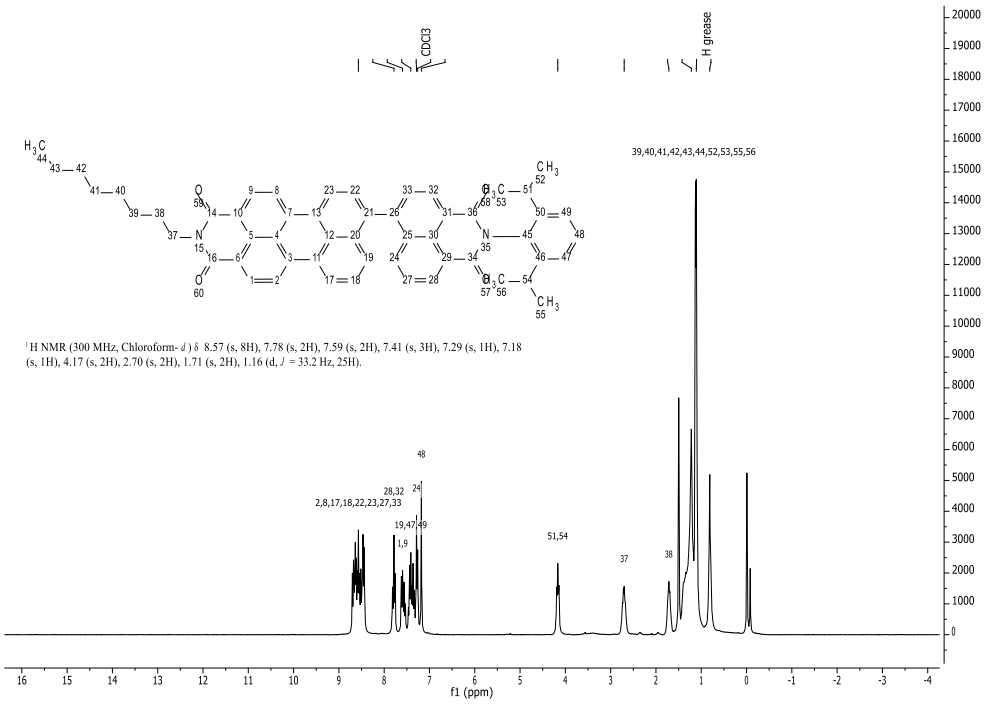

Figure 5-15 ^{1}H-NMR spectrum of **10** in chloroform-d at room temperature (300 MHz).

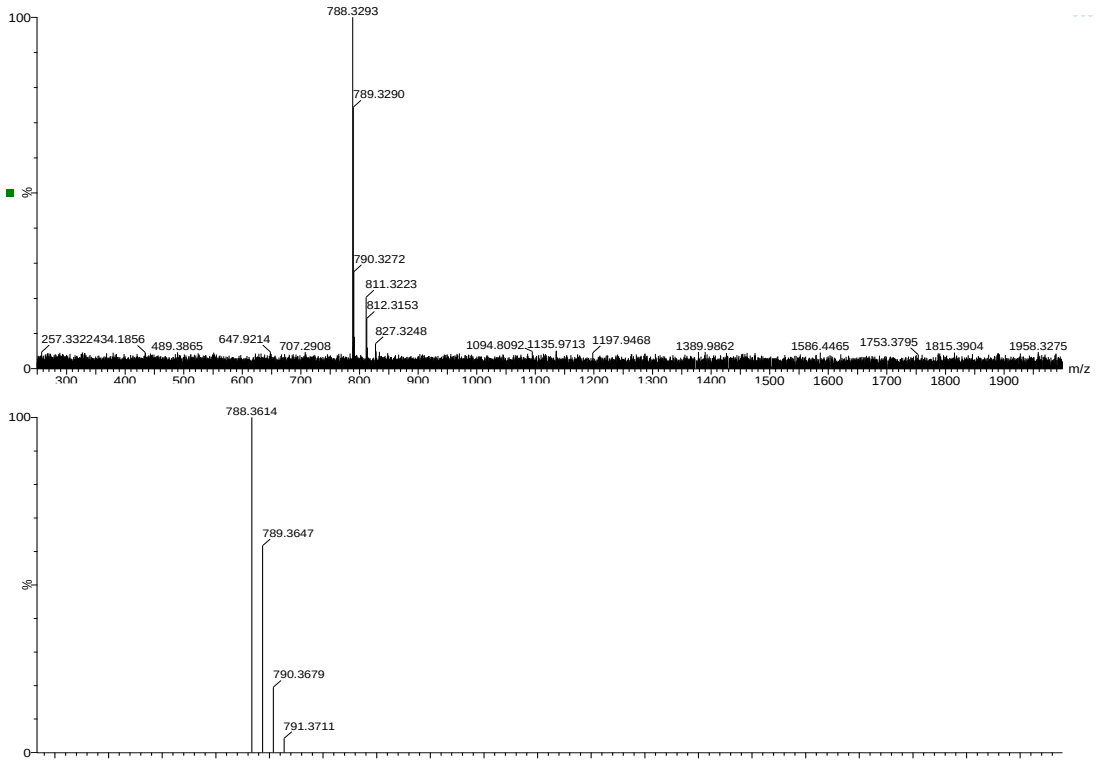

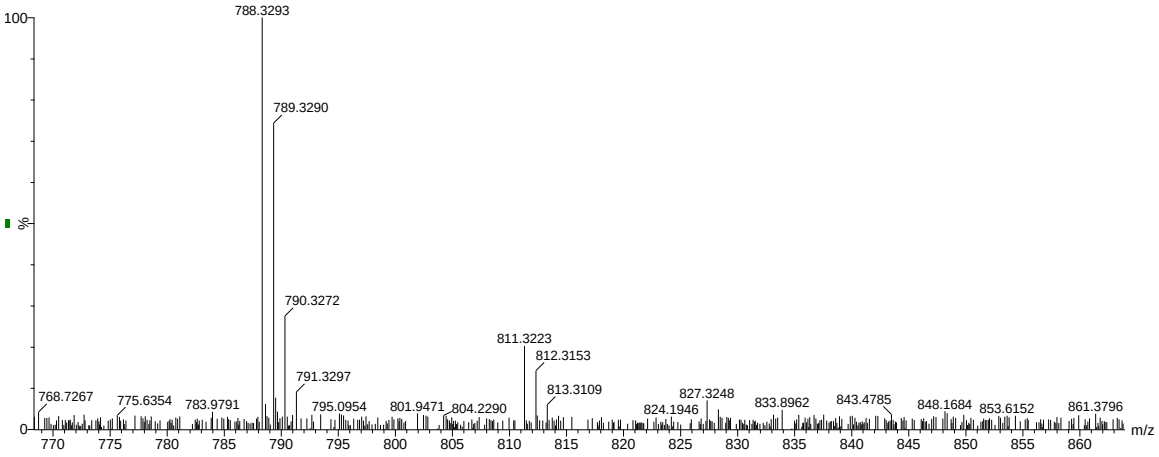

Figure 5-16 Experimental MALDI-TOF Mass spectrum (upper part); mass relevant range for theoretical isotope pattern (middle) and experimental MALDI-TOF-Mass spectrum (lower part) of **10**.

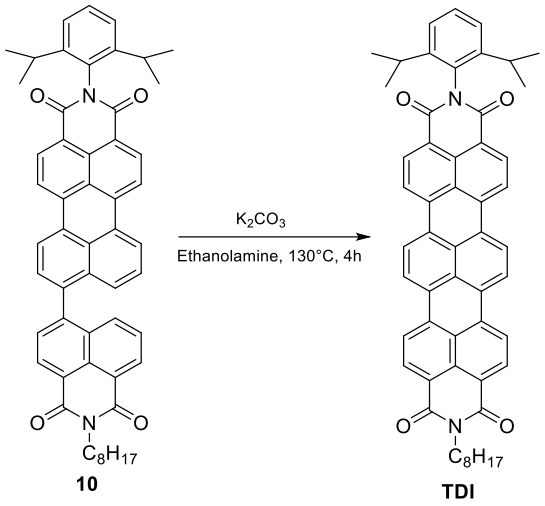

N,N'-(2,6-diisopropylphenyl)-(5-octyl)-terrylen-3,4:11,12-tetracarboxdiimide (TDI). The following reaction was carried out under argon atmosphere according to literature.[51,223] A 10 mL Schlenk tube was charged with 100 mg of terrylene precursor **10** (1.00 eq.) and potassium carbonate (1.02 mg, 58.0 eq.). Afterwards, 1.6 mL of ethanolamine were added and the reaction mixture was heated to 130 °C. The components were dissolved in heat and the color changed from red to blue within a few minutes. After 4 h a complete conversion of the reactants was observed via TLC. Purification of the crude product was conducted by washing the reaction mixture with cold H_2O. The blue precipitate was separated by centrifugation. Afterwards, several washing cycles with MeOH and a 1:2 mixture of DCM and MeOH were conducted until no more orange color was observed (83.8 mg, 84 %). Washing the precipitate several times, is sufficient for purification. Due to poor solubility, only mass spectrometry was used for analytical characterization.

MALDI-TOF-MS of **TDI** m/z: [M^+] calc. for $C_{54}H_{46}N_2O_4$: 786.3458; found: 786.5284.

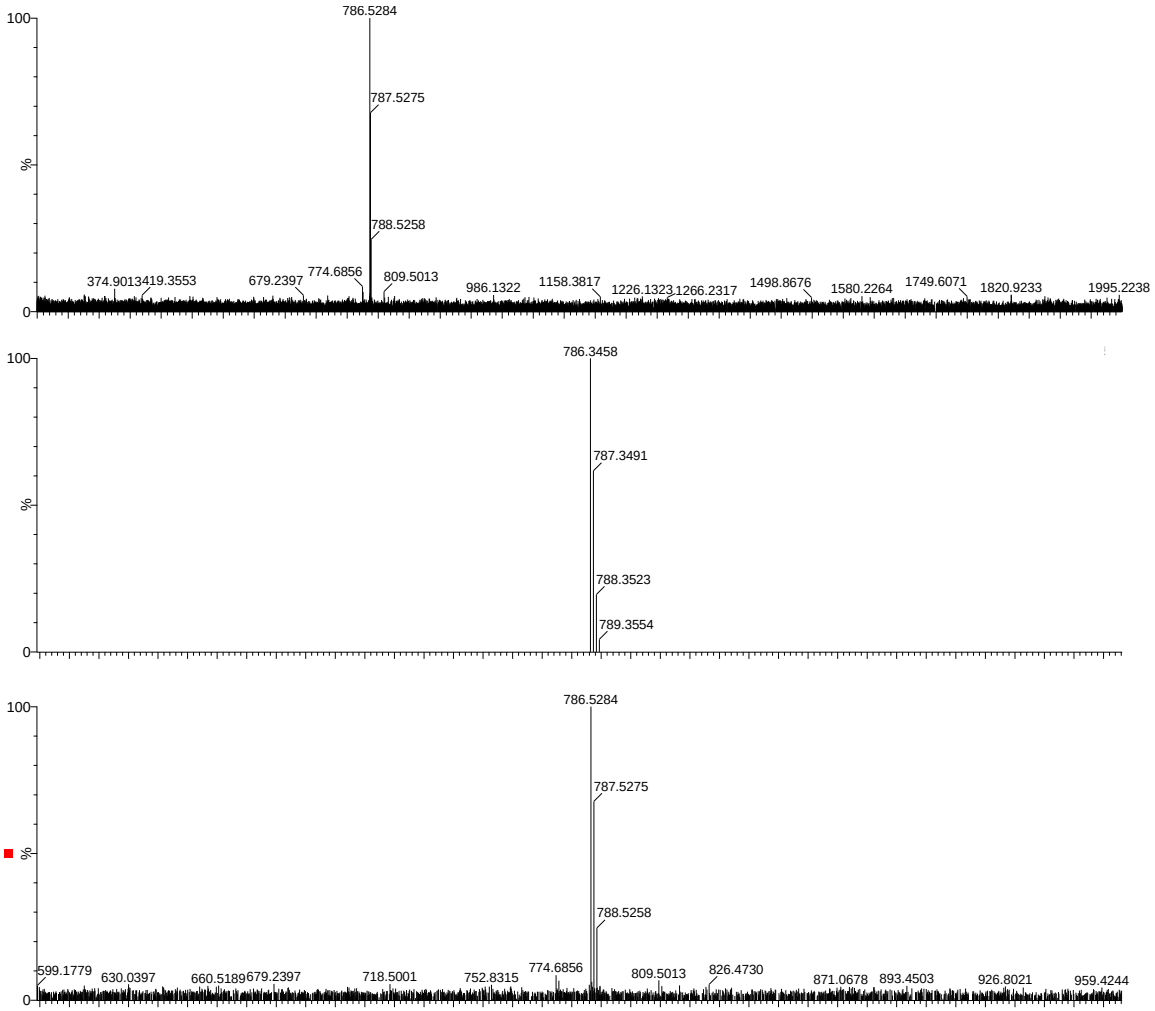

Figure 5-17 Experimental MALDI-TOF Mass spectrum (upper part); mass relevant range for theoretical isotope pattern (middle) and experimental MALDI-TOF-Mass spectrum (lower part) of **TDI.**

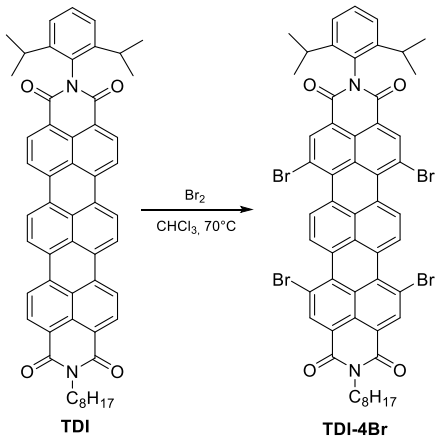

N,N'-(2,6-diisopropylphenyl)-(5-octyl)-1,6,9,13-tetrabromoterrylene-3,4:11,12-tetracarboxdiimide (TDI-4Br). The synthetic pathway was adapted from literature procedure.[58] In a dry 25 mL Schlenk tube, **TDI** (100 mg, 1.00 eq.) was dissolved in 10 mL $CHCl_3$ under argon atmosphere. 0.04 mL bromine (5.00 eq.) were added in one portion. The reaction

mixture was heated to reflux and stirred overnight with exclusion of light. The reaction was allowed to cool down to room temperature. Residual reactive bromine was quenched by addition of saturated Na_2SO_3 solution. The product was extracted with $CHCl_3$, dried over Na_2SO_4 and concentrated under reduced pressure. The resulting blue solid was purified via column chromatography (cyclohexane/DCM; 10/90 (fraction 1); educt at 1 % MeOH) yielding 89.8 mg of **TDI-4Br** (65 %). Resulting mono-, di-, and trisubstituted TDI can be converted to **TDI-4Br** under same reaction conditions due to the fact, that overbromination was not observed so far. ^{1}H NMR (300 MHz, Methylene Chloride-d_2) δ 9.14 (s, 4H), 8.89 (s, 2H), 8.60 (s, 2H), 7.56 (p, J = 9.4, 8.3 Hz, 1H), 7.40 (d, J = 7.8 Hz, 2H), 4.15 (t, J = 7.7 Hz, 2H), 2.88 (hept, J = 7.3 Hz, 2H), 1.75 (q, J = 7.8, 7.4 Hz, 2H), 1.50 – 1.01 (m, 25H).

MALDI-TOF-MS of **TDI-4Br** m/z: [M$^+$] calc. for $C_{54}H_{42}Br_4N_2O_4$: 1101.9847; found: 1102.1965.

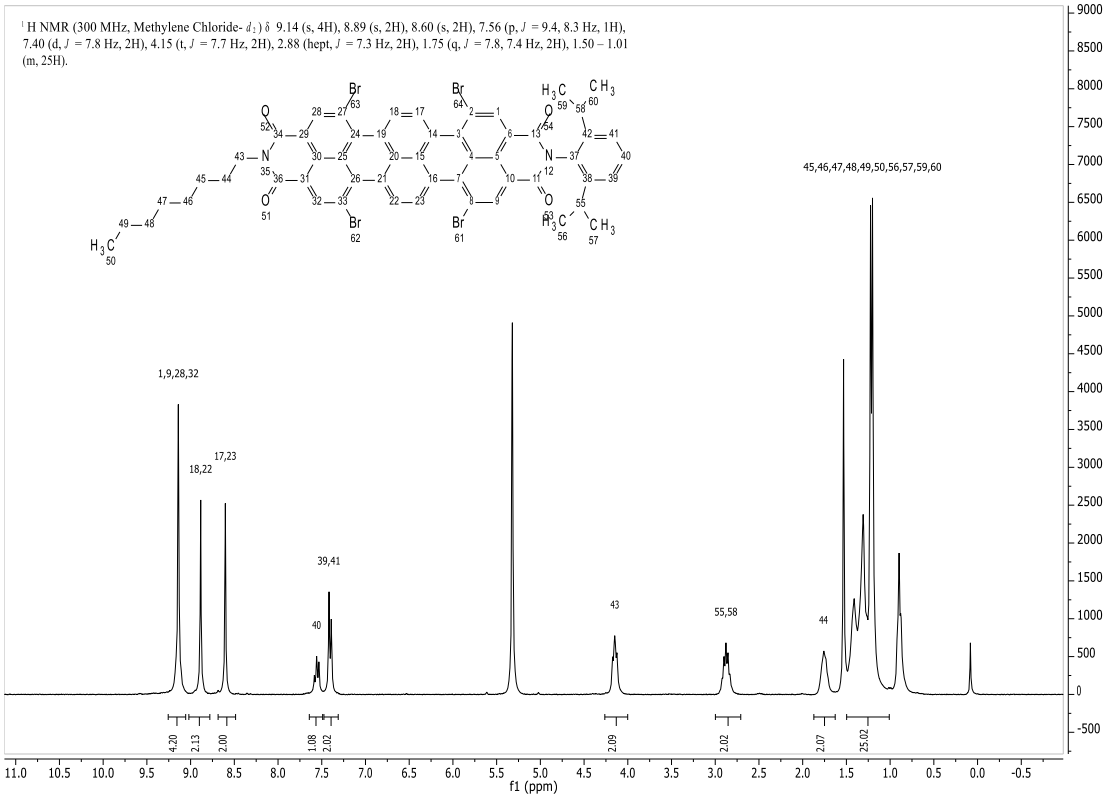

Figure 5-18 ^{1}H-NMR spectrum of **TDI-4Br** in methylene chloride-d_2 at room temperature (300 MHz).

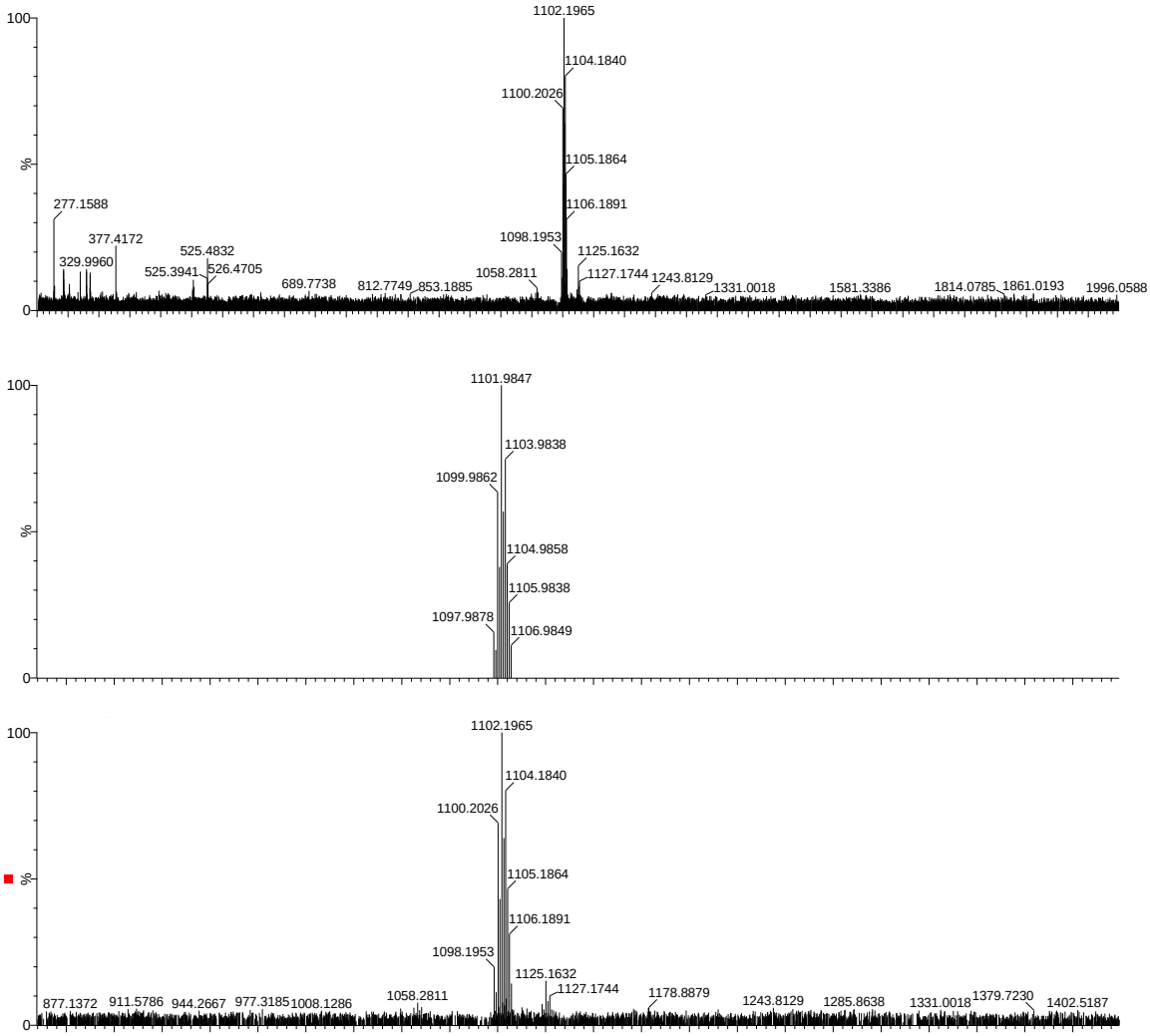

Figure 5-19 Experimental MALDI-TOF Mass spectrum (upper part); mass relevant range for theoretical isotope pattern (middle) and experimental MALDI-TOF-Mass spectrum (lower part) of **TDI-4Br.**

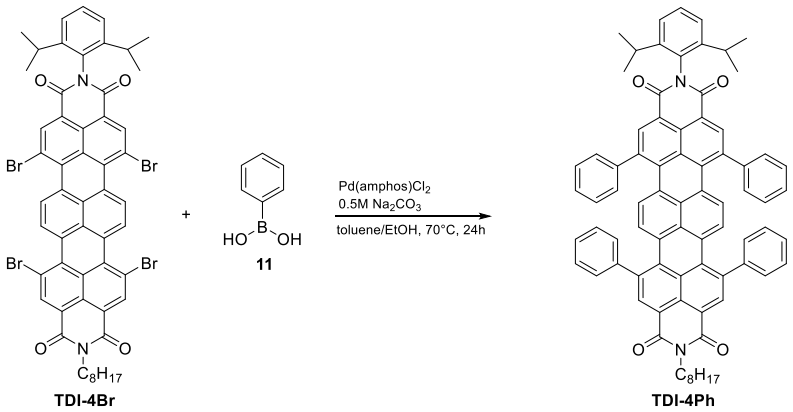

N,N'-(2,6-diisopropylphenyl)-(5-octyl)-1,6,9,13-tetraphenylterrylene-3,4:11,12-tetracarboxdiimide (TDI-4Ph). The synthesis of **TDI-4Ph** was carried out under argon atmosphere according to literature.[54] A 10 mL Schlenk tube was charged with **TDI-4Br** (20.0 mg, 1.00 eq.) and phenylboronic acid **11** (14.4 mg, 6.50 eq.) in 7 mL toluene/EtOH mixture and basic

0.5 M Na_2CO_3 solution (3.00 eq.) was added. In addition, a catalytic amount of Pd(amphos)Cl_2 was added. The reaction mixture was stirred for 24 h at 70 °C. The crude product was extracted using DCM/H_2O and dried over Na_2SO_4. Purification was conducted via column chromatography (cyclohexane/DCM; product: 0.5 % MeOH) yielding a green solid (10.2 mg; 52 %). ^{1}H NMR (300 MHz, Methylene Chloride-d_2) δ 8.49 (d, J = 14.7 Hz, 4H), 7.45 (s, 27H), 4.16 (s, 2H), 2.76 (s, 2H), 1.73 (s, 2H), 1.20 (d, J = 47.9 Hz, 25H).

MALDI-TOF-MS of **TDI-4Ph** m/z: [M$^+$] calc. for $C_{78}H_{62}N_2O_4$: 1090.4709; found: 1090.4076.

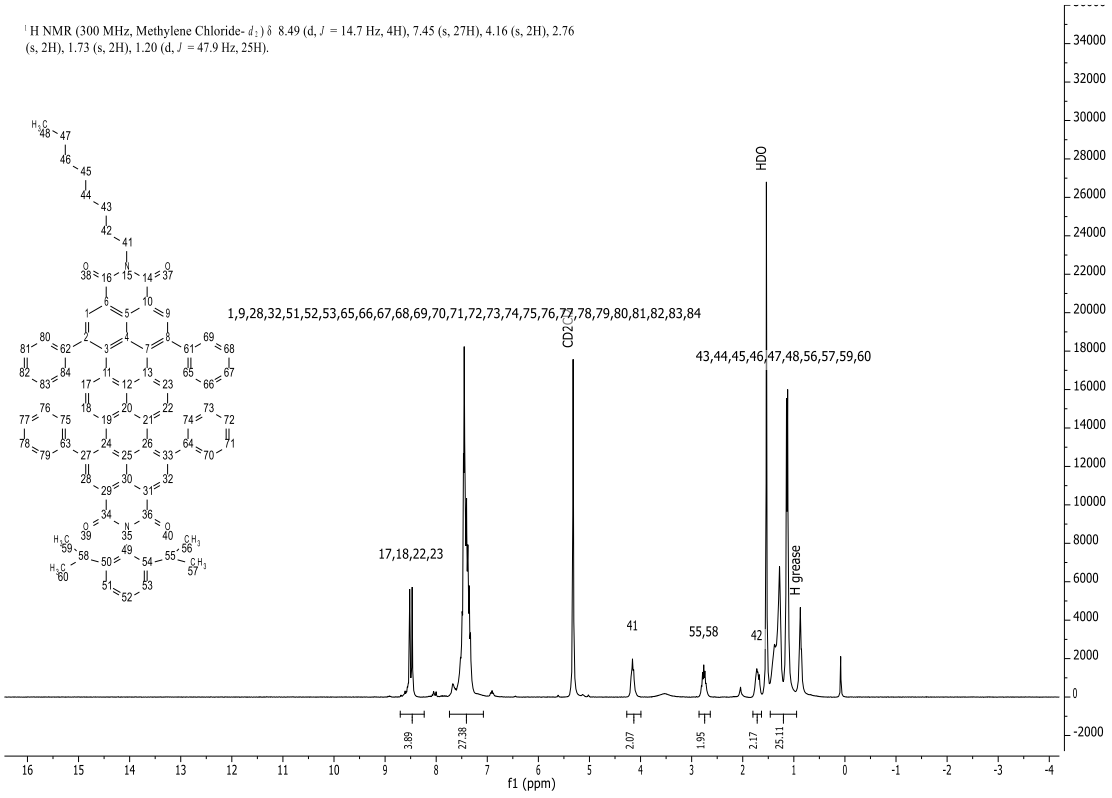

Figure 5-20 ^{1}H-NMR spectrum of **TDI-4Ph** in methylene chloride-d_2 at room temperature (300 MHz).

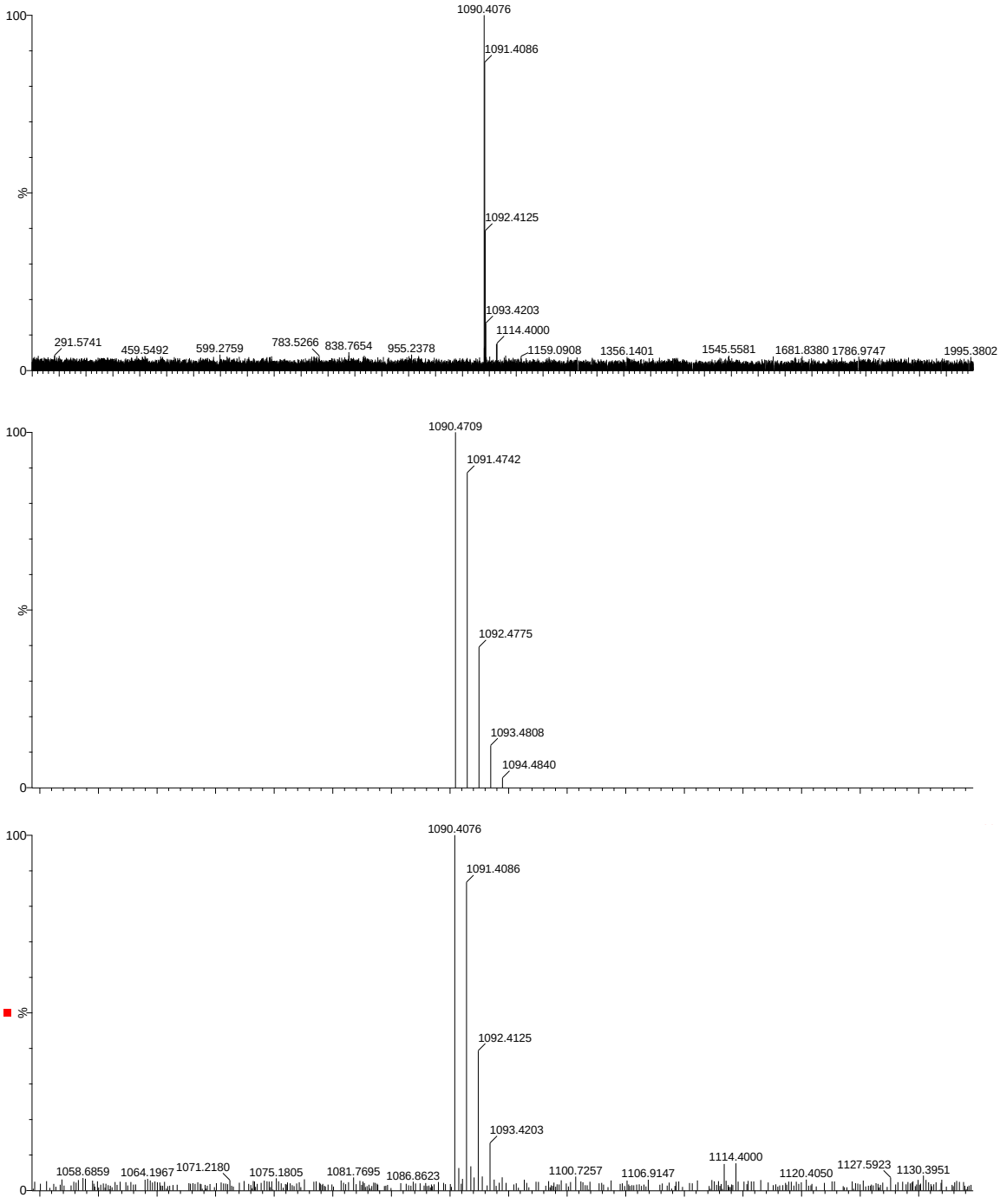

Figure 5-21 Experimental MALDI-TOF Mass spectrum (upper part); mass relevant range for theoretical isotope pattern (middle) and experimental MALDI-TOF-Mass spectrum (lower part) of **TDI-4Ph**.

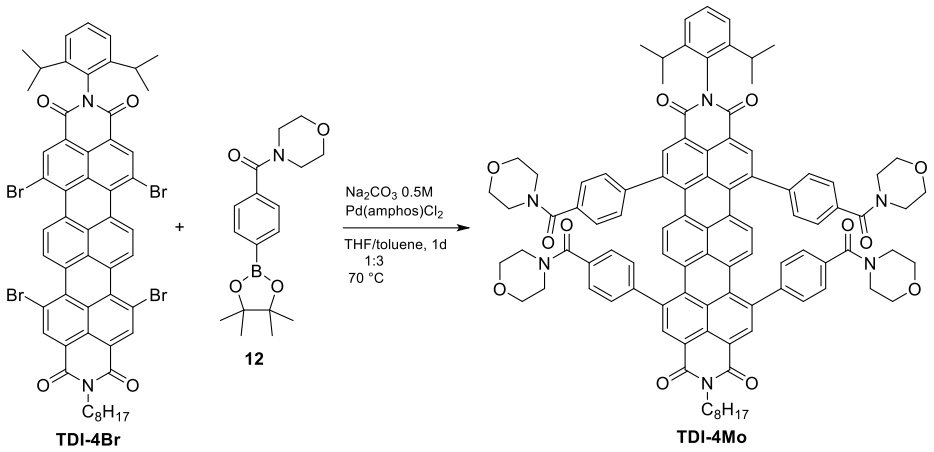

N,N'-(2,6-diisopropylphenyl)-(5-octyl)-1,6,9,13-tetra-4-benzoylmorpholinoterrylene-3,4:11,12-tetracarboxdiimide (TDI-4Mo). 50.1 mg of **TDI-4Br** (1.00eq.) and morpholino(4-(4,4,5,5-tetramethyl-1,3,2-dioxaborolan-2-yl)phenyl)methanone **12** (86.4 mg, 6.00 eq.) were combined in a 15 mL Schlenk tube and dissolved in dry 0.5 mL THF and 2.5 mL toluene under argon atmosphere. Basic 0.5 M Na_2CO_3 solution (3.00 eq.) was added to the reaction mixture and a catalytic amount of catalyst Pd(amphos)Cl_2 was added. The blue solution was heated to 70 °C and stirred for 27 h. The color changed from blue to green. Aqueous work-up was conducted by washing with water and extraction of the product with DCM. The green organic phase was dried over Na_2SO_4 and concentrated under reduced pressure. Separation of the mono-, di-, tri- and tetra substituted compound was performed via column chromatography (cyclohexane/DCM; product: 4 % MeOH; 67 % yield). ^{1}H NMR (300 MHz, Methylene Chloride-d_2) δ 8.75 – 8.33 (m, 3H), 8.09 (h, J = 8.5, 7.8 Hz, 1H), 8.00 – 7.86 (m, 1H), 7.81 – 7.40 (m, 17H), 7.34 (t, J = 7.6 Hz, 2H), 7.08 – 6.82 (m, 2H), 6.74 (d, J = 8.1 Hz, 0H), 4.15 (dt, J = 15.6, 7.3 Hz, 2H), 3.62 (dd, J = 54.3, 27.2 Hz, 30H), 3.00 (s, 1H), 2.75 (td, J = 15.5, 13.9, 8.5 Hz, 2H), 2.01 (d, J = 16.7 Hz, 1H), 1.81 – 1.64 (m, 2H), 1.44 – 1.06 (m, 25H).

MALDI-TOF-MS of **TDI-4Mo** m/z: [MNa$^+$] calc. for $C_{98}H_{90}N_6O_{12}$: 1566.6547; found: 1566.6859.

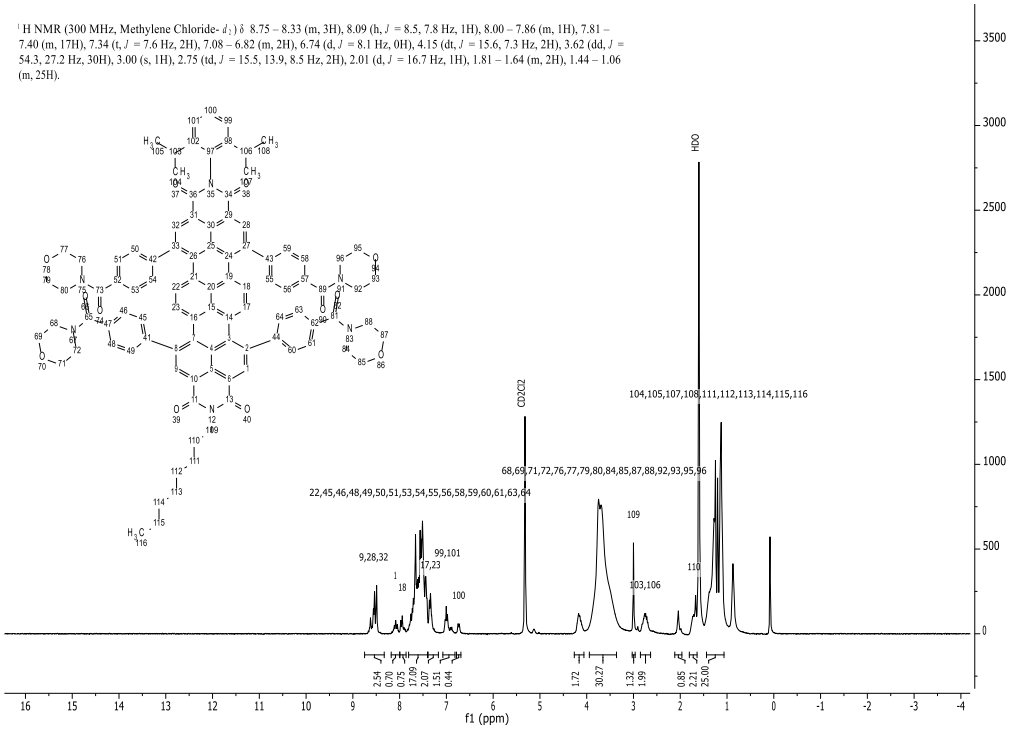

Figure 5-22 ^{1}H-NMR spectrum of **TDI-4Mo** in methylene chloride-d_2 at room temperature (300 MHz).

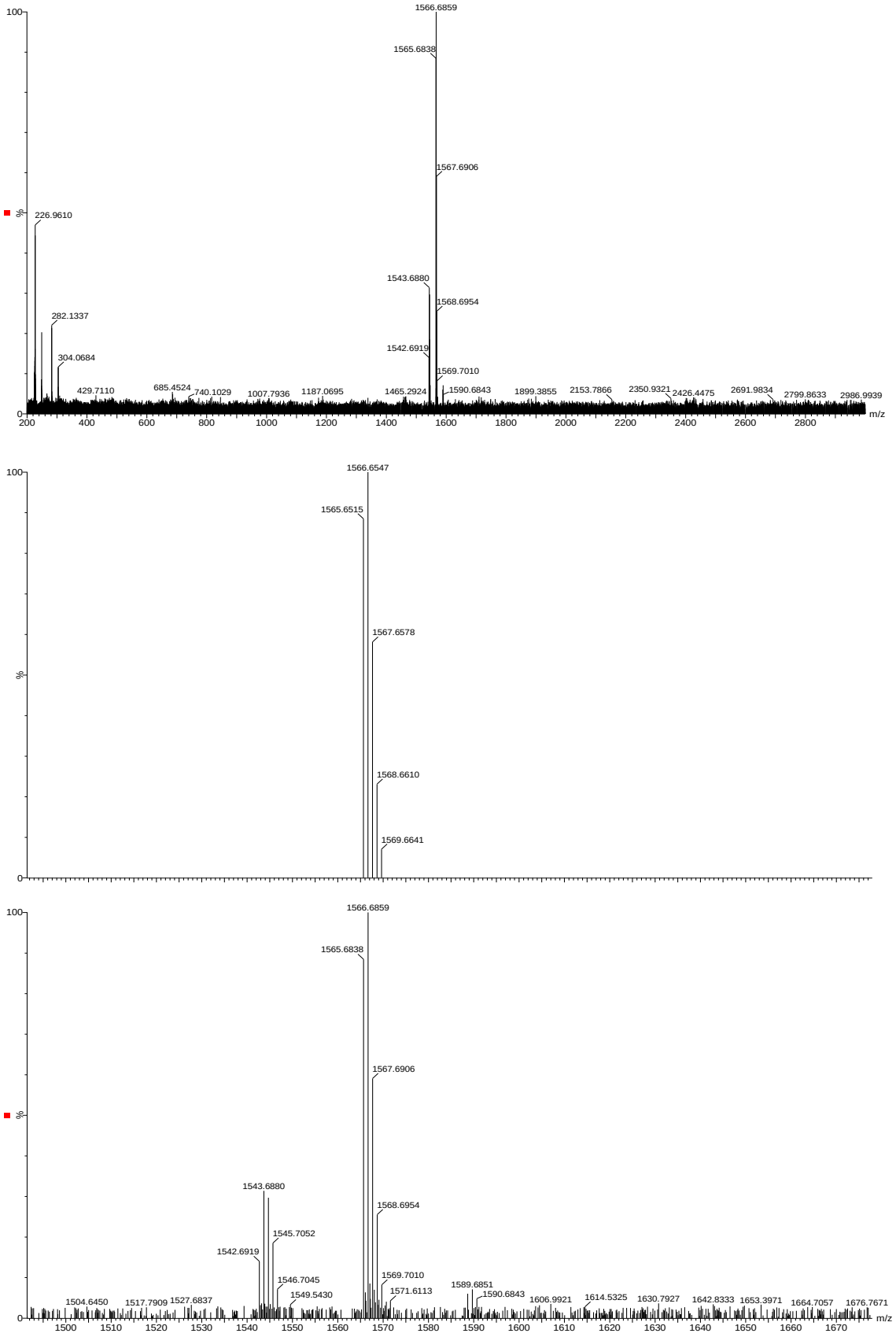

Figure 5-23 Experimental MALDI-TOF Mass spectrum (upper part); mass relevant range for theoretical isotope pattern (middle) and experimental MALDI-TOF-Mass spectrum (lower part) of **TDI-4Mo.**

5.6 Conclusions

In summary, synthesis of terrylene diimide proved to be a challenging and time-consuming task, due to laborious purification procedures, limited yields of various synthetic steps and poor solubility of several compounds. This lowers the accessibility of other terrylene derivatives. In this study we synthesized three bay-substituted terrylene diimide derivatives exhibiting rather high molar absorption coefficients, bright red to far-red fluorescence emission (albeit only in apolar solvents), and extraordinary high photostability. The attempts to introduce pH sensitivity via PET receptors to the terrylene structure in the imide-position or in bay-position were not successful. Recently, Uersfeld et al. reported a simplified method to build up terrylene dyes from naphthalene and perylene units *via* efficient Suzuki/C-H-arylation coupling cascade.[62] The presented synthetic development also allows purification by precipitation and crystallization and accessibility of terrylene monoimides, which may facilitate the synthesis of new dyes even with pH sensitive functionalities and thus, creating a platform for numerous new applications in optical sensors. However, for these applications it must be considered that the fluorescence quantum yields dropped significantly in polar solvents such as ethanol and thus potential pH sensitive dyes may show low brightness in the relevant (rather hydrophilic) matrices.

Acknowledgments

Financial support by the Austrian Academy of Science (ÖAW) at the Institute of Analytical Chemistry and Food Chemistry, Graz University of Technology (DOC-Fellowship of David Pfeifer) is gratefully acknowledged. Matthias Schwar at the Institute of Analytical Chemistry and Food Chemistry is thanked for photostability measurements of dibutoxy-aza-BODIPY.

Part III

Outlook and conclusions

6 Outlook and conclusion

The purpose of the dissertation was to investigate 3 different types of chromophres concerning the synthetic pathways, their photophysical and analyte-recognition properties and last but not least the suitability for applications in optical pH and carbon dioxide sensors. This thesis is focused on investigations including rylene dyes, especially core-extended perylene and terrylene derivatives as well as classical and π-extended BODIPY dyes.

In the first part of this thesis, we introduced a new class of pH indicators based on bay-modified perylene dyes which can be utilized for optical pH sensors as well as for optical carbon dioxide sensors. The indicators, which are accessible via a simple one-step reaction show high luminescence brightness, extraordinary good photostability and versatility in respect to chemical modification. Moreover, the di-substituted perylene shows unique behaviour with two protonation/deprotonation equilibria enabling sensing of carbon dioxide in unprecedentedly broad dynamic range. Due to the results presented in this thesis further design of pH sensors based on 2-phenyl-imidazole substituted perylenes is of high research intereset.

In conclusion of the second part, we prepared a series of new BODIPY pH indicators for application in optical carbon dioxide sensors. All the dyes feature excellent brightness in solution. Photodegradation studies reveal unmatched photostability of the π-extended dyes. The sensors prepared from the dyes based on combination of 3-carboxy-4-hydroxyphenyl receptor and π-extended chromophores show unmatched sensitivity, resolving ambient CO_2 levels which is particularly interesting for environmental applications.

Finally, synthesis of terrylene diimide turned out as a challenging and time-consuming task. The synthesized three bay-substituted terrylene diimide derivatives exhibiting rather high molar absorption coefficients, bright red to far-red fluorescence emission (albeit only in apolar solvents), and extraordinary high photostability. Even though, it was not possible to introduce pH-sensitivity via PET receptors to the terrylene structure in imide-position or in bay-position. In contrast to the two parts based on perylene and BODIPY dyes, terrylene diimides appear no to be promising for applications in pH sensors, at least in the current modification pattern.

Part IV

Appendix

7 Curriculum Vitae

David Pfeifer

Date of Birth	29.09.1990
Address	Schörgelgasse 66, 8010 Graz
Nationality	Austria
E-mail	david.pfeifer.dp@gmail.com

Education

01/2016 - 01/2020	PhD student in Technical Chemistry at Graz University of Technology; Topic: Highly photostable red-emitting pH Indicators for Optical Sensors. Supervisor: Assoc. Prof. kand. Sergey M. Borisov, Co-supervisor: Univ.-Prof. Dipl.-Chem. Dr.rer.nat. Ingo Klimant.
09/2013 - 10/2015	Master program of Technical Chemistry; Graz University of Technology and Karl-Franzens University Graz (NAWI Project). Master thesis: Near-Infrared Indicators and Optical pH Sensors with High Fluorescence Brightness. Supervisors: Univ.-Prof. Dipl.-Chem. Dr.rer.nat. Ingo Klimant & Assoc. Prof. kand. Sergey M. Borisov.
10/2009 - 08/2013	Bachelor program of Chemistry; Graz University of Technology and Karl-Franzens University Graz (NAWI Project), Bachelor thesis: Permethylierte Polycyclische Silane. Supervisor: Prof. Dr. Harald Stüger
09/2000 – 06/2008	A-Level at BG/BRG Oeverseegasse, Graz

International Experience

07/2018	Arkansas Food Industries and Culinary Traditions Summer school, Fayetteville (USA)
07/2015	9th ASCOS Summer school, Porto (Portugal)
01-06/2014	Erasmus at Universidad de Oviedo (Spain)

Grants and Awards

08/2017-07/2020	DOC-fellowship of the Austrian Academy of Science (ÖAW)
11/2019	Distinction of successful inventors of TU Graz
11/2017	Distinction of successful inventors of TU Graz

List of Publications in Peer Reviewed Journals

Pfeifer, D.; Klimant, I. & Borisov, S. M. Ultra-bright Red-Emitting Photostable Perylene Bisimide Dyes: New Indicators for Ratiometric Sensing of High pH or Carbon Dioxide. *Chemistry - A European Journal*, *24*(42), 10711-10720. https://doi.org/10.1002/chem.201800867, **2018**

Pfeifer, D.; Russegger, A.; Klimant, I & Borisov, S. M. Green to red emitting BODIPY dyes for fluorescent sensing and imaging of carbon dioxide, *Sensors and Actuators B: Chemical*. 304, 127312. https://doi.org/10.1016/j.snb.2019.127312, **2020**

Oral Presentations

Pfeifer, D.; Borisov, S. M.; Klimant, I.: Ultra-bright and highly photostable perylene indicator dyes for optical carbon dioxide and pH sensing – 13th ASCS JunganalytikerInnen-Forum, Vienna, **2017**

Poster Presentations

Pfeifer D.; Russegger A.; Klimant I.; Borisov S. M.: Bright fluorescent carbon dioxide sensors on basis of NIR BODIPY dyes – Europt(r)ode XIV, Naples, **2018**

Maierhofer M.; Strobl M.; **Pfeifer D.**; S. M.; Mayr T.; Optical ammonia sensor for continuous bioprocess monitoring – Europt(r)ode XIV, Naples, **2018**

Pfeifer, D.; Borisov, S. M.; Klimant, I.: Near-Infrared-Emitting pH Indicators for Optical pH Sensors – ÖAW Grant ceremony, Vienna, **2017**

Pfeifer, D.; Borisov, S. M.; Klimant, I.: Ultra-Bright Red Emitting Perylene Indicator Dyes for Optical pH Sensors – Europt(r)ode XIII, Graz, **2016**

Haas, M.; Groß, U.; Hasken, B.; **Pfeifer, D.**; Six, B.; Torvisco Gomez, A.; Stüger, H.; Grogger, C.: Separation of Inorganic Isomers via Silica Gel Column. - 15. Österreichische Chemietage. Graz, **2013**

8 References

[1] B. Valeur, Wiley InterScience (Online service), *Molecular Fluorescence Principles and Applications*, Wiley-VCH, New York, **2001**.

[2] J. R. Lakowicz, *Principles of Fluorescence Spectroscopy*, Springer, New York, **2006**.

[3] T. W. J. Gadella, Ed. , *FRET and FLIM Techniques*, Elsevier, Amsterdam ; Boston, **2009**.

[4] G. Orellana, in *Optical Chemical Sensors* (Eds.: F. Baldini, A.N. Chester, J. Homola, S. Martellucci), Springer Netherlands, Dordrecht, **2006**, pp. 99–116.

[5] D. Wencel, T. Abel, C. McDonagh, *Analytical Chemistry* **2014**, *86*, 15.

[6] J. Han, K. Burgess, *Chemical Reviews* **2010**, *110*, 2709.

[7] M. Beija, C. A. M. Afonso, J. M. G. Martinho, *Chem. Soc. Rev.* **2009**, *38*, 2410.

[8] T. Doussineau, S. Trupp, G. J. Mohr, *Journal of Colloid and Interface Science* **2009**, *339*, 266.

[9] O. Wolfbeis, E. Furlinger, H. Kroneis, H. Marsoner, *Fresenius Zeitschrift Fur Analytische Chemie* **1983**, *314*, 119.

[10] A. Mills, S. Hodgen, in *Topics in Fluorescence Spectroscopy* (Eds.: C.D. Geddes, J.R. Lakowicz), Springer US, Boston, MA, **2005**, pp. 119–161.

[11] S. M. Borisov, D. L. Herrod, I. Klimant, *Sensors and Actuators B: Chemical* **2009**, *139*, 52.

[12] C. Staudinger, S. M. Borisov, *Methods and Applications in Fluorescence* **2015**, *3*, 042005.

[13] A. Mishra, R. K. Behera, P. K. Behera, B. K. Mishra, G. B. Behera, *Chem. Rev.* **2000**, *100*, 1973.

[14] W. Sun, S. Guo, C. Hu, J. Fan, X. Peng, *Chem. Rev.* **2016**, *116*, 7768.

[15] F. Würthner, *Chem. Commun.* **2004**, 1564.

[16] T. Weil, T. Vosch, J. Hofkens, K. Peneva, K. Müllen, *Angewandte Chemie International Edition* **2010**, *49*, 9068.

[17] A. Loudet, K. Burgess, *Chemical Reviews* **2007**, *107*, 4891.

[18] G. Ulrich, R. Ziessel, A. Harriman, *Angewandte Chemie International Edition* **2008**, *47*, 1184.

[19] R. Scholl, Chr. Seer, R. Weitzenböck, *Ber. Dtsch. Chem. Ges.* **1910**, *43*, 2202.

[20] E. Clar, *Chem. Ber.* **1948**, *81*, 52.

[21] E. Clar, W. Kelly, R. M. Laird, *Monatshefte für Chemie* **1956**, *87*, 391.

[22] H. Quante, K. Müllen, *Angewandte Chemie International Edition in English* **1995**, *34*, 1323.

[23] F. O. Holtrup, G. R. J. Müller, H. Quante, S. De Feyter, F. C. De Schryver, K. Müllen, *Chemistry - A European Journal* **1997**, *3*, 219.

[24] Y. Avlasevich, S. Müller, P. Erk, K. Müllen, *Chemistry - A European Journal* **2007**, *13*, 6555.

[25] Y. Avlasevich, C. Li, K. Müllen, *Journal of Materials Chemistry* **2010**, *20*, 3814.

[26] L. Zang, Y. Che, J. S. Moore, *Acc. Chem. Res.* **2008**, *41*, 1596.

[27] T.-L. Chiu, K.-H. Chuang, C.-F. Lin, Y.-H. Ho, J.-H. Lee, C.-C. Chao, M.-K. Leung, D.-H. Wan, C.-Y. Li, H.-L. Chen, *Thin Solid Films* **2009**, *517*, 3712.

[28] J. Fortage, M. Séverac, C. Houarner-Rassin, Y. Pellegrin, E. Blart, F. Odobel, *Journal of Photochemistry and Photobiology A: Chemistry* **2008**, *197*, 156.

[29] S. Schols, S. Verlaak, C. Rolin, D. Cheyns, J. Genoe, P. Heremans, *Advanced functional materials* **2008**, *18*, 136.

[30] P. Tinnefeld, K. D. Weston, T. Vosch, M. Cotlet, T. Weil, J. Hofkens, K. Müllen, F. C. De Schryver, M. Sauer, *J. Am. Chem. Soc.* **2002**, *124*, 14310.

[31] A. Rademacher, S. Märkle, H. Langhals, *Chemische Berichte* **1982**, *115*, 2927.

[32] K. Peneva, G. Mihov, F. Nolde, S. Rocha, J. Hotta, K. Braeckmans, J. Hofkens, H. Uji-i, A. Herrmann, K. Müllen, *Angew. Chem. Int. Ed.* **2008**, *47*, 3372.

[33] Y. Zhang, Z. Zhao, X. Huang, Y. Xie, C. Liu, J. Li, X. Guan, K. Zhang, C. Cheng, Y. Xiao, *RSC Advances* **2012**, *2*, 12644.

[34] W. Fan, N. Liang, D. Meng, J. Feng, Y. Li, J. Hou, Z. Wang, *Chem. Commun.* **2016**, *52*, 11500.

[35] Z. Chen, A. Lohr, C. R. Saha-Möller, F. Würthner, *Chem. Soc. Rev.* **2009**, *38*, 564.

[36] D. Aigner, S. A. Freunberger, M. Wilkening, R. Saf, S. M. Borisov, I. Klimant, *Analytical Chemistry* **2014**, *86*, 9293.

[37] H. Langhals, J. Karolin, L. B.-Å. Johansson, *Journal of the Chemical Society, Faraday Transactions* **1998**, *94*, 2919.

[38] C. Kohl, T. Weil, J. Qu, K. Müllen, *Chemistry - A European Journal* **2004**, *10*, 5297.

[39] H. Langhals, R. Ismael, O. Yürük, *Tetrahedron* **2000**, *56*, 5435.

[40] J. Qu, C. Kohl, M. Pottek, K. Müllen, *Angewandte Chemie* **2004**, *116*, 1554.

[41] D. Aigner, S. M. Borisov, I. Klimant, *Analytical and Bioanalytical Chemistry* **2011**, *400*, 2475.

[42] D. Aigner, S. M. Borisov, P. Petritsch, I. Klimant, *Chemical Communications* **2013**, *49*, 2139.

[43] F. Würthner, C. Thalacker, S. Diele, C. Tschierske, *Chemistry – A European Journal* **2001**, *7*, 2245.

[44] R. Gvishi, R. Reisfeld, Z. Burshtein, *Chemical Physics Letters* **1993**, *213*, 338.

[45] A. S. Lukas, Y. Zhao, S. E. Miller, M. R. Wasielewski, *J. Phys. Chem. B* **2002**, *106*, 1299.

[46] Y. Avlasevich, K. Müllen, *Chem. Commun.* **2006**, 4440.

[47] H. G. Löhmannsröben, H. Langhals, *Appl. Phys. B* **1989**, *48*, 449.

[48] F. Würthner, V. Stepanenko, Z. Chen, C. R. Saha-Möller, N. Kocher, D. Stalke, *The Journal of Organic Chemistry* **2004**, *69*, 7933.

[49] H. Langhals, A. J. Esterbauer, S. Kinzel, *New Journal of Chemistry* **2009**, *33*, 1829.

[50] D. Aigner, R. I. Dmitriev, S. M. Borisov, D. B. Papkovsky, I. Klimant, *J. Mater. Chem. B* **2014**, *2*, 6792.

[51] F. Nolde, J. Qu, C. Kohl, N. G. Pschirer, E. Reuther, K. Müllen, *Chemistry - A European Journal* **2005**, *11*, 3959.

[52] C. S. Fischer, C. Jenewein, S. Mecking, *Macromolecules* **2015**, *48*, 483.

[53] M. Berberich, F. Würthner, *Chemical Science* **2012**, *3*, 2771.

[54] N. Liang, K. Sun, J. Feng, Y. Chen, D. Meng, W. Jiang, Y. Li, J. Hou, Z. Wang, *Journal of Materials Chemistry A* **2018**, *6*, 18808.

[55] R. Gronheid, J. Hofkens, F. Köhn, T. Weil, E. Reuther, K. Müllen, F. C. De Schryver, *J. Am. Chem. Soc.* **2002**, *124*, 2418.

[56] G. Schweitzer, R. Gronheid, S. Jordens, M. Lor, G. De Belder, T. Weil, E. Reuther, K. Müllen, F. C. De Schryver, *J. Phys. Chem. A* **2003**, *107*, 3199.

[57] P. Schlichting, B. Duchscherer, G. Seisenberger, T. Basché, C. Bräuchle, K. Müllen, *Chemistry–A European Journal* **1999**, *5*, 2388.

[58] T. Weil, E. Reuther, C. Beer, K. Müllen, *Chemistry – A European Journal* **2004**, *10*, 1398.

[59] T. Sakamoto, C. Pac, *J. Org. Chem.* **2001**, *66*, 94.

[60] T. Ishiyama, M. Murata, N. Miyaura, *J. Org. Chem.* **1995**, *60*, 7508.

[61] Norio. Miyaura, Akira. Suzuki, *Chem. Rev.* **1995**, *95*, 2457.

[62] D. Uersfeld, S. Stappert, C. Li, K. Müllen, *Advanced Synthesis & Catalysis* **2017**, *359*, 4184.

[63] A. Treibs, F.-H. Kreuzer, *Justus Liebigs Annalen der Chemie* **1968**, *718*, 208.

[64] N. Boens, V. Leen, W. Dehaen, *Chem. Soc. Rev.* **2012**, *41*, 1130.

[65] R. P. Haugland, The Handbook: A Guide to Fluorescent Probes and Labeling Technologies, Univerza v Ljubljani, Fakulteta za farmacijo, **2005**.

[66] H. Lu, J. Mack, Y. Yang, Z. Shen, *Chem. Soc. Rev.* **2014**, *43*, 4778.

[67] T. Kowada, H. Maeda, K. Kikuchi, *Chemical Society Reviews* **2015**, *44*, 4953.

[68] K. Umezawa, D. Citterio, K. Suzuki, *Analytical Sciences* **2014**, *30*, 327.

[69] K. Umezawa, Y. Nakamura, H. Makino, D. Citterio, K. Suzuki, *J. Am. Chem. Soc.* **2008**, *130*, 1550.

[70] K. Rurack, M. Kollmannsberger, J. Daub, *New Journal of Chemistry* **2001**, *25*, 289.

[71] E. Deniz, G. C. Isbasar, Ö. A. Bozdemir, L. T. Yildirim, A. Siemiarczuk, E. U. Akkaya, *Org. Lett.* **2008**, *10*, 3401.

[72] T. Kowada, S. Yamaguchi, K. Ohe, *Organic letters* **2009**, *12*, 296.

[73] T. Kowada, S. Yamaguchi, H. Fujinaga, K. Ohe, *Tetrahedron* **2011**, *67*, 3105.

[74] T. Rappitsch, I. Klimant, S. M. Borisov, *Dyes and Pigments* **2019**, 108037.

[75] J. Killoran, L. Allen, J. F. Gallagher, W. M. Gallagher, F. O. Donal, *Chemical Communications* **2002**, 1862.

[76] A. Loudet, R. Bandichhor, L. Wu, K. Burgess, *Tetrahedron* **2008**, *64*, 3642.

[77] T. Werner, C. Huber, S. Heinl, M. Kollmannsberger, J. Daub, O. S. Wolfbeis, *Fresenius J Anal Chem* **1997**, *359*, 150.

[78] T. Gareis, C. Huber, O. S. Wolfbeis, J. Daub, *Chemical Communications* **1997**, *0*, 1717.

[79] M. Hecht, W. Kraus, K. Rurack, *The Analyst* **2013**, *138*, 325.

[80] K. Cammann, E. Guibault, H. Hall, R. Kellner, O. Wolfbeis, **1996**.

[81] P. Gründler, *Chemical Sensors: An Introduction for Scientists and Engineers*, Springer, Berlin ; New York, **2007**.

[82] C. McDonagh, C. S. Burke, B. D. MacCraith, *Chemical Reviews* **2008**, *108*, 400.

[83] S. Nagl, O. S. Wolfbeis, *The Analyst* **2007**, *132*, 507.

[84] G. Orellana, D. Haigh, *Current Analytical Chemistry* **2008**, *4*, 273.

[85] M. Schäferling, *Angewandte Chemie International Edition* **2012**, *51*, 3532.

[86] O. S. Wolfbeis, *Journal of Materials Chemistry* **2005**, *15*, 2657.

[87] J. Lin, *TrAC Trends in Analytical Chemistry* **2000**, *19*, 541.

[88] M. Strobl, T. Rappitsch, S. M. Borisov, T. Mayr, I. Klimant, *Analyst* **2015**, *140*, 7150.

[89] J. Qi, D. Liu, X. Liu, S. Guan, F. Shi, H. Chang, H. He, G. Yang, *Analytical Chemistry* **2015**, *87*, 5897.

[90] G. J. Mohr, O. S. Wolfbeis, *Analytica Chimica Acta* **1994**, *292*, 41.

[91] G. Mohr, H. Müller, B. Bussemer, A. Stark, T. Carofiglio, S. Trupp, R. Heuermann, T. Henkel, D. Escudero, L. González, *Analytical and Bioanalytical Chemistry* **2008**, *392*, 1411.

[92] I. Klimant, C. Huber, G. Liebsch, G. Neurauter, A. Stangelmayer, O. S. Wolfbeis, in *New Trends in Fluorescence Spectroscopy* (Eds.: P.B. Valeur, D.J.-C. Brochon), Springer Berlin Heidelberg, **2001**, pp. 257–274.

[93] J. E. Whitaker, R. P. Haugland, F. G. Prendergast, *Analytical Biochemistry* **1991**, *194*, 330.

[94] Z. Xu, A. Rollins, R. Alcala, R. E. Marchant, *Journal of Biomedical Materials Research* **1998**, *39*, 9.

[95] N. Klonis, W. H. Sawyer, *J Fluoresc* **1996**, *6*, 147.

[96] C. R. Schröder, B. M. Weidgans, I. Klimant, *Analyst* **2005**, *130*, 907.

[97] M. Cajlakovic, A. Lobnik, T. Werner, *Analytica Chimica Acta* **2002**, *455*, 207.

[98] M. M. Martin, L. Lindqvist, *Journal of Luminescence* **1975**, *10*, 381.

[99] H. Offenbacher, O. S. Wolfbeis, E. Fürlinger, *Sensors and Actuators* **1986**, *9*, 73.

[100] Z.-Z. Li, C.-G. Niu, G.-M. Zeng, Y.-G. Liu, P.-F. Gao, G.-H. Huang, Y.-A. Mao, *Sensors and Actuators B: Chemical* **2006**, *114*, 308.

[101] C.-G. Niu, G.-M. Zeng, L.-X. Chen, G.-L. Shen, R.-Q. Yu, *Analyst* **2004**, *129*, 20.

[102] G. J. Mohr, *Sensors and Actuators B: Chemical* **2018**, *275*, 439.

[103] A. P. de Silva, H. Q. N. Gunaratne, J.-L. Habib-Jiwan, C. P. McCoy, T. E. Rice, J.-P. Soumillion, *Angewandte Chemie International Edition in English* **1995**, *34*, 1728.

[104] I. Grabchev, X. Qian, Y. Xiao, R. Zhang, *New Journal of Chemistry* **2002**, *26*, 920.

[105] O. S. Wolfbeis, H. Marhold, *Chemische Berichte* **1985**, *118*, 3664.

[106] O. S. Wolfbeis, E. Koller, P. Hoghmuth, *Bulletin of the Chemical Society of Japan* **1985**, *58*, 731.

[107] Z. Zhujun, W. R. Seitz, *Analytica Chimica Acta* **1984**, *160*, 305.

[108] S. Hulth, R. C. Aller, P. Engström, E. Selander, *Limnology and Oceanography* **2002**, *47*, 212.

[109] S. G. Schulman, Shangxian Chen, F. Bai, M. J. P. Leiner, L. Weis, O. S. Wolfbeis, *Analytica Chimica Acta* **1995**, *304*, 165.

[110] A. Lobnik, I. Oehme, I. Murkovic, O. S. Wolfbeis, *Analytica Chimica Acta* **1998**, *367*, 159.

[111] A. Burns, H. Ow, U. Wiesner, *Chemical Society Reviews* **2006**, *35*, 1028.

[112] O. S. Wolfbeis, B. M. Weidgans, in *Optical Chemical Sensors* (Eds.: F. Baldini, A.N. Chester, J. Homola, S. Martellucci), Springer Netherlands, Dordrecht, **2006**, pp. 17–44.

[113] Y. Tian, F. Su, W. Weber, V. Nandakumar, B. R. Shumway, Y. Jin, X. Zhou, M. R. Holl, R. H. Johnson, D. R. Meldrum, *Biomaterials* **n.d.**, *In Press, Corrected Proof*, DOI: 10.1016/j.biomaterials.2010.06.023.

[114] R. P. Haugland, The Molecular Probes® Handbook, http://www.lifetechnologies.com/at/en/home/references/molecular-probes-the-handbook.html, accessed: Nov., 2013.

[115] S. A. Vinogradov, D. F. Wilson, *Chemistry – A European Journal* **2000**, *6*, 2456.

[116] J. Zhang, M. Yang, C. Li, N. Dorh, F. Xie, F.-T. Luo, A. Tiwari, H. Liu, *Journal of Materials Chemistry B* **2015**, *3*, 2173.

[117] T. Jokic, S. M. Borisov, R. Saf, D. A. Nielsen, M. Kühl, I. Klimant, *Analytical Chemistry* **2012**, *84*, 6723.

[118] M. Y. Berezin, K. Guo, W. Akers, R. E. Northdurft, J. P. Culver, B. Teng, O. Vasalatiy, K. Barbacow, A. Gandjbakhche, G. L. Griffiths, S. Achilefu, *Biophysical Journal* **2011**, *100*, 2063.

[119] T. Myochin, K. Kiyose, K. Hanaoka, H. Kojima, T. Terai, T. Nagano, *J. Am. Chem. Soc.* **2011**, *133*, 3401.

[120] K. Umezawa, A. Matsui, Y. Nakamura, D. Citterio, K. Suzuki, *Chemistry - A European Journal* **2009**, *15*, 1096.

[121] G. M. Fischer, A. P. Ehlers, A. Zumbusch, E. Daltrozzo, *Angewandte Chemie International Edition* **2007**, *46*, 3750.

[122] X. Wan, D. Wang, S. Liu, *Langmuir* **2010**, *26*, 15574.

[123] D. Jacquemin, E. A. Perpète, G. Scalmani, I. Ciofini, C. Peltier, C. Adamo, *Chemical Physics* **2010**, *372*, 61.

[124] Y. Tian, F. Su, W. Weber, V. Nandakumar, B. R. Shumway, Y. Jin, X. Zhou, M. R. Holl, R. H. Johnson, D. R. Meldrum, *Biomaterials* **2010**, *31*, 7411.

[125] S. Thyagarajan, T. Leiding, S. P. Årsköld, A. V. Cheprakov, S. A. Vinogradov, *Inorg. Chem.* **2010**, *49*, 9909.

[126] Y. Li, Y. Wang, S. Yang, Y. Zhao, L. Yuan, J. Zheng, R. Yang, *Analytical Chemistry* **2015**, *87*, 2495.

[127] L. He, W. Lin, Q. Xu, H. Wei, *ACS Applied Materials & Interfaces* **2014**, *6*, 22326.

[128] Y. Ni, J. Wu, *Organic & Biomolecular Chemistry* **2014**, *12*, 3774.

[129] R. Gotor, P. Ashokkumar, M. Hecht, K. Keil, K. Rurack, *Analytical Chemistry* **2017**, *89*, 8437.

[130] J. Killoran, S. O. McDonnell, J. F. Gallagher, D. F. O'Shea, *New J. Chem.* **2008**, *32*, 483.

[131] S. O. McDonnell, D. F. O'Shea, *Org. Lett.* **2006**, *8*, 3493.

[132] M. M. Salim, E. A. Owens, T. Gao, J. Heon Lee, H. Hyun, H. Soo Choi, M. Henary, *Analyst* **2014**, *139*, 4862.

[133] J. Murtagh, D. O. Frimannsson, D. F. O'Shea, *Organic Letters* **2009**, *11*, 5386.

[134] C. Staudinger, J. Breininger, I. Klimant, S. M. Borisov, *Analyst* **2019**, *144*, 2393.

[135] D. Ekeberg, G. Ogner, M. Fongen, E. J. Joner, T. Wickstrøm, *Journal of Environmental Monitoring* **2004**, *6*, 621.

[136] J. W. Severinghaus, A. F. Bradley, *Journal of Applied Physiology* **1958**, *13*, 515.

[137] J. Zosel, W. Oelßner, M. Decker, G. Gerlach, U. Guth, *Measurement Science and Technology* **2011**, *22*, 072001.

[138] X.-D. Wang, O. S. Wolfbeis, *Anal. Chem.* **2013**, *85*, 487.

[139] J. Hodgkinson, R. P. Tatam, *Measurement Science and Technology* **2013**, *24*, 012004.

[140] J. Hodgkinson, R. Smith, W. O. Ho, J. R. Saffell, R. P. Tatam, *Sensors and Actuators B: Chemical* **2013**, *186*, 580.

[141] A. Mills, Q. Chang, *Analytica Chimica Acta* **1994**, *285*, 113.

[142] R. N. Dansby-Sparks, J. Jin, S. J. Mechery, U. Sampathkumaran, T. W. Owen, B. D. Yu, K. Goswami, K. Hong, J. Grant, Z.-L. Xue, *Analytical Chemistry* **2010**, *82*, 593.

[143] M. Uttamlal, D. R. Walt, *Nat Biotech* **1995**, *13*, 597.

[144] C. Munkholm, *Talanta* **1988**, *35*, 109.

[145] D. Nivens, *Talanta* **2002**, *58*, 543.

[146] X. Ge, Y. Kostov, G. Rao, *Biosensors and Bioelectronics* **2003**, *18*, 857.

[147] S. M. Borisov, C. Krause, S. Arain, O. S. Wolfbeis, *Adv. Mater.* **2006**, *18*, 1511.

[148] O. S. Wolfbeis, B. Kovács, K. Goswami, S. M. Klainer, *Mikrochim Acta* **1998**, *129*, 181.

[149] M. D. Fernández-Ramos, M. L. Aguayo-López, E. de los Reyes-Berbel, F. Santoyo-González, L. F. Capitán-Vallvey, *Analyst* **2019**, *144*, 3870.

[150] S. Schutting, T. Jokic, M. Strobl, S. M. Borisov, D. de Beer, Ingo. Klimant, *J. Mater. Chem. C* **2015**, *3*, 5474.

[151] E. Fritzsche, P. Gruber, S. Schutting, J. P. Fischer, M. Strobl, J. D. Müller, S. M. Borisov, I. Klimant, *Analytical Methods* **2017**, *9*, 55.

[152] L. Lochman, P. Zimcik, I. Klimant, V. Novakova, S. M. Borisov, *Sensors and Actuators B: Chemical* **2017**, *246*, 1100.

[153] S. Schutting, S. M. Borisov, I. Klimant, *Analytical Chemistry* **2013**, *85*, 3271.

[154] M. L. Aguayo-López, L. F. Capitán-Vallvey, M. D. Fernández-Ramos, *Talanta* **2014**, *126*, 196.

[155] N. B. Borchert, J. P. Kerry, D. B. Papkovsky, *Sensors and Actuators B: Chemical* **2013**, *176*, 157.

[156] A. Mills, Q. Chang, *Analyst* **1993**, *118*, 839.

[157] A. Mills, A. Lepre, L. Wild, *Sensors and Actuators B: Chemical* **1997**, *39*, 419.

[158] A. Mills, L. Monaf, *The Analyst* **1996**, *121*, 535.

[159] A. Mills, D. Yusufu, *The Analyst* **2016**, *141*, 999.

[160] C. Malins, B. D. MacCraith, *The Analyst* **1998**, *123*, 2373.

[161] A. Mills, Q. Chang, *The Analyst* **1993**, *118*, 839.

[162] B. H. Weigl, A. Holobar, N. V. Rodriguez, O. S. Wolfbeis, *Analytica Chimica Acta* **1993**, *282*, 335.

[163] Andrew. Mills, Qing. Chang, Neil. McMurray, *Analytical Chemistry* **1992**, *64*, 1383.

[164] E. Fritzsche, C. Staudinger, J. P. Fischer, R. Thar, H. W. Jannasch, J. N. Plant, M. Blum, G. Massion, H. Thomas, J. Hoech, K. S. Johnson, S. M. Borisov, I. Klimant, *Marine Chemistry* **2018**, *207*, 63.

[165] C. Staudinger, M. Strobl, J. P. Fischer, R. Thar, T. Mayr, D. Aigner, B. J. Müller, B. Müller, P. Lehner, G. Mistlberger, E. Fritzsche, J. Ehgartner, P. W. Zach, J. S. Clarke, F. Geißler, A. Mutzberg, J. D. Müller, E. P. Achterberg, S. M. Borisov, I. Klimant, *Limnology and Oceanography: Methods* **2018**, *16*, 459.

[166] J. Sipior, L. Randers-Eichhorn, J. R. Lakowicz, G. M. Carter, G. Rao, *Biotechnology Progress* **1996**, *12*, 266.

[167] J. W. Severinghaus, *Annals of the New York Academy of Sciences* **1968**, *148*, 115.

[168] J. M. Cook, R. L. Karelitz, D. E. Dalsis, *Journal of Chromatographic Science* **1985**, *23*, 57.

[169] P. Puligundla, J. Jung, S. Ko, *Food Control* **2012**, *25*, 328.

[170] C. von Bültzingslöwen, A. K. McEvoy, C. McDonagh, B. D. MacCraith, I. Klimant, C. Krause, O. S. Wolfbeis, *The Analyst* **2002**, *127*, 1478.

[171] M. Aresta, *Carbon Dioxide Recovery and Utilization*, Springer Science & Business Media, **2013**.

[172] H. Langhals, A. J. Esterbauer, S. Kinzel, *New J. Chem.* **2009**, *33*, 1829.

[173] X. Wang, R. J. Meier, C. Schmittlein, S. Schreml, M. Schäferling, O. S. Wolfbeis, *Sensors and Actuators B: Chemical* **2015**, *221*, 37.

[174] A. S. Jeevarajan, S. Vani, T. D. Taylor, M. M. Anderson, *Biotechnology and Bioengineering* **2002**, *78*, 467.

[175] G. T. John, D. Goelling, I. Klimant, H. Schneider, E. Heinzle, *Journal of Dairy Research* **2003**, *70*, 327.

[176] M. Kühl, in *Methods in Enzymology*, Elsevier, **2005**, pp. 166–199.

[177] M. Larsen, S. M. Borisov, B. Grunwald, I. Klimant, R. N. Glud, *Limnology and Oceanography: Methods* **2011**, *9*, 348.

[178] M. J. P. Leiner, *Analytica Chimica Acta* **1991**, *255*, 209.

[179] R. Narayanaswamy, O. S. Wolfbeis, *Optical Sensors: Industrial, Environmental and Diagnostic Applications*, Springer Science & Business Media, **2004**.

[180] R. J. Meier, S. Schreml, X. Wang, M. Landthaler, P. Babilas, O. S. Wolfbeis, *Angewandte Chemie International Edition* **2011**, *50*, 10893.

[181] D. Willoughby, R. C. Thomas, C. J. Schwiening, *Pflügers Arch* **1998**, *436*, 615.

[182] H. R. Kermis, Y. Kostov, G. Rao, *The Analyst* **2003**, *128*, 1181.

[183] Q. Wan, S. Chen, W. Shi, L. Li, H. Ma, *Angewandte Chemie* **2014**, *126*, 11096.

[184] S. Charier, O. Ruel, J.-B. Baudin, D. Alcor, J.-F. Allemand, A. Meglio, L. Jullien, *Angewandte Chemie International Edition* **2004**, *43*, 4785.

[185] W. Niu, L. Fan, M. Nan, Z. Li, D. Lu, M. S. Wong, S. Shuang, C. Dong, *Analytical Chemistry* **2015**, *87*, 2788.

[186] X.-D. Liu, Y. Xu, R. Sun, Y.-J. Xu, J.-M. Lu, J.-F. Ge, *The Analyst* **2013**, *138*, 6542.

[187] G. Seybold, *Dyes and Pigments* **1989**, *11*, 303.

[188] G. Schnurpfeil, *Dyes and Pigments* **1995**, *27*, 339.

[189] D. Baumstark, H.-A. Wagenknecht, *Angewandte Chemie International Edition* **2008**, *47*, 2612.

[190] C. D. Dimitrakopoulos, P. R. L. Malenfant, *Advanced Materials* **2002**, *14*, 99.

[191] F. Würthner, M. Stolte, *Chemical Communications* **2011**, *47*, 5109.

[192] A. Sanguineti, M. Sassi, R. Turrisi, R. Ruffo, G. Vaccaro, F. Meinardi, L. Beverina, *Chemical Communications* **2013**, *49*, 1618.

[193] L. B.-Å. Johansson, H. Langhals, *Spectrochimica Acta Part A: Molecular Spectroscopy* **1991**, *47*, 857.

[194] www.advbiomaterials.com/products/hydrophilic/HydroMed.pdf, **2015**.

[195] J. P. Broomfield, *Corrosion of Steel in Concrete Understanding, Investigation and Repair*, E & FN Spon [Etc.] : [Online:] Taylor & Francis, London [Etc.], **1997**.

[196] Q. Zhou, J. Hill, E. A. Byars, J. C. Cripps, C. J. Lynsdale, J. H. Sharp, *Cement and Concrete Research* **2006**, *36*, 160.

[197] K. J. Bowers, J. Wiegel, *Extremophiles* **2011**, *15*, 119.

[198] H. G., T. R., T. R., D. N., B. Q., *Applied Microbiology and Biotechnology* **2002**, *59*, 409.

[199] R. Jayakumar, S. Jayashree, B. Annapurna, S. Seshadri, *Applied Biochemistry and Biotechnology* **2012**, *168*, 1849.

[200] A. Mills, Q. Chang, *Sensors and Actuators B: Chemical* **1994**, *21*, 83.

[201] J. E. Baur, M. B. Baur, David A Franz, *Journal of Chemical Education* **2006**, *83*, 577.

[202] N. P. Revsbech, E. Garcia-Robledo, S. Sveegaard, M. H. Andersen, K. V. Gothelf, L. H. Larsen, *Sensors and Actuators B: Chemical* **2019**, *283*, 349.

[203] M. D. DeGrandpre, T. R. Hammar, S. P. Smith, F. L. Sayles, *Limnology and Oceanography* **1995**, *40*, 969.

[204] M. D. DeGrandpre, *Analytical Chemistry* **1993**, *65*, 331.

[205] X. Ge, Y. Kostov, R. Henderson, N. Selock, G. Rao, *Chemosensors* **2014**, *2*, 108.

[206] J. S. Clarke, E. P. Achterberg, D. P. Connelly, U. Schuster, M. Mowlem, *TrAC Trends in Analytical Chemistry* **2017**, *88*, 53.

[207] Q. Xu, S. Lee, Y. Cho, M. H. Kim, J. Bouffard, J. Yoon, *Journal of the American Chemical Society* **2013**, *135*, 17751.

[208] R. Ali, T. Lang, S. M. Saleh, R. J. Meier, O. S. Wolfbeis, *Analytical Chemistry* **2011**, *83*, 2846.

[209] D. Pfeifer, I. Klimant, S. M. Borisov, *Chemistry - A European Journal* **2018**, *24*, 10711.

[210] B. J. Mueller, S. M. Borisov, Ingo. Klimant, *Adv. Funct. Mater.* **2016**, *26*, 7697.

[211] S. M. Borisov, C. Würth, U. Resch-Genger, I. Klimant, *Analytical Chemistry* **2013**, *85*, 9371.

[212] W. Zhao, E. M. Carreira, *Chemistry - A European Journal* **2006**, *12*, 7254.

[213] A. G. Hortmann, D. A. Robertson, B. K. Gillard, *The Journal of Organic Chemistry* **1972**, *37*, 322.

[214] C. Eggeling, J. Widengren, R. Rigler, C. A. M. Seidel, *Anal. Chem.* **1998**, *70*, 2651.

[215] T. Gareis, C. Huber, O. S. Wolfbeis, J. Daub, *Chem. Commun.* **1997**, 1717.

[216] Y. Tokoro, A. Nagai, Y. Chujo, *Tetrahedron Letters* **2010**, *51*, 3451.

[217] D. Marushchak, S. Kalinin, I. Mikhalyov, N. Gretskaya, L. B. -Å. Johansson, *Spectrochimica Acta Part A: Molecular and Biomolecular Spectroscopy* **2006**, *65*, 113.

[218] R. J. Meier, L. H. Fischer, O. S. Wolfbeis, M. Schäferling, *Sensors and Actuators B: Chemical* **2013**, *177*, 500.

[219] X. Wang, H. H. Gorris, J. A. Stolwijk, R. J. Meier, D. B. M. Groegel, J. Wegener, O. S. Wolfbeis, *Chem. Sci.* **2011**, *2*, 901.

[220] C. Huber, I. Klimant, C. Krause, O. S. Wolfbeis, *Anal. Chem.* **2001**, *73*, 2097.

[221] Kameradetails, https://www.alliedvision.com/de/produkte/kameras/kameradetails/Marlin/F-201.html, accessed: Jun., 2019.

[222] S. K. Lee, Y. Zu, A. Herrmann, Y. Geerts, K. Müllen, A. J. Bard, *J. Am. Chem. Soc.* **1999**, *121*, 3513.

[223] E. A. Margulies, J. L. Logsdon, C. E. Miller, L. Ma, E. Simonoff, R. M. Young, G. C. Schatz, M. R. Wasielewski, *J. Am. Chem. Soc.* **2017**, *139*, 663.

[224] S. M. Dyar, E. A. Margulies, N. E. Horwitz, K. E. Brown, M. D. Krzyaniak, M. R. Wasielewski, *The Journal of Physical Chemistry B* **2015**, *119*, 13560.

[225] C. Jung, B. K. Müller, D. C. Lamb, F. Nolde, K. Müllen, C. Bräuchle, *Journal of the American Chemical Society* **2006**, *128*, 5283.

[226] P. W. Zach, S. A. Freunberger, I. Klimant, S. M. Borisov, *ACS Appl. Mater. Interfaces* **2017**, *9*, 38008.

[227] G. M. Bilmes, J. O. Tocho, S. E. Braslavsky, *J. Phys. Chem.* **1989**, *93*, 6696.

[228] G. A. Crosby, J. N. Demas, *The Journal of Physical Chemistry* **1971**, *75*, 991.

9 List of Figures

10 List of Tables

11 Abbreviations

BODIPY	Borondipyrromethene
DLR	Dual Lifetime Referencing
DPP	Diketopyrrolopyrrole
ICT	Intramolecular Charge Transfer
τ	Luminescence Lifetime
ε	Molar Absorption Coefficient
NIR	Near Infrared
NMR	Nuclear Magnetic Resonance
PBI/PDI	Perylene bisimide/ Perylene diimide
PET	Photoinduced Electron Transfer
PET-support	Polyethylene terephthalate support
PPT	Photoinduced Proton Transfer
QY (Φ)	Quantum Yield
TBI/TDI	Terrylene bisimide/ Terrylene diimide
UV-Vis	Ultraviolet-Visible Spectroscopy